Remodelling of Store-Operated Ca^{2+} Entry and G0/G1 Cell Cycle Arrest

Marwa Etfat Eliwa

Thesis submitted for the degree of Doctor of Philosophy

Institute for Cell and Molecular Biosciences

Faculty of Medical Sciences

Newcastle University

June 2017

Abstract

The concentration of intracellular free Ca^{2+} ($[Ca^{2+}]_i$) plays an essential role in cell cycle progression. Understanding the Ca^{2+} signalling mechanisms that drive and maintain cell cycle arrest in the quiescent state, or stimulate quiescent cells to re-enter the cell cycle and proliferate, will be crucial for developing therapeutic potentials for highly detrimental diseases such as cancer and aging disorders. The work in this thesis investigates remodelling of the Store-Operated Ca^{2+} Entry (SOCE) signalling pathway that is associated with cell cycle arrest in the quiescent G0/G1 phase.

Serum starvation was used to induce cell cycle arrest in quiescent G0/G1 phase to allow investigation of remodelling of SOCE when cells exit the cell cycle. Cancer HeLa, precancerous NIH 3T3 and immortal non-cancerous hTERT RPE-1 cell lines were used in this comparative study. Serum starvation induced cell cycle arrest in G0/G1 phase in HeLa and NIH 3T3 cells that was accompanied by a marked down regulation in SOCE. In hTERT RPE-1 cells, serum starvation induced a modest down regulation in SOCE that was not accompanied by cell cycle arrest. Further experiments revealed that SOCE downregulation was attributed to changes in expression and localisation of the Ca^{2+} sensing protein STIM1 and the Ca^{2+} release-activated channel (CRAC) protein Orai1.

Serum was added-back in order to induce arrested cells to re-enter the cell cycle. Cell cycle re-entry was associated with restoration of SOCE, STIM1 and Orai1 expression in NIH 3T3 cells, and the restoration of only Orai1 expression in HeLa cells. By comparing these changes to that of hTERT RPE-1 cells, which were not arrested in G0/G1 cells, it appears that there may be a significant role for cell cycle arrest in quiescent G0/G1 phase in SOCE remodelling. In addition, these results suggest an additional role for Orai1 as a positive regulator of cell cycle progression in HeLa cells. In NIH 3T3 cells, SOCE and its proteins, STIM1 and Orai1, were remodelled with cell cycle arrest in quiescent G0/G1 phase and restored with cell cycle re-entry, indicating that each of STIM1 and Orai1 appears to have a role in SOCE and cell cycle progression. SOCE seems to be coupled to cell proliferation in NIH 3T3 cells but not in HeLa cells.

This study provides evidence that there are significant differences in SOCE remodelling with cell cycle arrest in quiescent G0/G1 phase in cancerous and pre-cancerous cells, and identifies potential targets for drug therapy aimed at regulating the cell cycle.

Acknowledgements

First, I would like to thank my supervisor Dr Tim Cheek for his help and great support during my PhD. Without his guidance and constant feedback this PhD would not have been completed.

Many many thanks to my supervisor Dr Mark Levasseur for his support throughout my PhD. Thanks for teaching me the techniques in the lab, for guidance in the overall plan of my work and being there to sort out any problems I had on the way.

Big thank you to Maureen Sinclair for her assistance with different techniques in the lab.

Thank you to Dr Claire Whitworth for providing me with the excellent tool for data analysis.

My heartfelt gratitude is extended to my friend Dr Rouaa Yassin who was always there when I needed her, pushing me to stay motivated and be patient when it was all too much.

A huge thank you to my friend Professor Wafaa Saleh for her valuable advises throughout my writing up.

Huge thanks for my parents in low for their constant prayers and love.

This work would not have been done without the endless support, help, encourage and love from my husband; Mohamed and my lovely sons; Abdelrahman, Ahmed and Yahia, thank you for bearing with me and my mood swings and being the source of happiness in my life.

Finally, many thanks for my **MUM** who always believes in me, whatever I say or do, I wouldn't be able to thank her. I wish if my dad was a life to thank him for believing in me and in my potentials. He would have been the happiest dad in the world! This thesis is dedicated to my **PARENTS**.

Again, thank you **Mohamed** for the countless things you have been doing for me and for funding my PhD.

Structure of the thesis

- Chapter 1 Introduction
- Chapter 2 Materials and Methods
  - **Part I - Results - G0/G1 Cell Cycle Arrest**
- Chapter 3 Morphology and Flow cytometry
- Chapter 4 Store-Operated Ca^{2+} Entry (SOCE)
- Chapter 5 Store-Operated Ca^{2+} Entry Proteins
- Chapter 6 Serum Starvation Time Course
  - **Part II - Results - Cell Cycle Re-entry**
- Chapter 7 Morphology and Flow cytometry
- Chapter 8 Store-Operated Ca^{2+} Entry (SOCE)
- Chapter 9 Store-Operated Ca^{2+} Entry Proteins
- Chapter 10 Final Discussion
- Chapter 11 References

Table of Contents

List of figures

List of tables

List of abbreviations

9cRA	9-cis-retinoic acid
2-APB	2-Aminoethoxydiphenyl borate
ANOVA	Analysis of variance
ARPE-19	
AUP	Area under peak
BSA	Bovine serum albumin
BCA	Bicinchoninic acid
BTP2	3, 5-bis (trifluoromethyl) pyrazole
$[Ca^{2+}]_i$	Intracellular free Ca^{2+} concentration
cADPr	cyclic ADP ribose
CAI	carboxyamidotriazole
CaM	Calmodulin
CaMKII	Ca^{2+}-calmodulin-dependent protein kinase II
CaSR	Ca^{2+} sensing receptor
CC	Coiled-coil
CCE	Capacitative Ca^{2+} entry
CICR	Ca^{2+}-induced Ca^{2+} release
CRACM1	Ca^{2+} release-activated Ca2+ modulator 1 (also known as **Orai1**)
DAG	Diacylglycerol
DIC	Differential interference contrast
DMEM	Dulbecco's Modified Eagle's Medium
DMSO	Dimethyl sulfoxide
ECL	Enhanced chemiluminescent
EDTA	Ethylenediaminetetraacetic acid
ER	Endoplasmic reticulum
ERM	Ezrin-radixin-moesin
EthD-1	Ethidium homodimer-1
FCS	Fetal calf serum
FR	Fluorescence ratio

FRUs	Fluorescence ratio units
FSC	Forward scatter
Fura-2/AM	Fura-2 acetoxymethyl
G0	Gap 0 phase
G1	Gap 1 phase
G2	Gap 2 phase
GPCR	G-protein coupled receptors
HEK293	Human embryonic kidney cells 293
HOP	Height of peak
HRP	Horseradish peroxidise
HUVEC	Human umbilical vein endothelial cells
ICRAC	Ca^{2+} release-activated Ca^{2+} current
InsP3	Inositol 1,4,5-trisphosphate
IP3Rs	Inositol 1,4,5-trisphosphate receptors
IU	International units
M phase	Mitosis
mRNA	messenger RNA
NAADP	Nicotinic acid adenine dinucleotide phosphate
NEB	nuclear envelope breakdown
NP	Nucleus Pulposus Cells
PBS	Phosphate buffered saline
PIP2	Phosphatidyl inositol 4,5-bisphosphate
PKC	Protein kinase C
PLC	Phospholipase C
PM	Plasma membrane
PMCA	Plasma membrane Ca^{2+}-ATPase
PMT	photomultiplier tubes
R	Restriction point
RBL cells	Rat Basophilic Leukemia cells
ROC	Receptor-operated Ca^{2+} channel
ROD	Rate of decline

ROR	Rate of rise
RPE	Retinal pigment epithelium
RT	Room temperature
RYRs	Ryanodine receptors
SAM	Sterile ά-motif
SCID	Severe combined immunodeficiency disorder
SCC	Side scatter
SDS-PAGE	Sodium dodecyl sulphate-polyacrylamide gel electrophoresis
SEM	Standard error of the mean
SERCA	Sarco/endoplasmic reticulum Ca2+-ATPase
siRNA	small interfering RNA
S phase	Synthesis phase
SOC	Store-operated Ca^{2+} channel
SOCE	Store-operated Ca^{2+} entry
SR	Sarcoplasmic reticulum
STIM1	Stromal-interaction molecule 1
TB	Trypan blue
TG	Thapsigargin
TPCs	Two-pore channels
TRPC1	Transient receptor potential channel 1
VOC	Voltage-operated Ca^{2+} channel

Chapter 1 Introduction

Dysfunctional cell cycle progression is associated with many diseases and disorders which affect human lifespan and health, for example cancer, age-related disorders and pre-natal developmental disorders (Zhivotovsky and Orrenius, 2010). Of central importance in developing therapeutic treatment for diseases such as cancer (Chen *et al.*, 2013) and aging disorders (Peacock, 2010), will be understanding how Ca^{2+} signals drive or maintain cell cycle arrest in the quiescent state, or stimulate quiescent cells to re-enter the cell cycle and proliferate. The work in this thesis aims to address this 'knowledge gap' by mapping the remodelling of Ca^{2+} signals that is associated with cell cycle progression.

1.1 Cell proliferation and the cell cycle

Uncontrolled proliferation is a hallmark of cancer. Cancer cells have the ability to escape normal regulatory mechanisms that control how many times a cell can divide. Cell proliferation is directly linked to cell cycle progression.

The cell cycle consists of two main phases. The two major phases of cell cycle are interphase; the phase between mitotic events during which growth and regeneration take place and mitosis (Figure1.1). The interphase is further subdivided into three phases: G1-phase (Gap 1) during which the cells synthesize RNA and proteins to induce growth and prepare for DNA synthesis and chromosome duplication that occur in the S-phase (Synthesis). The S-phase is then followed by the G2-phase (Gap 2). During G2-phase which is the last phase of interphase the cell is preparing for mitosis in which the nuclear division (mitosis) and cytoplasmic division (cytokinesis) occur (Mitchison, 1971; Prescott, 1976; Prescott, 1987).

A further phase is known as G0 phase or quiescence. Cellular quiescence is a reversible non-proliferating state where the cells exit the cell cycle and no longer divide. Some cells become quiescent when they reach maturity and enter a state of terminal differentiation but continue to do their main functions (e.g. neurones). Other cells that can re-enter the cell cycle are known to be in G0 phase in response to a lack of growth factors or nutrients (e.g. stem cells).

1.1.1 Cell cycle checkpoints

Cell cycle events occur in a unidirectional way which is vital to ensure precise chromosomal duplication and segregation into daughter cells (Murray and Hunt, 1993).

Regulation of the cell cycle is critical to the survival of mammalian species. Therefore, the cell cycle is controlled by an independent system which consists of numerous mechanisms ensuring correct cell division in the right order. These independent mechanisms are known as checkpoints which operate at crucial transitions in the cell cycle to verify whether the processes at each phase of the cell cycle have been accurately completed before progression into the next phase (Hartwell and Weinert, 1989). The main check points are defined as: 1) Restriction point (R) (Pardee, 1992) which occurs at the end of G1 phase just before entry into S phase. 2) G2/M checkpoint which controls entry to mitosis. 3) Spindle Checkpoint that prevents separation of the sister chromatids until the completion of spindle assembly and attachment of chromosomes kinetochore to spindle fibres occur (Hoyt *et al*., 1991; Li and Murray, 1991).

The cell cycle is also controlled by both endogenous and exogenous signals. One of the main exogenous signals are the growth factors that stimulate cells to move from G0 to G1 phase. Early in G1 phase, before reaching R point, removal of growth factor results in a return to G0, while later on, after passing the R point, removal of growth factor has no effect and the cell will continue to enter the S phase (Rossow *et al.*, 1979). At R point, the key decision of whether the cell should divide, delay division, or enter a resting stage is made.

Ca^{2+} signalling is one of the main endogenous signals that operate at checkpoints and has been known to control some of these crucial transitions of the cell cycle. For example, Ca^{2+} /calmodulin-dependent protein kinase and calcineurin have been shown to be essential for quiescent cells to re-enter the proliferative pathway (G0 re-entry), G1/S, G2/M and metaphase of mitosis (Lu and Means, 1993; Means, 1994). In addition, a transient increase in intracellular free Ca^{2+} has been shown to control cell cycle progression by translational and post-translational regulation of the cell cycle control proteins pp34 and cyclin (Whitaker and Patel, 1990) and to control chromosome disjunction in early sea urchin embryos (Groigno and Whitaker, 1998).

1.1.2 Quiescent G0/G1 arrest

Quiescent G0/G1 arrest occurs before the cell reaches the R point where some cells enter the G0 phase and others remain in early G1 phase. The quiescent G0/G1 arrest is reversible; although the arrested cell stops dividing, it can be reactivated into proliferation by external signals e.g. growth factors (Figure1.1).

Cancer cells are able to ignore signals that can arrest cells in G0/G1 phase and can therefore continue to proliferate. This is usually a result of alterations to genes known as tumor suppressor genes, which normally control cells' response to external and internal cues to exit the cell cycle. In addition, some cancer cells remain dormant for prolonged periods where they persist in G0/G1 phase (Udagava, 2008; Almog, 2013). This stage makes the dormant cells below the threshold of diagnostic detection for months to decades. Elucidation of how remodelling of signalling mechanisms involved in the regulation of cell cycle arrest in G0/G1 phase might contribute to development of novel strategies in treatment and prevention of cancer.

In vitro, serum starvation has been extensively used in cell cycle research since Pardee established the restriction point concept (Zetterberg and Larsson, 1985; Pardee, 1992; Kerkhoff and Rapp, 1997; Pardee, 1974) and has continued as a principal and a valuable experimental technique to induce cell cycle arrest in a quiescent G0/G1 phase (Lemos *et al.*, 2007; Kothapalli *et al.*, 2008; Van Rechem *et al.*, 2010; Xiong *et al.*, 2012).

In this study, serum starvation has been used to induce cells to enter quiescent G0/G1 phase.

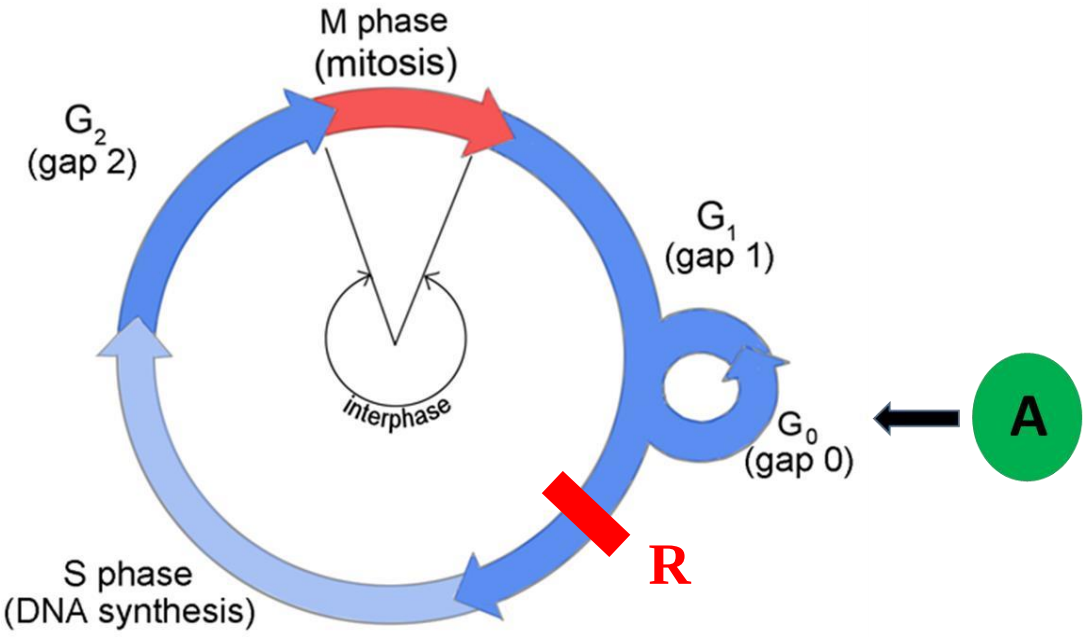

Figure 1.1 The Cell Cycle

The cell cycle consists of Interphase (G1, S and G2 phases) and Mitotic phase (M). Cells exit the cell cycle and stay in G0 phase (quiescence) upon either reaching maturity or due to lack of nutrients. Upon stimulation with an agonist (A) e.g. growth factor, cells in G0 phase re-enter the cell cycle. R (restriction point).

1.2 Ca^{2+} signalling

Mammalian cells use Ca^{2+} ions as a universal second messenger to control a diverse range of cellular processes, including cell proliferation, development, migration and apoptosis (Berridge *et al.*, 1998; Berridge *et al.*, 2000; Bootman *et al.*, 2001; Berridge *et al.*, 2003). These processes are triggered by different stimuli such as hormones, growth factors, cytokines, and neurotransmitters that cause a rise in intracellular Ca^{2+} concentration. The increase in cytosolic Ca^{2+} concentration generates transients that vary in temporal and spatial nature, thus enabling cells to adjust their response to a certain stimulus (Berridge *et al.*, 2003; Berridge, 2009; Laude and Simpson, 2009). This increase in cytosolic Ca^{2+} occurred either from entry of Ca^{2+} through the plasma membrane or release from internal stores.

The resting level of cytosolic Ca^{2+} is maintained at 50–200 nM by the concurrent interaction of several processes, which can be divided into Ca^{2+} 'on' and 'off' mechanisms depending on whether they serve to increase or decrease cytosolic Ca^{2+} respectively. When cells are activated the Ca^{2+} levels rise to create various signals that are characterised by being highly versatile in that they vary in space, time and amplitude (Berridge *et al.*, 1998; Berridge *et al.*, 1999; Berridge *et al.*, 2000; Bootman *et al.*, 2001). These signals can be in the form of micro domains with very high level of Ca^{2+} concentration (50–100 μM) in the vicinity of the Ca^{2+} channels that propagate over ~ 20 nm (Berridge *et al.*, 2000; McCarron *et al.*, 2006; Parekh, 2008) and stimulate highly localised processes. These cellular processes vary depending on the type of Ca^{2+} channel opened and its location (Berridge *et al.*, 1998).

These signals are called elementary events (Berridge *et al.*, 1998) and form the 'basic building blocks of Ca^{2+} signalling' that generate global Ca^{2+} signal that can spread over large distances (10–100 μm) in the range of nM by activating nearby channels to open and release Ca^{2+} through the process of Ca^{2+}-induced Ca^{2+} release (CICR) (Berridge *et al.*, 1998; Berridge *et al.*, 1999). These elementary events are rapidly removed by the process of simple diffusion (Berridge *et al.*, 1998). As the internal Ca^{2+} stores are limited, the sustained bouts of signalling depend on the influx of external Ca^{2+} through (SOCs) (Berridge *et al.*, 1998).

1.2.1 The Ca^{2+} 'on' mechanisms

Ca^{2+} 'on' mechanisms are Ca^{2+} channels that cause increase in the cytosolic Ca^{2+} level and consequently trigger Ca^{2+} signals that regulate many cellular processes including cell proliferation, migration and invasion by cancer cells (Berridge *et al.*, 2000; Berridge *et al.*, 2003). These channels are either located at the internal stores using the internal Ca^{2+} to generate Ca^{2+} signals or channels located at the plasma membrane (PM) which utilise Ca^{2+} from the extracellular space.

The internal stores are held within the membrane systems of the endoplasmic reticulum (ER) or, the sarcoplasmic reticulum (SR) of muscle cells which release the Ca^{2+} from finite intracellular Ca^{2+} stores. These channels include ryanodine receptors (RYRs) and Inositol 1,4,5-trisphosphate receptors (InsP3Rs) (Berridge *et al.*, 2000). One principal activator of these channels is Ca^{2+} itself and this process of Ca^{2+}-induced Ca^{2+} release (CICR) is fundamental to the mechanism of Ca^{2+} signalling (Berridge *et al.*, 1998; Berridge *et al.*, 1999).

Channels located at the plasma membrane (PM) are channels classified by the way in which they are activated. They are the Voltage-Operated- Channels (VOCs), Receptor-Operated Ca^{2+} -Channels (ROCs), ligand-gated channels, stretch-activated, second-messenger gated channels and Store-Operated -Channels (SOCs) (Berridge *et al.*, 2000; Bootman *et al.*, 2001; Clapham, 2007) . VOCs are activated by depolarisation to selectively permit Ca^{2+} entry from the extracellular space (Bootman *et al.*, 2001) and they typically exist in excitable cells such as neuronal and muscle cells (Berridge *et al.*, 2000). ROCs open in response to receptor activation by external stimuli such as ATP or acetylcholine (Berridge *et al.*, 2000; Bootman *et al.*, 2001). Store-Operated -Channels (SOCs) are one of the channels that allow Ca^{2+} entry from extracellular space in response to internal store depletion (Berridge *et al.*, 2000; Bootman *et al.*, 2001). Another source of Ca^{2+} influx is the two G-protein coupled receptors sensing extracellular Ca^{2+}, Ca^{2+}-sensing receptor (CaSR) and GPRC6a. These receptors are present in many cell types (Riccardi and Gamba, 1999). They are G-protein coupled receptors (GPCR) and when activated by increasing external Ca^{2+} concentrations they trigger intracellular Ca^{2+} transients (Breitwieser and Gama, 2001; Rey *et al.*, 2010). At rest Ca^{2+} 'on' mechanisms work in balance with the Ca^{2+} 'off' mechanisms (Bootman *et al.*, 2001).

1.2.2 The Ca^{2+} 'off' mechanisms

A more diverse set of 'off' mechanisms is recruited by cells to remove Ca^{2+} from the cytosol. These include the plasma membrane Ca^{2+} ATPase (PMCA) and Na^{+}/Ca^{2+} exchanger which removes Ca^{2+} from the cytosol into the extracellular environment (Berridge *et al.*, 2000). The sarco-endoplasmic reticulum Ca^{2+} ATPase (SERCA) is another Ca^{2+} 'off' mechanism located on the ER/SR membrane which pumps Ca^{2+} from the cytoplasm back into the ER/SR (Berridge *et al.*, 2000). Mitochondria have been shown to be an 'off' mechanism as they control the amplitude of cytosolic Ca^{2+} increase by rapidly sequestering Ca^{2+} and then slowly returning it to the cytosol once resting levels have been restored. Also, Ca^{2+} binding proteins are known as 'off' mechanisms and include Ca^{2+} sensors and Ca^{2+} buffers. Sensors such as calmodulin bind Ca^{2+} and in response activate various cellular responses (Berridge *et al.*, 2000) and also buffers such as peroxisomes in the cytosol bind Ca^{2+} as it enters the cell (Raychaudhury *et al.*, 2006; Lasorsa *et al.*, 2008).

Ca^{2+} plays a vital role in processes that are affected in cancerous cells including cell proliferation, differentiation and invasion. It is therefore important that these processes are central aspects of current cancer research (Bergner and Huber, 2008). This project therefore concentrates on elucidating the remodelling of Ca^{2+} signals, specifically SOCE and its proteins, when cells enter a quiescent state.

1.3 Store-operated Ca^{2+} entry

The active interplay between Ca^{2+} release from internal stores and influx from the extracellular space outlines Ca^{2+}-signalling dynamics and subsequently the cellular response. These two pathways, internal release and influx, are coupled through the store-operated Ca^{2+} entry (SOCE) that occurs in response to depletion in Ca^{2+} stores. This control of Ca^{2+} influx at the cell membrane by Ca^{2+}-store depletion was first defined by Putney in 1986 in the context of the capacitative Ca^{2+}-entry model (Putney, 1986; Parekh and Putney, 2005).

This depletion is a result of CICR, whereby Ca^{2+} self-promotes its own release by activating RYRs and InsP3Rs (Berridge *et al.*, 2000). InsP3, a second messenger generated in the phosphoinositide signalling pathway, binds to InsP3R makes it ready to be activated by Ca^{2+}. In contrast RYRs can be either directly activated by Ca^{2+} or through binding of a second messenger cyclic ADP ribose (cADPr) (Berridge *et al.*, 2000; Bootman *et al.*, 2001).

InsP3 and diacylglycerol (DAG) are produced by activation of Phospholipase C and phospholipase A2 following stimulation of plasma membrane G-protein coupled receptors (Miyazaki *et al.*, 1993). InsP3 diffuses through the cytosol, binds to and activates InsP3Rs located on the ER/SR membrane. Opening of these channels result in store depletion as Ca^{2+} moves down its concentration gradient from the ER (~500µM) into the cytosol (~100nM) (Bootman *et al.*, 2001). Depletion of the store then stimulates SOCE via opening of SOCs channels located in the plasma membrane in response to store depletion (Putney *et al.*, 2001) generating what is known as the Ca^{2+}-release activated Ca^{2+} current (ICRAC).

Recently, the molecular mechanisms underlying SOCE were identified. Three proteins have been implicated in the integration of this signalling pathway; STIM, Orai and TRPC1.

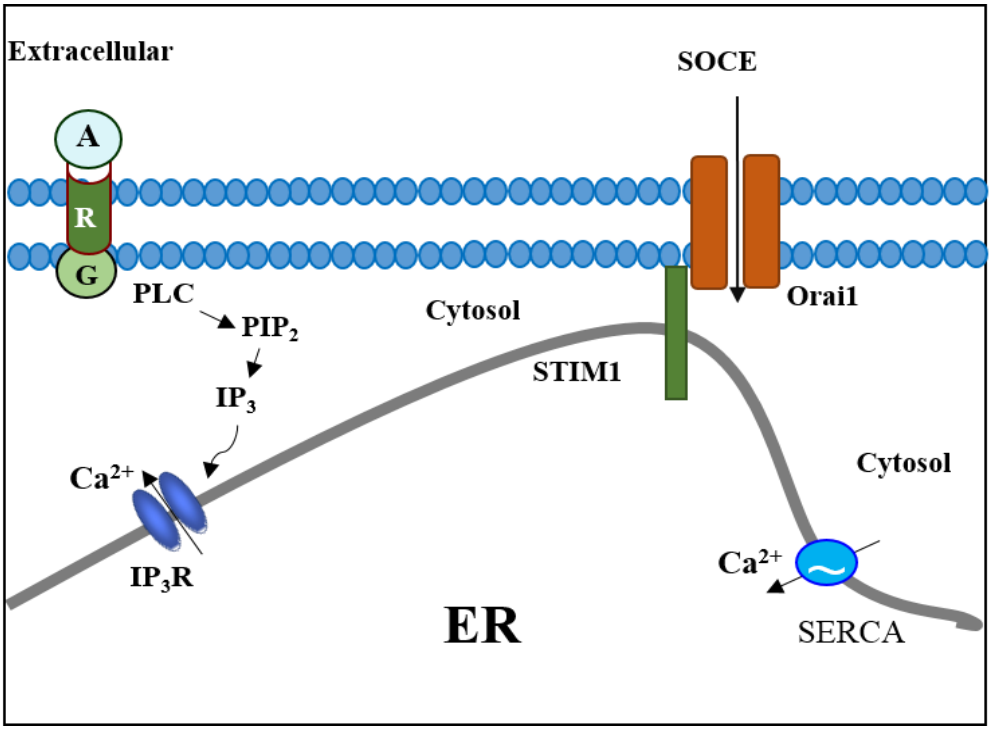

Figure 1.2 SOCE

Binding of an agonist (A) to a G-protein-coupled receptor (R) activates phospholipase C (PLC) which hydrolyses PIP2 to generate the second messenger IP3. IP3 diffuses through the cell cytosol and binds to IP3 receptors (IP3Rs) located in the ER membrane. Opening of IP3Rs results in ER store depletion. Depletion of ER Ca^{2+} stores is signalled, most likely by STIM1, to SOCs located in the PM. SERCA is a Ca^{2+} ATPase that pumps Ca^{2+} from the cytosol into the ER to replenish depleted stores.

1.3.1 STIM proteins

RNAi screens had a key role identifying STIM 1 and STIM2 (Stromal interaction molecule 1 and 2) genes in mammals (Liou *et al.*, 2005; Roos *et al.*, 2005). STIM1 and STIM2 are type I ER transmembrane proteins which were identified as the sensors of luminal ER Ca^{2+}.

STIM1 is a 77kDa type 1 single-pass TM proteins (Lewis, 2007). Up to 25% of these proteins are localized to the PM (Manji *et al.*, 2000; Zhang *et al.*, 2005), while the vast majority is localized to the ER membrane (Lewis, 2007) where the function of these regulatory molecules is best recognised (Williams *et al.*, 2001; Williams *et al.*, 2002; Zhang *et al.*, 2005).

STIM1 consists of an N-terminal region (STIM1-N) located in the ER lumen and a C-terminal region (STIM1-C) in the cytosol (Zeng *et al.*, 2008; Hogan *et al.*, 2010), and both possess an EF-hand domain that is able to bind Ca^{2+} in the ER lumen (Williams *et al.*, 2001; Liou *et al.*, 2005; Zhang *et al.*, 2005; Wu *et al.*, 2006; Brandman *et al.*, 2007; Zeng *et al.*, 2008) with binding affinity in the normal 0.5–1 mM range for ER $[Ca^{2+}]_i$ (Stathopulos *et al.*, 2006; Zeng *et al.*, 2008).

The C terminus has the ability to open all channels gated by STIM1 (Huang *et al.*, 2006) as it plays a key role in the translocation of STIM1 oligomers to ER-PM junctions (Baba *et al.*, 2006; Huang *et al.*, 2006; Liou *et al.*, 2007).

STIM1 phosphorylation at multiple serine residues has been recognised and shown to have a role in STIM1 activation during ER Ca^{2+} store depletion (Manji *et al.*, 2000; Pozo-Guisado *et al.*, 2013). On the other hand, STIM1 phosphorylation has also been shown to inhibit SOCE (Smyth *et al.*, 2009; Sundivakkam *et al.*, 2012; Sundivakkam *et al.*, 2013). STIM1 can also be glycosylated (Manji *et al.*, 2000; Dziadek and Johnstone, 2007) which can affect PM localisation (Williams *et al.*, 2002). Interference with STIM glycosylation prevents clustering of STIM1 (Korzeniowski *et al.*, 2010).

The extent of SOCE is closely related to level of STIM1 expression. STIM1 overexpression increases SOCE while knockdown causes a reduction in SOCE in many cell types such as endothelial progenitor cells (Kuang *et al.*, 2010; Shin *et al.*, 2010) endothelial cells (Abdullaev *et al.*, 2008), vascular smooth muscle cells (Takahashi *et al.*, 2007b; Aubart *et al.*, 2009; Potier *et al.*, 2009), SH-SY5Y neuroblastoma cells (Bell *et al.*, 2013) Jurkat T cells (Roos *et*

al., 2005; Huang *et al.*, 2006), HEK293 cells (Mercer *et al.*, 2006; Abdullaev *et al.*, 2008) and HeLa cells (Liou *et al.*, 2005).

Recently, STIM1 has been shown to exist in two isoforms; STIM1S and STIM1L (Darbellay *et al.*, 2011; Sauc *et al.*, 2015). The shorter STIM1S isoform has been identified as the predominant STIM1 isoform whereas the longer STIML isoform has only recently been recognised to activate SOCE in cells lacking STIM1S (Darbellay *et al.*, 2011; Sauc *et al.*, 2015).

STIM2 structurally, shares 66% sequence homology with STIM1 (Williams *et al.*, 2001; Zheng *et al.*, 2008) and is only expressed in the ER membrane, unlike STIM1 which is also expressed in the PM (Zheng *et al.*, 2008). STIM2 has been found to induce store independent Ca^{2+} entry (Parvez *et al.*, 2008). However it has been also found to activate SOCE and respond to smaller decreases in ER [Ca^{2+}] than STIM1 (Brandman *et al.*, 2007).

STIM2 knockdown reduces basal $[Ca^{2+}]_i$ and overexpression increases basal $[Ca^{2+}]_i$ (Brandman *et al.*, 2007) and also inhibits SOCE (Soboloff *et al.*, 2006b). In addition knockdown of STIM2 in HeLa cells caused a reduction in SOCE (Liou *et al.*, 2005) but has also been shown to have no effect in Jurkat T cells (Roos *et al.*, 2005), therefore role of STIM2 in SOCE still not clear.

As STIM1 activates SOCE, expression of STIM1 is investigated in this study (Chapter 5, 6 and 9).

1.3.2 Orai proteins

The Orai proteins were found to mediate the highly Ca^{2+} selective Ca^{2+} release activated current (ICRAC) (Feske *et al.*, 2006; Vig *et al.*, 2006; Zhang *et al.*, 2006). Each subunit of the Orai channels has four transmembrane spans with cytoplasmic N and C termini. There are three human homologues of the Orai protein; Orai1, Orai2 and Orai3.

Orai1 is a 33kDa tetra-pass PM spanning protein that forms the SOC pore. Orai1 was first identified in 2006 as an essential component of SOCE (Feske *et al.*, 2006; Vig *et al.*, 2006; Zhang *et al.*, 2006). T cells from patients with severe combined immunodeficiency (SCID) syndrome failed to activate SOCE following store depletion (Feske *et al.*, 2006) which later on was attributed to depletion of Orai1 and transfection with wild-type Orai1 in cells from SCID patients restored SOCE (Feske *et al.*, 2006)

Like STIM1, many studies showed that Orai1 has a key role in SOCE in many cell types. Knockdown of Orai1 cause a reduction of SOCE in neural progenitor cells (Hao *et al.*, 2014), HEK293 cells (Gwack *et al.*, 2007; Kawasaki *et al.*, 2010), neuroblastoma cells (Bell *et al.*, 2013), osteoclasts (Zhou *et al.*, 2011), endothelial cells (Abdullaev *et al.*, 2008), Jurkat T cells (Gwack *et al.*, 2007) and acinar cells (Hong *et al.*, 2011). Moreover, Orai1 overexpression was shown to restore SOCE in SCID T cells and fibroblasts (Gwack *et al.*, 2007), causes an increase in SOCE in HEK293 cells (Fukushima *et al.*, 2012) and in differentiated neuroblastoma cells (Bell *et al.*, 2013).

Indeed, Orai1has been shown to form the pore forming subunit of SOCs. This was confirmed by mutant studies in which substitution of acidic residues in transmembrane domains 1 and 3 and in the extracellular loop region between transmembrane domains 1 and 2 altered Ca^{2+} permeability and selectivity of ICRAC (Prakriya *et al.*, 2006; Vig *et al.*, 2006; Yeromin *et al.*, 2006). In addition, the R91W point mutation in SCID patients with dysfunctional ICRAC is located in transmembrane domain 1 (Feske *et al.*, 2006).

Orai2 and Orai3 show high sequence similarity to Orai1, particularly in their transmembrane segments (Takahashi *et al.*, 2007a; Shuttleworth, 2012), yet they are different at the cytosolic N- and C termini, at which SOCs channels are known to be activated (Takahashi *et al.*, 2007a; Shuttleworth, 2012).

Co-expression of Orai2 with STIM1 results in an increase in ICRAC, though to a lesser extent than Orai1 (Mercer *et al.*, 2006). Similarly, co-expression of STIM1 with Orai1 that had the Orai2 N-terminal tail only slightly increased SOCE while co-expression of STIM1 with Orai2 containing the Orai1 N-terminus cause robust increase in SOCE to levels observed with Orai1-STIM1 co-expression (Takahashi *et al.*, 2007a).

Orai3 does not generally appear to be involved in SOCE as, unlike Orai1 and Orai2, co-expression of Orai3 with STIM1 does not produce detectable Ca^{2+} selective currents (Mercer *et al.*, 2006; DeHaven *et al.*, 2007) and expression of a dominant-negative mutant Orai3 in HEK293 cells had no effect on SOCE (Mignen *et al.*, 2008).

Given that Orai1 co-expression with STIM1 has consistently been shown to increase SOCE to a greater extent than that observed with Orai2 or Orai3 expression (Mercer *et al.*, 2006; Peinelt *et al.*, 2006; Soboloff *et al.*, 2006a; Takahashi *et al.*, 2007a) this implies that the Orai1 isoform has a more prominent role in SOCE. Therefore, expression of Orai1 is investigated in this study (chapter 5, 6 and 9).

1.3.3 STIM1/Orai1 interaction

Interaction between STIM1 and Orai1underlies SOCE (Figure1.2). Ca^{2+} release from the endoplasmic reticulum causes a conformational change of STIM1 which is converted from monomers into oligodimers (Stathopulos *et al.*, 2006; Stathopulos *et al.*, 2008). STIM1 oligodimers induce formation of distinct puncta at ER-PM junctions that mediated by its sterile alpha motif (SAM) domain (Liou *et al.*, 2005; Zhang *et al.*, 2005; Park *et al.*, 2009; Yuan *et al.*, 2012) where they directly interact with the C-terminus of Orai1. This STIM1 interaction traps Orai1 at the PM and sequesters Orai1 into cortical STIM1 clusters (Hodeify *et al.*, 2015) inducing a conformational change in Orai1 (Luik *et al.*, 2006; Kawasaki *et al.*, 2009; Yuan *et al.*, 2012) which result in opening of Orai1 channels and triggering SOCE to refill depleted stores. Interestingly, the Orai1 channels open only in the immediate vicinity opposite STIM1 puncta which exists in close proximity (~20 nm) to the PM (Luik *et al.*, 2006; Wu *et al.*, 2006; Hodeify *et al.*, 2015). After refilling of ER Ca^{2+} stores STIM oligomers dissociate and its uniform distribution throughout the ER membrane is restored (Luik *et al.*, 2006; Liou *et al.*, 2007). Hence direct physical coupling between STIM1 (the ER Ca^{2+} sensor)

and Orai1 (the Ca^{2+} channel at the cell membrane) derives functional coupling between Ca^{2+} levels in the ER lumen and extracellular Ca^{2+} entry.

Therefore, STIM1 is essential for the function of Orai1 as a SOC (Mercer *et al.*, 2006; Peinelt *et al.*, 2006; Zhang *et al.*, 2006; Frischauf *et al.*, 2016) and it has been shown that knockdown of STIM1 significantly reduced SOCE (Roos *et al.*, 2005; Mercer *et al.*, 2006; Abdullaev *et al.*, 2008; Bell *et al.*, 2013).

STIM1 co-localisation with Orai1 at PM has been observed upon Ca^{2+} store depletion in sinoatrial node cells (Liou *et al.*, 2005), Xenopus oocytes (Courjaret and Machaca, 2014) and HEK293 cells (Fukushima *et al.*, 2012).

STIM1 not only interacts with Orai1 but also interacts with and gates members of the TRPC channel family (Huang *et al.*, 2006; Yuan *et al.*, 2007; Zeng *et al.*, 2008) which may play a role in cellular proliferation.

Recently, SOCE remodelling has been associated with cancer cell proliferation, migration and invasion (Targos 2005; Chen 2013; Prevarskaya *et al.*, 2011). SOCE mediated by Orai and STIM proteins has recently been implicated in various cellular processes associated with carcinogenesis (Bergmeier *et al.*, 2013).

1.3.4 TRPC

Transient Receptor Potential-Canonical (TRPC) channels are non-selective Ca^{2+}-permeable channel involved in cation transport in a variety of biological processes (Yuan *et al.*, 2003). TRPC1 is a 90kDa PM protein that has been implicated in SOCE (Parekh and Putney, 2005) and was initially thought to be the primary SOC involved in SOCE before the discovery of Orai1 (Parekh and Putney, 2005). For example, knockdown of TRPC1 in submaxillary mouse acinar cells causes a reduction in SOCE (Liou *et al.*, 2007). TRPC1 has been found to function as a SOC via interactions with STIM1 (Berna-Erro *et al.*, 2012; Lee *et al.*, 2014; Yuan *et al.*, 2007; Alicia *et al.*, 2008; Jardin *et al.*, 2008). The role of TRPC1 as a SOC is controversial, as several studies have shown that TRPC1 is not involved in SOCE. Most of the controversy surrounding the role of TRPC1 as a SOC is due to its well established role as a ROC. However, recent studies suggest that TRPC1 may also function as a SOC without the

requirement of STIM1 interactions (DeHaven *et al.*, 2009) and can be activated by other non-SOCE pathways (Putney, 2005).

This inconsistent evidence showed that TRPC1 role in SOCE is not clear and for this reason it was not included in this study.

1.4 Ca^{2+} signalling and the cell cycle

Ca^{2+} is a cell messenger that plays a central part in cell cycle control. Much of the evidence that points to Ca^{2+} as a signal that triggers cell cycle has been detected in almost every type of normal and transformed cell lines.

The notion that Ca^{2+} signalling may have a role in cell cycle progression originated in 1970s, when microinjection of Ca^{2+} chelators and antagonists into sea urchin egg blocked nuclear envelope breakdown (NEB), inhibited mitosis exit and consequently blocked the cell cycle (Zucker and Steinhardt, 1978), injection of Ca^{2+} chelators in somatic cells also delays mitosis exit (Izant, 1983) and the reverse result showing that artificially increasing $[Ca^{2+}]_i$ induced premature mitosis entry was also observed (Zucker *et al.*, 1978; Whitaker and Steinhardt, 1982).

By the early 1980s, with the development of fluorescent Ca^{2+} indicators (e.g. fura, fluo, indo and others), a further understanding of intracellular Ca^{2+} homeostasis was attained. Ca^{2+} transients have been recorded in mammalian at exit from mitosis (Poenie *et al.*, 1985; Poenie *et al.*, 1986) and Ca^{2+} gradients centred on the mitotic pole have been also seen (Ratan and Shelanski, 1986).

Furthermore, it has been known that a critical external Ca^{2+} concentration is necessary for mammalian cells to pass R checkpoint and enter the cell cycle (Whitfield *et al.*, 1976; Hazelton *et al.*, 1979; Tupper *et al.*, 1980).

Understanding of Ca^{2+} regulation of cell growth and division is further reinforced by genetic and biochemical studies demonstrating that calmodulin (CaM); a Ca^{2+} target and Ca^{2+}-calmodulin-dependent protein kinase II (CaMKII) play an essential role at several transition points during cell cycle progression. Calmodulin (CaM) was shown to regulate mitosis (Lu and Means, 1993; Takuwa *et al.*, 1995; Whitaker, 1995; Whitaker and Larman, 2001), G1 phase (Rasmussen and Means, 1989) and to be essential for movement of quiescent cells into the cell cycle as well as for proliferating cells to move from G1 to S, G2 to M and through mitosis (Rasmussen and Means, 1989; Means, 1994; Kahl and Means, 2003). Ca^{2+} has been also shown to be required for centrosome duplication which is necessary for spindle formation

and chromosome segregation (Matsumoto and Maller, 2002). Furthermore, the Ca^{2+}-dependent phosphatase calcineurin has been involved in G1-S progression (Kahl and Means, 2003).

Great progress has been made in the last few decades in understanding key Ca^{2+}-dependent pathways that regulate cell cycle progression. SOCE is a ubiquitous Ca^{2+}influx pathway that functions in all non-excitable cells in response to agonist stimulation (Parekh and Putney, 2005) and is known to play a key role in cell proliferation. One of the strong lines of evidence of a role of for Ca^{2+} influx in cell proliferation comes from the use of Ca^{2+} channel blockers. For example, 2-APB (Bootman *et al.*, 2002), BTP2 (Ohga *et al.*, 2008) and carboxyamidotriazole (CAI) (Perabo *et al.*, 2004) have been shown to inhibit cell proliferation.

SOCE has been known to be vital for lymphocyte proliferation (Feske *et al.*, 2006). In addition, blocking of SOCE resulted in an alteration of intracellular signalling pathways linked to cell proliferation (Berna-Erro *et al.*, 2012) and SOCE inhibition using (BTP-2) reduced cell proliferation in human metastatic melanoma cell lines (Umemura *et al.*, 2014). Furthermore, it has been shown that inhibition of Ca^{2+}influx through SOCs can slow down the growth of certain aggressive cancer cells (Kohn *et al.*, 1996).

The relation between SOCE and cell cycle is bidirectional, remodelling of SOCE has been well defined at mitosis (Arredouani *et al.*, 2010). The first suggestion that Ca^{2+} influx is inhibited during cell division was reported in 1988 in a study of HeLa cells (Volpi and Berlin, 1988). Recently, it has been confirmed that SOCE is inactivated during mitosis in HeLa and HEK293 cells (Smyth *et al.*, 2009), Cos-7 cells (Russa *et al.*, 2008) Smyth et al., 2009; RBL-2H3 cells (Tani *et al.*, 2007). Investigating SOCE levels throughout the cell cycle showed that there is a slight enhancement of SOCE during the G1-S transitions and dramatic down-regulation during M phase (Tani *et al.*, 2007).

1.5 Knowledge gap

Ca^{2+} signalling at mitosis has been studied most extensively. However, Ca^{2+} signalling, especially SOCE when cells enter and /or exit from a quiescent G0/G1 phase has been poorly investigated. Cancer cells have been shown to escape quiescence and go into uncontrolled proliferation (Sherr, 1996; Hanahan and Weinberg, 2000). Furthermore, tumour dormancy has been attributed to cell cycle arrest in a quiescent G0/G1 stage the time before which cells switch and enter the rapid growth phase (Udagava, 2008; Almog, 2013). Elucidating the remodelling of SOCE when cells enter/exit this phase may provide insight into the mechanisms that control cancer cell proliferation or keep cells dormant before they switch to proliferation and cause cancer metastases.

1.6 Cell lines

1.6.1 HeLa cell line

The HeLa cell line is a well-known aggressive cancerous cell line that has been widely used in studying the cell cycle. Cancer cells are known to have capability to overcome signals that can arrest cells in G0/G1 phase and consequently continue to proliferate. Investigating Ca^{2+} signalling during quiescent G0/G1 phase in an aggressive cell line like HeLa would be interesting and the findings possibly contribute to designing new drug therapies to drive cancer cells into quiescence and hence stop proliferating.

1.6.2 NIH 3T3 cell line

NIH 3T3 mouse embryonic fibroblast cells come from a cell line isolated and initiated in 1962 at the New York University. NIH 3T3 cells have been shown to be a pre-neoplastic cell line that exhibits subpopulations of cells that express malignant properties which can grow and transform into invasive colonies (Greig *et al.*, 1985; Rubin and Xu, 1989) and have been extensively used in studying cell cycle quiescence (Donohue *et al.*, 1996; Kerkhoff and Rapp, 1997; Litovchick *et al.*, 2011; Spencer *et al.*, 2013; Yao, 2014). It has been shown that some cancer cells remain dormant for prolonged periods where they persist in a stage of cell cycle arrest in G0/G1 phase (Udagava, 2008; Almog, 2013). Dormant cancer cells present a huge challenge for oncologists as they are the major source of metastasis, which is the main cause of cancer-related deaths. Understanding the Ca^{2+} signalling during quiescent G0/G1 phase in pre-neoplastic cells might provide new approaches to prevent metastasis and to target this crucial step in cancer progression.

1.6.3 hTERT RPE-1 cell line

Normal human somatic cells go through a limited number of divisions in culture after which they enter a non-replicative state called cellular senescence (Hayflick and Moorhead, 1961). Cell senescence is a growth-arrest program which can be triggered by alterations of telomeres. It is believed to provide a protection against the infinite proliferation and occurrence of cancer (Campisi, 2000). Human RPE-1 cells express telomerase reverse transcriptase which extends

their replicative lifespan beyond senescence without inducing aneuploidy or neoplastic transformation (Jiang *et al.*, 1999). In addition, previous studies have shown that hTERT RPE-1 cells are not arrested in G0/G1 phase after 3 days of serum starvation (Jiang *et al.*, 1999; Liang *et al.*, 2012). Hence these cells have been used in this study as a control for other cell types.

1.7 Aim

The aim of this study is to investigate the remodelling of SOCE during cell cycle arrest in quiescent G0/G1 phase in a comparison between cancerous HeLa cells, precancerous NIH 3T3 cells and an immortalised but noncancerous hTERT RPE-1 cells, using the following strategy;

- Induce cell cycle arrest in G0/G1 phase by serum starvation in HeLa, NIH 3T3 and hTERT RPE-1 cells and characterise them morphologically and by flow cytometry before and after serum starvation (Chapter 3) to measure the percentage of each entering G0/G1
- Characterise the degree of SOCE and SOCE protein remodelling with cell cycle arrest in G0/G1 phase in the three cell lines (chapter 4 and 5).
- Study the sequences of these changes over the serum starvation time-course (Chapter 6) to investigate whether they occur as a consequence of G0/G1 arrest or are involved in triggering it.
- Stimulate quiescent G0/G1 cells to re-enter the cell cycle by adding the serum back and define the response both morphologically and by flow cytometry (Chapter 7).
- Investigate the remodelling of SOCE and its proteins when cells re-enter the cell cycle (chapter 8 and 9).

Chapter 2 Materials and Methods

2.1 Materials

Three cell lines have been used in this study; cancerous HeLa cells, precancerous NIH 3T3 cells and an immortalised noncancerous; hTERT RPE-1 cells. All chemicals were from Sigma-Aldrich (Dorset, UK) unless stated otherwise.

2.2 Cell culture

HeLa and NIH 3T3 cells were cultured in complete medium comprising Dulbecco's Modified Eagle's Medium (DMEM) with foetal calf serum (10%), glutamine (2 mM), penicillin (100 IU ml-1) and streptomycin (100 IU ml-1). hTERT RPE-1 cells were cultured in complete medium comprising DMEM: F-12 Medium plus 2.5 mM L-glutamine, 15 mM HEPES, 0.5 mM sodium pyruvate, and 1200 mg/L sodium bicarbonate with foetal calf serum (10%), penicillin (100 IU ml-1) and streptomycin (100 IU ml-1). Cells were kept at 37 °C in a humidified atmosphere (95% air, 5% CO_2 for HeLa and NIH 3T3 cells and 10% CO_2 for hTERT RPE-1 cells). Cells were grown in 75cm^2 flasks (Corning, Flintshire, UK) and split once a week when ~ 90% confluent and were discarded beyond passage 28.

In order to split the cells into fresh culture medium, phosphate buffered saline (PBS) and Trypsin 0.02% (v/v) ethylene-diamine-tetra-acetic acid (EDTA) were pre-warmed to 37°C. Cells were washed three times with PBS (10ml) and detached from the flask by incubation with Trypsin EDTA (3ml) for 5 minutes at 37°C. DMEM (7ml) was added to the flask and the cell suspension was pipetted across the surface of the flask three times to fully remove adherent cells. The cell suspension (10ml) was centrifuged at 1000rpm for 5 minutes, the supernatant was discarded and the cell pellet re-suspended in DMEM (5ml). The resultant cell suspension was used for seeding of cells into flasks and onto dishes as required.

2.3 Serum starvation

Cells were split and left to grow to 60% confluence prior to starvation. In order to induce quiescence, the medium was removed and the cells were washed 3 times with PBS. Control cells were cultured again in DMEM containing 10% FCS, the experimental cells were cultured in low serum DMEM (DMEM with 0.1% FCS) for 5 days. 0.1% FCS medium was replaced every day and cells were used at required time points of starvation.

2.4 Cell counts

A Cellometer automated cell counter (Nexcelom Biosciences Ltd. Massachusetts, USA), a PC-based instrument for one-step bright field image capture and analysis, was used with a cellometer counting slide to count cells in suspension. Each chamber has two chambers. Prior to counting, cells were split and 20µl of cell suspension was loaded into one slide. The chamber was then inserted into the Cellometer instrument. Cells were imaged directly from the centre of the counting chamber using the Auto T4 which utilizes bright field imaging and pattern-recognition software. After inserting the chamber, the images were adjusted to best focus and the cell type was chosen from the dropdown menu. The count button was clicked to give the number of cells / ml. The counting was done twice and the average was calculated. The required volume of cells was then seeded onto flasks or dishes.

2.4.1 Trypan blue staining

Trypan blue (TB) stain is a vital stain used to selectively colour dead cells blue whilst live cells with intact cell membranes are not coloured. This test is based upon the concept that viable cells do not take up impermeable dyes (like Trypan Blue), but dead cells are permeable and take up the dye. Trypan blue staining was done while doing the cell count. After splitting the cells, the cell sample was diluted in TB dye by preparing a 1:1 dilution of the cell suspension using a 0.4% TB solution (10µl of cell suspension to 10 µl of TB). Trypan Blue is sterile filtered before using it in order to get rid of particles in the solution that would disturb the counting process. The number of whole and viable cells was determined as described above (Method 2.4).

2.5 Flow cytometry

Flow cytometry is an analytical technique which simultaneously measures and then analyses physical and/or chemical characteristics of single particles, typically cells, while they pass through a beam of light in a heterogeneous fluid mixture. It has been extensively used for cell analysis both in research and clinical laboratories.

A flow cytometer is made up of three main systems: fluidics, optics, and electronics. The fluidics system transports particles in a stream to the laser beam for interrogation, while the optics system consists of lasers that illuminate the particles in the stream and optical filters that direct the resulting light signals to the appropriate detectors. Lastly, the electronics system consists of detectors that detect the light signals and a digital convertor that converts light signals into electronic signals that can be processed by the computer. These electronic signals are proportional to the optical signals striking the electronic detectors.

For optimal illumination, only one cell or particle should move through the centre of the laser beam at a given moment. To accomplish this, the sample is injected into a stream of sheath fluid within the flow chamber. The design of the flow chamber causes the sample core to be focused in the centre of the sheath fluid where the laser beam will then interact with the particles.

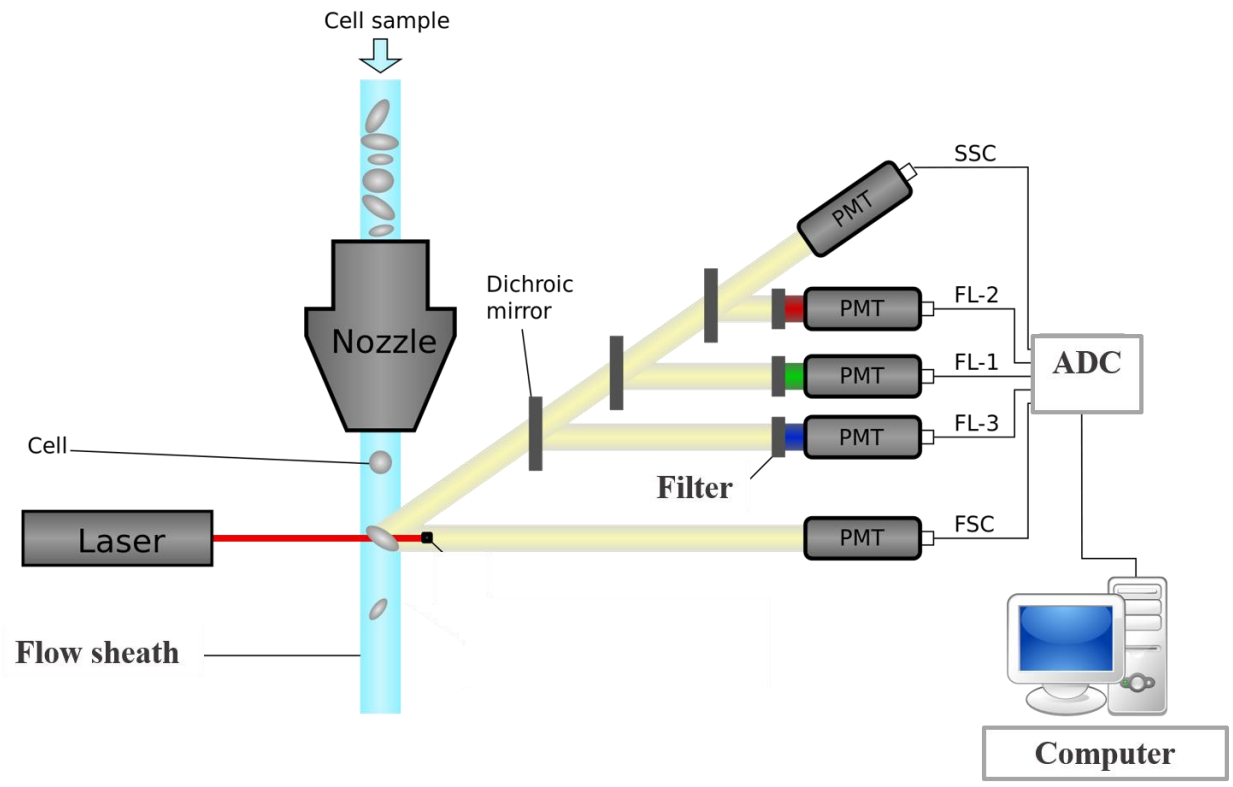

Figure 2.1 Flow cytometer

A schematic diagram of a flow cytometer. Flow cytometer is made up of three main systems: fluidics; flow sheath, optics; laser and filters and electronics; detectors (photomultiplier tubes (PMT)) and analogue- digital convertor (ADC). The flow sheath transports particles in a stream to the laser beam for interrogation. The design of the flow sheath causes one cell to pass through the centre of the laser beam at a given moment to get optimal illumination. The optics system consists of lasers that illuminate the particles in the stream and optical filters that direct the resulting light signals to the appropriate detectors (PMT). Detectors (PMT) detect the light signals and transfer it to ADC that converts light signals into electronic signals that can be processed by the computer. Different PMT types: SCC (side scatter), FSC (forward scatter), Fl -1, Fl- 2 and Fl-3 (Fluorescence channels 1, 2 and 3 respectively). (Adapted from O'Neill *et al*., 2013)

2.5.1 G0/G1 Separation

In this study flow cytometry was used to analyse cell cycle stage by taking cell viability, DNA and RNA contents into account by what is called Multiparametric analysis which was performed by using viability dye, Zombie NIR (BioLegened, UK Ltd), DNA dye; Hoechst (Thermo Fisher Scientific, USA) and RNA dye; Pyronin Y (Sigma-Aldrich Company Ltd. Dorset, England).

For the last two dyes the emitted fluorescence is proportional to DNA and RNA contents present in cells respectively (Andreeff *et al.*, 1980; Shapiro, 1981; Kerker *et al.*, 1982).

Staining cells with Hoechst and Pyronin Y is a method for the separation of G0 and G1 cell cycle phases. Hoechst is an exclusive DNA dye while Pyronin Y reacts with both DNA and RNA. When cells are stained first with Hoechst33342 and then with Pyronin Y, Pyronin Y reaction with DNA is blocked and Pyronin Y stains RNA only. Therefore, it is possible to distinguish DNA from RNA. Cells in S/G2/M phases were identified as the population with double DNA content and high RNA content (Darzynkiewicz *et al.*, 2011). Cells in G1 phase are identified as the population with single DNA content and high RNA content. Finally, cells in G0 phase were identified as the population with single DNA content and an RNA content lower than that in cells in S and G2/M phases as it is known that RNA content of cells is higher during proliferation than during quiescence (Crissman *et al.*, 1985; Lemons *et al.*, 2010; Darzynkiewicz *et al.*, 2011).

The cell viability was detected according to strength of the signals from the cells where dead cells exhibit significant fluorescence signal while live cells do not.

To prepare cells for flow cytometry, cells grown in 75cm^2 flasks were split as in method 2.2 to the resuspension step where 1×10^6 cells were resuspended in 1ml cell culture medium containing 10µg/ml Hoechst33342, and then incubated at 37ºC for 45 minutes. Cells then were washed three times in PBS and resuspended in 1ml PBS, and then 5µl of 100µg/ml Pyronin Y was added and cells were incubated at 37ºC for 15 minutes. 1µl of Zombie NIR was then added to the cells and incubated for a further 15 minutes at RT. Samples were then transferred into 12x75mm Polystyrene Test Tube, FACS, non-sterile and analysed by flow cytometry.

2.5.2 Flow cytometry data analysis

FACS Canto II cell analyser and FACs DIVA software were used to do cell cycle analysis. On the initial run all of the available channels and lasers on a Canto II flow cytometer (BD Biosciences, Oxford) were utilised to determine which lasers and detectors to use, FACs DIVA software was used to produce dot plots, histograms and to analyse data. Each dot appearing on the dot plots represent an 'event' recorded on the flow cytometer. Gating was designed based on the signals recorded from the samples so cells inside the gate move to the next checkpoint, while cells outside the gate are excluded. The gating tree was set as follows. A: Live gate (Zombie NIR/FSC; dead cells within the sample analysed exhibit significant fluorescence signal which is excluded from the gate). B: Hoechst Height/Area intensity this excludes events that could represent more than 1 cell; as shown in Figure 2.2, cell clumps, when they pass through the laser intercept, will take longer than single cells. This in turn, affects the area of the signal. Using a pulse geometry gate (such as Hoechst Height/ Hoechst Area), doublets can be easily eliminated. C: Cell number/ Hoechst intensity to detect normal cell cycle shape histogram based on DNA content. D: Pyronin Y intensity / Hoechst intensity to classify cells in different cell cycle phases; G0, G1, S/G2/M as described above.

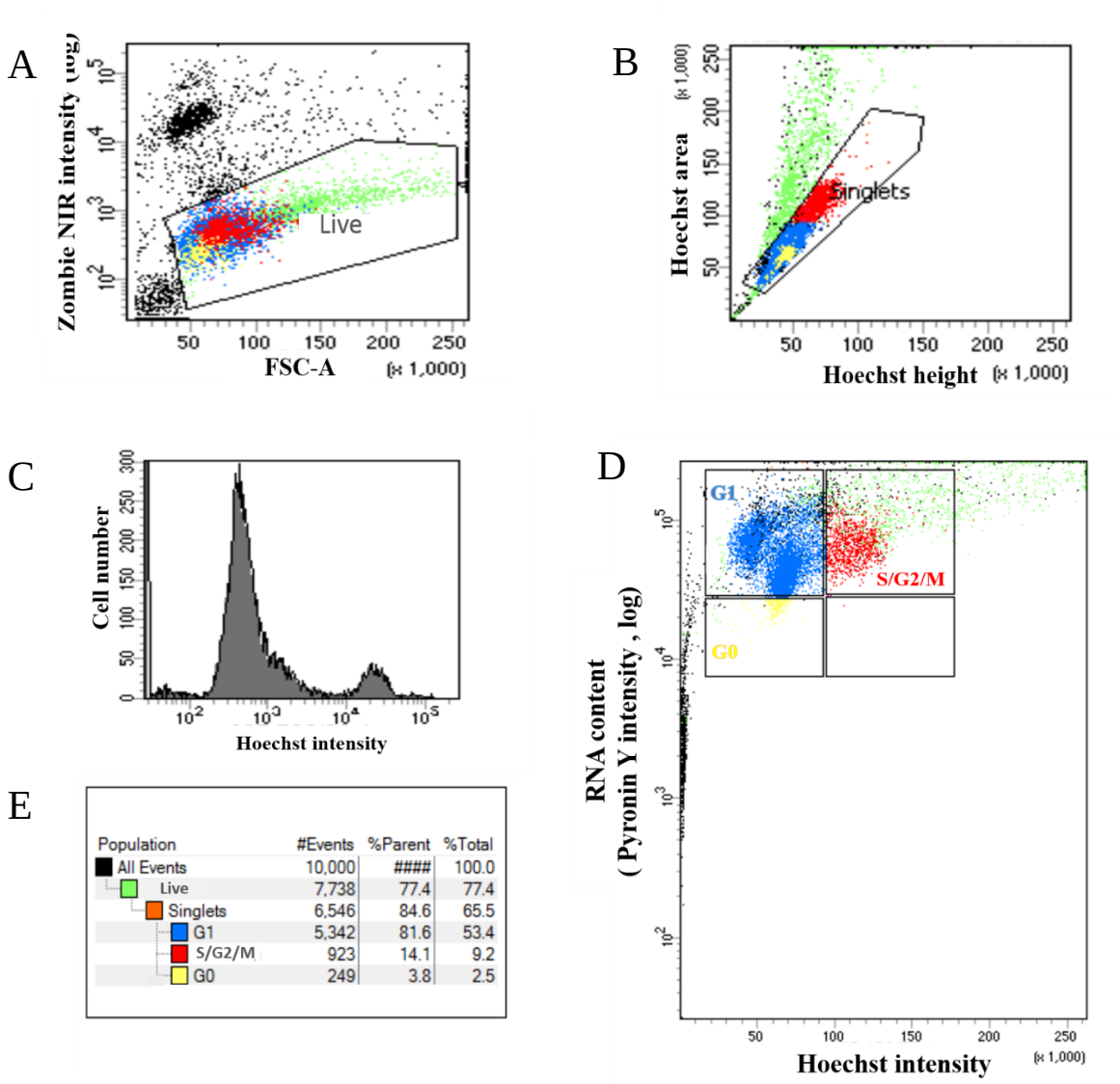

Figure 2.2 Example of FACS Diva data analysis sheet

HeLa cells were grown in 10% FCS medium (proliferating). Cells were stained with viability stain; Zombie NIR, DNA stain; Hoechst and RNA stain; Pyronin Y. FACS Diva software was used to produce dot plot, histogram and to analyse data. Each dot appearing on the dot plots represent an 'event' recorded on the flow cytometer. Gating was designed based on the signals recorded from the sample so cells inside the gate moved to the next checkpoint, while cells outside the gate were excluded. **A**) Live gate (Zombie NIR/FSC; dead cells (black dots) within the sample analysed exhibit significant fluorescence signal which is excluded from the gate). **B**) Singlets gate (Hoechst Area/ Height intensity gate; a pulse geometry gate) this excludes

events (doublets; green dots) that could represent more than 1 cell. **C**) Cell cycle analysis gate (cell number/ Hoechst intensity) to detect normal cell cycle shape histogram based on DNA content and to calculate G0/G1 and S/G2/M cells. **D**) G0/G1 separation gate (Pyronin Y intensity / Hoechst intensity) Cells were classed G1 if they exhibited single DNA content and were RNA positive (blue dots), cells were classed S/G2/M if they exhibited double DNA content and were RNA positive (red dots) and cells were classed G0 if they exhibited single DNA content and were RNA negative (yellow dots). **E)** Table of data shows number of events in each gate, events of each gate as a percentage of parent gates and as a percentage of total events.

2.6 Western blotting

Western blotting is an analytical technique used to detect specific proteins whereby proteins are separated based on their molecular weight by sodium dodecyl sulfate-polyacrylamide gel electrophoresis **(**SDS-PAGE) 2.6.4, transferred onto a membrane 2.6.5, detected with the use of antibodies and x-ray film 2.6.7 and 2.6.8 and analysed using densitometry 2.6.9.

2.6.1 Protein extraction

Cells in 75cm flasks were washed in PBS (4°C) three times and then lysed by the addition of 1ml lysis buffer (4°C) for ~20 minutes on ice; 1mM EDTA (pH 8), 1mM EGTA (pH 8), 1.28mM sucrose, 2mM Tris (pH 7.6), 10% (v/v) Triton X-100, dH_20 and 1 protease inhibitor tablet (Roche Products Ltd, Hertfordshire, UK) per 10mls. Cells were scraped off flasks and then broken up by being passed through a 20-gauge needle ~10 times. They were then were spun at 12,000g for 10 minutes at 4°C to remove cellular debris. The supernatant was aliquoted and stored at -20°C.

2.6.2 Protein concentration

Protein concentration was determined using bicinchoninic acid (BCA) protein assay (Pierce, BCA Protein Assay Kit, Cat. number: 23225). The BCA assay is used for detection and quantitation of total protein. A stock BSA solution (1mg/ml in lysis buffer) was used to provide a range of protein standards (0µg, 0.05µg, 1µg, 2µg, 5µg, 10µg, 20µg and 40µg). BSA standards and protein samples (3µl) were made up to 50µl with dH_20. 5ml of BCA Reagent A, containing sodium carbonate, sodium bicarbonate, bicinchoninic acid and sodium tartrate in 0.1M sodium hydroxide and 100 µl of BCA Reagent B, containing 4% cupric sulphate were mixed together and then 200 µl of this mixture was added to the standards and samples in a 96 well plate. The plate was mixed thoroughly on a plate shaker for 30 seconds and covered and left to stand for 30 minutes at 37°C. This method combines the well-known reduction of Cu^{2+} to Cu^{1+} by protein in an alkaline medium (the biuret reaction) with the highly sensitive and selective colorimetric detection of the cuprous cation (Cu^{1+}) using a unique reagent containing bicinchoninic acid (Smith *et al.*, 1985). The purple-coloured

reaction product of this assay is formed by the chelation of two molecules of BCA with one cuprous ion. This water-soluble complex exhibits a strong absorbance at 562nm that is nearly linear with increasing protein concentrations over a broad working range (20-2000µg/mL). The absorbance measurements from BSA standards at 562 nm were plotted to form a standard curve to which a line of best fit was added (Figure 2.3). The absorbance measured from the 0µg BSA standard was subtracted from each reading. The value of the slope (Y), calculated from the line of best fit, was used to calculate the concentration of protein samples which were measured in triplicate. The average absorbance from the protein samples (divided by 3 as 3µl of protein samples) was divided by the slope (Y) of the standard curve. This provided an estimate of protein concentration in µg/µl which was used to calculate the volume required to load 5µg samples onto gels.

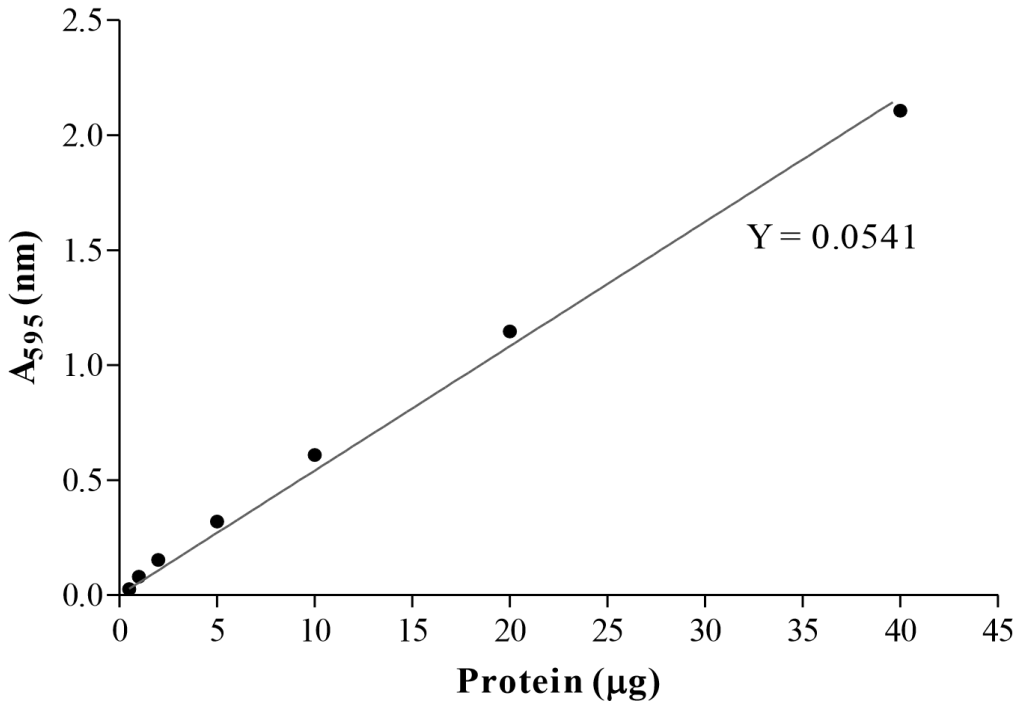

Figure 2.3 BSA standard curve

An example of a standard curve generated from BSA standards of 0.05µg, 1µg, 2µg, 5µg, 10µg, 20µg and 40µg. The absorption of each standard was measured at 562nm. A best fit linear regression line forced through the origin was added using GraphPad Prism software. The value for the slope of the line (Y) was used to calculate the concentration of protein samples.

If protein concentrations were too low for SDS-PAGE, Vivaspin (GE Health Care Life Science) sample concentrators were used to concentrate the protein solution. It is a fast, nondenaturing concentration of protein samples by membrane ultrafiltration. The entire process is performed in a single tube for each sample with an upper compartment containing sample and a lower compartment separated by a semipermeable membrane with a molecular weight cut-off (MWCO) 10,000. The samples were spun at 6500 rpm for 12 minutes. The concentrated sample in the upper chamber was collected and protein concentration was detected again by BCA protein assay. 1 x sample buffer 2.6.3 was added to the protein samples containing 5µg protein/15µl. Samples could then be loaded directly onto gels or stored at -20°C until required.

2.6.3 Sample buffer

Sample buffer (1x) was consists of 2% w/v sodium dodecyl sulfate (SDS), 5% v/v β–Mercaptoethanol, 10% w/v glycerol and 0.1% w/v bromophenol blue in 60mM Tris (pH 6.8). SDS is an anionic detergent that disrupts noncovalent bonds causing denaturation of proteins. SDS coats proteins with a negative charge relative to molecular weight. Mercaptoethanol reduces disulfide bonds. Heating of protein with sample buffer for 5 minutes at 95°C helps denature the proteins and aids binding of SDS. Glycerol increases the viscosity of the protein sample causes samples to sink into wells before the current is turned on. Bromophenol blue is a dye used to monitor progression of protein separation in SDS-PAGE as it is a small molecule which migrates through the gel quickly.

2.6.4 Sodium dodecyl sulfate polyacrylamide gel electrophoresis SDS-PAGE

Proteins were separated using an electric field where the negatively charged proteins move toward the positive electrode located at the bottom of the gel. A discontinuous polyacrylamide gel was used as a support medium and sodium dodecyl sulphate (SDS) to denature the proteins. Proteins are separated based on their molecular weight where small proteins move through the porous polyacrylamide gel quickly and large proteins move through the gel more slowly.

5µg protein samples were made up to 15µl with dH20 so that the same volume of sample was loaded into each well. 1x sample buffer was added to each protein sample. Samples were heated for 5 minutes at 95°C and centrifuged for 10 seconds at 12,000g to remove condensation on the underside of the lid.

NuPAGE gels (10% Bis-Tris) were clamped into a gel tank (Invitrogen, Life Technologies Ltd, Paisley, UK). The inner chamber was filled with NuPAGE 1x MOPS SDS buffer (200ml) with antioxidant (500µl). The addition of antioxidant to the inner chamber maintains proteins in a reduced state during electrophoresis. The outer chamber was filled with NuPAGE 1x MOPS SDS buffer (600ml). The comb was removed and the molecular weight marker (10µl) (Precision Plus Dual Colour Protein Standards were from Bio-Rad Laboratories Ltd, Hertfordshire, UK) were loaded into the first well and then protein samples were loaded into following wells using 20 µl pipette and fine tips. Electrophoresis was carried out at a constant voltage of 200V for ~1 hour or until Bromophenol Blue dye reached the bottom of the gel.

2.6.5 Transfer

Separated proteins were transferred to a nitrocellulose membrane (Bio-Rad, UK) at constant voltage of 60 V for ~2 hour using a wet transfer system at 4°C in a cold room to prevent overheating during transfer. The transfer cassette (BioRad), foam sponges, blotting paper and nitrocellulose membranes were pre-equilibrated in transfer buffer (25mM Tris, 192mM glycine, 20% v/v methanol) and set up to transfer the proteins from the membrane in an orientation so that the nitrocellulose membrane was closest to the positive electrode and the gel was closest to the negative electrode (Figure 2.4). Therefore, when the electric field was applied, the negatively charged proteins moved towards the positive electrode and were bound to the nitrocellulose membrane.

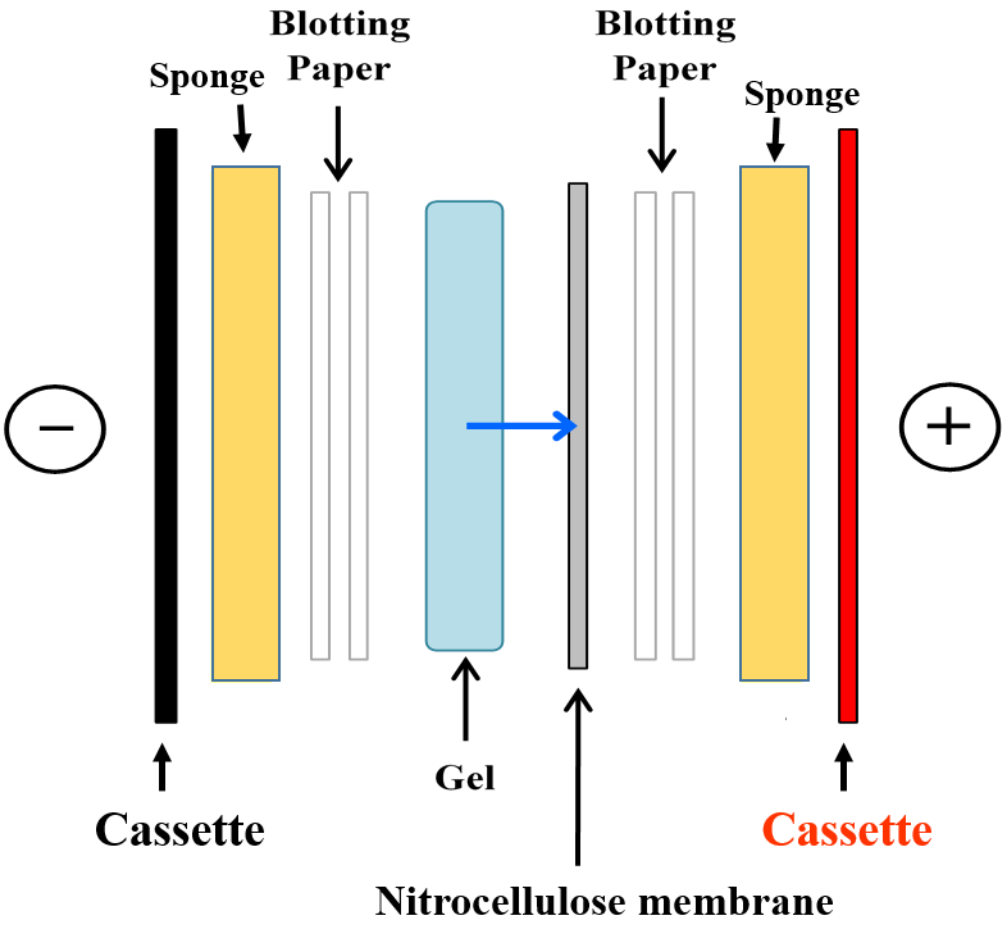

Figure 2.4 Transfer Cassette

Proteins were transferred from gels onto nitrocellulose membranes (represented by blue arrow) using a wet transfer system. The transfer cassette was set up in a 'sandwich' formation; sponge, blotting paper, gel, nitrocellulose membrane, blotting paper, sponge. Transfer cassettes were placed in the transfer tank in an orientation so that the gel was closest to the negative electrode (-) and the nitrocellulose membrane was closest to the positive electrode (+). Application of an electric field causes the negatively charged proteins to move toward the positive electrode and bind to the nitrocellulose membrane. Transfers were performed at a constant voltage of 60V for 2 hours.

2.6.6 Blocking

Following the transfer of proteins onto nitrocellulose membranes the cassette was disassembled and the gel was discarded. The membrane was washed in PBS and blocked in a mix of Blotting-Grade Blocker non-fat dry milk powder (Bio-Rad Laboratories Ltd, Hertfordshire, UK) (5% w/v) with Triton X-100 (0.1 % v/v) in PBS for 1 hour at RT with gentle agitation to block unoccupied sites on membranes and prevent non-specific binding of antibodies.

2.6.7 Immunodetection of protein expression

Nitrocellulose membranes were placed in 50ml falcon tubes (with the side that was in contact with the gel facing inwards) with 3mls of incubation buffer (PBS, 0.1 % v/v Triton X-100, 5% w/v non-fat dried milk) containing primary antibody (Table 2.1). Membranes were incubated overnight at 4°C on rollers. Following incubation with primary antibody membranes were washed (3 x 10 minutes) in wash buffer (PBS, 0.1 % v/v Triton X-100) to remove any unbound primary antibody.

Membranes were then incubated with horseradish peroxidise (HRP) conjugated secondary antibody in 10mls of incubation buffer (Table 2.1) for 1 hours at RT on rollers. Following secondary antibody incubation membranes were washed (3 x 10 minutes) in wash buffer to remove any unbound secondary antibody.

Antibody	Dilution used	Supplier
Anti-β-Actin	1/5000	Sigma-Aldrich, USA
Anti-Orai1	1/200	BD Biosciences, San Jose, NJ, USA
Anti-STIM1	1/200	Abcam, Cambridge, UK
*Anti-Mouse-HRP	1/20000	Abcam, Cambridge, UK
*Anti-Rabbit -HRP	1/40000	Abcam, Cambridge, UK

Table 2.1 Antibodies used for western blotting

Primary antibodies used for western blotting. All primary antibodies were incubated with blots overnight at 4°C. * denotes secondary antibodies used for western blotting. The appropriate corresponding secondary antibody was used following primary antibody incubation. Secondary antibodies were incubated with blots for 1hour at room temperature. All antibody dilutions were made up in incubation buffer.

2.6.8 Chemiluminescent Western blotting detection

Enhanced chemiluminescent (ECL) detection was used to develop immunoreactive bands on membrane by processing in a mix of 2ml of Solution A; luminol solution and 2ml of Solution B; peroxide solution (ECL select kit, GE Healthcare, Life Sciences, Amersham, Bucks, UK) for 3 minutes at RT. ECL is based on antibodies conjugated to horseradish peroxidase (HRP). HRP catalyses the oxidation of luminol in the presence of peroxide, generating emission of low intensity light at 428 nm. The signal intensity is dependent of the number of HRP molecules and is proportional to the amount of antibody bound to the target molecule. Membranes then were wrapped in saran wrap, placed in a film cassette and exposed to x-ray film (HyperfilmTM, GE Healthcare, Life Sciences, Amersham, Bucks, UK) for various times (2 seconds - 5 minutes) depending on the primary antibody used. Regions of film exposed to light (i.e. from HRP) darken. Exposed film was placed in an x-ray film processing machine.

2.6.9 Densitometry analysis

X-ray films were scanned onto a computer so the bands could be analysed by densitometry using ImageJ software (Rasband, 1997-2014). The integrated pixel density (sum of pixel values in selected area) of each band was measured. The selection area remained constant for each set of bands analysed. A background value was also subtracted from each band (Figure 5.2.A). For Orai1 protein, the protein showed a multiple band. The multiple band was measured as a whole and individually (Figure 5.2.B). Values were then expressed as a ratio of β-actin as a loading control in order to determine the expression levels of proteins.

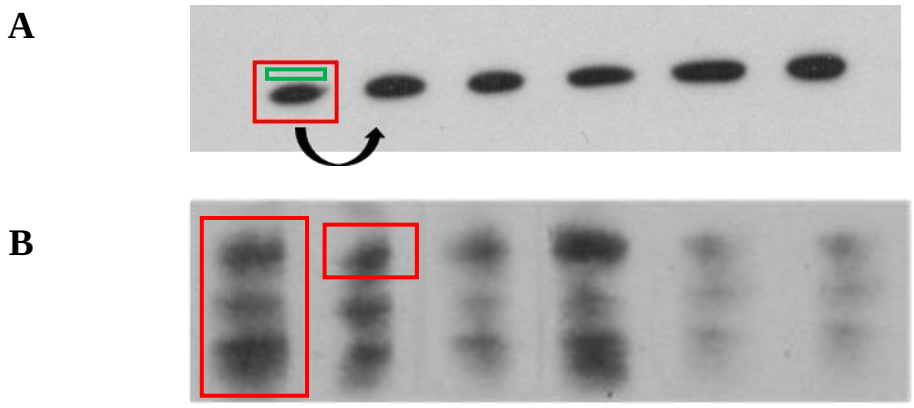

Figure 2.5 Densitometry analysis of western blots

Blots were analysed using ImageJ software. **A)** The same area was measured for each band using the same box (red). A background value (green box) was subtracted from each band. **B)** Orai1 protein multiple band was measured as a whole (large red box) and individually (small red box).

2.7 Immunofluorescence

Cells on 22mm glass coverslips were washed with PBS (2 x 5 minutes) and then fixed by incubation with paraformaldehyde (PFA) (4% w/v) in 1x PBS for 10 minutes at RT. Fixed cells were washed with PBS (2 x 5 minutes) then permeabilised using Triton X-100 (0.1% v/v) for 10 minutes at RT and then washed with PBS (2 x 5 minutes) and blocked with blocking solution; bovine serum albumin (BSA, 5% w/v) in PBS for 30 minutes at 4°C. Primary antibodies were diluted in 5% BSA (Table 2.2) and then incubated with cells for 1 hour at 37°C in humidified incubator in the dark. Following incubation with unconjugated antibodies, coverslips were washed with PBS (2 x 5 minutes) and incubated with secondary antibodies diluted in 5%BSA for 30 minutes at 37°C in humidified incubator in the dark (Table 2.2). Cells were again washed in PBS (2 x 5 minutes) before incubation with the nucleic acid dye, ethidium homodimer-1 (EthD-1), at a 1/500 dilution, for 10 minutes at RT. Cells were washed in PBS (2 x 5 minutes) and then in dH_20 (1 x 5 minutes) before being mounted on microscope slides with FluorSave Reagent and left to dry overnight at RT in the dark and then stored at 4°C until use.

Images were taken using a laser scanning confocal microscope (LSM 510, Carl Zeiss Ltd). The excitation and emission wavelengths of the fluorophores used in experiments are shown in (Figure 2.6). The emission wavelengths of Alexa Fluor 647 and EthD-1 overlap and were therefore collected separately using multi-track configuration to prevent cross-talk. When a multi-track configuration was used one track is active and the other track is switched off thereby preventing cross-talk.

Track one was set up to detect the Orai1 signal (Figure 2.7) and track two was set up to detect the STIM 1 and EthD-1 signals (Figure 2.8). Images were acquired with 12-bit data depth, a frame size of 512 x 512 and a scan speed of 9.

Antibody	Dilution used	Supplier
Anti-Orai1 - Rabbit	1/ 100	BD Biosciences, San Jose, NJ, USA
Anti-STIM1 - Mouse	1/50	Abcam, Cambridge, UK
*Anti-Mouse Alexa 647	1/2000	Abcam, Cambridge, UK
*Anti-Rabbit Alexa 488	1/2000	Abcam, Cambridge, UK

Table 2.2 Antibodies used for immunofluorescence

All primary antibodies were incubated with cells for 1 hour at 37°C. * denotes secondary antibodies used for immunofluorescence. The appropriate corresponding secondary antibody was used following primary antibody incubation. Secondary antibodies were incubated with blots for 30 minutes at 37°C. All antibody dilutions were made up in BSA.

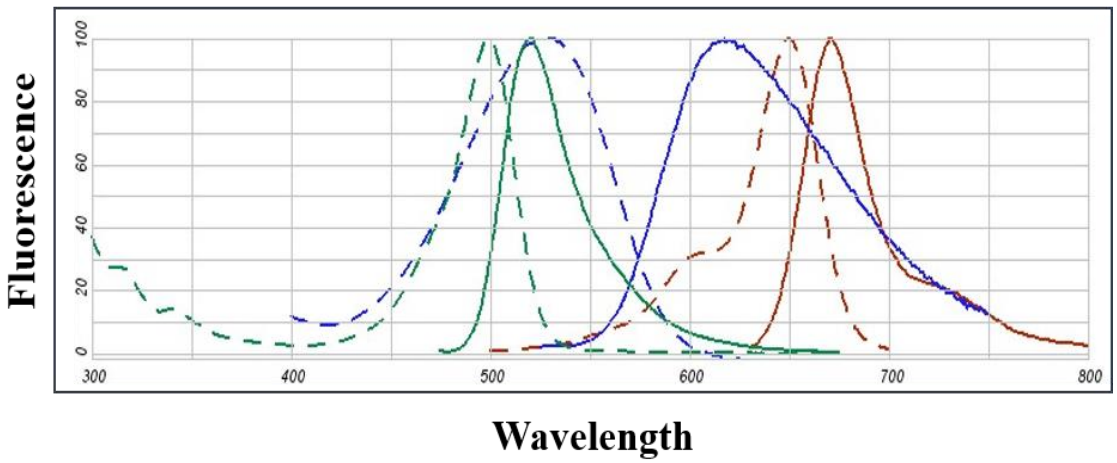

Figure 2.6 Excitation and emission spectra of fluorophores

Excitation (dashed line) and emission (solid line) spectra of ■ Alexa Fluor 647, ■ Alexa Fluor 488 and ■ EthD-1 (from Invitrogen; Fluorescence Spectra Viewer). The emission of Alexa Fluor 647 and EthD-1 overlap and were therefore collected separately.

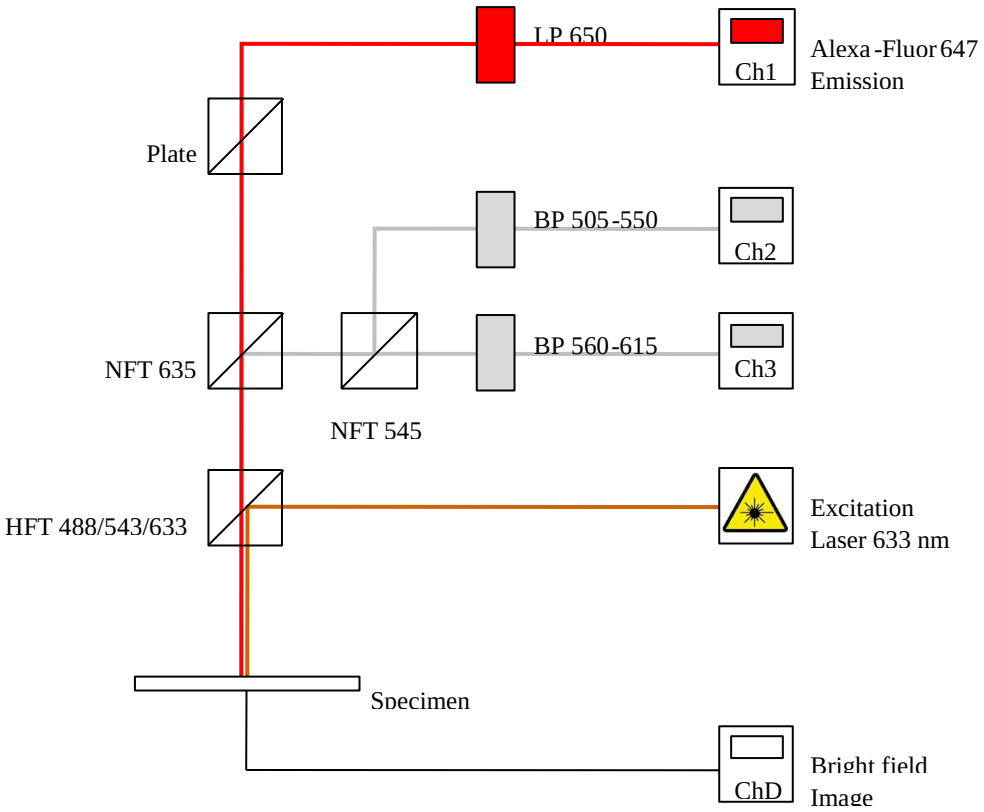

Figure 2.7 Track one set up – Orai 1 detection

This track was set up to collect the emission wavelengths of alexa-fluor 647 (peak emission ~670nm). It also takes a bright field image of the cells in channel D (ChD). The HeNe laser sends an excitation wavelength of 633nm to the main dichroic mirror (HFT 488/543/633) which is reflected 90° to the cells. Light emitted from the cells then passes through the main dichroic mirror to a secondary dichroic mirror (NFT 635) which only allows light above 635nm to pass through. The light is then directed to a long pass (LP) filter of 650nm. Only wavelengths above 650nm can pass through to be detected by the photomultiplier tube in channel 1 (Ch1) (Adapted from Bell, 2011).

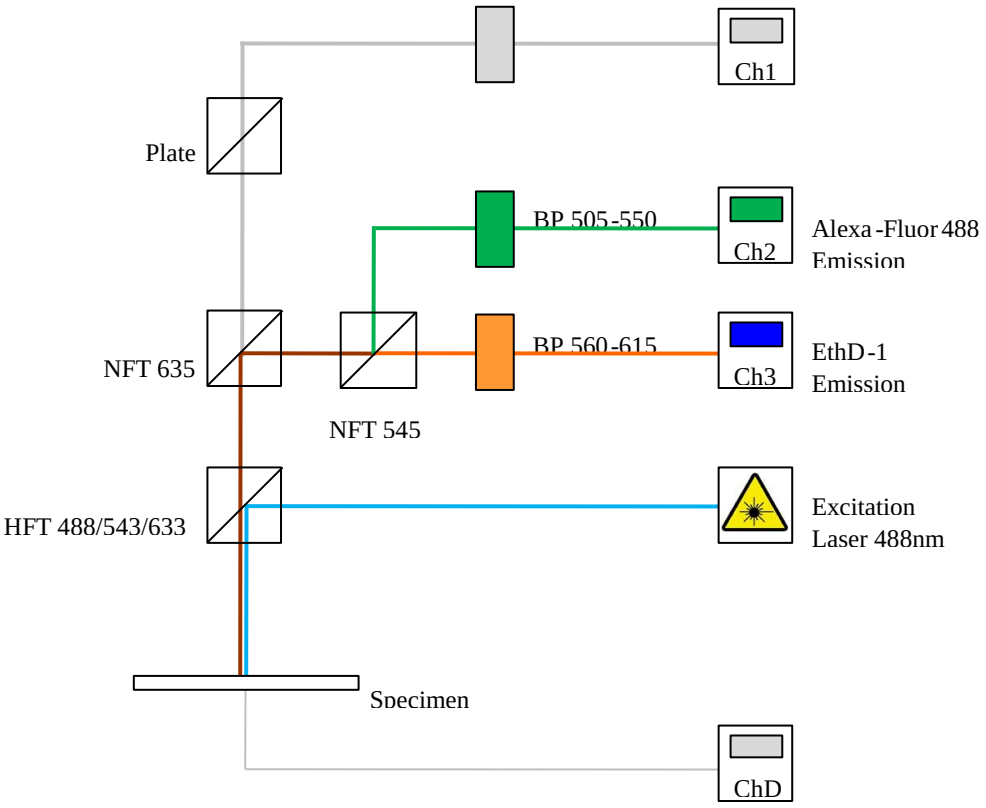

Figure 2.8 Track two set up – STIM 1 and EthD-1 detection

This track was set up to collect the emission wavelengths of Alexa Fluor 488 (peak emission ~519) and EthD-1 (peak emission ~615nm). The argon (Ar) laser sends an excitation wavelength of 488nm to the main dichroic mirror (HFT 488/543/633) which is reflected 90° to the cells. Light emitted from the cells then passes through the main dichroic mirror to a secondary dichroic mirror (NFT 635) which reflects light below 635nm 90° to another secondary dichroic mirror (NFT 545). Light below 545nm (Alexa Fluor 488) is reflected 90° to a band pass (BP) filter of 505-550nm which only allows light of 505-550nm to pass through to be detected by the photomultiplier tube in channel 2 (Ch2). Light above 545nm (EthD-1) passes through the mirror and is directed to a band pass (BP) filter of 560-615nm which only allows light of 560-615nm to pass through to be detected by the photomultiplier tube in channel 3 (Ch3)(Adapted from Bell, 2011).

2.8 Single cell Ca^{2+}-add-back experiments

Ca^{2+} add-back experiments were performed in order to measure both store depletion and resultant Ca^{2+} entry (i.e. SOCE). Fura-2/AM (Calbiochem, Germany), a fluorescent Ca^{2+} indicator was used in the measurement of intracellular Ca^{2+} concentration $[Ca^{2+}]_i$ (Grynkiewicz *et al.*, 1985) in single live cells. The cells were seeded onto 22mm glass cover-slips and used when ~50% confluent. Ca^{2+} measurements were made on individual coverslips at RT.

Cells were washed in Krebs buffer (4.2 mM $NaHCO_3$, 1.2 mM $MgSO_4$, 1.2 mM KH_2PO_4, 4.7 mM KCl, 118 mM NaCl, 10 mM glucose, 2 mM $CaCl_2$, 800 μM sulfinpyrazone, 10mM HEPES, pH 7.4) and loaded with the Ca^{2+}- sensitive fluorescent dye, fura-2/AM (3 μM, for 45 minutes in the dark at RT).

Fura-2/AM is insensitive to Ca^{2+} due to acetoxymethyl (AM) esters disguising carboxylate groups. As it is membrane permeable, fura-2/AM diffuses across the PM upon loading and once inside the cell cytosol is activated by cleavage of AM esters to fura-2. Fura-2 is sensitive to Ca^{2+} (due to exposure of carboxylate groups) and cannot diffuse across the PM as it becomes polar (Tsien, 1981). However, fura-2 can be pumped out of cells or taken up into organelles by organic anion transporters (Divirgilio *et al.*, 1988b). Consequently, poor loading and/or inaccurate fluorescent readings may occur. Sulfinpyrazone (an organic anion transport inhibitor) is therefore added to Krebs buffer to prevent this from occurring (Divirgilio *et al.*, 1988a; Divirgilio *et al.*, 1990).

After loading, cells were washed in Krebs buffer and incubated for another 30 minutes to allow complete fura-2/AM de-esterification. Individual coverslips were washed in Ca^{2+}-free Krebs buffer (prepared as Krebs buffer but 2 mM $CaCl_2$ replaced with an equal volume of distilled water) and fixed into a coverslip holder (custom made), producing a chamber in which Ca^{2+}-free Krebs buffer was added.

Relative changes in $[Ca^{2+}]_i$ were monitored continuously using ratiometric imaging (Bird *et al.*, 2008) via detection of fura-2 fluorescence at an excitation wavelength of 340nm and 380nm and an emission wavelength of 510nm using an Olympus IX70 fluorescent

microscope. Images were acquired with a charge-coupled device (CCD) camera (MicroMax, Sony Interline Chip, Princeton Instruments, Trenton, NJ) and using a 20x objective lens. Collected data was analysed using Metafluor Software (Universal Imaging, Marlow, UK).

Ratiometric measurements take advantage of the dual excitability of fura-2, which shifts its absorbance maximum to lower wavelengths in its Ca^{2+} bound form. Alternating excitation at 340 nm and 380 nm ensures a maximal difference between the fluorescence emission of fura-2 in its unbound and Ca^{2+} bound state. This normalises for changes in fluorescence intensity that are unrelated to changes in $[Ca^{2+}]_i$, such as uneven cell thickness, unequal fura-2 distribution, or noise introduced by the detection equipment (e.g. changes in illumination intensity).

Images of bright field, wavelength 1 (340nM), wavelength 2 (380nM) and ratio between 340nm and 380nm were recorded. Regions of interest (ROI) were applied to ~ 20 individual cells per field of view and the ratio between 340nm and 380nm fluorescence intensity as a representation of $[Ca^{2+}]_i$ were shown in a graph (Figure 2.9). Following establishment of a steady baseline, 200 nm Thapsigargin (TG; Calbiochem, Germany) or equivalent volume of DMSO as a vehicle control was added (Figure 2.10). TG is a selective SERCA inhibitor that prevents reuptake of Ca^{2+} into the ER thus causing Ca^{2+} release from intracellular stores and subsequent Ca^{2+} rise in cell cytosol. The resultant increase in $[Ca^{2+}]_i$ is observed as an increase in fura-2 fluorescence (first peak in fluorescence ratio). Following store depletion (TG response) and after the trace returned to baseline, 2 mM $CaCl_2$ was added, which leads to increase in $[Ca^{2+}]_i$ concentration as extracellular Ca^{2+} enters the cell to replenish intracellular Ca^{2+} stores. The increase in $[Ca^{2+}]_i$, observed as an increase in fura-2 fluorescence (second peak in fluorescence ratio). TG is dissolved in DMSO and therefore control Ca^{2+} add-back traces were performed by adding the equivalent volume of vehicle control DMSO in place of TG. The mean areas obtained from calibrated control DMSO traces were subtracted from the mean areas obtained from calibrated TG traces. All histograms presented are basal-subtracted (i.e. DMSO response) and are hence response to stimulus only.

To calculate the percentage decrease in $[Ca^{2+}]_i$ following starvation, the mean Ca^{2+} response was divided by the control Ca^{2+} response and multiplied by 100 to obtain the starved mean as

a percentage of the control mean. This value was then subtracted from 100 to provide the percentage decrease.

A

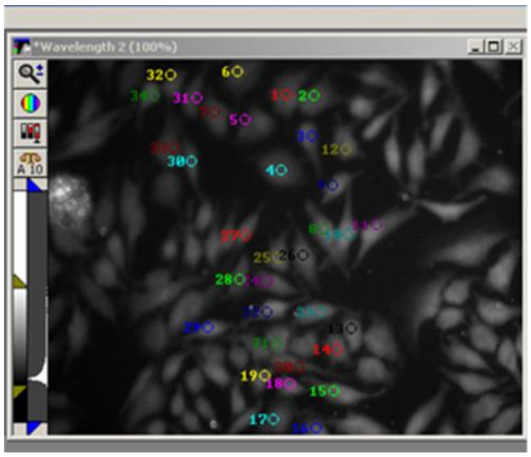

B

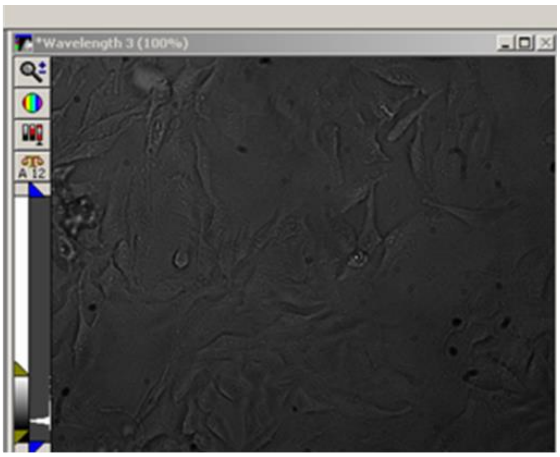

C

Date: Sun Mar 8 2015 11:11:35.206

Time (sec	R1 R1	R2 R1	R3 R1	R4 R1	R5 R1
21.82	0.99	0.98	1.04	1.03	1.03
41.82	0.98	0.98	1.04	1.03	1.02
61.82	0.98	0.99	1.04	1.02	1.03
81.82	0.97	0.99	1.05	1.03	1.03
101.82	0.98	0.99	1.04	1.02	1.03
121.82	0.97	0.98	1.04	1.02	1.03
141.82	0.98	0.98	1.05	1.04	1.03
161.82	1	1	1.06	1.06	1.04
181.82	1.01	1.02	1.1	1.08	1.07
201.82	1.04	1.05	1.13	1.12	1.09
221.82	1.08	1.08	1.18	1.16	1.11
241.82	1.12	1.12	1.21	1.19	1.12
261.82	1.15	1.15	1.22	1.21	1.12
281.82	1.16	1.16	1.24	1.22	1.11
301.82	1.16	1.15	1.24	1.21	1.12
321.82	1.16	1.16	1.23	1.21	1.11

D

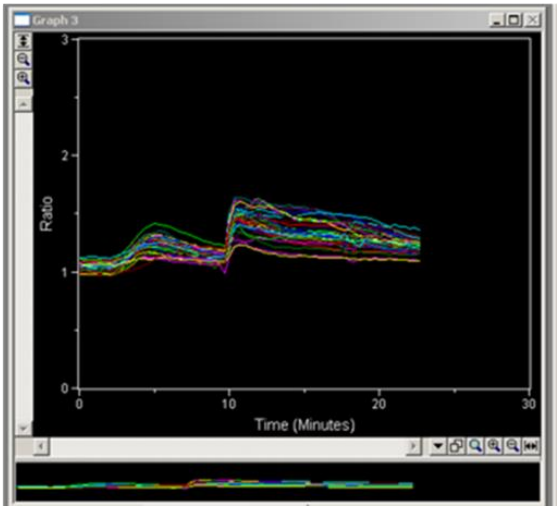

Figure 2.9 Single cell analysis of $[Ca^{2+}]_i$

Single cell $[Ca^{2+}]_i$ changes were determined using ratiometric imaging through detection of fura-2 fluorescence at an excitation wavelength of 340 nm and 380 nm and an emission wavelength of 510 nm using an Olympus IX70 fluorescent microscope. Charge-coupled device (CCD) camera (MicroMax, Sony Interline Chip, Princeton Instruments, Trenton, NJ) with a 20x objective lens were used to take images. (A) Fluorescence images and (B) bright field were used to identify cells in interphase (A) Regions of interest were created over cells in

interphase. (C and D) The experiment was run and fluorescence ratio data values were exported to an Excel sheet (C) and produce a trace for each region of interest (D).

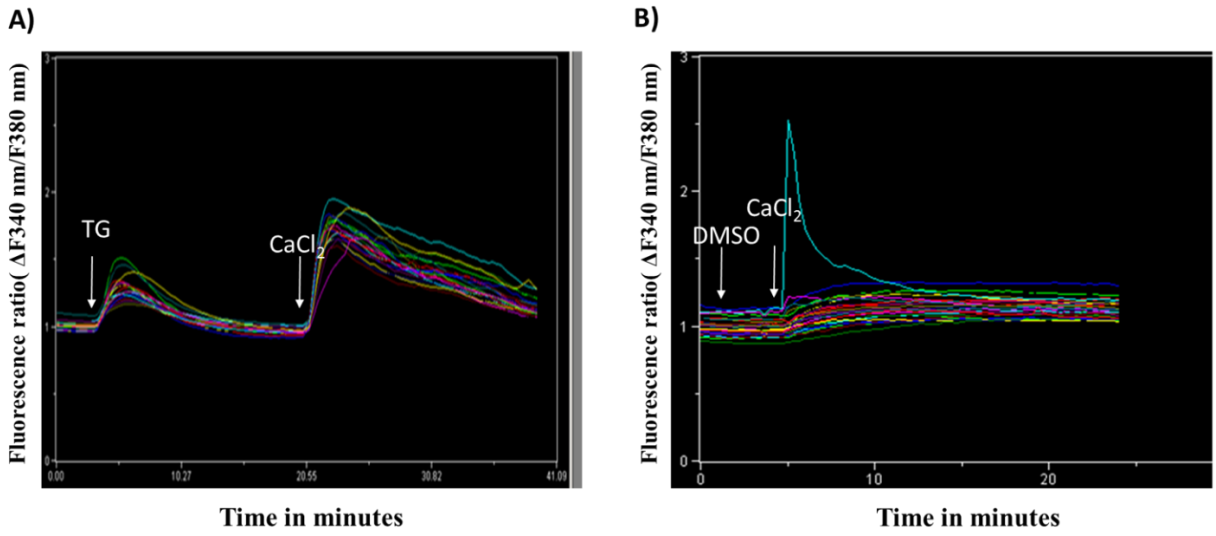

Figure 2.10 Typical Ca^{2+} add- back traces using the single cell Fura ratiometric technique (A) Ca^{2+} release from internal store in response to addition of 200nM TG leading to an increase in $[Ca^{2+}]_i$ and therefore an increase in fura-2 fluorescence and the ratio between the two excitation wavelengths. This activates SOCE pathway following addition Ca^{2+} (2mM $CaCl_2$) causes increase in $[Ca^{2+}]_i$ and fura-2 fluorescence. (B) Addition of DMSO as a control for TG doesn't cause any increase in $[Ca^{2+}]_i$ and therefore subsequent SOCE is reduced, this represents basal Ca^{2+} entry.

Fluorescence ratio data were recorded as mentioned before (Method 2.8, Figure 2.9). The experiments were then re-run to produce a trace for every cell in the field of view. The fluorescence ratio data was recorded on the computer in Microsoft Excel for each region of interest that could be related to cells in interphase (Figure 2.9). The height of peak (HOP), rate of rise (ROR), rate of decline (ROD) and area under the curve (AUC) for TG and Ca^{2+} responses were calculated using Excel functions in a template spread sheet (custom built by Dr Claire Whitworth and Dr Graham Scholefield) so that only three cell values needed to be altered manually for each data set (Figure 2.11).

The height of peak (HP) of each response was calculated by calculating the minimum and maximum ratio values in the TG and Ca^{2+} range.

To calculate the rate of rise (RR), the row number of the dataset at the minimum and maximum values in the TG or Ca^{2+} range is determined and then the minimum row number is subtracted from the maximum row number. This value is multiplied by 20 to give the time value of the TG or Ca^{2+} response range, since the time lapse between measurements is 20 seconds. The peak height is then divided by the time range to provide the RR (Figure 2.11).

The rate of decline (ROD) function determines the row number of the dataset at the maximum value and the minimum value following the peak in the TG or Ca^{2+} range and minuses the maximum row number from the minimum row number (Figure 2.11). This value is multiplied by 20 to give the time value of the TG or Ca^{2+} response range, since the time lapse between measurements is 20 seconds. The peak height is then divided by the time range to provide the total ROD (Figure 2.11).

The AUC is calculated by finding the area bound by the graph and within a specified time region above the specified minimum value. This function multiplies the minimum value by the time range and minuses this from the maximum to account for changes in baseline.

The cells in interphase were defined morphologically with the angular shaped cell bodies (cells in interphase stage) and not the spherical dividing cells (cells in mitotic phase).

Average DMSO control trace values were subtracted from the average responses following TG and $CaCl_2$ addition.

A

	A	B	C	D	E	F	G	H	I	J
1	ONLY EDIT **BOLD** VALUES							**Cell Type:**	**1**	**2**
2	DO NOT EDIT VALUES IN *ITALICS*									
3	Time Calcium added =		1155.36	sec				*Region #:*	*1n*	*2n*
4	Time between each image =		**20**	sec				*TG Range*	*Data!$B$11:$B$57*	*Data!$C$11:$C$57*
5	First time row number (in data tab) =		11					*Ca Range*	*Data!$B$58:$B$100*	*Data!$C$58:$C$100*
6	Last time row number (in data tab) =		100				TG	Min	1	1
7							TG	Max	1.2	1.21
8	Name of data sheet=		*Data*				TG	Height of peak (HP)	0.2	0.21
9	Time Range =		*Data!$A$11:$A$100*			**Analysis Formulas**	TG	Rate of rise (RR)	0.001111111	0.0013125
10							TG	Area under peak (AUP)	78	57.8
11	TG Lower Time =		*215.36*	sec			TG	Rate of decline (ROD)	0.00001234	0.0000278
12	TG Upper Time =		*1135.36*	sec				*Ca 'Peak Rise' Range*	Data!$B$58:$B$73	Data!$C$58:$C$67
13	Ca Lower Time =		*1155.36*	sec			Ca	Min	0.97	0.97
14	Ca Upper Time =		*1995.36*	sec			Ca	Max	1.77	1.7
15							Ca	Height of peak (HP)	0.8	0.73
16							Ca	Rate of rise (RR)	0.002666667	0.004055556
17							Ca	Area under peak (AUP)	439.2	350.8
18							Ca	Rate of decline (ROD)	0.000072398	0.00007832
19										
20										

B

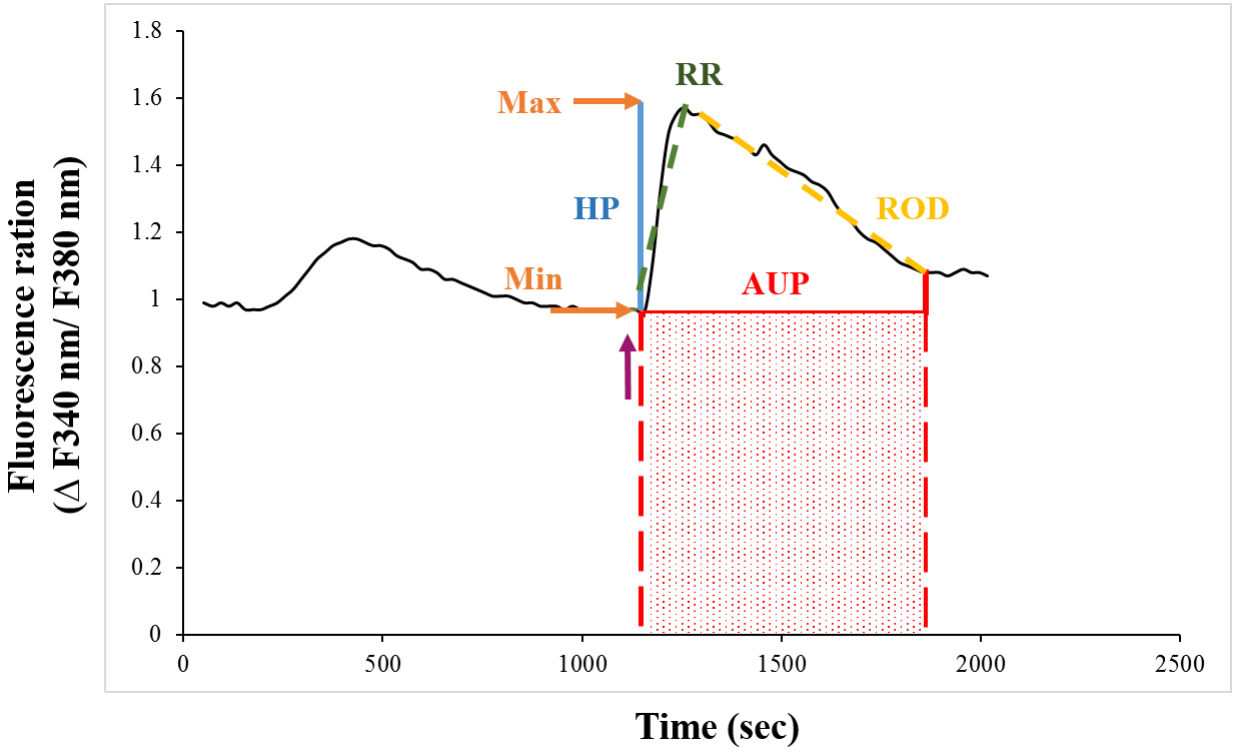

Figure 2.11 Example of template spread sheet

Example of template spread sheet showing calculated values of Ca^{2+} response attributed to each ROI. Colours correspond to those on the (B) example of single cell trace with spread sheet

function calculations for SOCE peak. The time of addition of $CaCl_2$ works as the start point of the SOCE response (green). For each region of interest (ROI) data set, the area under the peak (AUP) (area is bound by solid red line and trace) is calculated by finding the area that is bound by the graph within a specified time region (dashed red lines) and above the specified minimum value (solid red line). Then the result is multiplied by the minimum value (orange) by the time range (dashed red lines) and subtract this (dotted red area) from the maximum (total are under peak). To find height of peak (HP) (blue), the minimum value is subtracted from the maximum value (orange). The rate of rise (RR) function finds the row number of the dataset at the minimum and maximum values (orange) and minuses the minimum row number from the maximum row number. Since the time lapse between measurements is 20 seconds, this value is multiplied by 20 to give the time value of the response range (dotted red lines). The height of peak (blue) is then divided by the time range to provide the RR (green). The rate of decline (ROD) function determines the row number of the dataset at the maximum value and the minimum value (orange) following the peak and minuses the maximum row number from the minimum row number. since the time lapse between measurements is 20 seconds, this value is multiplied by 20 to give the time value of the response range (red green lines), The height of peak is then divided by the time range to provide the total ROD (yellow dashed line). The analysis of the TG – induced Ca^{2+} release was also performed using the same template spread sheet (Adapted from Whitworth, 2015).

2.9 Statistics

Data are generally presented as mean ± SEM of n determinations (Cumming *et al.*, 2007). Statistical comparisons of mean values were performed using Excel and GraphPad Prism software. For unpaired groups a two-tailed Student's t-test was used. For groups of three or more, one-way analysis of variance (ANOVA) was used. Statistical significance was accepted at $P<0.05$. The level of significance was also indicated on graphs ($P<0.05$*, $P<0.01$**, $P<0.001$***, $P<0.0001$****). N= number of repeated experiments. n= number of cells

Part I - Results - G0/G1 Cell Cycle Arrest

Chapter 3 Morphology and Flow cytometry

3.1 Introduction

Serum starvation-induced cell cycle arrest has been extensively used in cell cycle research since (Pardee, 1974) established the restriction point concept (Zetterberg and Larsson, 1985; Pardee, 1992; Kerkhoff and Rapp, 1997) and has continued as a principal and a valuable experimental technique to induce cell cycle arrest in G0/G1 phase (Lemos *et al.*, 2007; Kothapalli *et al.*, 2008; Van Rechem *et al.*, 2010; Xiong *et al.*, 2012).

The aim of this chapter was to induce cell cycle arrest in G0/G1 phase by serum starvation in cancer HeLa cells, pre-cancerous NIH 3T3 cells and immortalised noncancerous hTERT RPE-1 cells and to define the cell cycle arrest both morphologically and by Flow cytometry as a preface to the study of Ca^{2+} signalling when cells exit cell cycle which is presented in subsequent chapters.

In this chapter, HeLa, NIH 3T3 and hTERT RPE-1 cells were grown in 0.1% FCS medium for 5 days in order to induce cell cycle arrest in quiescent G0/G1 phase. Cells grown in 0.1 % FCS will henceforth be referred to by the corresponding day of the serum starvation time course. Cells grown in 10 % FCS (control cells) will henceforth be referred to as proliferating cells.

3.2 Results – Morphological changes

Cells were grown in 10% FCS (proliferating) or in 0.1% FCS for 1-5 days in order to track the time point at which cells arrested in quiescent G0/G1 phase. To investigate the effect of serum starvation on cell proliferation and to define cell cycle arrest, cell viability, total and mitotic cell number and cell diameter were determined before and over the 5-day serum starvation time course.

3.2.1 HeLa cells

Proliferating (control) cells (10% FCS) display a patchy monolayer growth pattern with angular shaped flattened cell bodies representing cells in interphase, and spherical dividing cells representing cells in mitosis. With serum starvation, cells grew in clusters and showed a decrease in total cell number, mitotic cell number and cell diameter with an obvious increase in debris (Figure 3.1).

Mitotic cells were counted and expressed as a percentage of total cell population in both proliferating (10% FCS) and serum starved cells (0.1% FCS). Mitotic cells were significantly decreased at day two by 60% (4.16± 0.09%, $P = 0.0026$), day three by 63% (3.69 ± 0.11%, $P = 0.0032$), day four by 90% (0.96 ± 0.04%, $P < 0.001$) and day five by 90% (0.92 ± 0.06%, $P < 0.001$) compared to proliferating (10.19%±0.92) (Figure 3..A and Table 3.1).

Consistent with the above data, cell counts showed that serum starvation inhibited cell proliferation in HeLa cells. This can be observed by comparing the cell counts for proliferating (3542×10^3 cells) and starved cells (522×10^3 cells) where cells were seeded at the same density prior to the 5 day serum starvation time-course (Figure 3.3.B). This can also be seen when serum starved cell populations (Figure 3.3.A.iii) were far less confluent compared to proliferating cell populations (Figure 3.3.A.ii), demonstrating that serum starvation inhibits proliferation. The effect of inhibition of proliferation can be seen when seeding cells for experiments; for starved cells to have an equal confluency to proliferating cells after 5 days of serum starvation, 6 times as many cells need to be seeded.

Cell diameter was significantly decreased at day two by 16.5% (14.16± 0. 06μm, $P = 0.0013$), day three by 18% (13.92 ± 0.13μm, $P = 0.0016$), day four by 15% (14.42 ± 0.10μm, $P < 0.002$), and day five by 15.5% (14.29 ± 0.1μm, $P < 0.002$) compared to proliferating (16.5±0.108μm) (Figure 3.2.B and Table 3.1).

Cell viability was determined using trypan blue stain which is a vital stain used to selectively colour dead cells blue whilst live cells with intact cell membranes are not coloured. Cells were stained with trypan blue then cell viability were calculated using a Cellometer (Method 2.4.1).

Cell viability was significantly decreased at day five by 30% (67.5± 1.7%, $P = 0.0335$) compared to proliferating (96.18 ± 0.72%) (Figure 3.2.C and Table 3.1).

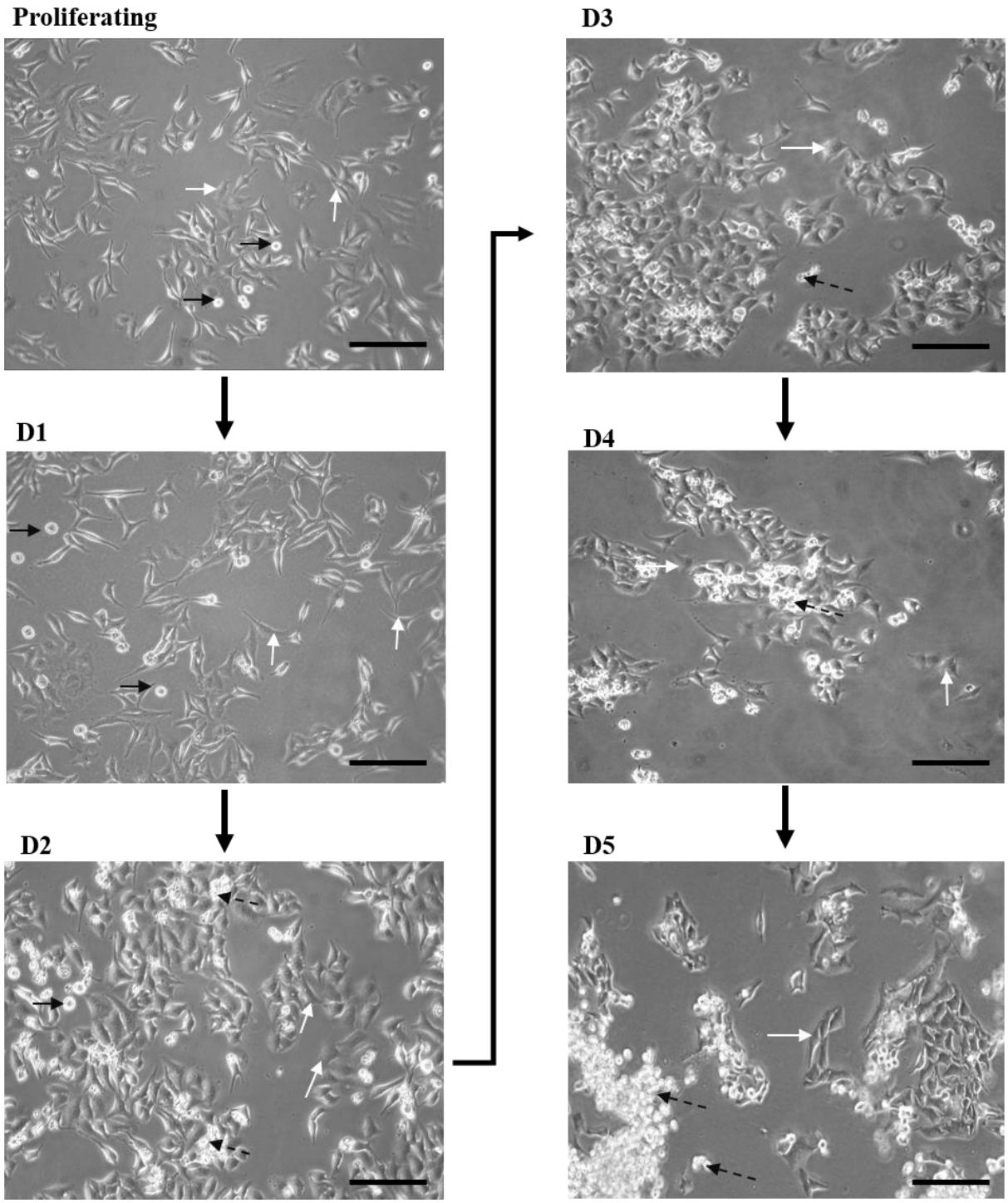

Figure 3.1 Serum starvation of HeLa cells induces morphological changes

Cells were starved by decreasing the FCS from 10% to 0.1% in culture medium for five (1-5) days. Bright field images of cells were taken before and after starvation. D1, D2, D3, D4 and

D5 represent day one, two, three, four and five of serum starvation. Proliferating cells display a patchy monolayer growth pattern with angular shaped cell bodies; cells in interphase (white arrows) and spherical dividing cells; cells in mitosis (solid black arrows). At D1 cells resemble proliferating cells. In D2 and D3, cells grew in clusters showing a decrease in the number of mitotic cells and a reduction of cell size of interphase cells and debris appear (dashed black arrows). From D4, mitotic cell are not seen and debris markedly increased. Images are representative of >20 images. Scale bars represent 50µm.

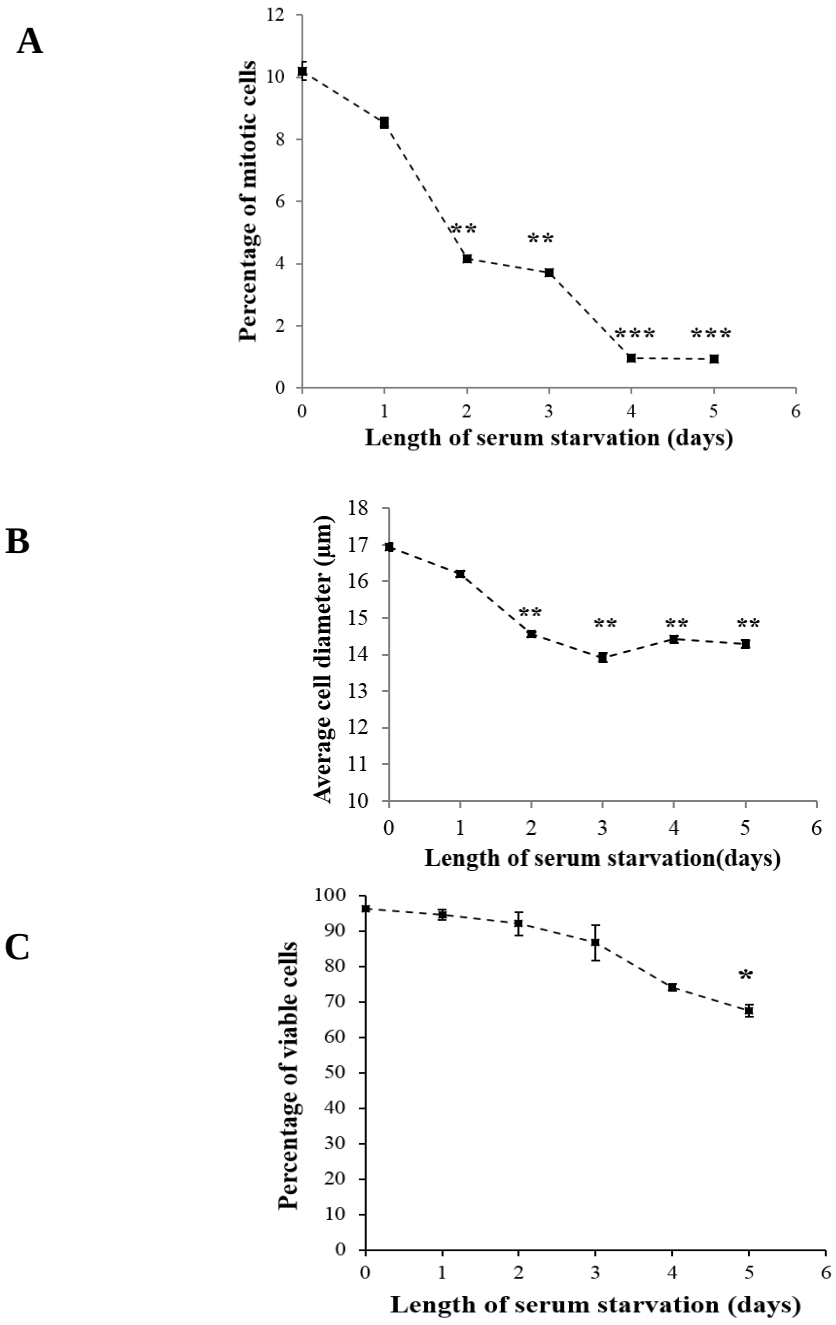

Figure 3.2 Growth characteristics changes with 5-day serum starvation time course in HeLa cells

HeLa cells were starved by decreasing the FCS from 10% to 0.1% in culture medium for 5 days. Mitotic cells were counted and expressed as a percentage of the total cell population. **A)** Mitotic cells were significantly decreased by ~ 60% (P = 0.0026**), ~ 63% (P = 0.0032**), ~

90% (P < 0.001***) and ~ 90% (P < 0.001***) in two, three, four and five days of serum starvation respectively. **B)** Cell diameter was significantly decreased by ~ 16.5% (P = 0.0013**), ~ 18% (P = 0.0016**), ~ 15 % (P = 0.002**) and ~ 15.5 % (P < 0.002**) in two, three, four and five days respectively compared to proliferating. **C)** Cell viability was detected by trypan blue stain (Method 2.4.1) cell viability was significantly decreased in day five by ~ 30 % (P = 0.0335) compared to proliferating. Error bars represent S.E.M.N=4.

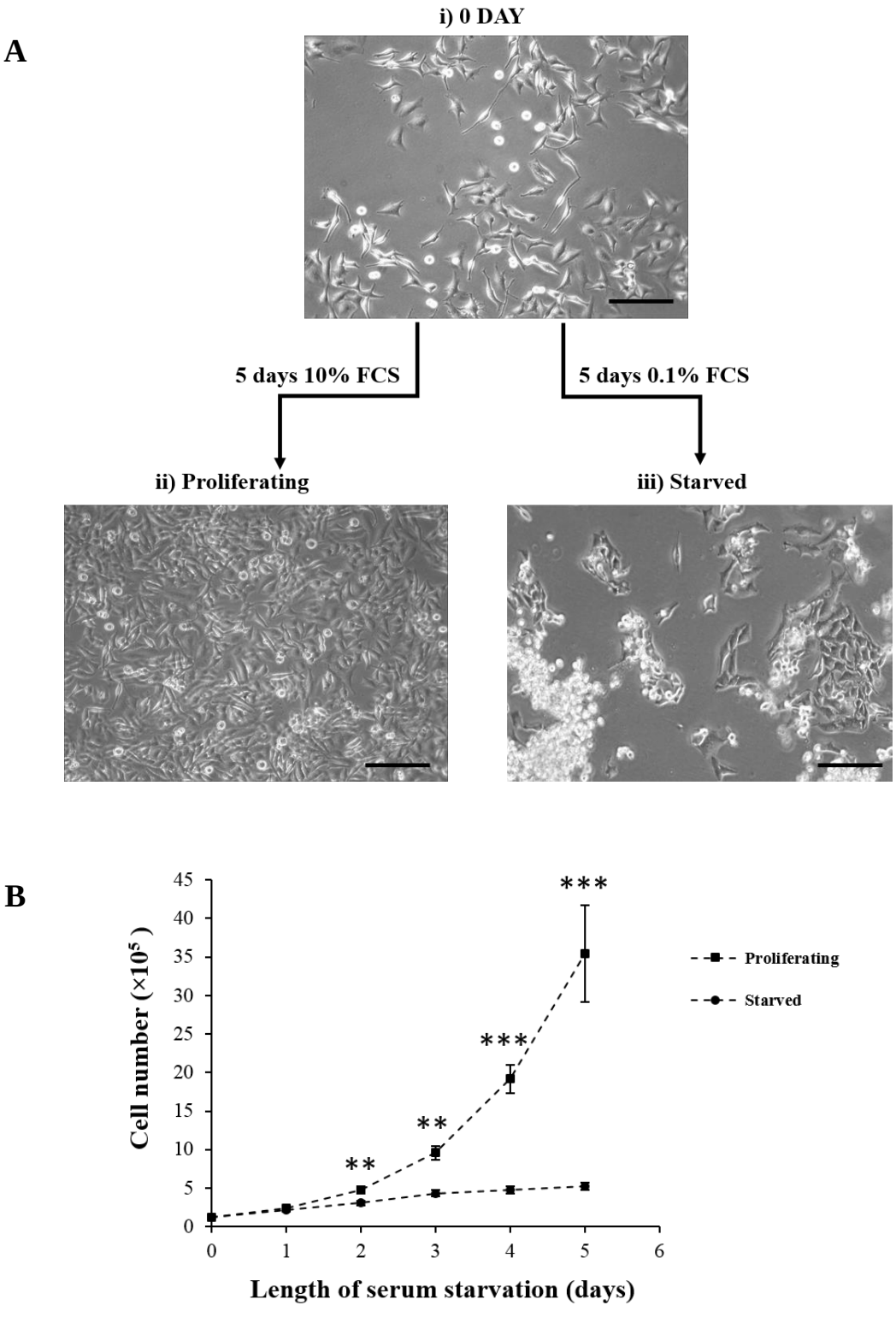

Figure 3.3 Serum starvation inhibited cell proliferation in HeLa cells

HeLa cells were grown in 10% FCS (proliferating) or 0.1%FCS (starved) for 5 days. The same numbers of cells were seeded onto coverslips prior to starvation. **A)** Bright field images were taken of cells before and after 5 days of serum starvation. **B)** Quantification of cells/ml culture medium was done by Cellometer (Method 2.4). Day 0; proliferating cells, n=7 (120×10^3 cells), starved cells *n*=7 (120×10^3 cells). Day 1; proliferating cells, *n*=6 (238×10^3 cells), starved cells *n*=7 (220×10^3 cells), P=0.8037. Day 2; proliferating cells, *n*=6 (479×10^3 cells), starved cells, *n*=6 (308×10^3 cells), $P<0.0031^{**}$. Day 3; proliferating cells, *n*=6 (958×10^3 cells), starved cells *n*=4 (431×10^3 cells), $P=0.0017^{**}$. Day 4; proliferating cells, *n*=6 (1914×10^3 cells), starved cells *n*=6 (474×10^3 cells), $P<0.001^{***}$. Day 5; proliferating cells, *n*=6 (3542×10^3 cells), starved cells *n*=6 (522×10^3 cells), $P<0.001^{***}$.

	Mitotic cells (%)	Cell diameter (µm)	Cell viability (%)
Proliferating (control)	10.19±0.92	16. 5±0.10	96.18±0.72
D1	8.52±1.7 (P= 0.3521)	16.21±0.07 (P=0.0783)	94.53±1.5 (P= 0.9959)
D2	4.16± 0.09 (P = 0.0026)	14.16±0.06 (P=0.0013)	92.03± 3.31 (P= 0.8188)
D3	3.69 ± 0.11 (P = 0.0032)	13.92±0.13 (P=0.0016)	86.6± 4.88 (P = 0.1578)
D4	0.96 ± 0.04 (P < 0.001)	14.42 ± 0.1 (P < 0.002)	74.07 ± 1.04 (P = 0.0579)
D5	0.92 ± 0.06 (P < 0.001)	14.29 ± 0.1 (P <0.001)	67.5 ± 1.7 (P = 0.0335)

Table 3.1 Growth characteristics changes of HeLa cells over the 5-day serum starvation time course (means ± SEM)

3.2.2 NIH 3T3 cells

Morphologically, proliferating NIH 3T3 cells (10% FCS) display a patchy monolayer growth pattern with angular shaped cell bodies (cells in interphase) and spherical dividing cells (cells in mitosis). Starved cells (0.1 %FCS) showed a gradual decrease in mitotic cell number and a marked increase in debris. At day four and five, images clearly exhibit that almost cells are non-viable (Figure 3.4).

As seen in HeLa cells, mitotic NIH 3T3 cells were significantly decreased over the 5-day serum starvation (Figure 3.4 and Figure 3.5.A). At day one mitotic cells were decreased by 63% (4.14± 0.24%, $P < 0.001$), at day two by 66% (3.84 ± 0.55%) ($P < 0.001$), at day three by 93.5% (0.71 ± 0.35%, $P < 0.0001$) and at day four and day five by ~ 100% (0.0) ($P < 0.0001$) compared to proliferating (11.22±0.85%) (Table 3.2).

In addition, cell count showed that serum starvation inhibited cell proliferation in NIH 3T3 cells, this can be detected by comparing the cell counts for proliferating (5991×10^3cells) and starved cells (23×10^3 cells) where cells were seeded at the same density prior to the 5-day serum starvation time-course (Figure 3.6). This was confirmed by the observation that serum starved cell populations (Figure 3.6.A.iii) were far less confluent compared to proliferating cell populations (Figure 3.6.A.ii), indicating that serum starvation inhibits cell proliferation.

Unlike HeLa cells, cell diameter of NIH 3T3 cells was not significantly altered over the 3-day serum starvation (Figure 3.5.B). At day one (9.70 ± 0.49μm), day two (11.9 ± 0.19μm), and day three (10.91 ± 0.1μm) compared to proliferating (9.28±0.46μm), (All $P > 0.999$) suggesting that cell diameter could not be an indicative for cell cycle arrest in NIH 3T3 cells. In day four and day five of serum starvation nearly almost cells were non-viable (Figure 3.4) and thus cell diameter could not be measured (Table 3.2).

Cell viability was measured by trypan blue stain which showed that the viability was significantly decreased at day four by ~ 50.5% (40.3± 4.1%, $P < 0.01$) and day five by ~ 71.5% (23.3 ± 5.2 %, $P < 0.001$) compared to proliferating (81.6 ± 13.3%) (Figure 3.5.C and Table 3.2).

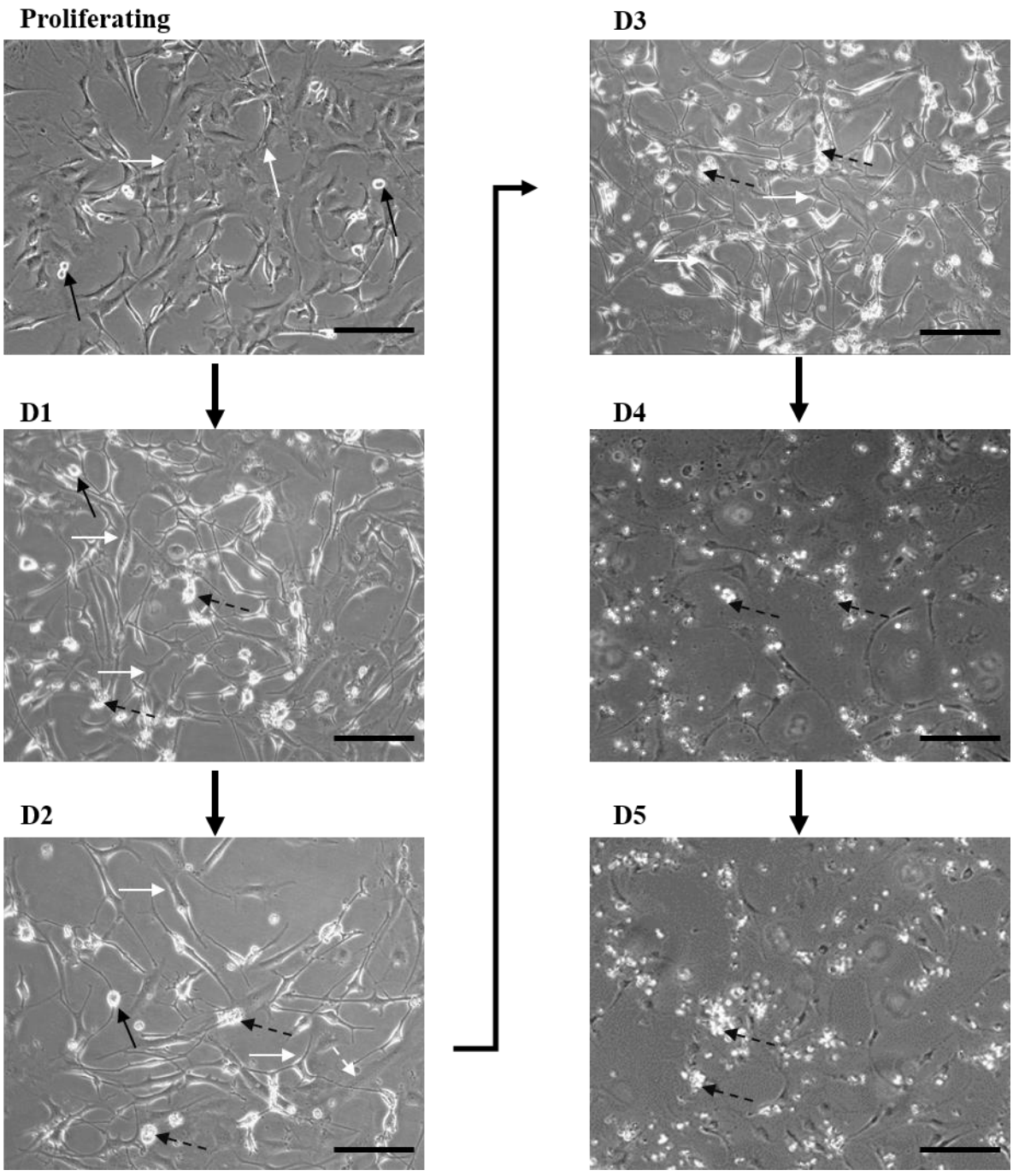

Figure 3.4 Serum starvation of NIH 3T3 cells induces morphological changes

Cells were starved by decreasing the FCS from 10% to 0.1% in culture medium for 5 (1-5) days. Bright field images of cells were taken before and after starvation. D1, D2, D3, D4 and D5 represent day one, two, three, four and five of serum starvation. Proliferating cells display a patchy monolayer growth pattern with angular shaped cell bodies; cells in interphase (white

arrows) and spherical dividing cells; cells in mitosis (solid black arrows). From D1, **c**ells show a decrease in the number of mitotic cells. Debris increases with increase time of serum starvation (dashed black arrows). From D4, nearly almost cells are non-viable and debris markedly increased. Images are representative of >15 images. Scale bars represent 50µm.

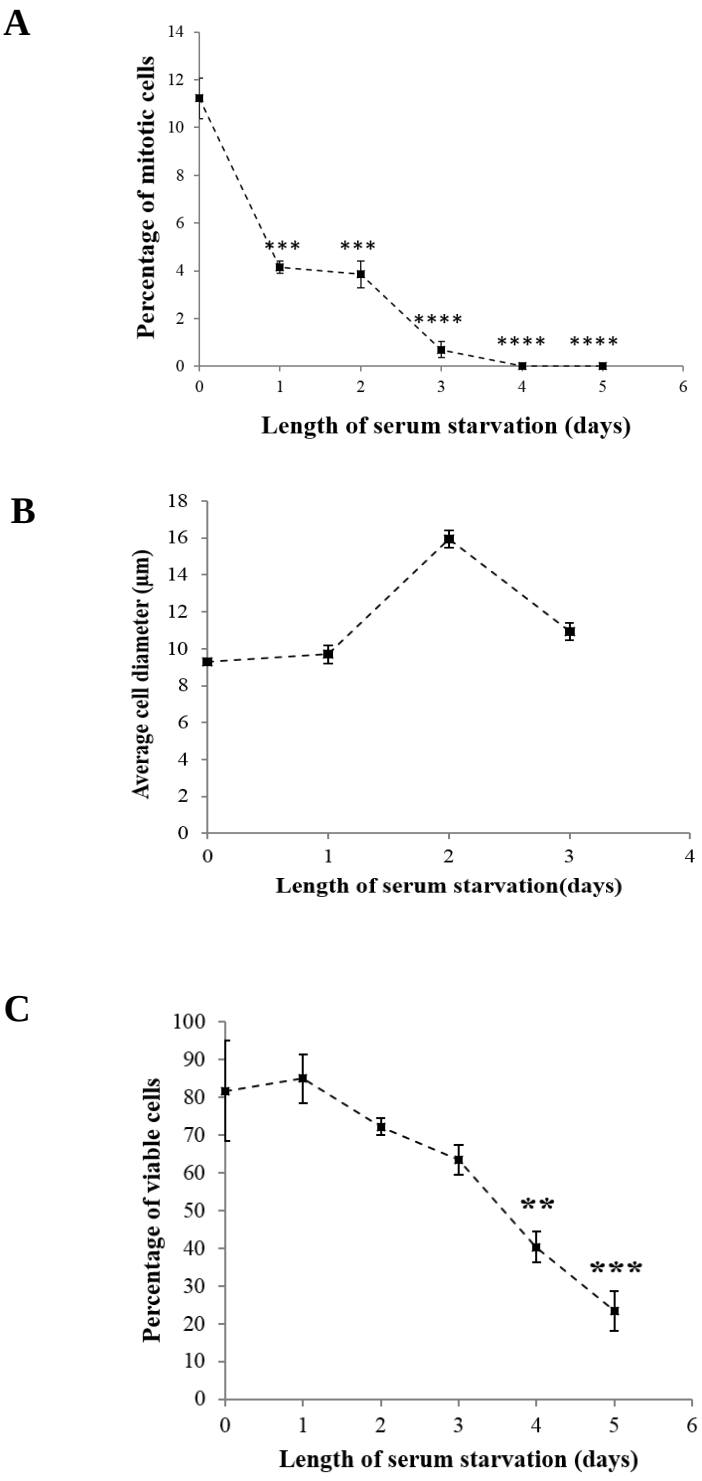

Figure 3.5 Growth characteristics changes of NIH 3T3 cells over 5-day serum starvation

NIH 3T3 cells were starved by decreasing the FCS from 10% to 0.1% in culture medium for 5 days. **A)** Mitotic cells were counted and expressed as a percentage of the total cell population, mitotic cells were significantly decreased by ~ 63% (P<0.001***), ~ 66% (P<0.001***) , ~

93.5% (P < 0.0001****), ~100 % (P < 0.0001****) and ~ 100% (P < 0.0001****) in day one, day two, day three, day four and day five of serum starvation respectively. B) Cell diameter was not significantly different in starved cells compared to proliferating (P > 0.999). In day four and five days nearly almost cells were non-viable (Figure) and thus cell diameter could not be measured. Cell viability was detected by trypan blue stain (method 2.4.1), cell viability was significantly decreased in day four and day five by ~ 50.5% (P < 0.01**) and ~ 71.5% (P < 0.001***) compared to proliferating Data represent the mean ± S.E.M. For proliferating cells n =836, for D1 n = 932, D2 n = 816, D3 n = 729, D4 n= 215, D5 n= 431. N=4.

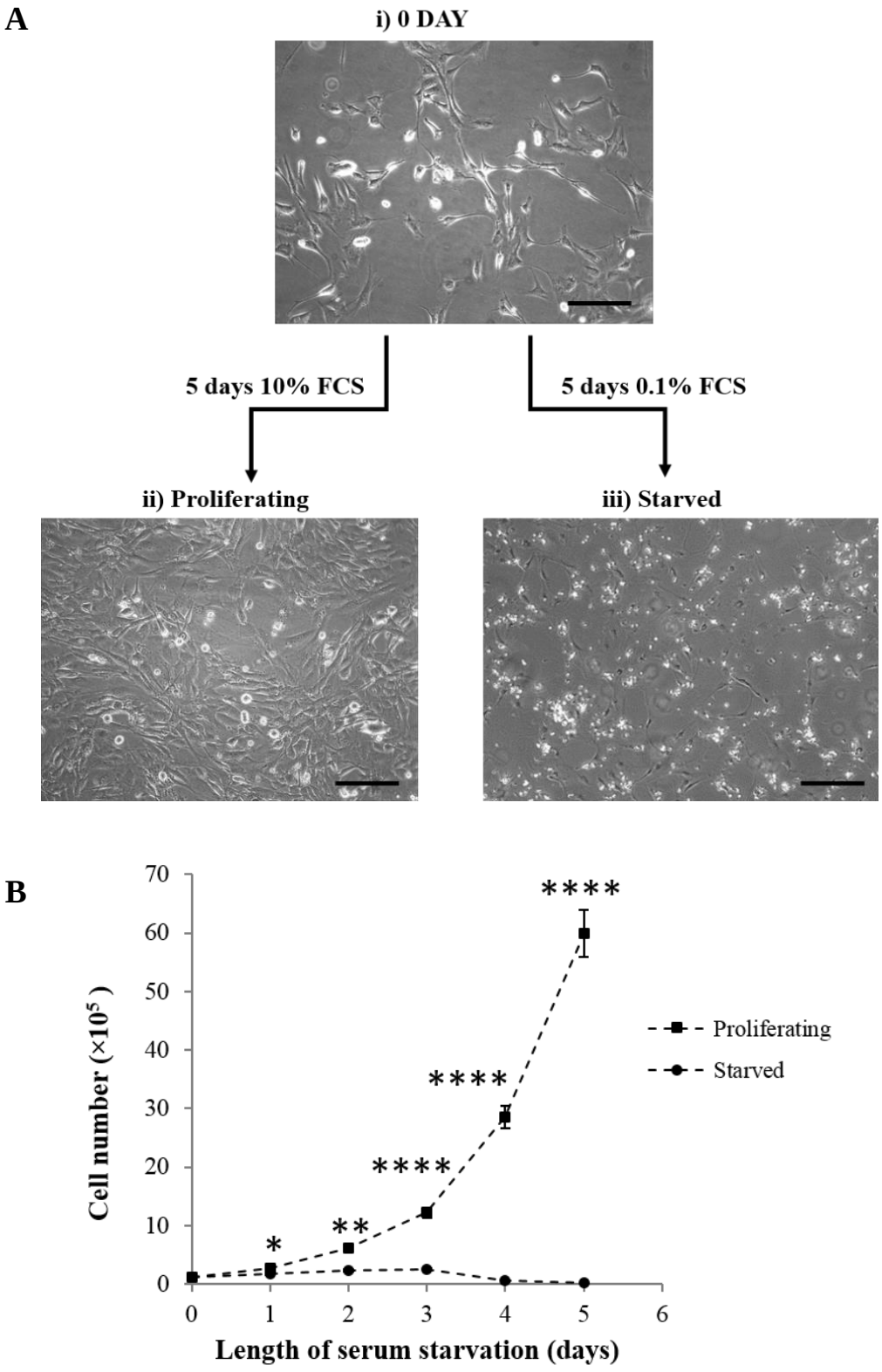

Figure 3.6 Serum starvation inhibited cell proliferation in NIH 3T3 cells

NIH 3T3 cells were grown in 10% FCS (proliferating) or 0.1%FCS (starved) for 5 days. The same numbers of cells were seeded onto coverslips prior to starvation. **A)** Bright field images were taken of cells before and after serum starvation. **B)** Quantification of cells/ml culture medium was done by Cellometer (Method 2.4). Day 0; proliferating cells, n=7 (120×103 cells), starved cells n=7 (120 ×103 cells). Day 1; proliferating cells, n=5 (257×103 cells), starved cells n=7 (165 ×103 cells), P=0.022*. Day 2; proliferating cells, n=3 (605 ×103 cells), starved cells, n=6 (226×103 cells), P<0.003**. Day 3; proliferating cells, n=6 (1224×103 cells), starved cells n=4 (250×103 cells), P=0.0001****. Day 4; proliferating cells, n=5 (2854 ×103 cells), starved cells n=3 (54 ×103 cells), P<0.0001****. Day 5; proliferating cells, n=5 (5991×103 cells), starved cells n=6 (23×103 cells), P<0.0001****.

	Mitotic cells (%)	Cell diameter (μm)	Cell viability (%)
Proliferating (control)	11.22±0.85	9.2±0.46	81.63±13.31
D1	4.14±0.24 (P<0.001)	9.7± 0.49 (P > 0.05)	84.93±6.4 P = 0.8821
D2	3.84± 0.55 (P < 0.001)	11.91±0.19 (P > 0.05)	72.16± 2.2 P = 0.4236
D3	0.7 ± 0.35 (P < 0.0001)	10.92±0.46 (P > 0.05)	63.46± 3.52 P = 0.0912
D4	0 ± 0 (P < 0.0001)	N/A	40.3 ± 4.1 (P< 0.01)
D5	0 ± 0 (P < 0.0001)	N/A	23.3 ± 5.23 (P< 0.001)

Table 3.2 Growth characteristics of NIH 3T3 cells with 5-day serum starvation (means ± SEM)

N/A, not applicable to measure cell diameter at D4 and D5 as almost all cells were non-viable.

3.2.3 hTERT RPE-1 cells

In contrast to HeLa and NIH 3T3 cells, there was no alterations in the growth pattern over the five-day serum starvation time course in hTERT RPE-1 cells. Proliferating (control) cells (10% FCS) and starved cells (0.1% FCS) exhibit the normal patchy monolayer growth pattern with angular shaped cell bodies (cells in interphase) and spherical dividing cells (cells in mitosis) (Figure 3.7).

Furthermore, mitotic cell number was not significantly changed over the 5-day serum starvation (Figure 3.7 and Figure 3.8.A). At day one the percentage of mitotic cells was (3.1± 0.72%), day two (2.6± 0.56%), day three (2.76 ± 0.71%), day four (2.86 ± 0.56%) and day five (2.89 ± 0.61%) compared to proliferating (2.48±0.81), (All P >0.999) (Figure 3.8.A and Table 3.3).

Similarly, cell counts showed that serum starvation did not inhibit cell proliferation in hTERT RPE-1 cells, this can be observed by comparing the cell counts for proliferating (40×10^4 cells) and starved cells (35×10^4 cells) where cells were seeded at the same density prior to the 5 day serum starvation time-course (Figure 3.9.B). In addition to the observation that serum starved cell populations (Figure 3.9.A.iii) were similarly confluent compared to proliferating cell populations (Figure 3.9.A**Figure** .ii) demonstrating that serum starvation does not affect cell proliferation. This lack of inhibition of proliferation can also be seen when seeding cells for experiments; for starved cells to have an equal confluency to proliferating cells after 5 days of serum starvation, the same number of cells need to be seeded.

Cell diameter was also not significantly changed over the 5-day serum starvation. At day one (12.48± 1.1µm), day two (12.71± 0.91 µm), day three (12.86 ± 1.2 µm), day four (13.45 ± 1.01 µm) and day five (14.02 ± 0.89 µm) (All P >0.999) compared to proliferating (13.29±1.02 µm) (Figure 3.8.B and Table 3.3).

Consistent with these observations, cell viability was not significantly altered over the 5-day serum starvation. At day one (83.73± 13.09), day two (87.23± 5.61), day three (94.13 ± 0.37), day four (94.86 ± 1.8) and day five (96.63 ± 0.96) (All P >0.999) compared to proliferating (97.43±1.32) (Figure 3.8.C and Table 3.3).

The results so far revealed that serum starvation inhibited cell proliferation with no significant effect on cell viability till day four in HeLa cells and till day three in NIH 3T3 cells, while in hTERT RPE-1 cells, serum starvation did not induce any changes on cell proliferation suggesting that serum starvation induced cell cycle arrest in HeLa and NIH 3T3 cells but not hTERT RPE-1 cells. These results were further confirmed by investigating cell cycle analysis using flow cytometry.

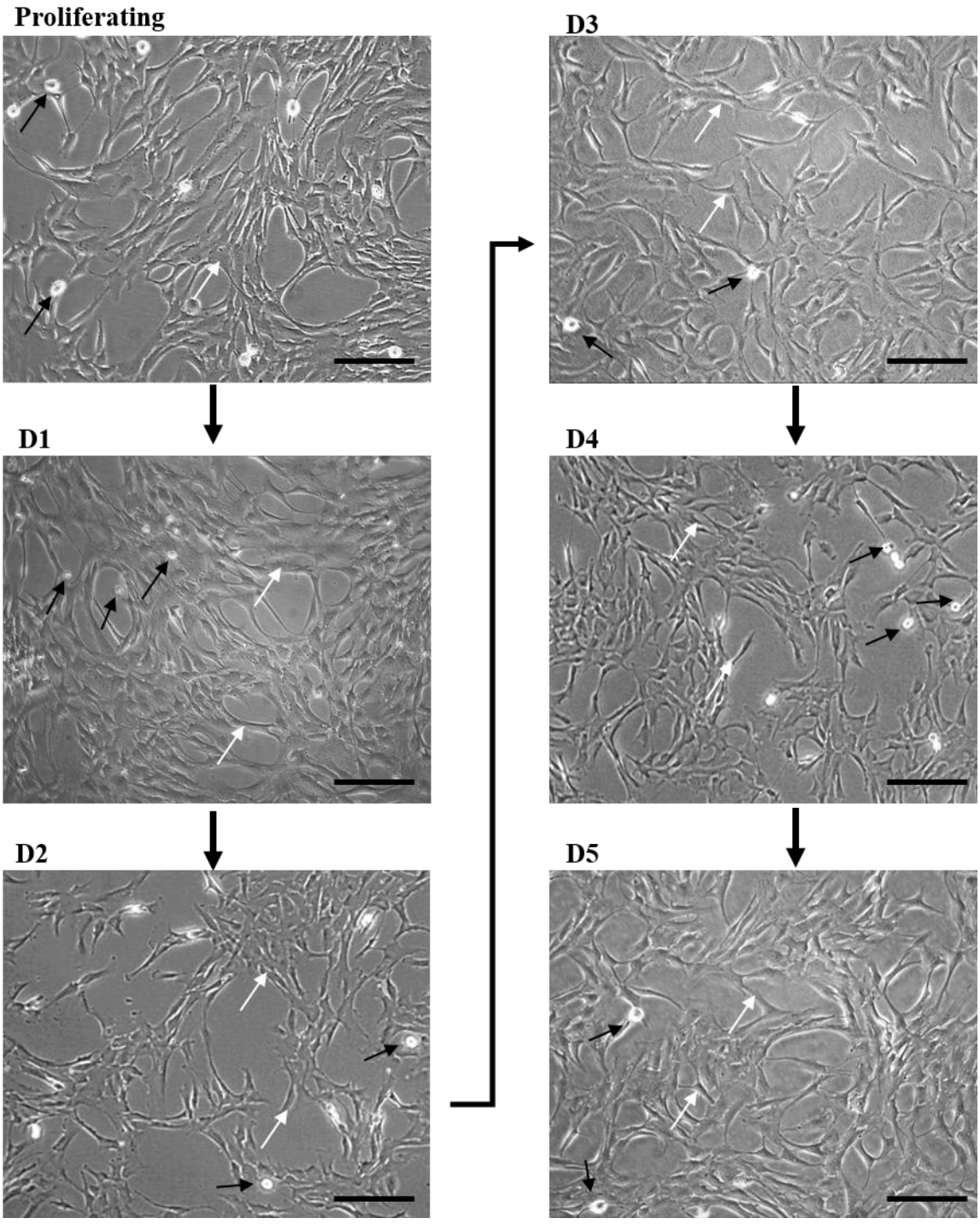

Figure 3.7 Serum starvation does not induce morphological changes in hTERT RPE-1 cells

Cells were starved by decreasing the FCS from 10% to 0.1% in culture medium for 5 (1-5) days. D1, D2, D3, D4 and D5 represent one day, two days, three days, four and five days of serum starvation. Bright field images of cells were taken before and after starvation. Proliferating cells

display patchy monolayer growth pattern with angular shaped cell bodies (cells in interphase stage; white arrows) and spherical dividing cells (cells in mitotic phase, black arrows).In D1, D2, D3, D4 and D5 there is no changes in the pattern of cell growing with no apparent debris or died cells. The same numbers of cells were seeded onto coverslips prior to starvation. Images are representative of >20 images. Scale bars represent 50µm.

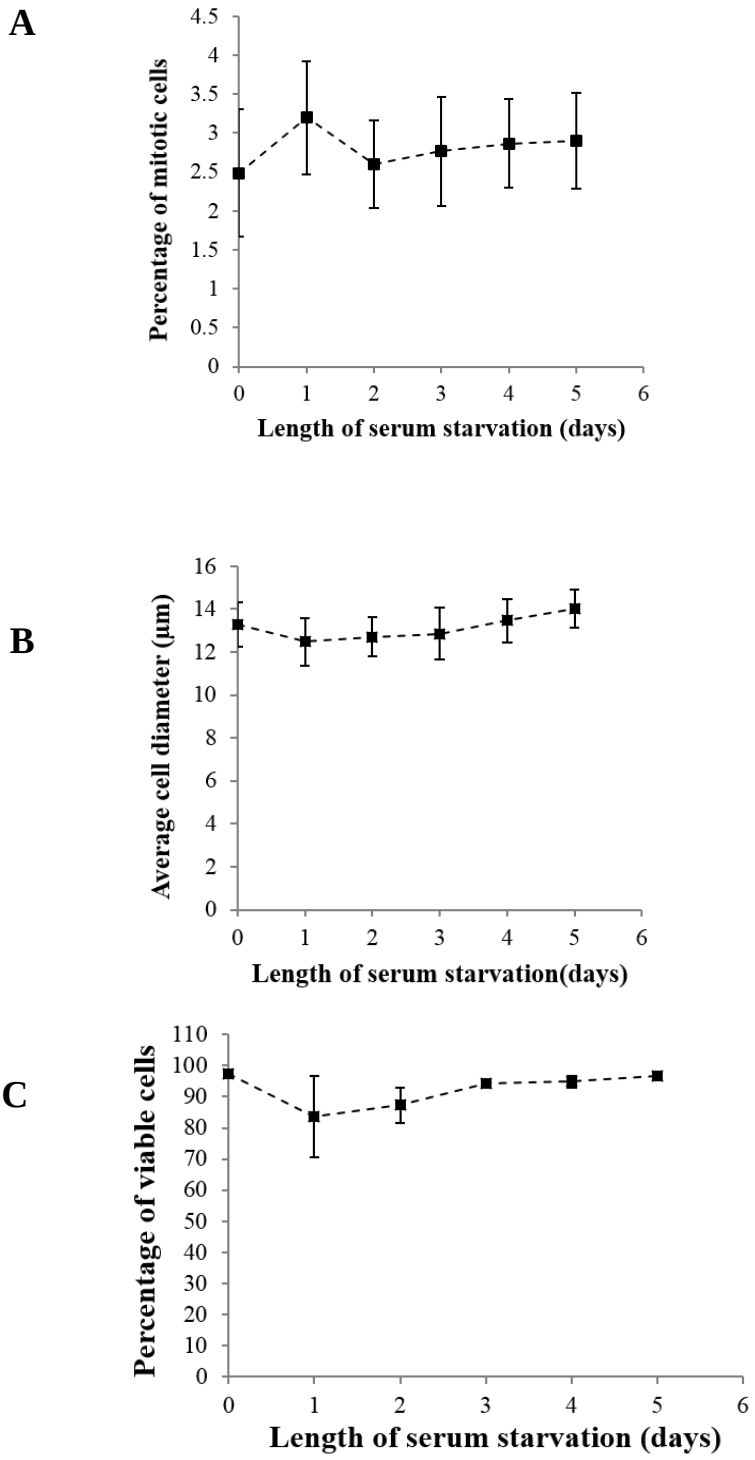

Figure 3.8 Growth characteristics changes of hTERT RPE-1 cells over 5-day serum starvation

hTERT RPE-1 cells were starved by decreasing the FCS from 10% to 0.1% in culture medium for 5 days. **A)** Mitotic cells were counted and expressed as a percentage of the total cell

population, mitotic cells were not significantly altered over the 5-day serum starvation time course ($P > 0.999$). **B)** Cell diameter was not significantly different in starved cells compared to proliferating ($P > 0.999$). **C)** Cell viability was detected by trypan blue stain (Method 2.4.1), cell viability was not significantly changed in starved cells compared to proliferating ($P > 0.999$). Data represent the mean ± S.E.M. For proliferating cells n =935, for D1 n = 982, D2 n = 954, D3 n = 1203, D4 n= 1034, D5 n=984. N=4.

A

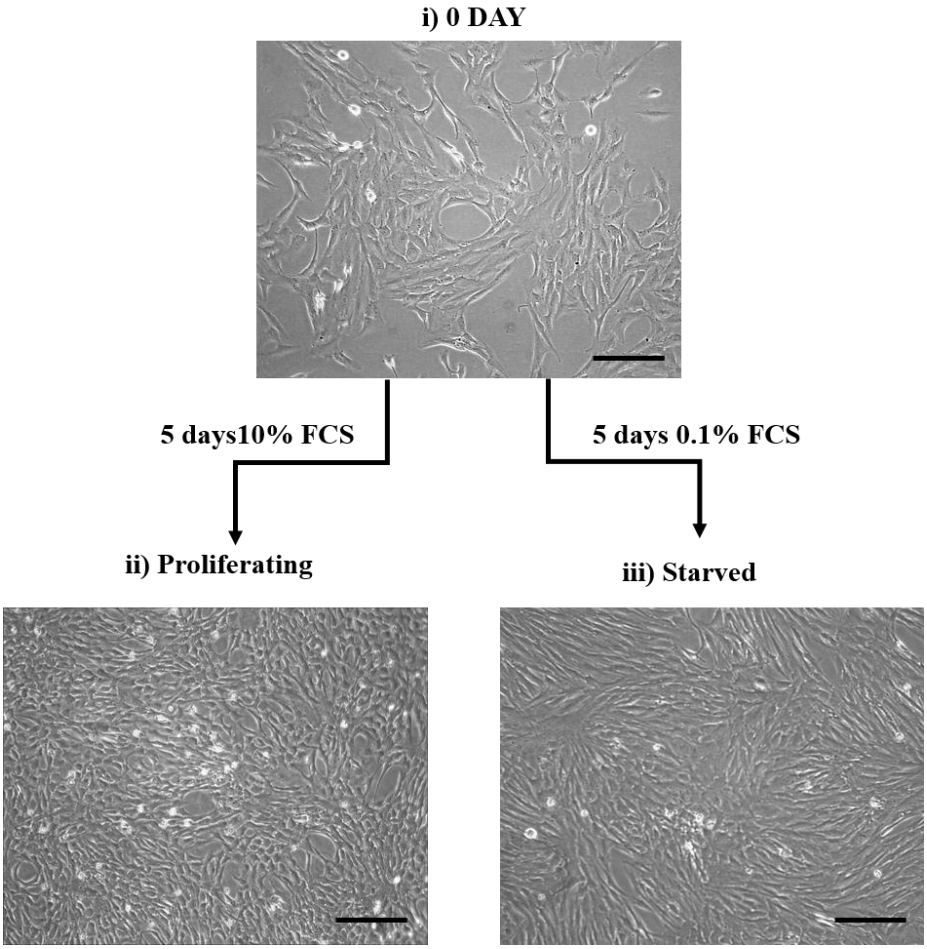

B

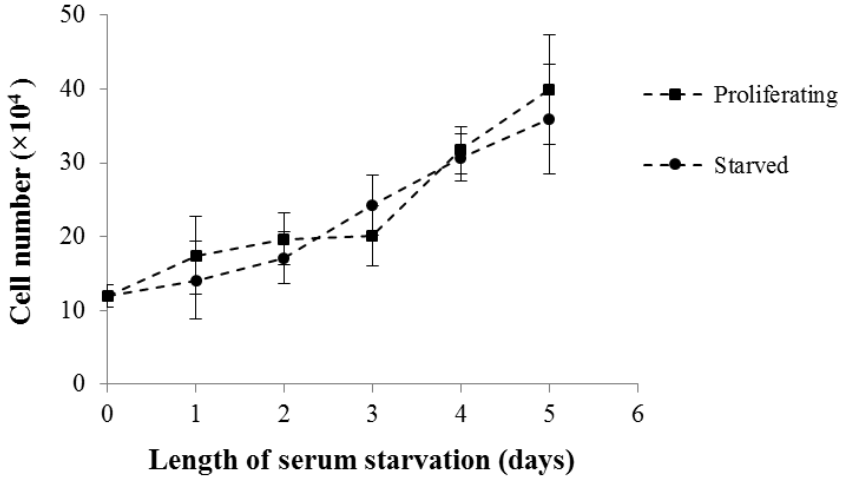

Figure 3.9 Serum starvation of hTERT RPE-1 cells does not alter cell proliferation in hTERT RPE-1 cells

hTERT RPE-1 cells were grown in 10% FCS (proliferating) or 0.1%FCS (starved) for 5 days. The same numbers of cells were seeded onto coverslips prior to starvation. **A)** Bright field images were taken of cells before and after serum starvation. **B)** Quantification of cells/ml culture medium was done by Cellometer (Method 2.4). Day 0; proliferating cells, n=7 (120×10^3 cells), starved cells n=7 (120×10^3 cells). Day 1; proliferating cells, n=6 (154×10^3 cells), starved cells n=7 (140×10^3 cells). Day 2; proliferating cells, n=6 (196×10^3 cells), starved cells, n=6 (171×10^3 cells). Day 3; proliferating cells, n=6 (200×10^3 cells), starved cells n=4 (242×10^3 cells). Day 4; proliferating cells, n=6 (316×10^3 cells), starved cells n=6 (306×10^3 cells). Day 5; proliferating cells, n=6 (398×10^3 cells), starved cells n=6 (359×10^3 cells) (All $P > 0.999$). Data represent means ± SEM.

	Mitotic cells (%) (All P > 0.999)	Cell diameter (μm) (All P > 0.999)	Cell viability (%) (All P > 0.999)
Proliferating	2.48±0.81	13.29±1.02	97.43±1.32
D1	3.1± 0.72	12.48± 1.1	83.73± 13.09
D2	2.6± 0.56	12.71±0.91	87.23± 5.61
D3	2.76 ± 0.71	12.86 ± 1.2	94.13 ± 0.37
D4	2.86 ± 0.56	13.45±1.01	94.86 ± 1.8
D5	2.89 ± 0.61	14.02±0.98	96.63 ± 0.96

Table 3.3 Growth characteristics of hTERT RP-1 cells with five-day serum starvation (means ± SEM)

3.3 Results – Flow cytometry

Flow cytometry is an analytical technique, in this study, it is used to analyse cell cycle phases by taking cell viability, DNA and RNA contents into account in order to determine the time point of 5-day serum starvation time course at which the cells enter G0/G1 phase and also to detect the percentage of G0 cells contributing to this phase.

This was done by analysing the DNA content of isolated cells in order to define cells according to cell cycle status (G0/G1 and S/G2/M) and by separating G1 and G0 phase cells based on their RNA content by using the Hoechst/pyronin Y method (Shapiro, 1981).

Proliferating (control) cells (10% FCS) and starved cells (0.1% FCS) were stained first with Hoechst33342 to stain DNA and then with Pyronin Y. As Pyronin Y reaction with DNA was blocked by Hoechst33342, Pyronin Y stains RNA only (Method 2.5.1). Cells in S/G2/M phases were identified as the population with double DNA content and high RNA content (Darzynkiewicz *et al.*, 2011). Cells in G1 phase are identified as the population with single DNA content and high RNA content. Finally, cells in G0 phase were identified as the population with single DNA content and an RNA content lower than that in cells in S and G2/M phases as it is known that RNA content of cells is higher during proliferation than during quiescence (Crissman *et al.*, 1985; Lemons *et al.*, 2010; Darzynkiewicz *et al.*, 2011).

Cells were also stained with Zombie NIR in order to detect cell viability. Zombie NIR is an amine reactive fluorescent dye that is excluded by live cells, while dead cells allowing the entry of the dye into the cytoplasm increasing the amount of total protein labelling thus enables to detect cell viability. Data were measured and analysed using a FACS Diva cell sorter.

Figure 3.10 shows how cell gating was done. The gating tree was set as follows. First, dead cells were excluded from the whole cell populations (Live gate). Then the doublet were excluded in order to analyse cells in singlets only (Singlets gate). Cell number were calculated in each cell phase according to DNA content (cell cycle analysis gate). The last gate where G0 and G1 phase separation was done according to DNA and RNA contents (Method 2.5.2).

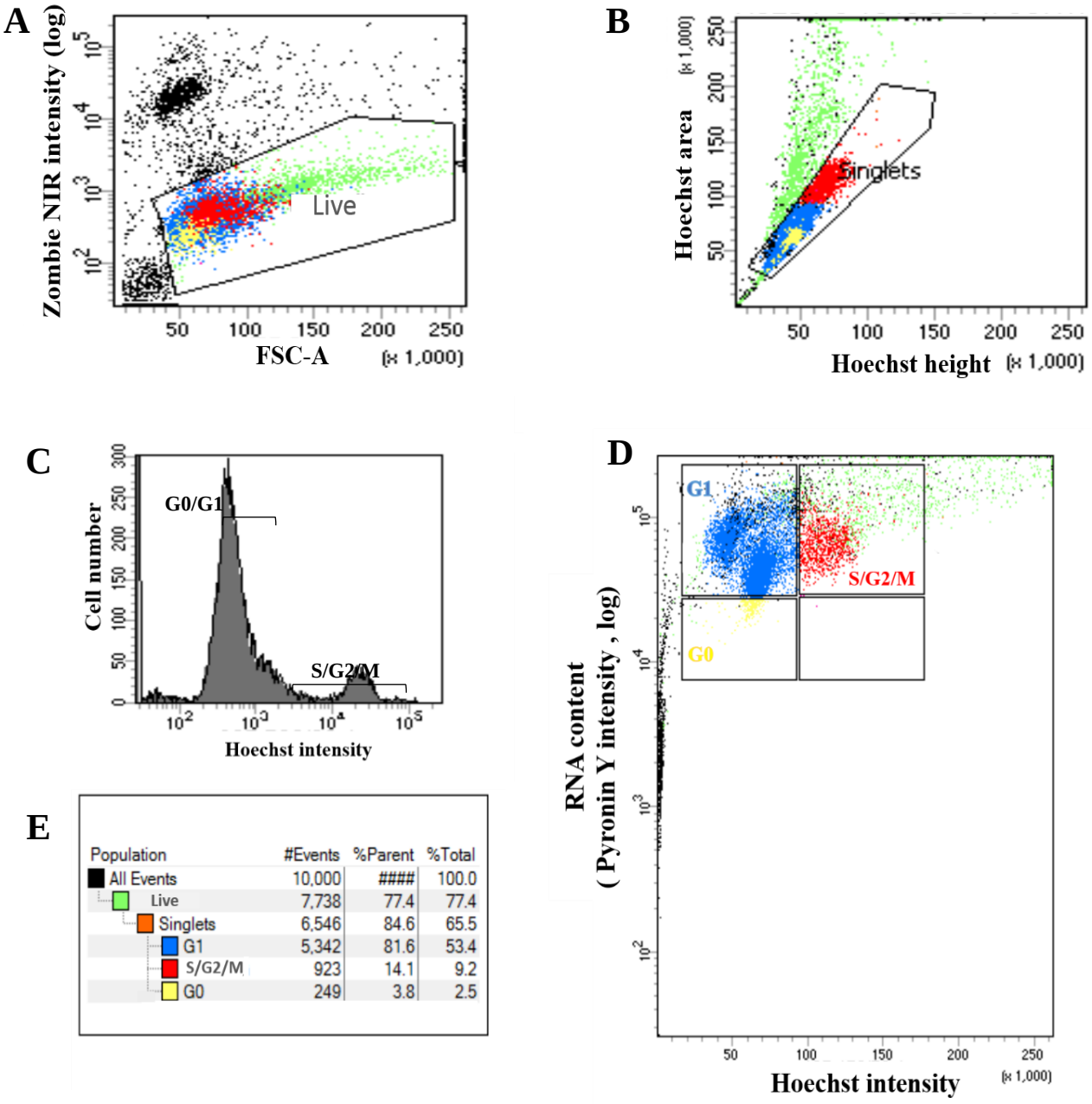

Figure 3.10 FACS Diva data analysis sheet of proliferating HeLa cells

HeLa cells were grown in 10% FCS medium (proliferating). Cells were stained with viability stain; Zombie NIR, DNA stain; Hoechst and RNA stain; Pyronin Y. FACS Diva software was used to produce dot plots, histograms and to analyse data. Each dot appearing on the dot plots represent an 'event' recorded on the flow cytometer. Gating was designed based on the signals recorded from the sample so cells inside the gate moved to the next checkpoint, while cells

outside the gate were excluded. **A)** Live gate (Zombie NIR/FSC; dead cells (black dots) within the sample analysed exhibit significant fluorescence signal which is excluded from the gate), coloured cells in the gate are the live cells which will be further subdivided in the following analysis (D). **B)** Singlets gate (Hoechst Area/ Height intensity gate; a pulse geometry gate) this excludes events (doublets; green dots) that could represent more than 1 cell, again coloured cells in the singlet gate will be subdivided in the following analysis (D). **C)** Cell cycle analysis gate (cell number/ Hoechst intensity) to detect normal cell cycle shape histogram based on DNA content and to calculate G0/G1 and S/G2/M cells. **D)** G0/G1 separation gate (Pyronin Y intensity / Hoechst intensity) Cells were classed S/G2/M if they exhibited double DNA content and were RNA positive (red dots), cells were classed G1 if they exhibited single DNA content and were RNA positive (blue dots), and cells were classed G0 if they exhibited single DNA content and were RNA negative (yellow dots). **E)** Table of data shows number of events in each gate, events of each gate as a percentage of parent gates and as a percentage of total events.

3.3.1 Four day-serum starvation time course induced cell cycle arrest of HeLa cells in G0/G1 phase

Flow cytometry analysis using viability Zombie NIR florescence dye showed that the percentage of viable cells was significantly decreased in D5 (35.85 ± 2.05%) compared to proliferating (82.63 ± 3.82) by ~ 56.5%, (P= 0.0078) (Figure 3.11). This result is consistent with the previous data obtained from trypan blue viability staining where the cell viability was significantly decreased at day five of serum starvation (Section 3.2.1).

Cell cycle analysis by flow cytometry showed that the percentage of G0 cells was significantly increased in D4 (26.43 ± 9.160%) by ~ 4934 %, (P = 0.0236) and D5 (25 ± 6.34%), by 4661%, (P = 0.0364) compared to proliferating (0.525 ± 0.33%) (Figure 3.12, Figure 3.13 and Table 3.4).

Corresponding to this increase in G0 cells, the percentage of S/G2/M cells was significantly decreased in D2 by ~ 40 % (13.82 ± 0.55%, P = 0.0084), D3 by ~ 46% (12.3 ± 0.89%, P = 0.0037), D4 by ~70% (6.86 ± 0.77%, P = 0.0003) and D5 by 81 % (4.3 ± 1.38%, P = 0.0004) compared to proliferating (23.1± 2.4%) (Figure 3.12, Figure 3.13 and Table 3.4).

The percentage of G1 cells decreased over the serum starvation time course with maximum decrease at day four by ~ 12% (66.7± 8.1%) compared to proliferating (76.3± 1.52%), however, these changes were not significant (P > 0.999) (Table 3.4).

These results revealed that four-day serum starvation induced cell cycle arrest in G0/G1 phase where more than 93% of cells were in G0/G1 phase (~26% in G0 and 67% in G1 phase).

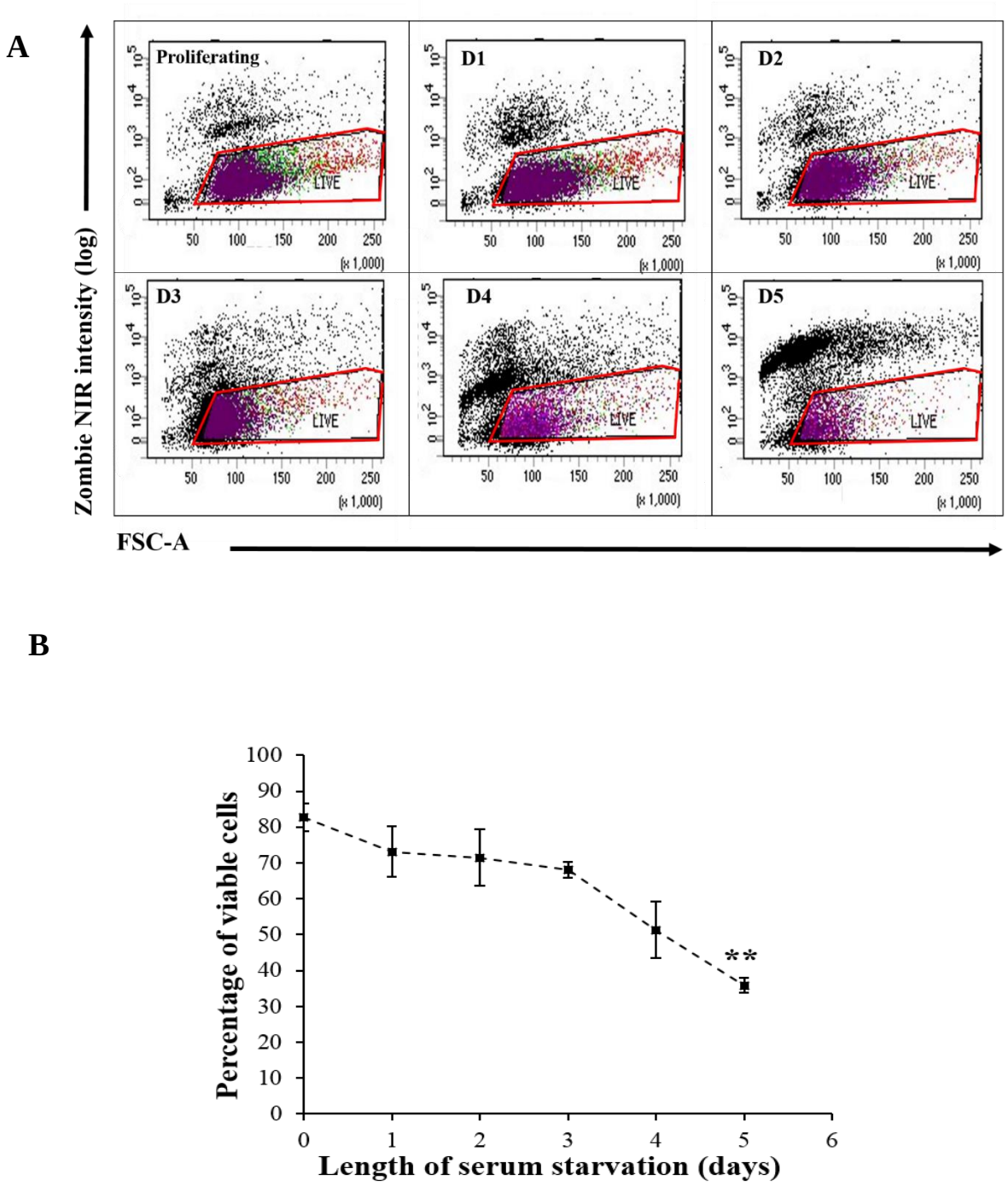

Figure 3.11 Cell viability over five-day serum starvation time-course in HeLa cells

HeLa cells were grown in 10% FCS medium (proliferating) or 0.1% FCS medium (starved) for 5 days. **A)** Dot plots of flow cytometric analysis performed on HeLa cells stained with viability stain; Zombie NIR. D1, D2, D3, D4 and D5 represent one day, two days, three days,

four and five days of serum starvation. FSC-A represents forwards scatter area. Each dot appearing on the dot plot represents a single cell. The proportion of viable cells were detected by Flow cytometry based on strength of fluorescence signal. The dot plots showing distribution of two cell populations represents the dead cells (black dots outside live gate; red box) that exhibit significant high Zombie NIR fluorescence signal, and live cells which do not (coloured dots within the live gate, colour code is shown in the next figure; Figure 3.12). The number of viable cells appeared to be decreased over the 5-day serum starvation time course. **B)** Graph shows quantitative measurements of the proportion of live cells as a percentage of total HeLa cells population. The percentage of viable cells was significantly decreased by ~ 56.5% (P= 0.0078**) at D5 compared to proliferating. n= 10,000. N= 4.

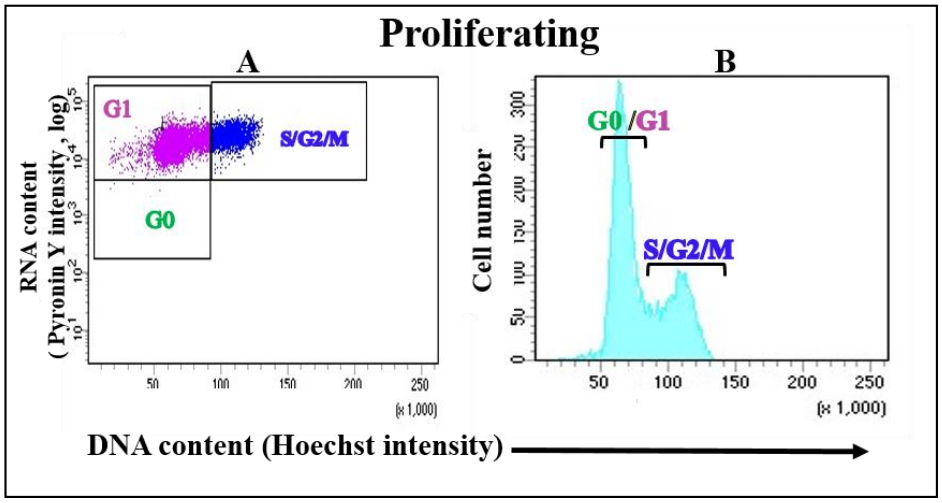
Proliferating
A
B
G1
S/G2/M
G0
RNA content
(Pyronin Y intensity, log)
Cell number
G0 /G1
S/G2/M
(× 1,000)
DNA content (Hoechst intensity)

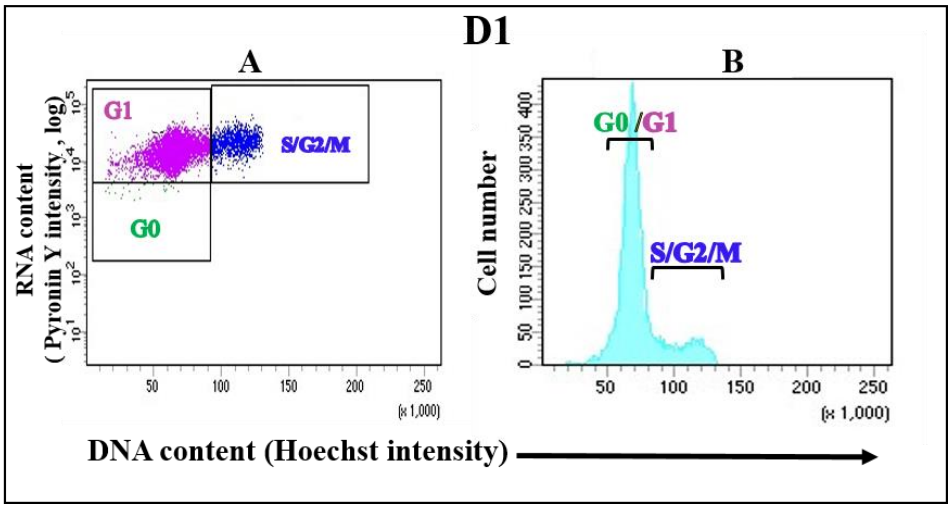
D1
A
B
G1
S/G2/M
G0
RNA content
(Pyronin Y intensity, log)
Cell number
G0 /G1
S/G2/M
(× 1,000)
DNA content (Hoechst intensity)

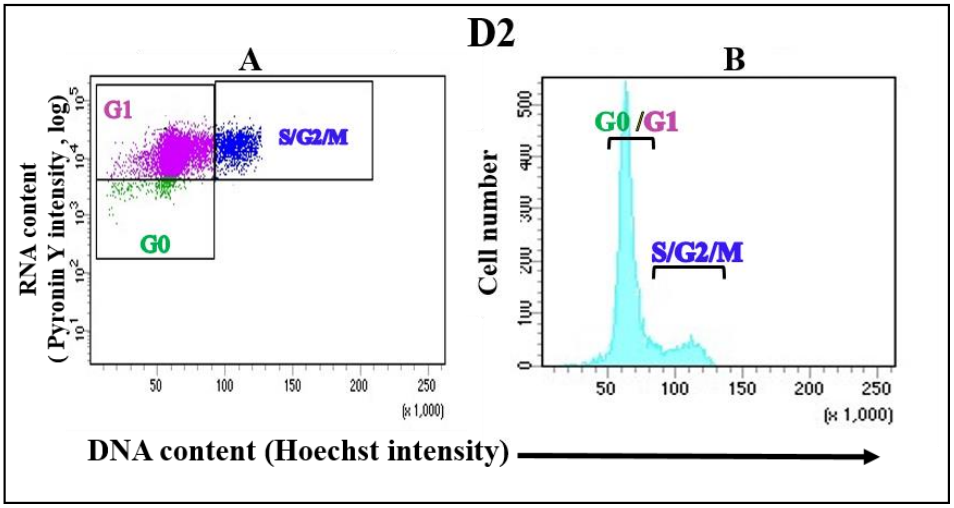
D2
A
B
G1
S/G2/M
G0
RNA content
(Pyronin Y intensity, log)
Cell number
G0 /G1
S/G2/M
(× 1,000)
DNA content (Hoechst intensity)

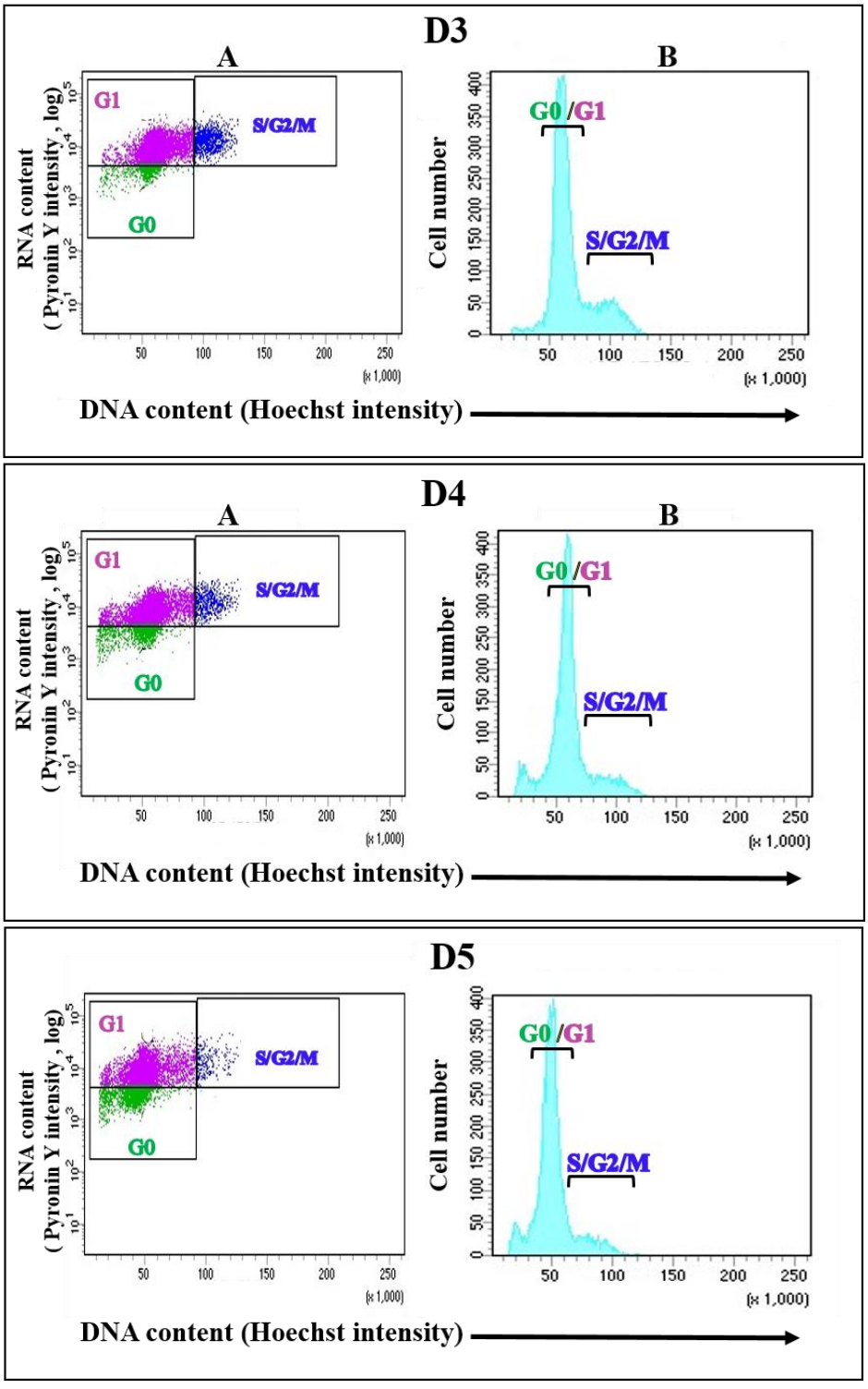

Figure 3.12 Five-day serum starvation time-course altered the proportion of S/G2/M, G1 and G0 subpopulations in HeLa cells

HeLa cells were grown in 10% FCS medium (proliferating) or 0.1% FCS medium (starved) for 5 days; D1, D2, D3, D4 and D5 represent one day, two days, three days, four and five days of serum starvation. **A)** Flow cytometry plots of HeLa cells stained with viability stain; Zombie NIR, DNA stain; Hoechst and RNA stain; Pyronin Y. Dead cells were excluded from the whole cell population (Figure 1). The proportions of cells in S phase, G2 phase and M phase (S/G2/M), cells in G1 phase and cells in G0 phase were detected by Flow cytometry based on DNA and RNA contents using FACsDIVA software. Cells were classed G1 if they exhibited single DNA content and were RNA positive (purple dots), cells were classed S/G2/M if they exhibited double DNA content and were RNA positive (blue dots) and cells were classed G0 if they exhibited single DNA content and were RNA negative (green). Each dot represents a single cell. A difference in distribution of dots in S/G2/M (blue) and G0 (green) gates is obvious over the 5-day serum starvation time-course. The extent of S/G2/M cells appear to be decreased over the 5-day serum starvation time-course while the extent of G0 cells appear to be increased. However, a difference in the extent of G1 cells is not obvious over the 5-day serum starvation time-course compared to proliferating. **B)** Histogram of HeLa cells stained with Hoechst stain show cell cycle analysis according to DNA content. There is an increase in cell number of G0/G1 and a decrease in cell number of S/G2/M over the 5-day serum starvation time-course compared to proliferating. n= 10,000. N=4.

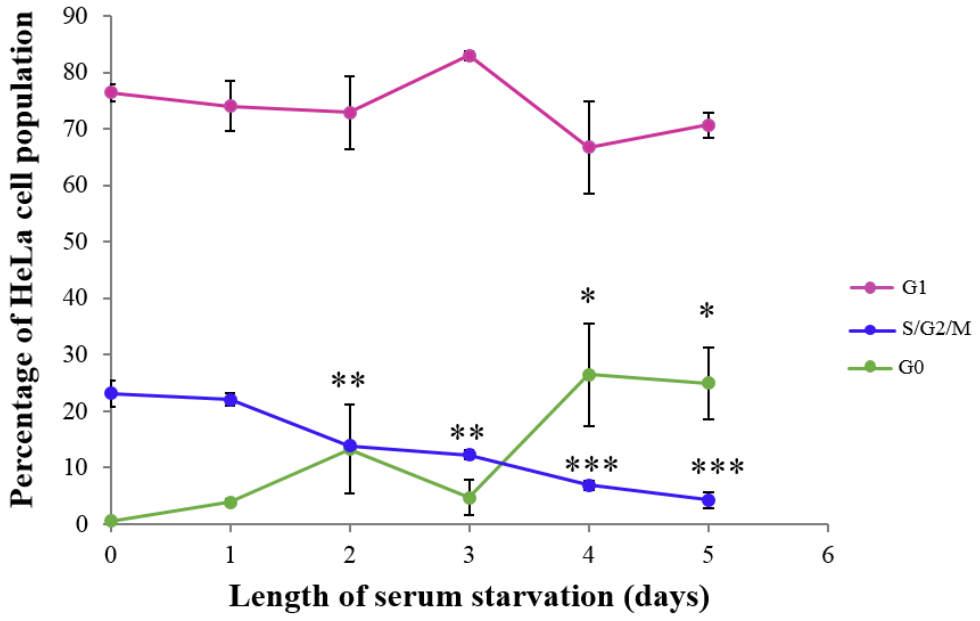

Figure 3.13 Quantitative measurement of the proportion of S/G2/M and G0 or G1 subpopulations over five-day serum starvation in HeLa cells

HeLa cells were grown in 10% FCS medium (proliferating) or 0.1% FCS medium (starved) for 5 days. The proportion of S/G2/M, G1 and G0 cell subpopulations was determined as a percentage of the total HeLa viable cell population over the five-day serum starvation time-course. Cells were stained with viability stain; Zombie NIR, DNA stain; Hoechst and RNA stain; Pyronin Y. Dead cells were excluded from the whole cell population. The proportion of S/G2/M, G1 and G0 cell subpopulations were calculated by Flow cytometry depending on DNA and RNA contents using FACsDIVA software. Cells were classed G1 if they exhibited single DNA content and were RNA positive, cells were classed S/G2/M if they exhibited double DNA content and were RNA positive while cells were classed G0 if they exhibited single DNA content and were RNA negative. Quantitative measurements of the proportions of G0 and S/G2/M cells were significantly changed with serum starvation. The percentage of G0

cells was significantly increased by ~ 4934 %, (P = 0.0236*) and 4661%, (P = 0.0364*) in day four and day five of serum starvation time course respectively compared to proliferating. The percentage of S/G2/M cells was significantly decreased by ~ 40 % (P = 0.0084**), ~46% (P = 0.0037**) , 70% (P = 0.0003***) and 81% (P = 0.0004***) in day two, day three, day four and day five of serum starvation time course respectively compared to proliferating. There were no significant changes in the percentage of G1 cells over the five-day serum starvation time-course (P > 0.999) n= 10,000. N=4.

	Viability (%)	G0 cells (%)	G1 cells (%)	S/G2/M cells (%)
Proliferating	82.63±3.82	0.52± 0.33	76.37±1.52	23.1±2.4
D1	73±7.042 P =0.2588	3.9 ± 0.55 P = 0.9999	74.02±4.43 (P > 0.999)	22.07±1.02 P= 0.1208
D2	71.46±7.85 P = 0.4921	13.3±7.86 P =0 .3675	72.87± 6.42 (P > 0.999)	13.82±0.55 P = 0.0084
D3	68.1±2.152 P = 0.1930	4.72±3.11 P =0.9802	82.97±0.83 (P > 0.999)	12.3± 0.89 P = 0.0037
D4	51.26±7.85 P= 0.0662	26.43±9.16 P = 0.0236	66.7±8.13 (P > 0.999)	6.86±0.77 P = 0.0003
D5	35.85±2.05 P = 0.0078	25 ± 6.345 P = 0.0264	70. 7± 2.22 (P > 0.999)	4.3± 1.385 P = 0.0004

Table 3.4 Flow cytometry data of HeLa cells viability and subpopulations over the five-day serum starvation time course (Means ± SEM)

3.3.2 Two day-serum starvation time course was sufficient to arrest NIH 3T3cells in G0/G1 phase

In NIH 3T3 cells, serum starvation markedly affected the cell viability at day five as seen previously (Figure 3.4 and Figure 3.5.C) and to do staining for flow cytometry analysis, cells pass through many steps of washing and staining. Therefore, it was not possible to do flow cytometry analysis to D5 cells as viable cells was too few to be detected.

Flow cytometry viability analysis over the four-day serum starvation time course showed that the percentage of viable cells was significantly decreased in D4 (33.46 ± 1.56 %) compared to proliferating (59.2 ± 0.617%) by ~ 43.5%, (P= 0.001) (Figure 3.14 and Table 3.5). This result is in consistent with the previously observed decrease in cell viability at D4 in NIH 3T3 cells detected by trypan blue viability staining (Section 3.2.2) where cell viability was significantly decreased at D4.

In consistence to inhibition of proliferation observed previously, the percentage of G0 cells was significantly increased in D1 by ~ 1092 % (39.36±17.84%, P = 0.0262), D2 by ~ 1529% (53.7±14.3%, P = 0.0002), D3 by ~1622% (56.8±20.9%, P = 0.0002) and D4 by ~ 1437% (50.7±21.07%, P = 0.0003) compared to proliferating (3.23 ± 0.5131%) (Figure 3.15, Figure 3.16 and Table 3.5).

Parallel to this increase in G0 cells, the percentage of G1cells was significantly decreased in D1 by ~ 34.5 % (50.8±16%, P = 0.059), D2 by ~ 51.5%, (37.6 ± 8.6%, P = 0.0035), D3 by ~57% (33.5 ± 9.1%, P = 0.0024) and D4 by ~ 48% (40.9 ± 9 %, P = 0.0038) compared to proliferating (77.7 ± 3.4%) (Figure 3.15, Figure 3.16 and Table 3.5).

Similarly, the percentage of cells in S, G2, M phases (S/G2/M (+ve) cells was significantly decreased in D1 by ~ 48 % (9.8±2%, P= 0.041), D2 by ~ 52% (8.9±1.2%, P = 0.037), D3 by ~47% (9.9±2.8%, P = 0.0412) and D4 by ~52% (9.1 ± 1.6%, P = 0.0321) compared to proliferating (19 ± 4.1 %) (Figure 3.15, Figure 3.16 and Table 3.5).

A new class of cells, S/G2/M (-ve) cells, appeared with serum starvation, these cells have double DNA content and very low RNA content. Though these S/G2/M (-ve) cells appeared with serum starvation but it did not show any significant changes. At D1 (1.3 ± 0.3 %), D2

(2.6 ± 1.4%), D3 (1.3 ± 0.9%) and D4 (1.43 ± 0.43 %), proliferating (0.05 ± 0.001%) (All P>0.05) (Figure 3.15, Figure 3.16 and Table 3.5).

These results showed that two-day serum starvation was sufficient to induce cell cycle arrest in G0/G1 phase where ~ 92 % of viable cells were in G0/G1 phase (~54% in G0 and 38% in G1 phase).

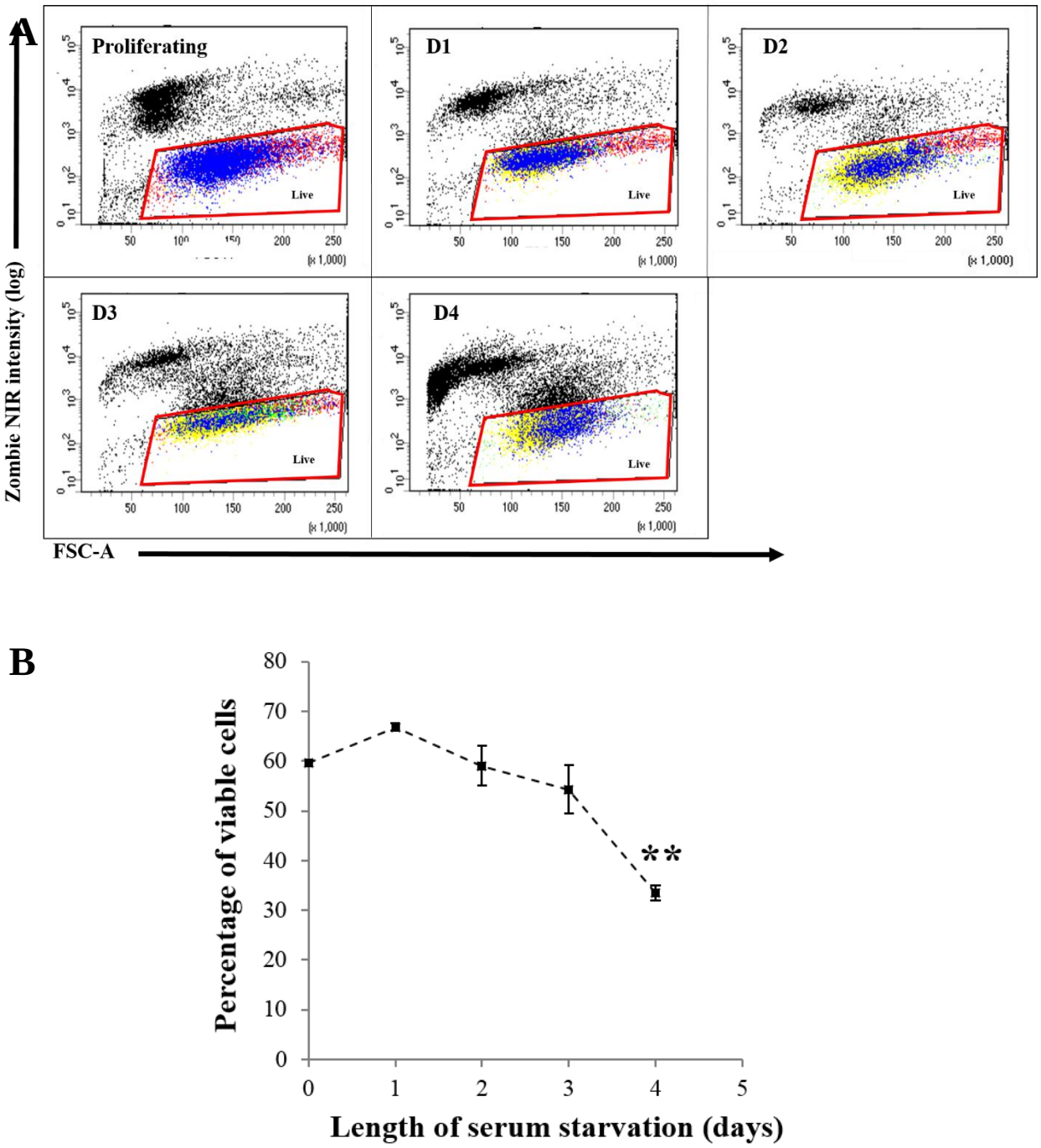

Figure 3.14 Cell viability over four-day serum starvation time-course in NIH 3T3 cells

NIH 3T3 cells were grown in 10% FCS medium (proliferating) or 0.1% FCS medium (starved) for 4 days. A) Dot plots of flow cytometric analysis performed on NIH 3T3 cells stained with viability stain; Zombie NIR. D1, D2, D3and D4 represent one day, two days, three days and four days of serum starvation. FSC-A represents forwards scatter area. Each

dot appearing on the dot plot represents a single cell. The proportion of viable cells were detected by Flow cytometry based on strength of fluorescence signal. The dot plots showing distribution of two cell populations represents the dead cells (black dots outside live gate; red box) that exhibit significant Zombie NIR fluorescence signal, and live cells (coloured dots within the live gate; colour code is shown in the next figure; Figure 3.15) which do not. The number of viable cells appeared to be decreased over the 4-day serum starvation time course. **B)** Graph shows quantitative measurements of the proportion of live cells as a percentage of total NIH 3T3 cells population. The percentage of viable cells was significantly decreased by 43.5% in D4 compared to proliferating (P = 0.001**). n= 10,000. N= 3.

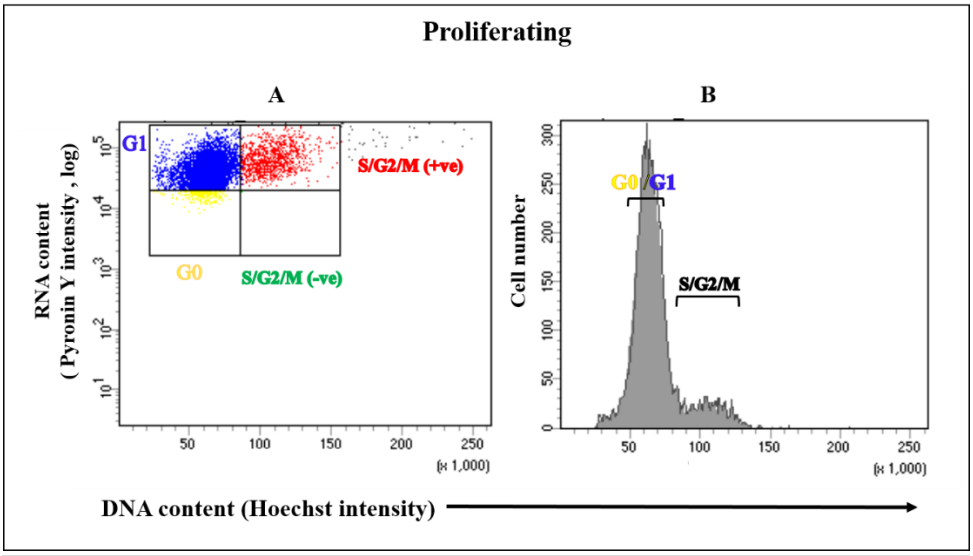
Proliferating
A
B
RNA content
(Pyronin Y intensity , log)
G1
S/G2/M (+ve)
G0
S/G2/M (-ve)
Cell number
G0/G1
S/G2/M
(x 1,000)
DNA content (Hoechst intensity)

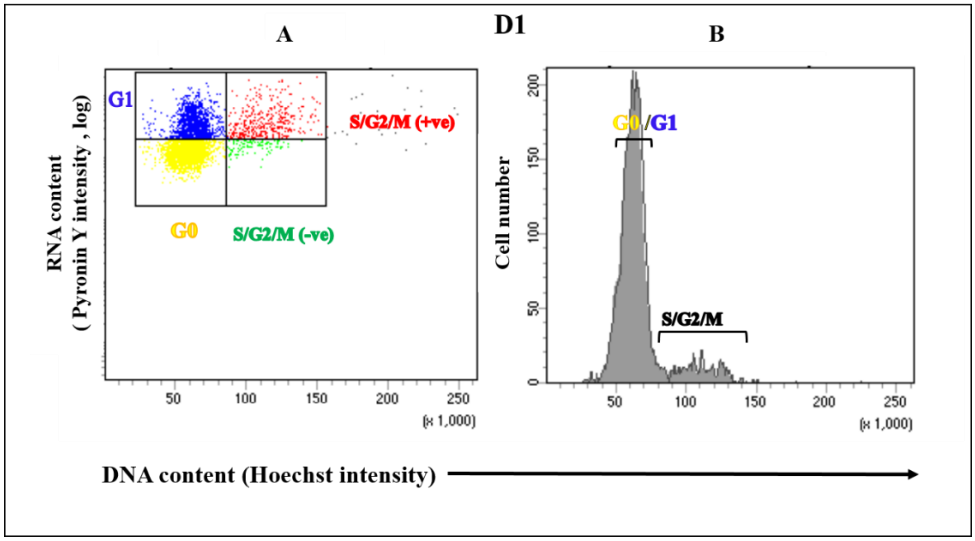
D1
A
B
RNA content
(Pyronin Y intensity , log)
G1
S/G2/M (+ve)
G0
S/G2/M (-ve)
Cell number
G0/G1
S/G2/M
(x 1,000)
DNA content (Hoechst intensity)

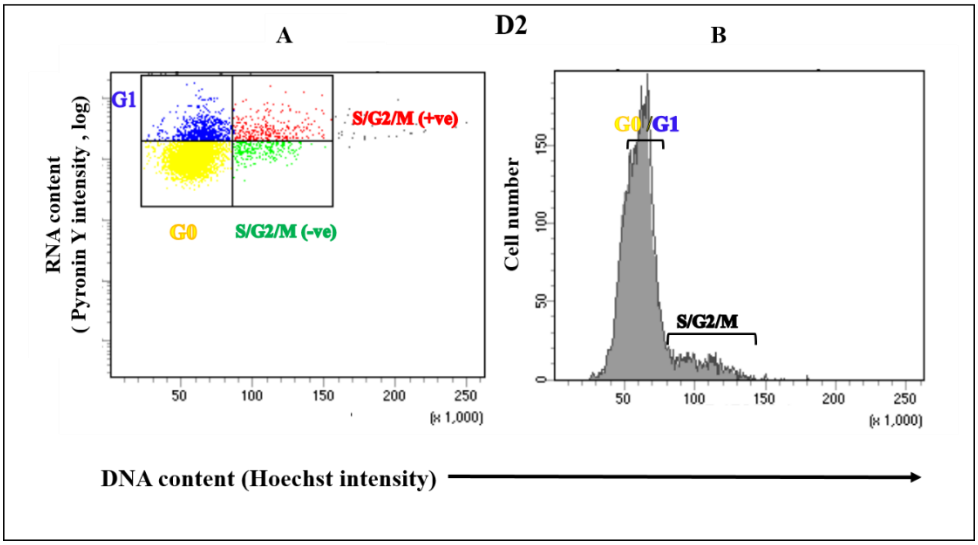
D2
A
B
RNA content
(Pyronin Y intensity , log)
G1
S/G2/M (+ve)
G0
S/G2/M (-ve)
Cell number
G0/G1
S/G2/M
(x 1,000)
DNA content (Hoechst intensity)

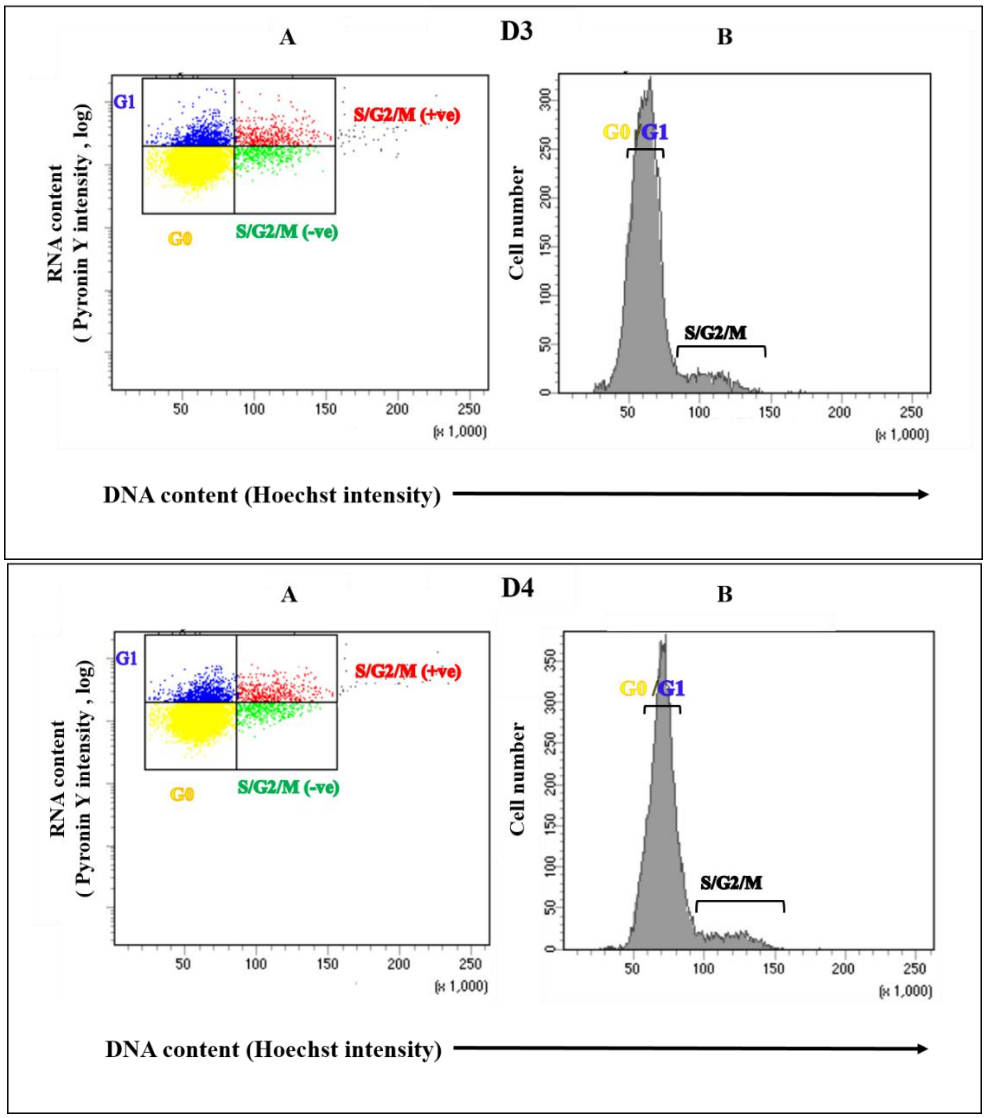

Figure 3.15 Four-day serum starvation time-course changes the proportion of S/G2/M, G1 and G0 subpopulations in NIH 3T3 cells

NIH 3T3 cells were grown in 10% FCS medium (proliferating) or 0.1% FCS medium (starved) for 4 days; D1, D2, D3 and D4 represent one day, two days, three days and four days of serum starvation. **A)** Flow cytometry plots of NIH 3T3 cells stained with viability stain; Zombie NIR, DNA stain; Hoechst and RNA stain; Pyronin Y. Dead cells were excluded from the whole cell population (Figure 3.). The proportions of cells in S phase, G2 phase and M phase (S/G2/M), cells in G1 phase and cells in G0 phase were detected by Flow cytometry based on DNA and RNA contents using FACsDIVA software. Cells were classed G1 if they exhibited single DNA

content and were RNA positive (blue dots), cells were classed S/G2/M (+ve) if they exhibited double DNA content and were RNA positive (red dots) and cells were classed G0 if they exhibited single DNA content and were RNA negative (yellow). Another group of cells appear with serum starvation exhibit double DNA content and were RNA negative S/G2/M (-ve) (green dots). Each dot represents a single cell. A difference in distribution of dots in S/G2/M (+ve) (red), G1 (blue), G0 (yellow) and S/G2/M (-ve) (green) gates is obvious over the 4-day serum starvation time-course compared to control. The extent of G1 cells and S/G2/M (+ve) cells appear to be decreased while the extent of G0 cells and S/G2/M (-ve) appear to be increased over the 4-day serum starvation time-course compared to proliferating. **B)** Histogram of NIH 3T3 cells stained with Hoechst stain shows cell cycle analysis according to DNA content. There is an increase in cell number of G0/G1 and a decrease in cell number of S/G2/M over the 4-day serum starvation time-course compared to proliferating. n= 10,000. N=3.

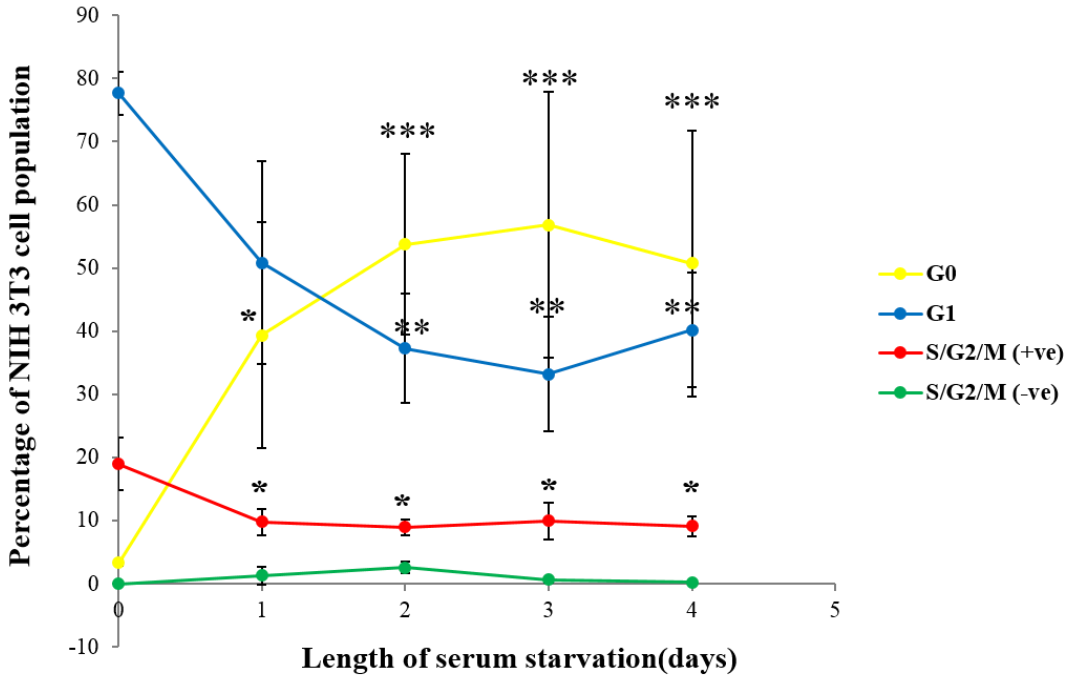

Figure 3.16 Quantitative measurement of the proportion of S/G2/M and G0 or G1 subpopulations over four-day serum starvation in time course in NIH 3T3 cells

NIH 3T3 cells were grown in 10% FCS medium (proliferating) or 0.1% FCS medium (starved) for 4 days. The proportion of S/G2/M, G1 and G0 cell subpopulations was determined as a percentage of the total NIH 3T3 viable cell population over the four-day serum starvation time-course. The proportion of S/G2/M, G1 and G0 cell subpopulations was determined as a percentage of the total NIH 3T3 viable cell population. Cells were stained with viability stain; Zombie NIR, DNA stain; Hoechst and RNA stain; Pyronin Y. Dead cells were excluded from the whole cell population. The proportion of S/G2/M, G1 and G0 cell subpopulations were calculated by Flow cytometry based on DNA and RNA contents using FACs DIVA software. Cells were classed G1 if they exhibited single DNA content and were RNA positive, cells were classed S/G2/M (+ve) if they exhibited double DNA content and were RNA positive, cells were classed S/G2/M (-ve) if they exhibited double DNA content and were RNA negative and cells were classed G0 if they exhibited single DNA content and were RNA negative. Quantitative measurements of the proportions of G0 and G1 cells were significantly changed with serum starvation. The percentage of G0 cells was significantly increased by 1092.92% ($P = 0.0262$*), 1529% ($P < 0.001$***), 1622% ($P < 0.001$***) and 1437% ($P < 0.001$***) in day one, day two, day three and day four of serum starvation

respectively compared to proliferating cells. The percentage of G1 cells was significantly decreased by 51.5 %, 57%, and 48% in day two, day three and day four of serum starvation respectively compared to proliferating (All P <0.01**). The percentage of S/G2/M (+ve) cells was decreased by 44.73%, 52.80%, 26.49 % and 25.78 % in day one, day two, day three and day four of serum starvation respectively compared to proliferating however the decrease was not significant. The percentage of S/G2/M (-ve) cells was not significantly different compared to proliferating (P > 0.05) n= 10,000. N=4.

	Viability (%)	G0 Cells (%)	G1 Cells (%)	S/G2/M (+ve) Cells (%)	S/G2/M (-ve) Cells (%)
Proliferating	59.2± 0.61	3.2 ± 0.5131	77.7 ± 3.431	19 ± 4.139	0
D1	66.8±0.731 P = 0.2588	39.36±17.84 P = 0.0262	50.83±16.09 P = 0.059	9.8±2.05 P= 0.041	1.3 ± 0.305 P = 0.7108
D2	59.06 ± 3.98 P = 0.9921	53.76±14.37 P = 0.0002	37.66 ± 8.68 P = 0.0035	8.96±1.234 P = 0.037	2.6 ± 1.47 P = 0.166
D3	54.3 ± 4.79 P = 0.9930	56.83±20.99 P = 0.0002	33.53 ± 9.11 P = 0.0024	9.96±2.88 P = 0.0412	0.6 ± 0.929 P = 0.7108
D4	35.4 ± 1.56 P = 0.001	50.73±21.07 P = 0.0003	40.9 ± 9.06 P = 0.0038	9.1 ± 1.60 P = 0.0321	0.26±0.437 P = 0.6368

Table 3.5 Flow cytometry data of NIH 3T3 cells viability and subpopulations over four-day serum starvation time course (means ± SEM)

3.3.3 Five day-serum starvation time course did not arrest hTERT RPE-1 cells in G0/G1 phase

Flow cytometry cell cycle analysis of hTERT RPE-1 cells was also done before and over 5-day serum starvation time course.

The percentage of viable cells was not significantly decreased in serum starved cells. At day one (74.2 ± 6.7%), day two (66.03 ± 4.7 %), day three (72.7 ± 9.4 %), day four (76.33 ± 7.26 %) and day five (66.8 ± 4.4 %) compared to proliferating (82.63 ± 9.4 %) ($P > 0.999$) (Figure 3.17 and Table 3.6). This result is in consistent with the previously observed results in cell viability detected by trypan blue.

Similarly, cell subpopulations did not show any significant changes over the 5-day serum starvation time course. For G0 cells, day one (1.06±4%), day two (1.6±1.7%), day three (3.7 ± 2.7%) and day four (2.9 ± 2.8%) and day five (3 ± 1.6%) compared to proliferating (1.1± 0.54%) ($P > 0.05$) (Figure 3.18, Figure 3.19 and Table 3.6).

For G1 cells, day one (80.7 ± 3.8%), day two (87.9 ± 2.6%), day three (82 ± 2.2%), day four (85.2±1.3%) and day five (83±0.9%) compared to proliferating (80 ± 3.8%) ($P > 0.05$). For S/G2/M cells, day one (17.1 ± 1.6%), day two (11 ± 4.8%), day three (14± 0.9%), day four (10.9±1.9%) and day five (14.7±0.12%) compared to proliferating (17 ± 0.5%) ($P > 0.05$) (Figure 3.18, Figure 3.19 and Table 3.6)

These result indicating that serum starvation did not induce cell cycle arrest in G0/G1 phase in hTERT RPE-1 even following five or more days of starvation.

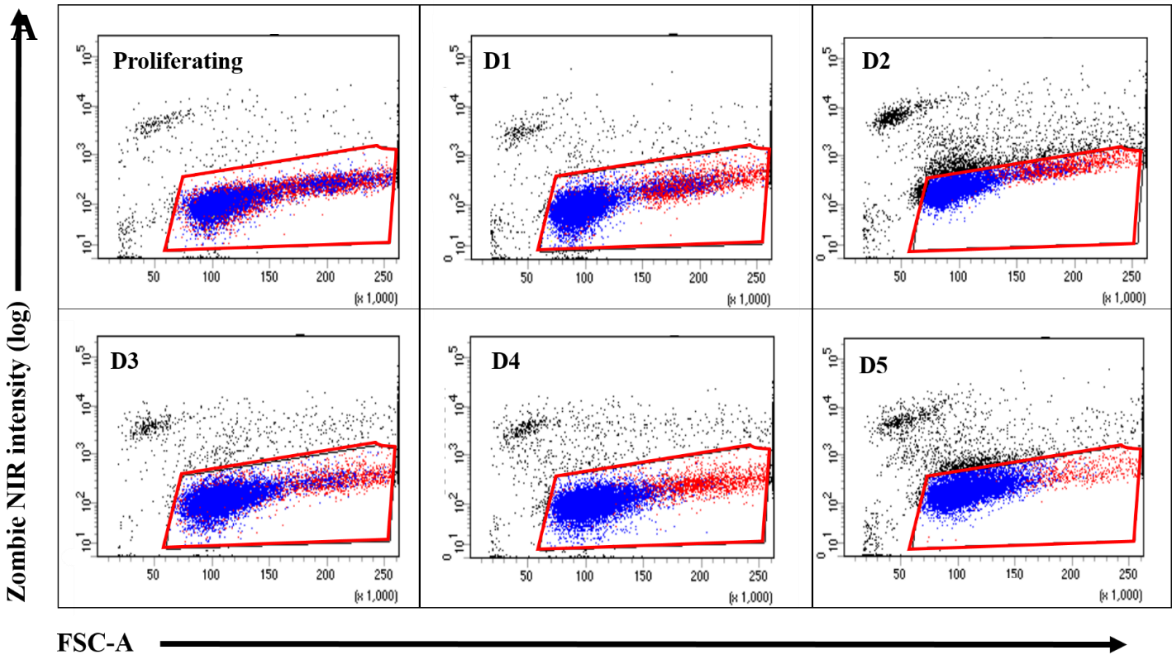

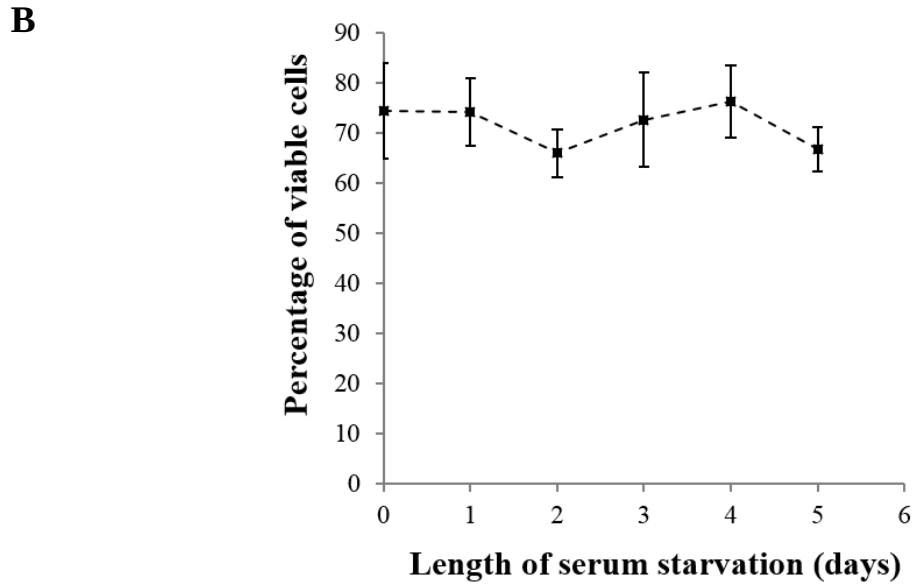

Figure 3.17 5-day serum starvation time-course does not affect the viability of RPE-1 cells

RPE-1 cells were grown in 10% FCS medium (proliferating) or 0.1% FCS medium (starved) for 5 days. A) Dot plots of flow cytometric analysis performed on RPE-1 cells stained with viability stain; Zombie NIR. D1, D2, D3, D4 and D5 represent one day, two days, three days, four and five days of serum starvation. FSC-A represents forwards scatter area. Each dot

appearing on the dot plot represents a single cell. The proportion of viable cells were detected by Flow cytometry based on strength of fluorescence signal. The dot plots showing distribution of two cell populations represents the dead cells (black dots outside live gate; red box) that exhibit significant Zombie NIR fluorescence signal, and live cells (coloured dots within the live gate; colour code is shown in the next figure; Figure 3.18) which do not. The number of viable cells appeared to be unaltered over the 5-day serum starvation time course. B) Graph shows quantitative measurements of the proportion of live cells as a percentage of total RPE-1 cells population. The percentage of viable cells was not significantly changed over the 5-day serum starvation time-course compared to proliferating (All $P>0.999$) n= 10,000. N= 3.

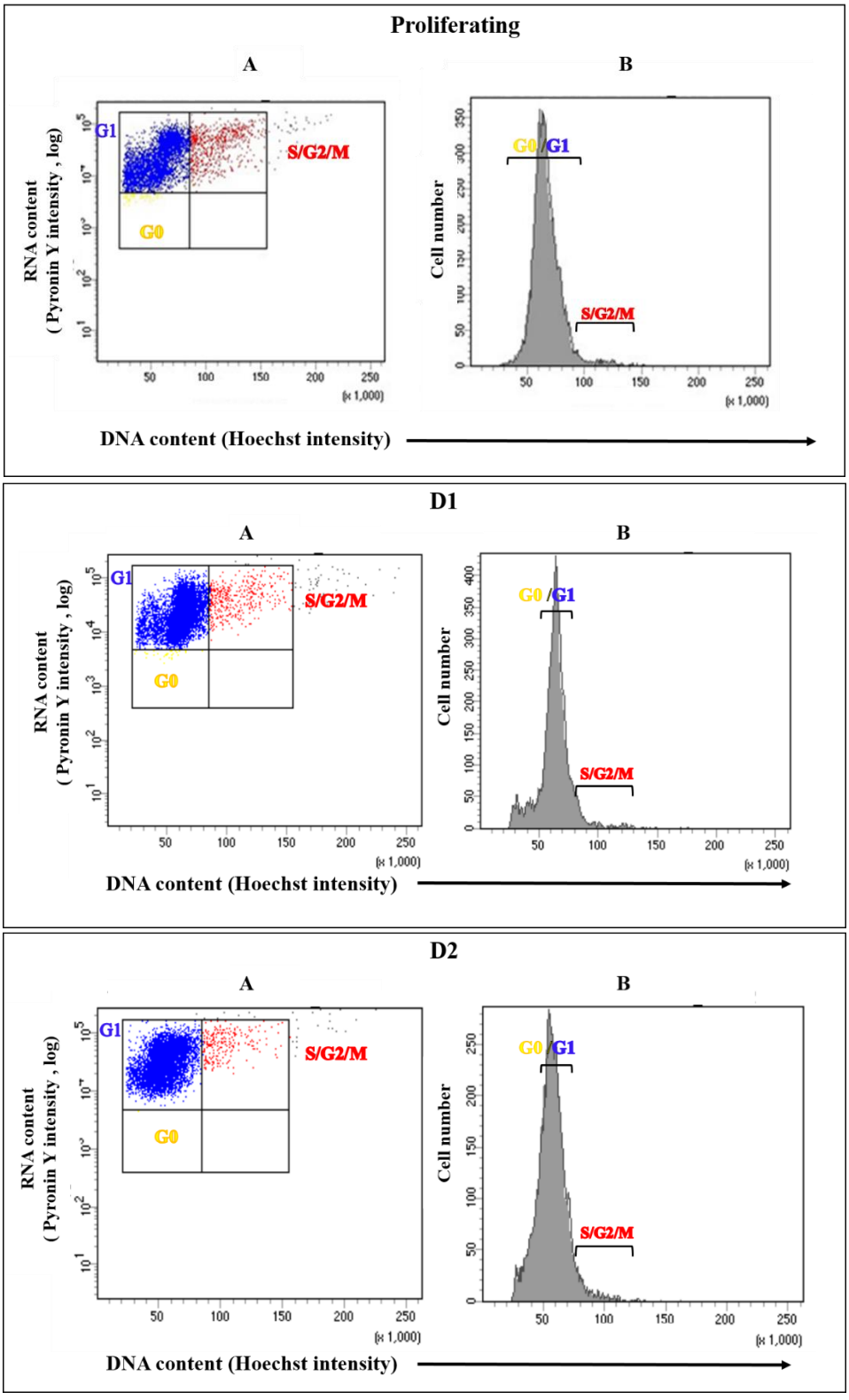
Proliferating
A
B
RNA content
(Pyronin Y intensity , log)
G1
S/G2/M
G0
Cell number
G0 /G1
S/G2/M
(x 1,000)
DNA content (Hoechst intensity)
D1
A
B
RNA content
(Pyronin Y intensity , log)
G1
S/G2/M
G0
Cell number
G0 /G1
S/G2/M
(x 1,000)
DNA content (Hoechst intensity)
D2
A
B
RNA content
(Pyronin Y intensity , log)
G1
S/G2/M
G0
Cell number
G0 /G1
S/G2/M
(x 1,000)
DNA content (Hoechst intensity)

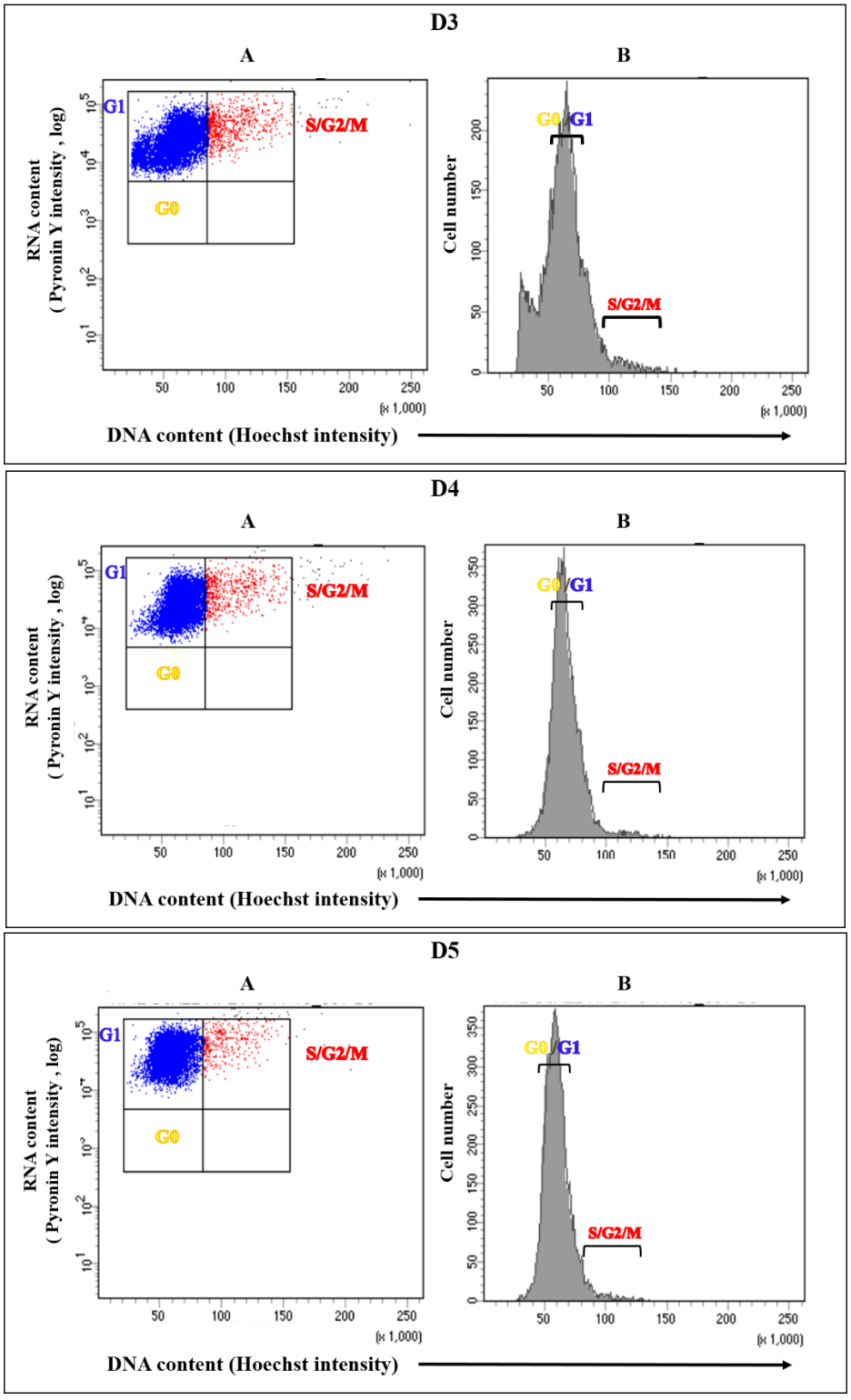

Figure 3.18 Five day serum starvation time-course does not affect the proportion of S/G2/M, G1 and G0 subpopulations in RPE-1 cells

RPE-1 cells were grown in 10% FCS medium (proliferating) or 0.1% FCS medium (starved) for 5 days; D1, D2, D3, D4 and D5 represent one day, two days, three days, four and five days of serum starvation. **A)** Flow cytometry plots of RPE-1 cells stained with viability stain; Zombie NIR, DNA stain; Hoechst and RNA stain; Pyronin Y. Dead cells were excluded from the whole cell population (Figure.1). The proportions of cells in S phase, G2 phase and M phase (S/G2/M), cells in G1 phase and cells in G0 phase were detected by Flow cytometry based on DNA and RNA contents using FACs DIVA software. Each dot represents a single cell. Cells were classed G1 if they exhibited single DNA content and were RNA positive (blue dots), cells were classed S/G2/M if they exhibited double DNA content and were RNA positive (red dots) and cells were classed G0 if they exhibited single DNA content and were RNA negative (yellow dots). The plots show that no cells enter G0 phase over the 5-day serum starvation time course. A difference in distribution of dots in G1 (blue) and S/G2/M (red) gates is not obvious over the 5-day serum starvation time-course compared to control. B) Histogram of RPE-1 cells stained with Hoechst stain showing DNA content distribution. There is no obvious change in the number of cells in different cell cycle phases over the 5-day serum starvation time-course compared to proliferating. n= 10,000. N=3.

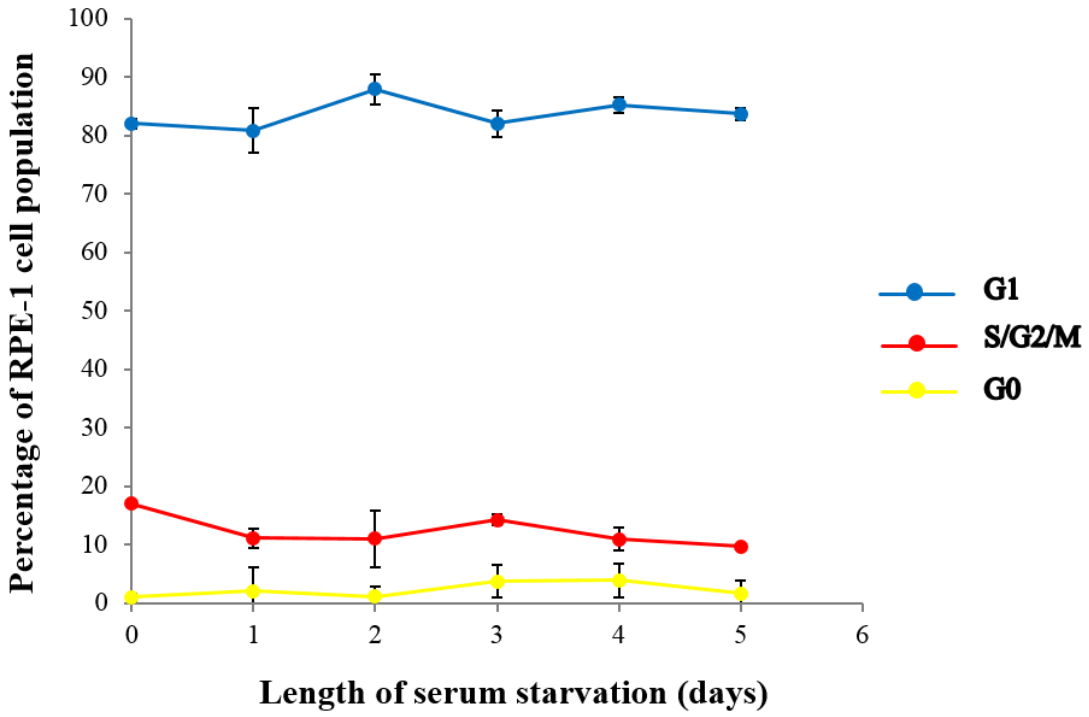

Figure 3.19 Quantitative measurement of the proportion of S/G2/M and G0 or G1 subpopulations over five-day serum starvation time course RPE-1 cells

The proportion of S/G2/M, G1 and G0 cell subpopulations was determined as a percentage of the total RPE-1viable cell population over the five-day serum starvation time-course. Cells were stained with viability stain; Zombie NIR, DNA stain; Hoechst and RNA stain; Pyronin Y. First, dead cells were excluded from the whole cell population to avoid false positive results then the proportion of S/G2/M, G1 and G0 cell subpopulations were calculated by Flow cytometry depending on DNA and RNA contents using FACsDIVA software. Cells were classed G1 if they exhibited single DNA content and were RNA positive, cells were classed S/G2/M if they exhibited double DNA content and were RNA positive while cells were classed G0 if they exhibited single DNA content and were RNA negative. Quantitative measurements show no significant changes occurred in the percentage of the G0 ($P = 0.9065$), G1 ($P = 0.6539$) or

S/G2/M (P = 0.7439) subpopulation over the five-day serum starvation time-course compared to proliferating. All n= 10,000. N= 3.

	Viability (%) (All P > 0.999)	G0 cells (%) (All P > 0.05)	G1 cells (%) (All P > 0.05)	S/G2/M cells (%) (All P > 0.05)
Proliferating	59.2 ± 0.617	1.167± 0.54	82.03 ± 0.84	17 ± 0.53
D1	74.26 ± 6.70	1.06 ± 4.03	80.77 ± 3.83	17.16±1.64
D2	66.03±4.712	1.63 ± 1.73	87.9 ± 2.62	11 ± 4.84
D3	72.7 ± 9.454	3.7 ± 2.75	82.06± 2.26	14.24±0.91
D4	76.33±7.263	2.93 ± 2.83	85.21±1.33	10.93±1.91
D5	66.80 ± 4.4	3 ± 1.6	83.67±0.97	14.73±0.12

Table 3.6 Flow cytometry data of hTERT RPE-1 cells viability and subpopulations over five day serum starvation time course (means ± SEM)

	HeLa cells		NIH 3T3 cells		hTERT RPE-1 cells (All P > 0.999)	
	Trypan blue	**Zombie NIR**	**Trypan blue**	**Zombie NIR**	**Trypan blue**	**Zombie NIR**
Proliferating	96.18±0.72	82.63±3.82	81.63±13.31	59.2 ± 0.617	97.43±1.32	82.03 ± 0.84
D1	94.53±1.5 (P= 0.9959)	73±7.042 P =0.2588	84.93±6.4 P = 0.8821	66.8±0.731 P = 0.2588	83.73± 13.09	80.77 ± 3.83
D2	92.03± 3.31 (P= 0.8188)	71.46±7.85 P = 0.4921	72.16± 2.2 P = 0.4236	59.06 ± 3.98 P = 0.9921	87.23± 5.61	87.9 ± 2.623
D3	86.6± 4.88 (P = 0.1578)	68.1±2.152 P = 0.1930	63.46± 3.52 P = 0.0912	54.3 ± 4.79 P = 0.9930	94.13 ± 0.37	82.06± 2.26
D4	74.07 ± 1.04 (P = 0.0579)	51.26±7.85 P= 0.0662	40.3 ± 4.1 (P< 0.01)	35.4 ± 1.56 P = 0.001	94.86 ± 1.8	85.21±1.33 P = 0.781
D5	67.5 ± 1.7 (P = 0.0335)	35.85±2.05 P = 0.0078	23.3 ± 5.23 (P< 0.001)		96.63 ± 0.96	83.67±0.977

Table 3.7 A comparison between cell viability data obtained from Trypan blue dye and Zombie NIR dye

3.4 Discussion

Serum starvation is a well-known experimental method to induce cell cycle arrest in the quiescent G0/G1 phase in mammalian cells (Langan and Chou, 2011; Xiong *et al.*, 2012). However, the duration of serum starvation to induce cell cycle arrest in G0/G1 phase was variable in various cell types and even within the same cell type. Previous studies have shown that duration of serum starvation to induce cell cycle arrest in G0/G1 phase was one day in RBL cells (Bodding, 2001; Tani *et al.*, 2007), two days in HeLa cells (Xiong *et al.*, 2012), in mouse embryonic fibroblast cells (Cooper, 2003) and porcine fibroblasts (Kues *et al.*, 2000) and three days in foreskin fibroblasts (Kim *et al.*, 2008) and HeLa S3 cells (Matsumura *et al.*, 1990). Furthermore, in NIH 3T3 cells, there was a controversy in the duration of serum starvation required to induce cell cycle arrest in G0/G1; it has been reported as 24hours (Cooper, 2003), 30hours (Nishikura and Murray, 1987) and 48 hours (Kerkhoff and Rapp, 1997).

Therefore, in the present study, serum starvation was carried out in order to induce HeLa, NIH 3T3 and hTERT RPE-1 cells to arrest in G0/G1 phase. The morphological and flowcytometry data were collected each day of starvation in order to determine the minimum time of serum starvation required to induce cell cycle arrest in the three cell types.

Total and mitotic cell count and cell viability have been shown to be indicatives of quiescent G0/G1 cell cycle arrest under serum starvation conditions, as cessation of growth and division are the fundamental features of quiescence (Kerkhoff and Rapp, 1997; Kues *et al.*, 2000). Hence, in the present study, total and mitotic cell count and cell viability were detected in HeLa, NIH 3T3 and hTERT RPE-1 cells with serum starvation.

Following 2 days of serum starvation, in HeLa cells, there was a significant decrease in the total cell number as well as mitotic cell number in starved cells compared to proliferating controls (Figure 3.2.A**Figure**). By day 4 of serum starvation ~1% of cells were in mitosis and the proportion of mitotic cells did not change following 5 or more days of serum starvation (Table 3.1 and Figure 3.2.A) **Figure 3.**. In NIH 3T3 cells, following one day of serum starvation there was a significant decrease in the total cell number as well as mitotic cell number in starved cells compared to proliferating controls. By 3 days of serum starvation less than ~ 0.5% of cells were in mitosis and the proportion of mitotic cells did

not change following 4 or more days of serum starvation (Table 3.2 and Figure Figure 3.5.A). In contrast, hTERT RPE-1 cells showed no changes in total and mitotic cell number with 5-day serum starvation (Table 3.3 and Figure 3.8.A).

Cell viability was also analysed to investigate whether the significant decrease in total and mitotic cell number with serum starvation in HeLa and NIH 3T3 cells is attributed to cell cycle arrest in G0/G1 or cell death. Cell viability when evaluated with a well-known viability stain trypan blue was decreased by ~ 21% in HeLa cells at day five of serum starvation (Figure 3.2.C) and markedly decreased by ~70% in NIH 3T3 cells at day four and five of serum starvation (Figure 3.5.C) while in hTERT RPE-1 cells, there was no change in cell viability over the five-day serum starvation time course (Figure 3.8.C).

These results indicated that serum starvation induced cell cycle arrest in HeLa and NIH 3T3 cells, as the cell proliferation was significantly inhibited without any significant effect on cell viability till day four in HeLa cells and day three in NIH 3T3 cells.

Results also showed that serum starvation did not alter cell proliferation or viability of hTERT RPE-1 cells and this observation was also reported by others (Jiang *et al.*, 1999; Liang *et al.*, 2012).

To further define the cell cycle arrest in G0/G1 phase of HeLa, NIH 3T3 and hTERT RPE-1 cells under serum starvation conditions and to detect the extent of G0 cells contributing to this phase, flow cytometry experiments measuring the cellular DNA and RNA content were performed. Measuring DNA and RNA content has been used for separation of G0 and G1 cells (Shapiro, 1981; Darzynkiewicz *et al.*, 2011) as G0 cells were identified as the population with single DNA content and an RNA content lower than that in cells in S and G2/M phases (Crissman *et al.*, 1985; Lemons *et al.*, 2010).

Before gating cells according to their DNA and RNA content, dead cells were excluded using a fluorescent viability dye; Zombie NIR (Figure 3.10). Both trypan blue dye and fluorescent Zombie NIR dye showed that cell viability was significantly decreased at day five in HeLa, at day four in NIH3T3 cells and was not altered in RPE-1 cells (Table 3.7). However, data obtained using trypan blue dye showed overestimation of cell viability compared to that obtained from flow cytometry analysis. On the basis of cell counts obtained using the flow cytometry analysis, in HeLa cells, ~ 45 % of the cells were viable at day five whereas cell viability was estimated at ~75% on the basis of cell counts obtained using the trypan blue dye. Similarly, in NIH 3T3 cells, data obtained from flow

cytometry analysis showed that ~ 33% the cells were viable at day four while with trypan blue staining viable cells were ~ 41% (Table 3.7). This observation has been reported by others (Altman *et al.*, 1993). The over estimation of cell viability by trypan blue may be due, possibly, to its insensitivity to nonviable cells, to the nature of the test and/or to the condition that cell counts be made rapidly following addition of the dye.

Flow cytometry cell cycle analysis revealed that, in HeLa cells, G0 cells increased in a multi-step manner which peaked and became significant at day four of serum starvation (~26%). A corresponding gradual significant decrease in S/G2/M cells was observed from day two (~ 13%) peaked at day four (~ 6.5%) of serum starvation while no significant changes detected in G1 cells (Figure 3.13 and Table 3.4).

In NIH 3T3 cells, the alteration in the profile of distribution of cell populations with serum starvation was somewhat different, G0 cells increased significantly in a gradual manner which peaked at day two of serum starvation (~ 52%). A parallel decrease in G1 was observed from first day of starvation (~34.5%) and peaked at day two (~ 40%) and a significant decrease in S/G2/M cells was detected from day one (~9%) (Figure 3.16 and Table 3.5)

It noteworthy that a new class of cells appeared with serum starvation in NIH 3T3 cells, these cells exhibit double DNA content and were very low RNA content (Figure 3.15). This observation suggests, at least in part, that cells exhibit different quiescent states and/or quiescence could not only be a prolonged pause in G0 or early G1 but also a state of distinct gene expression changes that may occurred in cells in all phases in response to serum deprivation.

These results so far clearly showed that the minimum period of serum starvation required to induce cell cycle arrest in G0/G1 phase was 4 days in HeLa cells and 2 days in NIH 3T3 cells.

In contrast to HeLa and NIH 3T3 cells, the cell subpopulations and cell viability in hTERT RPE-1 cells did not change in response to serum starvation suggesting that serum starvation did not induce cell cycle arrest in hTERT RPE-1cells. This result has also been observed by others (Jiang *et al.*, 1999; Liang *et al.*, 2012).

In hTERT RPE-1cells, the percentage of G0, G1 and S/G2/M cells were not significantly different compared to proliferating after 5 days of serum starvation. Furthermore, by using

the fluorescent Zombie NIR dye, cell viability was not altered over the 5-day serum starvation time course which confirming that results showed by using trypan blue dye. As previously observed in HeLa and NIH 3T3 cells, the trypan blue dye showed overestimation of cell viability compared to the results obtained from using fluorescent Zombie NIR dye (Table 3.7).

Jiang et al., 1999 showed that 3-day serum starvation did not affect cell viability and that hTERT RPE-1 cells exhibited normal growth rate under serum deprivation conditions. In addition, Liang et al, 2012 observed, by using flow cytometry cell cycle analysis, that 2-day serum starvation did not induce cell cycle arrest in hTERT NP cells and that overexpression of hTERT protect against serum starvation-induced apoptosis. Here this starvation was extended to 5 days and this was still insufficient to cause any arrest. These previous observations along with the results obtained in the present study might be explained by the fact that overexpression of telomerase reverse transcriptase in hTERT RPE-1 cells protects against apoptosis as hTERT helps to restore the DNA base pairs lost from the telomeres during cell division therefore extends their replicative lifespan beyond senescence.

In summary, these results revealed that the sufficient duration of serum starvation to induce cell cycle arrest in G0/G1 phase was four days in HeLa cells and two days in NIH 3T3 cells, whilst five days of serum starvation did not induce any cell cycle changes in hTERT RPE-1 cells. Hence, hTERT RPE-1cells was used as a control for HeLa and NIH 3T3 cells in order to investigate Ca^{2+} signalling responses that were specific to cell cycle arrest in G0/G1 phase.

On the basis of these findings, it was determined that when preparing G0/G1 arrested HeLa cells four-day serum starvation time course would be used throughout the remainder of this thesis. Similarly, for NIH 3T3 cells, two-day serum starvation time course would be used in order to prepare cells in G0/G1phase. For hTERT RPE-1 cells, however, four-day and two-day serum starvation time course were used for the remainder of this thesis to correspond with the duration of serum starvation selected for HeLa and NIH 3T3 cells respectively.

3.5 Conclusions

- In HeLa cells, four days of serum starvation induced G0/G1 cell cycle arrest shown by inhibition of proliferation and increase in the percentage of G0 cells which occurred in a multistep manner.
- In NIH 3T3 cells, two days of serum starvation induced G0/G1 cell cycle arrest shown by inhibition of proliferation and increase in the percentage of G0 cells which occurred in a gradual manner.
- In hTERT RPE-1 cells, serum starvation did not induce G0/G1 cell cycle arrest as neither inhibition of cell proliferation nor increase in the percentage of G0 cells were detected till five days of starvation.

Chapter 4 Store-Operated Ca^{2+} Entry (SOCE)

4.1 Introduction

SOCE is a major Ca^{2+} entry pathway involved in cell cycle progression in non-excitable cells whereby external Ca^{2+} enters cells via SOCs located on the PM in response to depletion of ER Ca^{2+} stores (Introduction 1.6). In this study, serum starvation induced cell cycle arrest in G0/G1 phase (increase in percentage of cells in G0/G1 phase) in HeLa cells (93%) and in NIH 3T3 cells (92%) but not in hTERT RPE-1 cell (Chapter 4). The aim of this chapter is to investigate SOCE responses in HeLa and NIH 3T3 when the cell cycle is arrested in quiescent G0/G1 phase by serum starvation and to make a comparison to hTERT RPE-1cells.

Cells were grown in 10% FCS medium (proliferating) or in 0.1% FCS medium (G0/G1). To measure SOCE, cells were loaded with the Ca^{2+} sensitive fluorescent indicator dye fura-2/AM, which enabled continuous measurement of cytosolic Ca^{2+}. Loaded cells, maintained in Ca^{2+}-free buffer, were then treated with TG in order to deplete ER Ca^{2+} stores. TG binds to and inhibits the SERCA pump located on the ER membrane causing a leak of Ca^{2+} from the ER into the cytosol. Depletion of ER Ca^{2+} stores activate SOCE whereby external Ca^{2+} enters the cytosol in order to replenish depleted stores. The addition of Ca^{2+} to the Ca^{2+} -free buffer, in what is termed an 'add-back' experiment, enabled the measurement of Ca^{2+} influx and therefore the activity of the SOCE pathway.

4.2 Results- SOCE

4.2.1 SOCE was markedly down-regulated in G0/G1 HeLa cells

HeLa cells were grown in 10% FCS medium (proliferating) or in 0.1% FCS medium (G0/G1) for 4 days, the time point at which the cells were arrested in G0/G1 phase (chapter 4). Then Ca^{2+} 'add-back' experiments were done to measure SOCE in proliferating and G0/G1 cells.

Typical Ca^{2+}-addback traces from 6 individual cells within one experiment were chosen randomly to show various profiles of single cell Ca^{2+} signals (Figure 4.1.A). As expected,

HeLa Ca^{2+}-addback traces from proliferating cells showed differences in the level of SOCE responses which are not observed in traces of G0/G1 HeLa cells (Figure 4.1.A). This might be explained by the fact that the proliferating cells were not synchronised; cells exist in different cell cycle phases and therefore giving a mixed pattern of Ca^{2+} responses while G0/G1 cells were synchronised; > 90% of cells in G0/G1 phase (Section 3.3.1).

Mean Ca^{2+}-addback traces from proliferating and G0/G1 HeLa cells indicated that both Ca^{2+} store release in response to TG addition (200nM) and SOCE following the addition of $CaCl_2$ (2mM) appeared to be reduced in G0/G1 cells compared to proliferating cells (Figure 4.1.B).

In order to quantify Ca^{2+} entry into the cell cytosol the area from under TG and $CaCl_2$ responses was calculated from calibrated fluorescence traces (Method 2.8). Area under peak (AUP) was presented in graphs as mean ± SEM of n determinations (Figure 4.2.A).

Total Ca^{2+} store release (TG response) was significantly down-regulated in G0/G1 HeLa cells by ~ 35% (48.8 ± 1.596 FRUs) compared to proliferating cells (75.38 ± 2.082 FRUs), $P<0.0001$ (Figure 4.2.A). SOCE ($CaCl_2$ response) following store depletion was also significantly down-regulated in G0/G1 HeLa cells by ~ 60% (184.8 ± 5.512 FRUs) compared to proliferating cells (451 ± 12.9 FRUs), $P<0.0001$. Therefore, cell cycle arrest of HeLa cells in G0/G1 phase is accompanied by down-regulation of Ca^{2+} store release suggesting a potential decrease in the size of the ER Ca^{2+} store and/or a decreased sensitivity to TG.

The extent of down regulation of SOCE (~ 60%) accompanied by cell cycle arrested was far more than that of Ca^{2+} store release (~ 35%) indicating an uncoupling of SOCE from Ca^{2+} store release.

These data were further confirmed by analysing maximal (as opposed to total) Ca^{2+} store release and maximal SOCE, using measurements of height of peak (HOP) of TG and $CaCl_2$ responses from calibrated fluorescence traces (Method 2.8), HOP was presented in graphs as mean ± SEM of n determinations (Figure 4.2.B). Consistent with the decrease in total Ca^{2+} store release and SOCE, maximal Ca^{2+} store release was significantly down-regulated in G0/G1 HeLa cells by ~ 40% (0.196 ± 0.006 FRUs) compared to proliferating cells (0.329 ± 0.008 FRUs), $P<0.0001$. Maximal SOCE was significantly down-regulated in G0/G1 HeLa cells by ~ 37% (0.403 ± 0.008 FRUs) compared to proliferating cells (0.64 ± 0.015 FRUs), $P<0.0001$ (Figure 4.2.B).

Rate of rise (reflecting the speed of Ca^{2+} store release and activation of SOCE) and rate of decline (reflecting the speed of Ca^{2+} store emptying and deactivation of SOCE) of TG and $CaCl_2$ responses respectively from calibrated fluorescence traces (Method 2.8) were also analysed. Rate of Ca^{2+} store release was significantly decreased in G0/G1 HeLa cells by ~ 48% (1.68± 0.5 $\times 10^{-3}$ FRUs) compared to proliferating cells (3.25± 0.1$\times 10^{-3}$ FRUs), P<0.0001. Rate of SOCE was significantly decreased in G0/G1 HeLa cells by ~ 80 % (5.5$\times$ 10^{-3} ± 0.0001 FRUs) compared to proliferating cells (5.897 ± 11.64 × 10^{-5} FRUs), P = 0.0229 (Table 4.1).

Decline rate of Ca^{2+} store release was significantly increased in G0/G1 HeLa cells by ~ 48% (29.46 ± 12.47 × 10^{-5} FRUs) compared to proliferating cells (3.25$\times 10^{-3}$ ± 0.0001 FRUs), P<0.0001. Decline rate of SOCE was increased in G0/G1 HeLa cells by ~ 54 % (10.41 ± 8.093 × 10^{-5} FRUs) compared to proliferating cells (4.82 ± 5.02 × 10^{-5} FRUs), however this increase was not significant, P = 0.7484 (Table 4.1).

These findings suggest that cell cycle arrest in G0/G1 is associated with marked reduction of total Ca^{2+} store release and SOCE. Also, rate of Ca^{2+} store release and the SOCE activation were shortened thus both Ca^{2+} store release and SOCE responses are smaller and shorter in G0/G1cellls compared to proliferating.

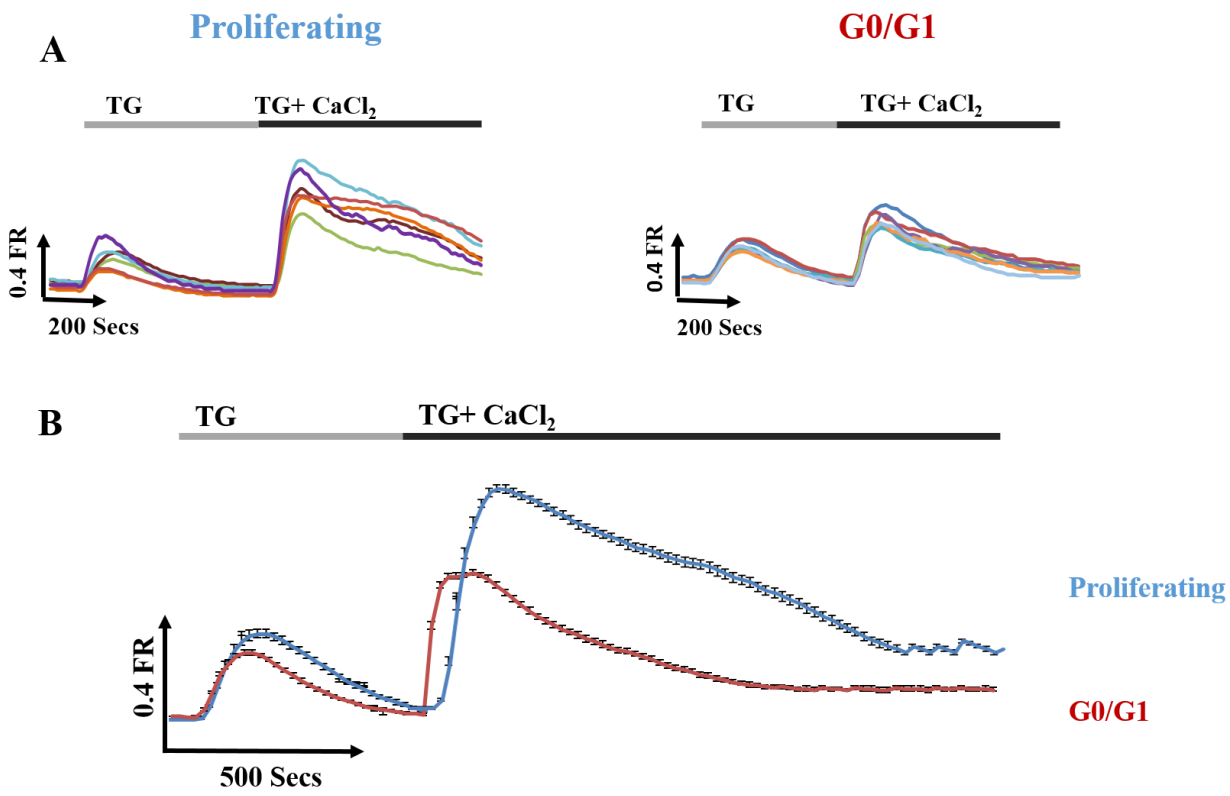

Figure 4.1 Single cell Ca^{2+} signal traces changes in G0/G1 HeLa cells

HeLa cells were grown for 5 days in 10% FCS medium (proliferating) or in 0.1% FCS medium (G0/G1). TG represents the addition of the SERCA inhibitor thapsigargin to induce Ca^{2+} store release and $CaCl_2$ represents Ca^{2+} addition to the Ca^{2+} free buffer to induce SOCE. **A)** Typical Ca^{2+}-addback traces from 6 individual cells within one experiment in proliferating and G0/G1 cells show variability in Ca^{2+} responses in proliferating compared to G0/G1 cells. **B)** Mean Ca^{2+} addback traces from proliferating (blue) and G0/G1 cells (red). Traces represent an average from 60 cells ± S.E.M from one experiment. Fura-2 fluorescence was measured at excitation wavelengths of 340 nm and 380 nm and an emission wavelength of 510 nm, with changes in fluorescence ratio (FR) reflect changes in $[Ca^{2+}]_i$. Addition of thapsigargin (TG, first peak) caused increase in FR in proliferating and G0/G1 cells indicating increase in $[Ca^{2+}]_i$ as Ca^{2+} is depleted from ER stores. Following Ca^{2+}-addback ($CaCl_2$, second peak) an increase in FR occurred, as Ca^{2+} enters the cytosol via SOCE to replenish depleted stores. Both Ca^{2+} store release and SOCE responses appear to be reduced in G0/G1 cells compared to proliferating cells.

		Total		Maximal		ROR		ROD	
		Values (FRUs)	**% change**	**Values (FRUs)**	**% change**	**Values ($FRUs \times 10^{-3}$)**	**% change**	**Values ($\times 10^{-5}$ FRUs)**	**% change**
Ca^{2+} store release	Proliferating	75.38± 0.08	------	0.32±0.008	------	3.25± 0.1	------	5.897 ±1.64	------
	G0/G1	48.8 ± 1.59 (P<0.0001)	- 35%	0.196±0.006 (P<0.0001)	- 40%	1.68± 0.5 (P<0.0001)	- 48%	29.46±2.47 (P<0.0001)	400%
SOCE	Proliferating	451 ± 12.9	------	0.64 ±0.015	------	7.9± 0.4	------	4.82 ±5.02	------
	G0/G1	184.8±5.51 (P<0.0001)	- 60%	0.403±0.008 (P<0.0001)	- 37%	5.5± 0.1 (P =0.0229)	- 30%	12.81±9.37 (P=0.7484)	165%

Table 4.1 Summary of quantifications of Ca^{2+} store release and SOCE responses in HeLa cells

The total response (area under the peak, AUP), maximal response (the height of peak, HOP), rate of rise (ROR) and rate of decline (ROD) for TG and $CaCl_2$ responses from calibrated fluorescence traces were calculated using Excel functions in a template spread sheet (Methodology chapter 2.8, figure 2.10) in proliferating and G0/G1 HeLa cells. Data represented as means ± SEM. FRUs (fluorescence ratio unit). For proliferating cells n =228 and for G0/G1cells n= 206. N=7.

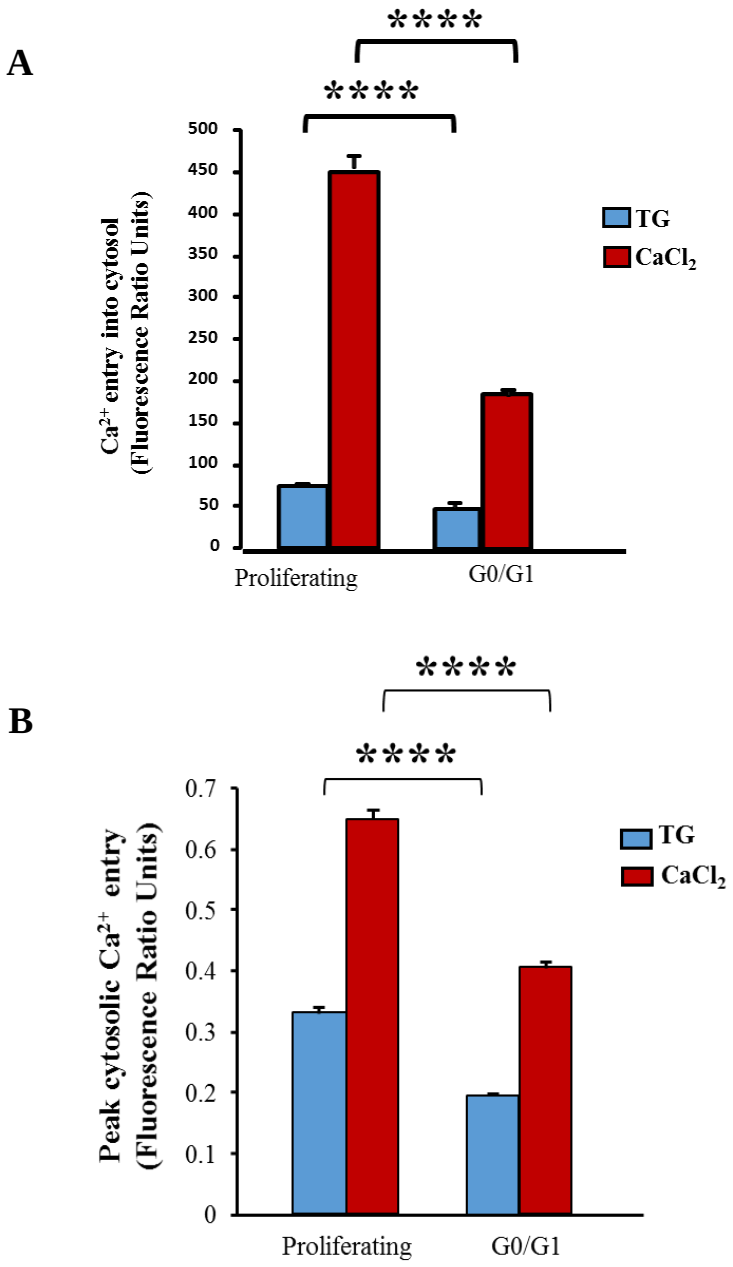

Figure 4.2 Ca^{2+} signals responses in HeLa cells

HeLa cells were grown in either 10% FCS medium (proliferating) or 0.1% FCS medium (G0/G1) for 4 days. **A)** Graph shows means of total Ca^{2+} entry into the cytosol following Ca^{2+} store release in response to stimulation with 200nM thapsigargin (TG) and subsequent SOCE following the addition of 2mM $CaCl_2$. Changes in fluorescence ratio units (FRUs) reflect changes in $[Ca^{2+}]_i$. Both total Ca^{2+} store release and SOCE were significantly reduced in G0/G1 cells compared to proliferating, P<0.0001****. **B)** Graph shows means of maximal

Ca^{2+} store release and maximal SOCE. Both maximal Ca^{2+} store release and SOCE were significantly reduced in G0/G1 cells compared to proliferating, P<0.0001****. Error bars represent S.E.M. For proliferating cells n =228 and for G0/G1cells n= 206. N=7.

4.2.2 SOCE was markedly down-regulated in G0/G1 NIH 3T3 cells

NIH 3T3 cells were grown in 10% FCS medium (proliferating) or in 0.1% FCS medium (G0/G1) for two days, the time point at which the cells were arrested in G0/G1 phase (chapter 4). Then Ca^{2+} 'add-back' experiments were done to measure Ca^{2+} store release and SOCE in proliferating and G0/G1 cells.

Typical Ca^{2+}-addback traces from 6 individual cells within one experiment were chosen randomly to show various profiles of single cell Ca^{2+} signals (Figure 4.3.A). As in HeLa cells, NIH 3T3 cells Ca^{2+}- addback traces from proliferating cells showed variations in level of Ca^{2+} responses which is not observed in traces of G0/G1 NIH 3T3 cells (Figure 4.3.A), this again might indicate that the proliferating cells exist in different cell cycle phases therefore generating varying Ca^{2+} responses while G0/G1 cells were synchronised; > 90% of cells in G0/G1 phase thus giving similar Ca^{2+} responses (Section 3.4.1).

Mean Ca^{2+}-addback traces from proliferating and G0/G1 NIH 3T3 cells indicated that both Ca^{2+} store release in response to TG addition (200nM) and SOCE following the addition of $CaCl_2$ (2mM) appeared to be reduced in G0/G1 cells compared to proliferating cells (Figure 4.3.B).

In order to quantify Ca^{2+} entry into the cell cytosol the area from under TG and $CaCl_2$ responses was calculated from calibrated fluorescence traces (see methodology section 2.8 for more details). Area under peak (AUP) was presented in graphs as mean ± SEM of n determinations (Figure 4.5.A).

Total Ca^{2+} store release (TG response) was significantly down-regulated in G0/G1 NIH 3T3 cells (10.55 ± 0.989 FRUs) compared to proliferating cells (46.4 ± 2.201 FRUs) by ~ 77%, $P<0.0001$ (Figure 4.5.A and Table 4.2). SOCE ($CaCl_2$ response) following store depletion was also significantly down-regulated in G0/G1 NIH 3T3 cells (32.49 ± 2.508) compared to proliferating cells (84.28 ± 3.826 FRUs) by ~ 61%, $P<0.0001$ (Figure 4.5.A and Table 4.2).

HOP (presenting maximal store release and SOCE) was shown in graphs as mean ± SEM of n determinations (Figure 3.5.B). Consistent with the decrease in total Ca^{2+} store release and SOCE, maximal Ca^{2+} store release was significantly down-regulated in G0/G1 NIH 3T3 cells (0.0428 ± 0.003 FRUs) compared to proliferating cells 0.12 ± 0.004 FRUs) by ~ 65%, $P<0.0001$. Maximal SOCE was significantly down-regulated in G0/G1 NIH 3T3 cells (0.15

± 0.011) compared to proliferating cells (0.24 ± 0.009 FRUs) by ~ 36%, P<0.0001 (Figure 4.5.B and Table 4.2).

Rate of Ca^{2+} store release was significantly decreased in G0/G1 NIH 3T3 cells (0.342 ± 0.024 $\times 10^{-3}$ FRUs) compared to proliferating cells (0.968 ± 0.047 $\times 10^{-3}$ FRUs) by ~ 65%, P = 0.0173. Rate of SOCE was not significantly different in G0/G1 NIH 3T3 cells (4.02 ± 0.511 $\times$ 10^{-3} FRUs) compared to proliferating cells (3.57 ± 0.28 $\times$ 10^{-3} FRUs), P = 0.813 (Table 4.2).

Decline rate of Ca^{2+} store release not significantly different in G0/G1 NIH 3T3 cells (5.22 ± 3.22 $\times 10^{-5}$ FRUs) compared to proliferating cells (13.35 ± 3.464 $\times$ 10^{-5} FRUs), P = 0.393. Decline rate of SOCE was increased in G0/G1 NIH 3T3 cells (5.76 ± 6.489$\times 10^{-5}$ FRUs) compared to proliferating cells (1.7 ± 9.172 $\times$ 10^{-5} FRUs) by ~ 70 %, however this increase was not significant, P = 0.5232 (Table 4.2).

These results revealed the cell cycle arrest of NIH 3T3 cells in G0/G1 phase is associated with down-regulation of both Ca^{2+} store release and SOCE suggesting a potential decrease in the size of the ER Ca^{2+} store and/or a decreased sensitivity to TG.

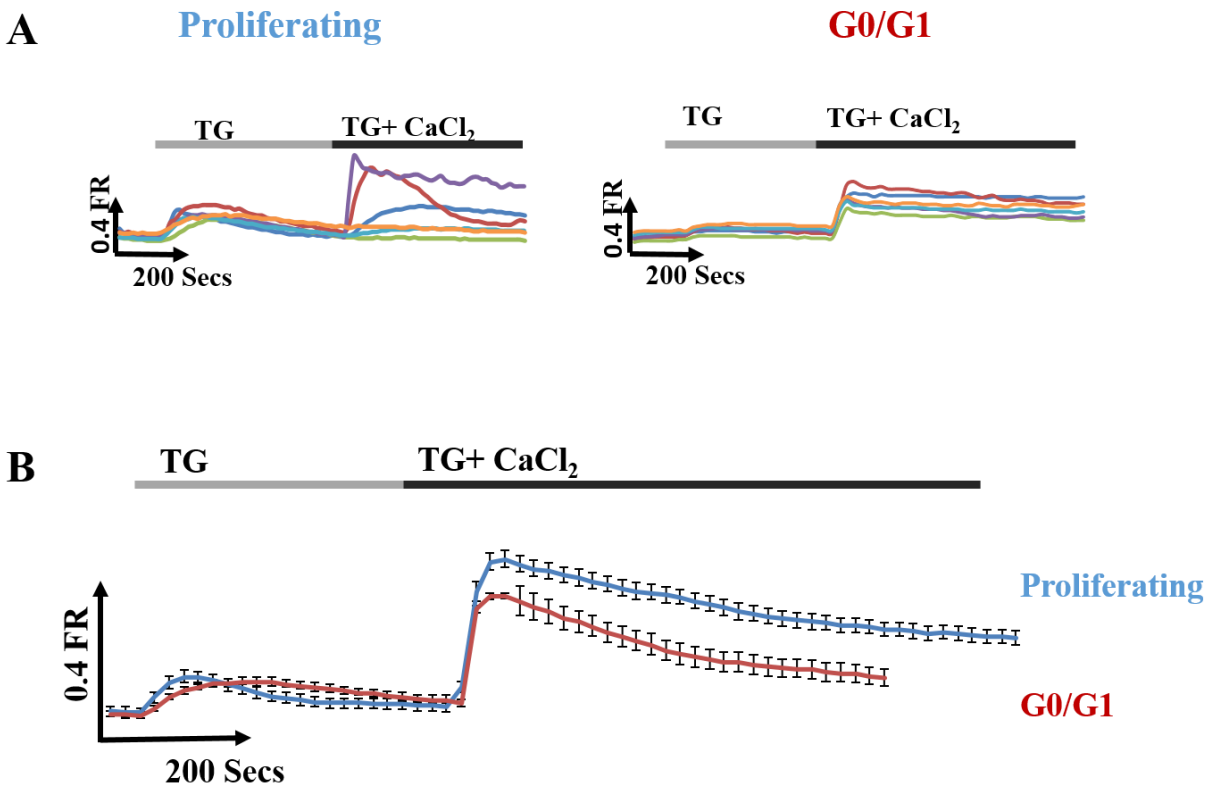

Figure 4.3 Single cell Ca^{2+} signal traces changes in G0/G1 NIH 3T3 cells

NIH 3T3 cells were grown for 3days in 10% FCS medium (proliferating) or in 0.1% FCS medium (G0/G1). TG represents the addition of the SERCA inhibitor thapsigargin to induce Ca^{2+} store release and $CaCl_2$ represents Ca^{2+} addition to the Ca^{2+} free buffer to induce SOCE. **A)** Typical Ca^{2+}-addback traces from 6 individual cells within one experiment in proliferating and G0/G1 cells show variability in Ca^{2+} responses in proliferating compared to G0/G1 cells. **B)** Mean Ca^{2+} addback traces from proliferating (blue) and G0/G1 cells (red). Traces represent an average from 60 cells ± S.E.M from one experiment. Fura-2 fluorescence was measured at excitation wavelengths of 340 nm and 380 nm and an emission wavelength of 510 nm, with changes in fluorescence ratio (FR) reflect of changes in $[Ca^{2+}]_i$. Addition of thapsigargin (TG, first peak) caused increase in FR in proliferating and G0/G1 cells indicating increase in $[Ca^{2+}]_i$ as Ca^{2+} is depleted from ER stores. Following Ca^{2+}-addback ($CaCl_2$, second peak) an increase in FR occurred, as Ca^{2+} enter the cytosol via SOCE to replenish depleted stores. Both store depletion and SOCE response appear to be reduced in G0/G1 cells compared to proliferating cells.

		Total		Maximal		ROR		ROD	
		Values (FRUs)	**% change**	**Values (FRUs)**	**% change**	**Values ($\times 10^{-3}$ FRUs)**	**% change**	**Values ($\times 10^{-5}$ FRUs)**	**% change**
Ca^{2+} store release	Proliferating	46.4 ± 2.20	------	0.12 ± 0.004	------	0.968±0.04	------	13.35±3.46	------
	G0/G1	10.55± 0.98 (P< 0.0001)	- 77**%**	0.0428 ± 0.003 (P< 0.0001)	- 65%	0.342±0.02 (P = 0.0173)	- 65%	5.22 ± 3.22 (P = 0.393)	-60%
SOCE	Proliferating	84.28±3.82	------	0.24 ± 0.009	------	3.57 ± 0.28	------	4.82 ± 9.172	------
	G0/G1	32.49±2.50 (P< 0.0001)	- 61**%**	0.15± 0.011 (P< 0.0001)	- 36%	4.02± 0.511 (P = 0.813)	- 13%	5.76± 6.489 (P= 0.5232)	25%

Table 4.2 Summary of quantifications of Ca^{2+} store release and SOCE responses in NIH 3T3 cells

The total response (area under the peak, AUP), maximal response (the height of peak, HOP), rate of rise (ROR) and rate of decline (ROD) for TG and $CaCl_2$ responses from calibrated fluorescence traces (Figure 4.3) were calculated using Excel functions in a template spread sheet (Methodology chapter 2.8, figure 2.10) in proliferating and G0/G1 NIH 3T3 cells. Data represented as means ± SEM. FRUs (fluorescence ratio unit). For proliferating cells n =249 and for G0/G1cells n= 128. N=5.

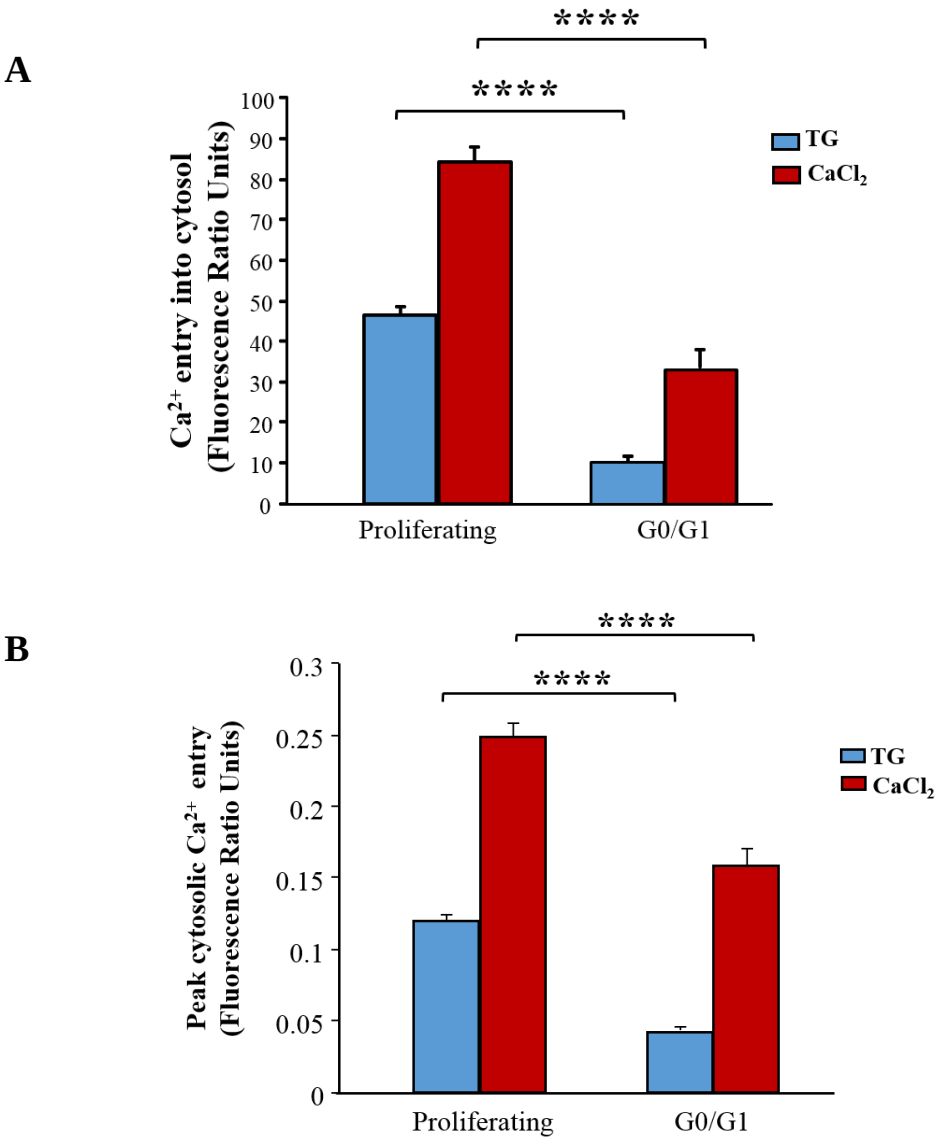

Figure 4.4 Ca^{2+} signals responses in NIH 3T3 cells

NIH 3T3 cells were grown in either 10% FCS medium (proliferating) or 0.1% FCS medium (G0/G1) for 2 days. **A)** Graph shows means of total Ca^{2+} entry into the cytosol following Ca^{2+} store release in response to stimulation with 200nM thapsigargin (TG) and subsequent SOCE following the addition of 2mM $CaCl_2$. Changes in fluorescence ratio units (FRUs) reflect changes in $[Ca^{2+}]_i$. Both total Ca^{2+} store release and SOCE were significantly reduced in G0/G1 cells compared to proliferating, P<0.0001****. **B)** Graph shows means of maximal Ca^{2+} store release and maximal SOCE. Both maximal Ca^{2+} store release and SOCE were significantly reduced in G0/G1 cells compared to proliferating, P<0.0001****. Error bars represent S.E.M. For proliferating cells n =249 and for G0/G1cells n= 128. N=5.

4.2.3 SOCE was slightly down-regulated in serum-starved hTERT RPE-1 cells

Serum starvation of hTERT RPE-1 cells did not affect cell cycle progression, consequently, did not induce cell cycle arrest in G0/G1 phase (Chapter 4). Therefore, Ca^{2+} signalling responses to serum starvation were investigated in hTERT RPE-1 cells in order to make a comparison with HeLa and NIH 3T3 cells to determine the level of contribution of cell cycle arrest in G0/G1 phase to the SOCE remodelling.

hTERT RPE-1 cells were grown in 10% FCS medium (proliferating) or in 0.1% FCS medium (serum-starved) for two time points, 2 days (D2 serum- starved) the time point at which NIH 3T3 cells were arrested in G0/G1 phase (Chapter 4) and 4 days (D4 serum-starved) the time point at which HeLa cells were arrested in G0/G1 phase (Chapter 4) in order to correspond with duration of serum starvation of each cell type to make a reliable comparison. Then Ca^{2+} 'add-back' experiments were done to measure SOCE in proliferating and serum- starved cells.

Typical Ca^{2+}-addback traces from 6 individual cells within one experiment were chosen randomly to show various profiles of single cell Ca^{2+} signals (Figure 1.5.A). As expected, hTERT RPE-1 cells Ca^{2+}-addback traces from D2 and D4 serum-starved cells showed differences in Ca^{2+} responses which is similar to that observed in traces of proliferating cells (Figure 4.5.A). This could be explained by the fact that serum starved cells were not synchronised; cells are in different cell cycle phases (Chapter 4) giving various levels of Ca^{2+} responses as that in proliferating.

Mean Ca^{2+}-addback traces from proliferating and D2 and D4 serum-starved cells indicated that both Ca^{2+} store release in response to TG addition (200nM) and SOCE following the addition of $CaCl_2$ (2mM) appeared to be slightly reduced in D2 and D4 serum-starved cells compared to proliferating cells (Figure 4.5.B).

In order to quantify Ca^{2+} entry into the cell cytosol the area from under TG and $CaCl_2$ responses was calculated from calibrated fluorescence traces (see methodology section 2.8 for more details). Area under peak (AUP) was presented in graphs as mean ± SEM of n determinations (Figure 4.6.A).

Total Ca^{2+} store release (TG response) was significantly down-regulated in D2 and D4 serum-starved cells (21.21 ± 1.043 FRUs) and (23.25± 0.933 FRUs) respectively compared to proliferating cells (38.89 ± 1.05 FRUs) by ~ 45% and ~ 40% respectively, $P<0.001$ (Figure

4.6). SOCE ($CaCl_2$ response) following store depletion was also significantly down-regulated in D2 and D4 serum-starved cells (52.88 ± 1.643 FRUs) and (46.58± 2.088 FRUs) compared to proliferating cells (61.21 ± 1.29 FRUs) by ~ 13.5 % and 23.5 %, P = 0.02638 and P = 0.01451 respectively (Figure 4.6.A and Table 4.3).

These results showed that an uncoupling of SOCE from Ca^{2+} store release with marked down-regulation of Ca^{2+} store release indicting a possible decrease in the size of the ER Ca^{2+} store and/or a decreased sensitivity to TG.

These data were further confirmed by analysing maximal (as opposed to total) Ca^{2+} store release and maximal SOCE, using measurements of height of peak (HOP) of TG and $CaCl_2$ responses from calibrated fluorescence traces (see methodology section 2.8 for more details), HOP was presented in graphs as mean ± SEM of n determinations (Figure 4.6.B). In consistent with the decrease in total Ca^{2+} store release and SOCE, maximal Ca^{2+} store release was significantly down-regulated in in D2 and D4 serum-starved cells (0.105 ± 0.007 FRUs) and (0.110 ± 0.004 FRUs) compared to proliferating cells (0.175 ± 0.003 FRUs) by ~ 39.5% and ~ 37.5%, all P<0.001. Maximal SOCE was significantly down-regulated in in D2 and D4 serum-starved cells (0.253 ± 0.005 FRUs) and (0.230± 0.009 FRUs) compared to proliferating cells (0.403± 0.008 FRUs) by ~ 37% and ~ 43% respectively, all P<0.01 (Figure 4.6.B and Table 4.3).

Rate of rise (reflecting the speed of Ca^{2+} store release and activation of SOCE) and rate of decline (reflecting the speed of Ca^{2+} store emptying and deactivation of SOCE) of TG and $CaCl_2$ responses respectively from calibrated fluorescence traces (see methodology section 2.8 for more details) were also analysed. Rate of Ca^{2+} store release was increased in D2 and D4 serum-starved cells (2.114 ± 0.258 $\times 10^{-3}$ FRUs) and (2.013± 0.262 $\times 10^{-3}$ FRUs) compared to proliferating cells (1.849 ± 0.08$\times 10^{-3}$ FRUs) by ~ 14% and ~ 9% respectively, however this increase was not significant, P = 0.471 and P = 0.562 respectively. Rate of SOCE was significantly decreased in D2 and D4 serum-starved cells (4.39 ± 0.327$\times 10^{-3}$ FRUs) and (4.601± 0.156 $\times 10^{-3}$ FRUs) compared to proliferating cells (6.479 ± 0.146$\times 10^{-3}$ FRUs) by ~ 32% and ~ 28 %, all P<0.0001 (Table 4.3).

Decline rate of Ca^{2+} store release was decreased in D2 and D4 serum-starved cells (14.15± 6.07$\times 10^{-5}$ FRUs) and (17.51± 5.08 $\times 10^{-5}$ FRUs) compared to proliferating cells (20.95 ± 7.5$\times 10^{-5}$ FRUs) by ~ 32% and ~ 16 %, P = 0.4317 and P = 0.8231 respectively. Decline rate of SOCE was increased in serum-starved cells (86.27±9.07$\times 10^{-5}$ FRUs) and (90.42 ±

10.06×10^{-5} FRUs) compared to proliferating cells ($133.7 \pm 11.9\times10^{-5}$ FRUs) by ~ 32% and ~ 16 %, P = 0.203 and P = 0.1953 respectively (Table 4.3).

The results so far showed that serum starvation induces marked down-regulation of SOCE in HeLa and NIH 3T3 cells and to a much lesser extent in hTERT RPE-1 suggesting a contribution of cell cycle arrest to the SOCE down-regulation.

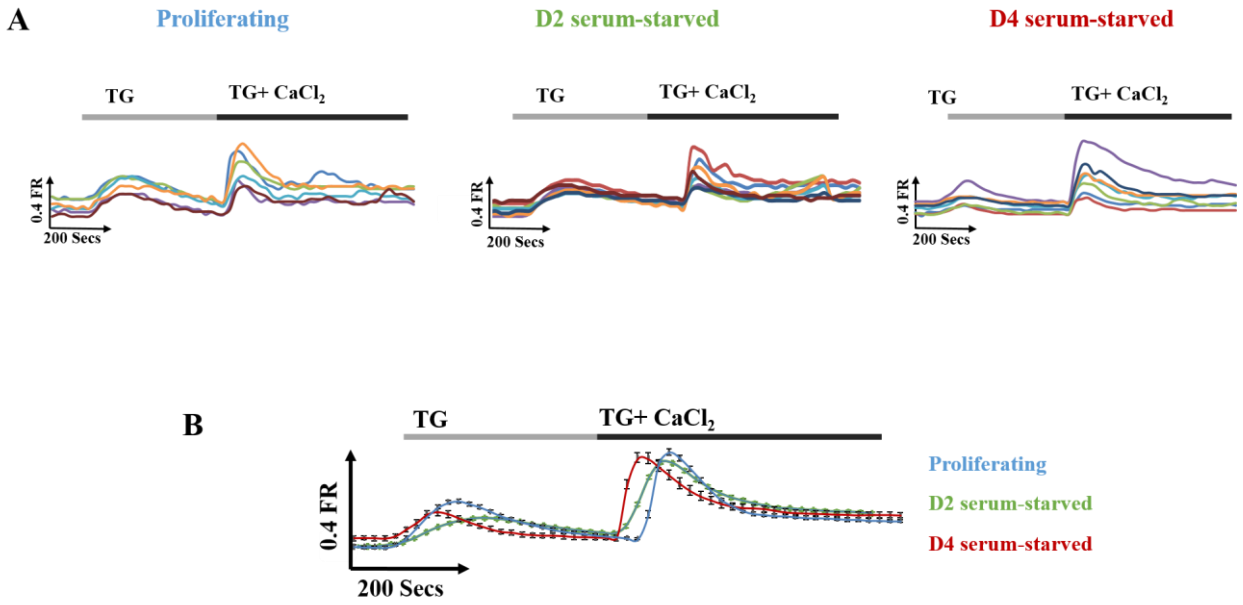

Figure 4.5 Single cell Ca^{2+} signal traces from hTERT RPE-1 cells

hTERT RPE-1 cells were grown in 10% FCS medium (proliferating) or in 0.1% FCS medium (serum- starved) for two time points, 2 days (D2 serum- starved) 4 days (D4 serum-starved). TG represents the addition of the SERCA inhibitor thapsigargin to induce Ca^{2+} store release and $CaCl_2$ represents Ca^{2+} addition to the Ca^{2+} free buffer to induce SOCE. A) Typical Ca^{2+}-addback traces from 6 individual cells within one experiment in proliferating, D2 serum- starved and D4 serum- starved exhibit variability in Ca^{2+} responses. **B)** Mean Ca^{2+} addback traces from proliferating (blue), D2 serum- starved (green) and D4 serum-starved (red). Traces represent an average from 60 cells ± S.E.M from one experiment. Fura-2 fluorescence was measured at excitation wavelengths of 340 nm and 380 nm and an emission wavelength of 510 nm, with changes in fluorescence ratio (FR) reflective of changes in $[Ca^{2+}]_i$. Addition of thapsigargin (TG, first peak) caused increase in FR indicating increase in $[Ca^{2+}]_i$ as Ca^{2+} is depleted from ER stores. Following Ca^{2+}-addback ($CaCl_2$, second peak) an increase in FR occurred, as Ca^{2+} enter the cytosol via SOCE to replenish depleted stores. Both store depletion and SOCE responses appear to be reduced in D2 serum-starved (green) and D4 serum-starved (red) cells compared to proliferating cells. However, the difference in SOCE response is minor.

		Total		Maximal		ROR		ROD	
		Values (FRUs)	**% change**	**Values (FRUs)**	**% change**	**Values($\times 10^{-3}$ FRUs)**	**% change**	**Values($\times 10^{-5}$ FRUs)**	**% change**
Ca^{2+} store release	Proliferating	38.89 ± 1.05	------	0.175 ± 0.003	------	1.849± 0.08	------	20.95 ± 7.5	------
	D2 serum-starved	21.21 ± 1.04 P < 0.001	- 45%	0.105± 0.007 P < 0.001	-39.5%	2.114±0.25 P = 0.471	14%	14.15± 6.07 P = 0.4317	-32%
	D4 serum-starved	23.25±0.93 P < 0.001	- 40%	0.11 ± 0.004 P<0.001	-37.5%	2.013±0.262 P = 0.562	9%	17.51± 5.08 P = 0.8231	-16%
SOCE	Proliferating	61.21 ± 1.29	------	0.403± 0.008	------	6.479 ± 0.146	------	133.7 ± 11.9	------
	D2 serum-starved	52.88 ± 1.64 P = 0.02638	-13.5%	0.25 ± 0.005 P<0.01	-37%	4.39 ± 0.327 P < 0.01	-32%	86.27±9.07 P = 0.203	-35%
	D4serum-starved	46.58± 2.088 P = 0.01451	- 23.5%	0.230± 0.009 P<0.01	-43%	4.601±0.156 P < 0.001	- 28%	90.42±10.06 P = 0.1953	-32%

Table 4.2 Summary of quantifications of Ca^{2+} store release and SOCE responses in hTERT RPE-1 cells

The total response (area under the peak, AUP), maximal response (the height of peak, HOP), rate of rise (ROR) and rate of decline (ROD) for TG and $CaCl_2$ responses from calibrated fluorescence traces (**Figure 4.5**) were calculated using Excel functions in a template spread sheet (Methodology

chapter 2.8, figure 2.10) in proliferating, D2 serum-starved and D4 serum-starved cells. Data represented as means ± SEM. FRUs (fluorescence ratio unit). For proliferating cells n = 211, D2 serum-starved n = 195 and D4 serum-starved n = 196, N=4.

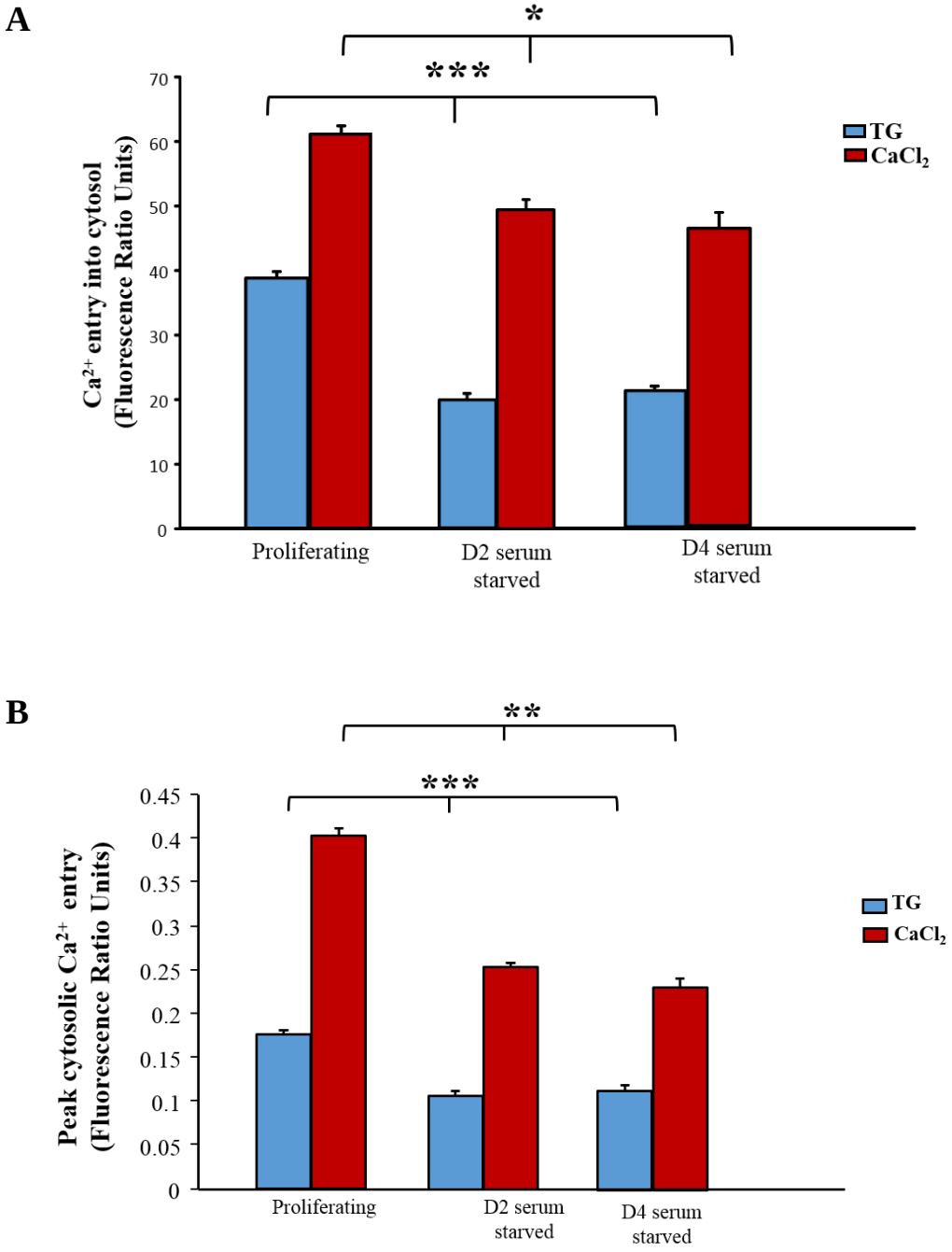

Figure 4.6 Ca^{2+} signals responses in hTERT RPE-1 cells

hTERT RPE-1 cells were grown in 10% FCS medium (proliferating) or in 0.1% FCS medium (serum- starved) for two time points, 2 days (D2 serum- starved) 4 days (D4 serum-starved). **A)** Graph shows means of total Ca^{2+} entry into the cytosol following Ca^{2+} store release in response to stimulation with 200nM thapsigargin (TG) and subsequent SOCE following the addition of 2mM $CaCl_2$. Changes in fluorescence ratio units (FRUs) reflect changes in $[Ca^{2+}]_i$. Total Ca^{2+} store release was significantly reduced in D2 serum- starved and D4 serum- starved cells compared to proliferating, all $P < 0.001$***. SOCE were

significantly reduced in D2 serum- starved and D4 serum- starved cells compared to proliferating, P = 0.02638* and P = 0.01451* respectively. **B)** Graph shows means of maximal Ca^{2+} store release and maximal SOCE. Both maximal Ca^{2+} store release and SOCE were significantly reduced in D2 serum- starved and D4 serum- starved cells compared to proliferating, P<0.001*** and P<0.01** respectively. Error bars represent S.E.M. For proliferating cells = 211, D2 serum-starved n = 195 and D4 serum-starved n = 196, N=4.

4.3 Discussion

SOCE is a ubiquitous Ca^{2+}influx pathway that functions in all non-excitable cells in response to agonist stimulation (Parekh and Putney, 2005) and has been known to be involved in cell cycle progression. The aim of the work presented in this chapter was to investigate SOCE remodelling in HeLa and NIH 3T3 when cell cycle is arrested in G0/G1 phase by serum starvation and to make a comparison to hTERT RPE-1 in order to determine the contribution of cell cycle arrest in G0/G1 phase to this remodelling.

The results show that serum starvation induced down-regulation of SOCE in the three cell types (HeLa, NIH 3T3 and hTERT RPE-1 cells) (Figure 4.2, 4.4 and 4.6). Previous studies (Bodding, 2001; Tani *et al.*, 2007; El Boustany *et al.*, 2010) reported that cell cycle arrest in G0/G1 by serum starvation was accompanied by a down-regulation in SOCE. However, (Bodding, 2001; El Boustany *et al.*, 2010) attributed this down-regulation to cell cycle arrest as the SOCE down-regulation was also observed in RBL cells where cell cycle was arrested by retinoic acid (Bodding, 2001), while (Tani *et al.*, 2007) attributed the SOCE down-regulation to serum starvation and not cell cycle arrest as it was observed that SOCE down-regulation did not occur when RBL cells were arrested in G0/G1 phase by Ca^{2+} deprivation.

In this chapter, the results show a clear difference in the extent of SOCE down-regulation with serum starvation only and with both serum starvation and cell cycle arrest in G0/G1 phase. The extent of SOCE down regulation was 60% in HeLa and 61% in NIH 3T3 cells (Table 4.1 and 4.2) where cell cycle was arrested and percentage of G0 cells was increased from ~ 0.5% to ~ 26% in HeLa cells and from ~ 3% to ~ 54% in NIH 3T3 cells (Table 3.4 and 3.5), while in hTERT RPE-1 cells, SOCE down-regulation was ~ 18% (Table 4.3) where no cell cycle arrest occurred and the percentage of G0 cells was not changed (Table 3.6). These results therefore imply that SOCE down-regulation occurred with cell cycle arrest in G0/G1 by serum starvation and can be attributed to a lesser extent to serum starvation and to greater extent to cell cycle arrest implying the level contribution of G0 cells to SOCE damping. Furthermore, in HeLa cells, the percentage of G1 cells did not significantly change before and after serum starvation confirming the contribution of the significant increase in G0 cells in SOCE down-regulation. Consistent with this, SOCE down-regulation has previously been observed in neuronal differentiation where cells exit cell cycle and arrested in G0 like phase. SOCE was observed to be down-regulated in

neuroblastoma cells upon differentiation (Brown *et al.*, 2005; Bell *et al.*, 2013; Whitworth, 2015). These finding so far indicate that down-regulation of SOCE is likely to be important for driving cells to exit the cell cycle.

SOCE has been previously shown to be remodelled during cell cycle progression. It is inactivated and uncoupled from store depletion in mitosis (Arredouani *et al.*, 2010) and in meiosis of frog oocytes (Machaca and Haun, 2000; Machaca and Haun, 2002) and to be upregulated in G1/S transition (Chen *et al.*, 2016).

The alteration in Ca^{2+} signalling responses with G0/G1 cell cycle arrest was different between cancerous HeLa cells and precancerous NIH 3T3 cells. In HeLa cells, an uncoupling of SOCE from Ca^{2+} store release with marked down-regulation of SOCE was observed. While in NIH 3T3 cells there was a marked down-regulation of SOCE which was still coupled to Ca^{2+} store release. This observation suggests that the mechanisms underlying the down-regulation of SOCE might be different between cancerous and precancerous cells or it might be cell type specific.

It is noteworthy that there was a marked decrease in Ca^{2+} store release in HeLa (~ 35%), NIH 3T3 (~77%) and hTERT RPE-1(~ 40%) cells with serum starvation. These changes suggest that the capacity of the Ca^{2+} store may be altered or there might be a change in sensitivity to TG with serum starvation and cell cycle arrest in G0 phase. Comparing Ca^{2+} store release changes in HeLa and NIH 3T3 cells to that in hTERT RPE-1cells, these findings, potentially, indicate that the down-regulation of Ca^{2+} store release in HeLa, NIH 3T3 and hTERT RPE-1cells may be attributed to serum starvation and not to cell cycle arrest in G0/G1 phase, this will be further investigated in a subsequent chapter by correlating Ca^{2+} signalling changes day by day with percentage of G0 subpopulations of all three cell types (Chapter 6: serum starvation time-course).

It was reported Ca^{2+} store release was unchanged when RBL cells were arrested in G0/G1 phase with 24 hours serum starvation (Bodding, 2001). The reason for this contrast with previous findings might be due to the length of serum starvation and this will be investigated in a subsequent chapter (Chapter 6: Serum starvation time-course). It has been reported that Ca^{2+} store release was slightly decreased in N-type cells within an N-type populations of neuroblastoma cells upon differentiation (Whitworth, 2015). In S-type population, however, the Ca^{2+} store release was increased with differentiation (Whitworth, 2015). The

observations in this chapter along with previous studies suggest that, possibly, the mechanisms underlying the Ca^{2+} store release alterations is a cell-type specific.

SOCE measurements in cells arrested in G0/G1 phase were done by identifying cells in interphase (cells with angular bodies). It remains unclear therefore whether G0/G1 cells have a fully down-regulated SOCE pathway (with the measured SOCE being a property of the contaminating cells in S or G2 phases) or whether a SOCE pathway may still be present and functioning in G0/G1 cells, albeit at a decreased level. Nevertheless, the data obtained is clearly informative as the serum starvation arrested ~90% of the cells in G0/G1 phase.

Given that SOCE pathway in cells arrested in G0/G1 phase are markedly down-regulated, a more likely possibility is a change in expression or function of one or more proteins involved in the pathway. These possibilities were examined in which the expression and localisation of the SOCE-associated proteins STIM1 and Orai1 were investigated further in this study (Chapter 5: SOCE proteins).

4.4 Conclusions

- An uncoupling of SOCE from Ca^{2+} store release with robust down-regulation of SOCE was observed in HeLa cells with the cell cycle arrest in G0/G1 phase.
- A marked down-regulation of SOCE and Ca^{2+} store release was detected with the cell cycle arrest in G0/G1 phase in NIH 3T3 cells.
- An uncoupling of SOCE from Ca^{2+} store release with slight down-regulation of SOCE occurred in hTERT RPE-1 cells with serum starvation.
- Compared to hTERT RPE-1, the SOCE down-regulation in HeLa and NIH 3T3 cells appeared to be attributed to cell cycle arrest in G0/G1 phase.

Chapter 5 Store-Operated Ca^{2+} Entry Proteins

5.1 Introduction

The STIM1and Orai1 proteins have been demonstrated to be involved in SOCE. Direct physical coupling between STIM1-the ER Ca^{2+} sensor- and Orai1 -the Ca^{2+} channel at the cell membrane, ensues functional coupling between Ca^{2+} levels in the ER lumen and extracellular Ca^{2+} entry (Hoover and Lewis, 2011). Cell cycle arrest in G0/G1 phase was associated with a significant down-regulation of SOCE in HeLa and NIH 3T3 cells. In addition, serum starvation induced slight SOCE down-regulation in hTERT RPE-1 cells (Chapter 4). A change in STIM1and Orai1 activity or expression may underlie these alterations in SOCE response. Therefore the aim of this chapter was to investigate the expression and localisation of SOCE proteins in HeLa and NIH 3T3 before and after cell cycle arrest in G0/G1 phase and in hTERT RPE-1 cells before and after serum starvation.

5.2 Result - STIM1 and Orai1 expression

Western blots were performed on protein extracted from HeLa, NIH 3T3, hTERT RPE-1 cells in order to determine STIM1 and Orai1 expression (Methods 2.6).

5.2.1 STIM1 and Orai1 expression in G0/G1 HeLa cells

STIM1 was expressed in proliferating (4 days 10% FCS) and G0/G1 (4 days 0.1% FCS) HeLa cells as determined by a band detected at 84kDa by an anti-STIM1 antibody (Figure 5.1.A). Blots were re-probed with β-actin, used as a loading control, and STIM1 was expressed as a ratio of β-actin in order to quantify changes in band intensity (Figure.5.1.B).

STIM1 protein expression was significantly decreased in G0/G1 cells by ~ 47.5 % compared to proliferating ($P = 0.0075$). The extent of down-regulation of SOCE was ~60% (Figure 4.2). The changes observed in SOCE are consistent with those seen in STIM1 expression and suggest that STIM1 is involved in the process of SOCE in HeLa cells.

As Orai1 is a PM protein that forms the SOC channel pore that STIM1 activates for SOCE regulation (Mignen *et al.*, 2008; Demuro *et al.*, 2011; Hoover and Lewis, 2011), the

relationship between Orai1 expression and SOCE was investigated in proliferating and G0/G1 HeLa cells.

Orai1 was expressed in both proliferating and G0/G1 cells as determined by a triple band detected between 37 and 50 kDa by an anti- Orai1 antibody (Figure 5.2.A). Blots were re-probed with β-actin, used as a loading control, and Orai1 was expressed as a ratio of β-actin in order to quantify changes in band intensity (Figure 5.2.B).

Orai1 protein expression was significantly decreased in G0/G1 cells by ~ 68 % compared to proliferating ($P = 0.0072$). This down-regulation would possible contribute to the dampened SOCE observed in G0/G1 HeLa cells of (Chapter 4).

When looking at Orai1 expression, this showed a triple band in proliferating and G0/G1 HeLa cells. The upper, middle and lower (Figure 5.2.C) Orai1 bands were analysed individually. The upper, middle and lower bands showed significant decrease in Orai1 expression in G0/G1 cells by ~ 62.5%, ~ 81% and ~ 80% compared to proliferating ($P > 0.01$) consistent with the analysis of the band as a whole. The existence of Orai1 expression in a pattern with several distinct molecular masses would suggest that Orai1may be subjected to post-translational modification(s).

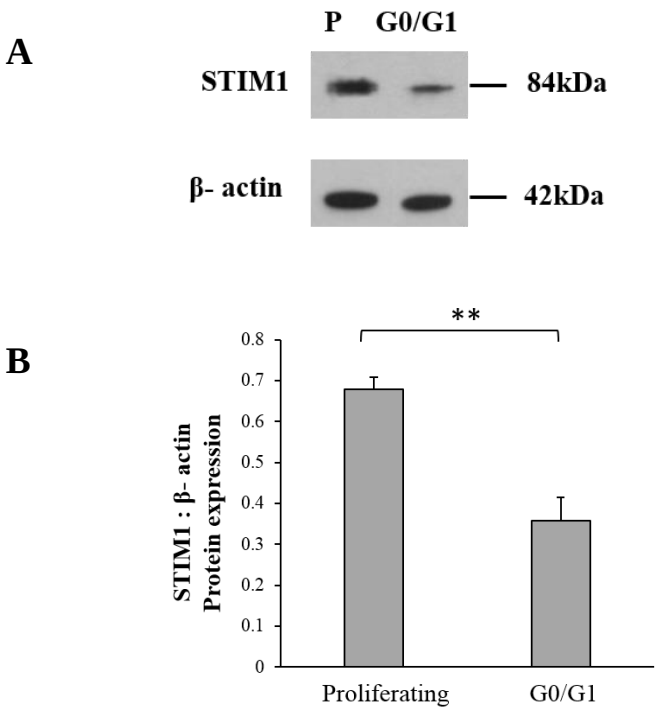

Figure 5.1 STIM1 expression in HeLa cells

Western blots were performed on protein extracted from HeLa cells following growth for 4 days in 10% FCS (proliferating = P) or 0.1% FCS (G0/G1). Blots were probed with anti-STIM1 antibody which detected a band at 84 kDa or β- actin antibody which was used as a loading control and detected a band at 42 kDa. **A)** STIM1 was expressed in both proliferating (P) and G0/G1 cells. **B)** Quantitative measurements of bands were performed using densitometry (ImageJ software, Methods 2.6.9) where STIM1 was expressed as a ratio of β-actin. There was a significant decrease in STIM1 expression in G0/G1 by ~47.5% compared to proliferating (P = 0.0075**). N=5.

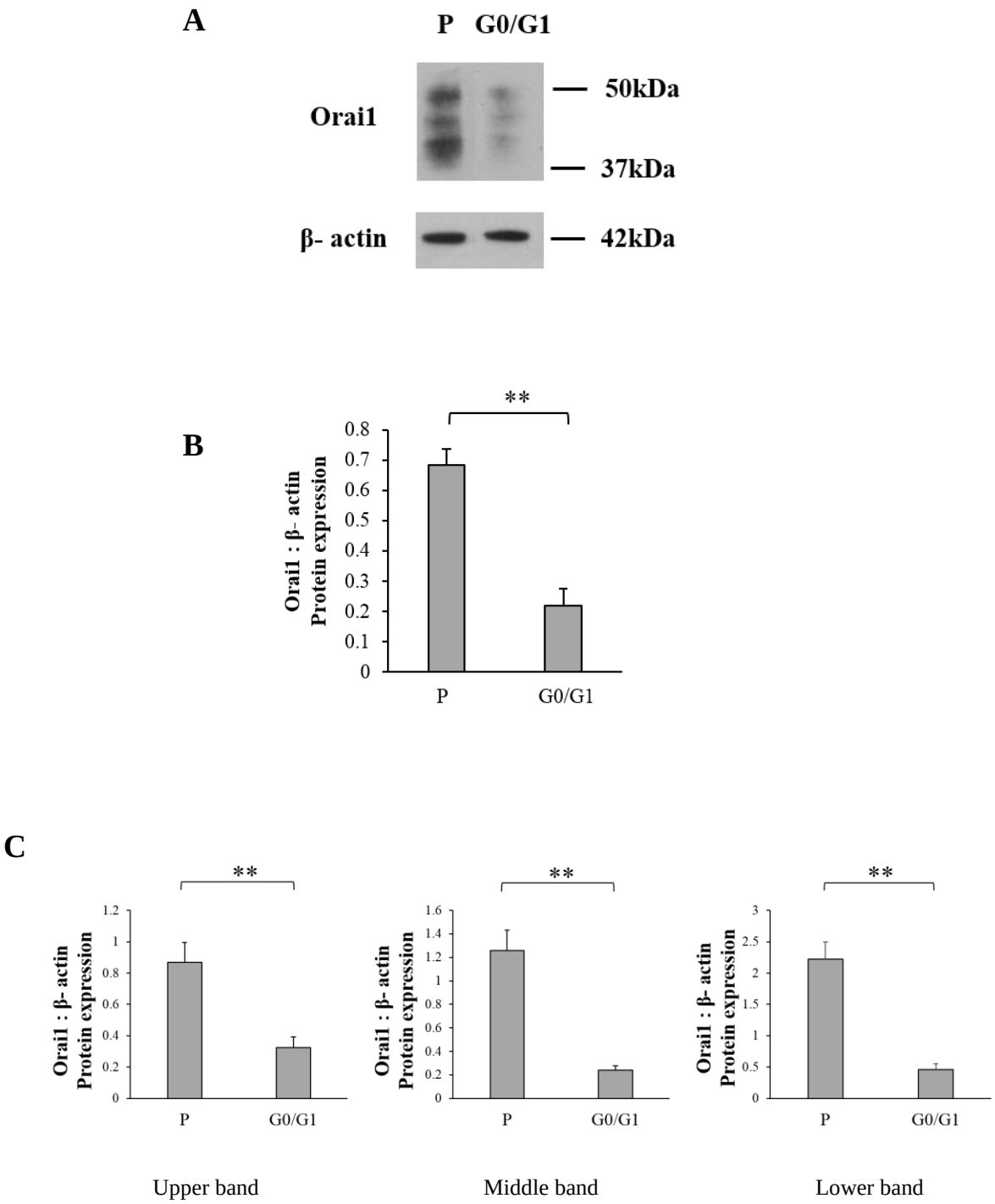

Figure 5.2 Orai1 expression in HeLa cells

Western blots were performed on protein extracted from HeLa cells following growth for 4 days in 10% FCS (proliferating = P) or 0.1% FCS (G0/G1). Blots were probed with anti-Orai1 antibody which detected a band between 37 and 50 kDa or β- actin antibody which was used as a loading control and detected a band at 42kDa A) Orai1 was expressed in both proliferating (P) and G0/G1 cells. **B)** Quantitative measurements of bands were performed using densitometry (ImageJ software, Methods 2.6.9) where Orai1 was

expressed as a ratio of β-actin. There was a significant decrease in Orai1 expression by ~68 % compared to proliferating (P= 0.0072*). **C)** Quantitative analysis of upper, middle and lower Orai1 bands. Orai1 expression was significantly decreased in G0/G1 cells by 62.5%, 81% and 80% respectively compared to proliferating cells (P=0.01**). N=4.

5.2.2 STIM1 and Orai1 expression in G0/G1 NIH 3T3 cells

STIM1 was expressed in proliferating (two days 10% FCS) and G0/G1 (two days 0.1% FCS) NIH 3T3 cells as determined by a band detected at 84kDa by an anti-STIM1 antibody (Figure 5.3.A). Blots were re-probed with β-actin, used as a loading control, and STIM1 was expressed as a ratio of β-actin in order to quantify changes in band intensity (Figure 5.3.B).

Similar to HeLa cells, STIM1 protein expression was significantly decreased in G0/G1 NIH 3T3 cells by ~49 % compared to proliferating cells (P = 0.0431). The extent of down-regulation of SOCE was ~60% (Figure 4.2). The changes observed in SOCE are consistent with those seen in STIM1 expression and indicate that STIM1 has a role in SOCE in NIH 3T3 cells.

The relationship between Orai1 expression and SOCE was also investigated in NIH 3T3 cells.

Orai1 was expressed in both proliferating and G0/G1 cells as determined by a double band detected between 37 and 50 kDa by an anti- Orai1 antibody (Figure 5.4.A). Blots were re-probed with β-actin, used as a loading control, and Orai1 was expressed as a ratio of β-actin in order to quantify changes in band intensity (Figure 5.4.B).

Orai1 protein expression was significantly decreased in G0/G1 cells by ~ 53 % compared to proliferating (P = 0.0197). This down-regulation could possible contribute to the observed down-regulation in SOCE in G0/G1 NIH 3T3 cells (Chapter 4).

As observed in HeLa cells, Orai1 expression appeared in distinct molecular weights. It showed a double band in both proliferating and G0/G1 NIH 3T3 cells. The upper (Figure 5.4.C) and lower (Figure 5.4.D) Orai1 band were analysed individually. The upper band showed significant down-regulation of Orai1expression in G0/G1 cells by ~ 67.5% compared to proliferating (P = 0.0052) whereas the lower band showed no significant difference in Orai1 expression in G0/G1 compared to proliferating (P=0.0662). This implies that Orai1 exists in two different states possibly due to post-translational modification.

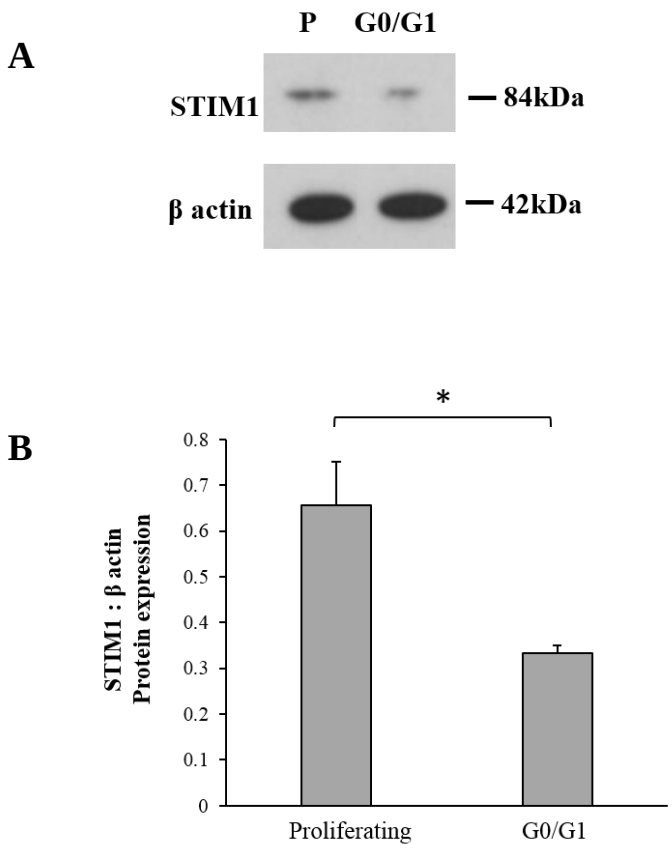

Figure 5.3 STIM1 expression in NIH 3T3 cells

NIH 3T3 cells were grown in 10% FCS medium (proliferating) or 0.1% FCS medium (G0/G1) for 2 days. Blots were probed with anti-STIM1 antibody which detected a band at 84 kDa or β- actin antibody which was used as a loading control and detected a band at 42 kDa. **A**) STIM1 was expressed in both proliferating (P) and G0/G1 cell populations. **B**) Quantitative measurements of bands were performed using densitometry (ImageJ software, Methods 2.6.9) where STIM1 was expressed as a ratio of β-actin. There was a significant decrease in STIM1 expression by ~ 49% compared to proliferating (P = 0.0431*). N=5.

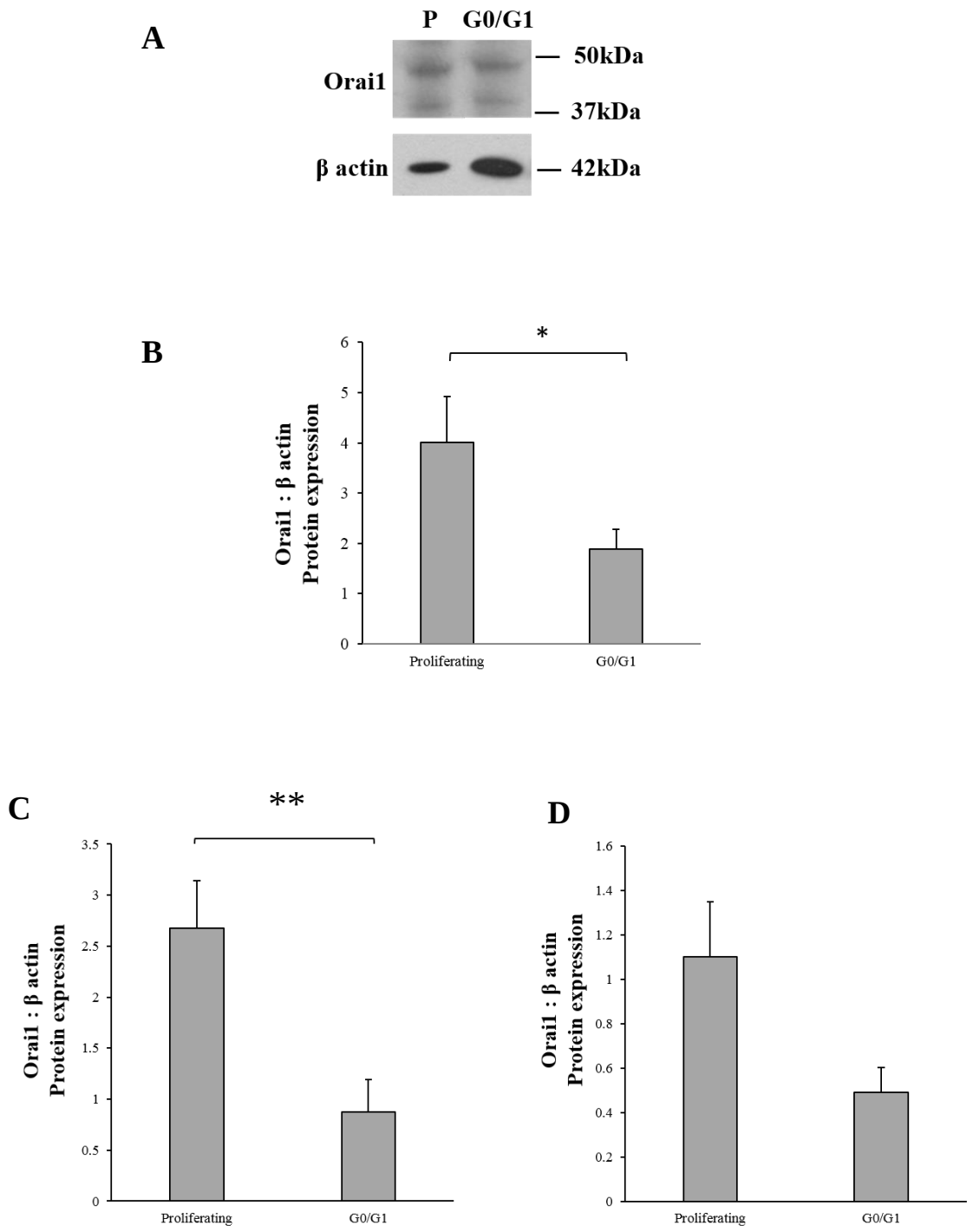

Figure 5.4 Orai1 expression in NIH 3T3 cells

Western blots were performed on protein extracted from NIH 3T3 cells following growing for 2 days in 10% FCS (proliferating = P) or 0.1% FCS (G0/G1). Blots were probed with anti-Orai1 antibody which detected a band between 37 and 50 kDa or β- actin antibody which was used as a loading control and detected a band at 42 kDa. **A**) Orai1 was expressed in both proliferating (P) and G0/G1 cell populations. **B**) Quantitative

measurements of bands were performed using densitometry (ImageJ software, Methods 2.6.9) where Orai1 was expressed as a ratio of β-actin. There was significantly decreased in Orai1 expression in G0/G1 cells by ~ 53% compared to proliferating (P = 0.0197*). **C)** Quantitative analysis of upper Orai1 band. Orai1 expression was significantly down-regulated in G0/G1 cells by ~ 67.5%compared to proliferating (P=0.0052**) cells. **D)** Quantitative analysis of lower Orai1 band. Orai1 expression was not significantly different in G0/G1cells compared to proliferating (P=0.0662) cells. N=4.

5.2.3 STIM1 and Orai1 expression in serum starved hTERT RPE-1 cells

SOCE becomes down-regulated with serum starvation in hTERT RPE-1 cells (Chapter 4). In order to determine any changes in STIM1and Orai1 protein expression associated with the observed changes in SOCE, western blots were performed on protein extracted from proliferating (10% FCS) and D2 and D4 serum starved (2 days and 4 days 0.1% FCS).

STIM1 was not expressed in proliferating cells. However, two patterns of STIM1 expression were observed in D2 and D4 serum starved cell extracts. In most cases (N=4), there was no STIM1 expression (Figure 5.5.A) and in others (N=2), STIM1 was slightly expressed at a higher molecular weight, as determined by a slight upward band shift (Figure 5.5.B) detected just above 84kDa by an anti-STIM1 antibody. Blots were re-probed with β-actin, used as a loading control.

These results showed that hTERT RPE-1 may lack or have undetectable levels of STIM1 protein, which will also be tested by immunofluorescent study in this chapter. The occasionally detected upshifted band could indicate phosphorylation of STIM1 or the presence of a different isoform or some other post-translational modifications which alter electrophoretic mobility and that could alter STIM1 function.

The relationship between Orai1 expression and SOCE following serum starvation was also investigated in hTERT RPE-1 cells. Orai1 was expressed in proliferating, D2 and D4 hTERT RPE-1 cells as determined by a double band detected between 37 and 50 kDa by an anti- Orai1 antibody (Figure 5.6.A). Blots were re-probed with β-actin as a loading control.

Orai1 protein expression as a ratio of β-actin was decreased in D2 and D4 by ~14% and ~18.5 % compared to proliferating however these changes were not significant (P= 0.0602 and P=0.0571 respectively) (Figure 5.6.B).
Orai1 expression showed a double band in proliferating and in D2 and D4. The upper and lower Orai1 bands (Figure 5.6.C) were analysed individually. This showed the same pattern as that of whole band analysis where there was a slight non-significant decrease in Orai1 expression in D2 and D4 compared to proliferating.

The extent of down-regulation of SOCE was ~ 13.5 % and 23.5 % (Section 4.2.3) in D2 and D4 respectively which are consistent with those seen in Orai1expression and suggest that Orai1 is involved in the process of SOCE in hTERT RPE-1cells.

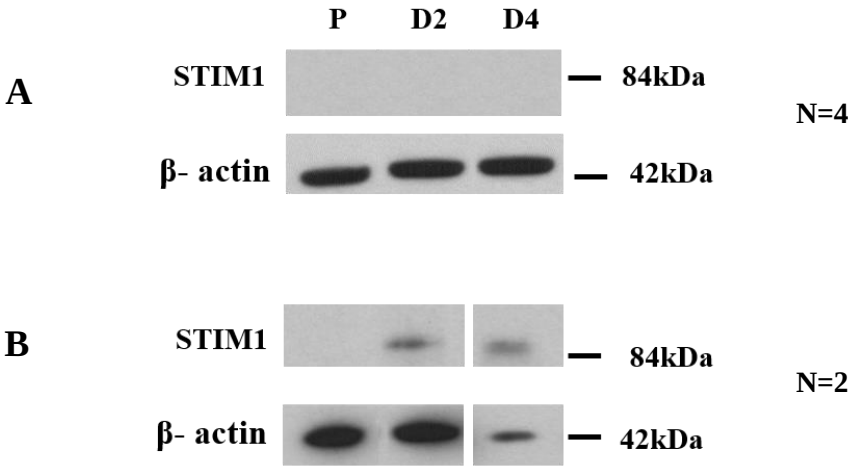

Figure 5.5 STIM1 expression in hTERT RPE-1 cells

Western blots were performed on protein extracted from hTERT RPE-1 cells following growing in 10% FCS (proliferating = P) or 0.1% FCS for two days (D2) and for four days (D4). Blots were probed with anti-STIM1 antibody which detected a band at 84 kDa or β-actin antibody which was used as a loading control and detected a band at 42 kDa. **A**) STIM1 expression was not detected in both proliferating (P), D2 and D4 cells. **B)** STIM1 expression was not detected in proliferating (P) while there was STIM1 expression in D2 and D4. N=6.

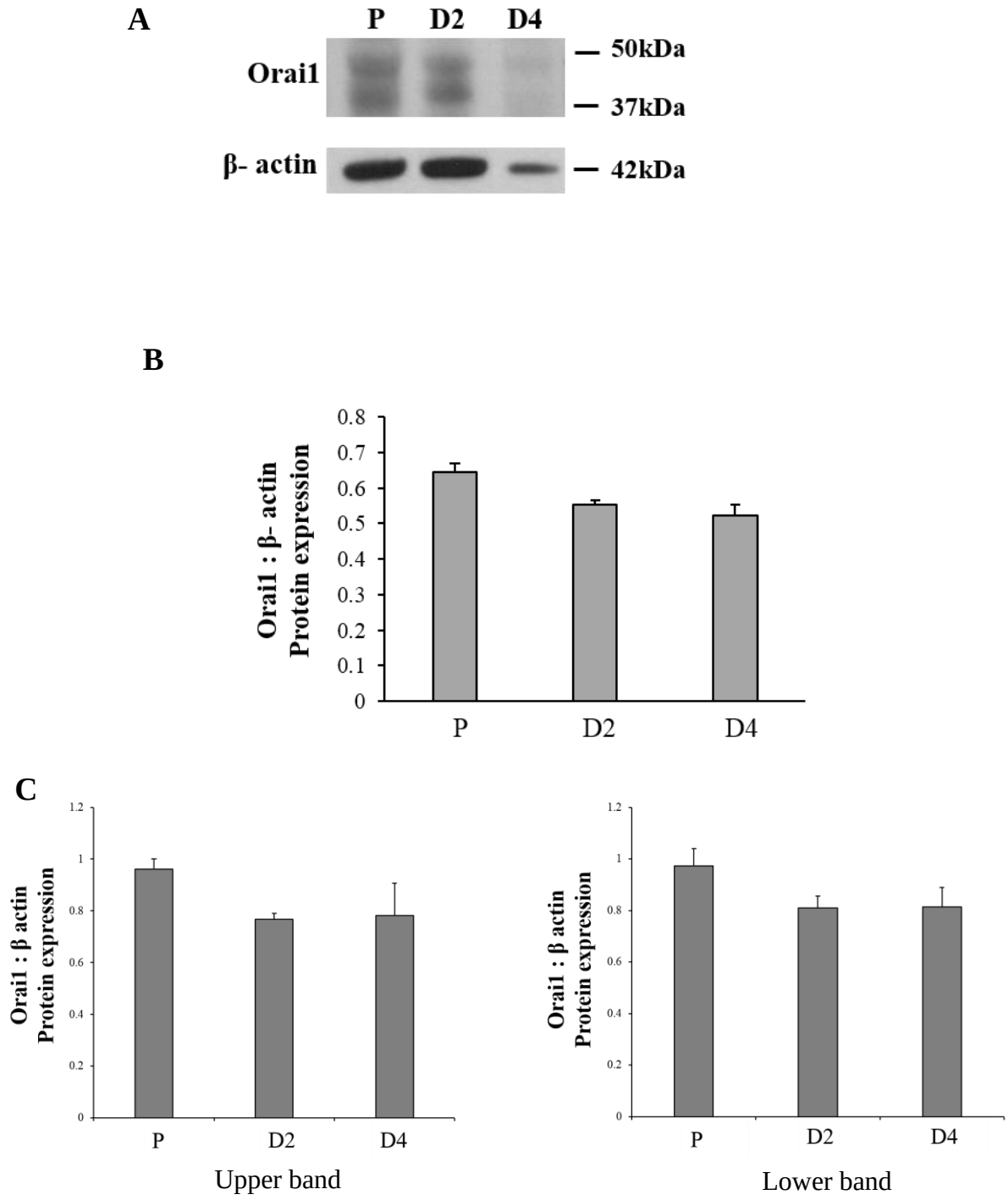

Figure 5.6 Orai1 expression in hTERT RPE-1 cells

Western blots were performed on protein extracted from hTERT RPE-1 cells following growing in 10% FCS (proliferating = P) or 0.1% FCS for 2 days (D2) and for 4 days (D4). Blots were probed with anti-Orai1 antibody which detected a band between 37 and 50 kDa or β- actin antibody which was used as a loading control and detected a band at 42 kDa. **A**) Orai1 was slightly expressed in both proliferating (P) and starved cell populations (D2 and D4). **B**) Quantitative measurements of bands were performed using densitometry (ImageJ

software, Methods 2.6.9) where Orai1 was expressed as a ratio of β-actin. There was no significant changes in Orai1 expression in starved cell populations (D2 and D4) compared to proliferating ($P > 0.05$). **C)** Quantitative analysis of upper and lower Orai1 bands. Orai1 expression showed the same pattern as that of whole band analysis (B). There was no significant differences in Orai1 expression in D2 and D4 compared to proliferating ($P > 0.05$). N=4.

5.3 Results - STIM1 and Orai1 localisation

The expression of STIM1 and Orai1 were altered in G0/G1 HeLa and NIH 3T3 cells and in serum starved hTERT RPE-1 cells compared to proliferating. STIM1 has been shown to redistribute to the PM and bind to Orai1 upon Ca^{2+} store depletion in sinoatrial node cells (Liu *et al.*, 2015), Xenopus oocytes (Courjaret and Machaca, 2014) and HEK293 cells (Fukushima *et al.*, 2012). Therefore, localisation of these SOCE proteins were investigated. Immunofluorescent studies were performed on HeLa, NIH 3T3 and hTERT RPE-1 cells; fixed cells were stained with either anti-STIM1 primary antibody or anti-Orai1 primary antibody followed by Alexa Fluor 647 secondary antibody or Alexa Fluor 488 secondary antibody respectively. Cells then were examined and images were taken by laser scanning confocal microscopy using an x63 objective (Method 2.7).

5.3.1 STIM1 and Orai1 localisation with cell cycle arrest in G0/G1 phase in HeLa cells

There was widespread expression of STIM1 throughout the cytoplasm in proliferating HeLa cells with higher levels of STIM1 in the cell nuclei and there was a clear evidence of localisation into foci near cell membrane (Figure 5.7.A). There was a similar expression pattern in G0/G1 cells (Figure 5.7.A) however, there was no apparent areas of clustering into foci (Figure 5.7A and B).

Obviously, these changes in localisation of STIM1 with cell cycle arrest in G0/G1 cells may affect STIM1 function and its ability to contribute to the observed uncoupling and down-regulation of SOCE response in G0/G1 HeLa cells (Section 4.2.1).

There was widespread expression of Orai1 throughout the cytoplasm and nuclei of proliferating cells and there were clear examples of clustering in the nucleus (Figure 5.8.A and B). There was a similar expression pattern in G0/G1 cells though nuclear Orai1 clustering was much less (Figure 5.8.A and B). These changes in Orai1 localisation with cell cycle arrest in G0/G1 cells possibly contribute to the extent of SOCE activity.

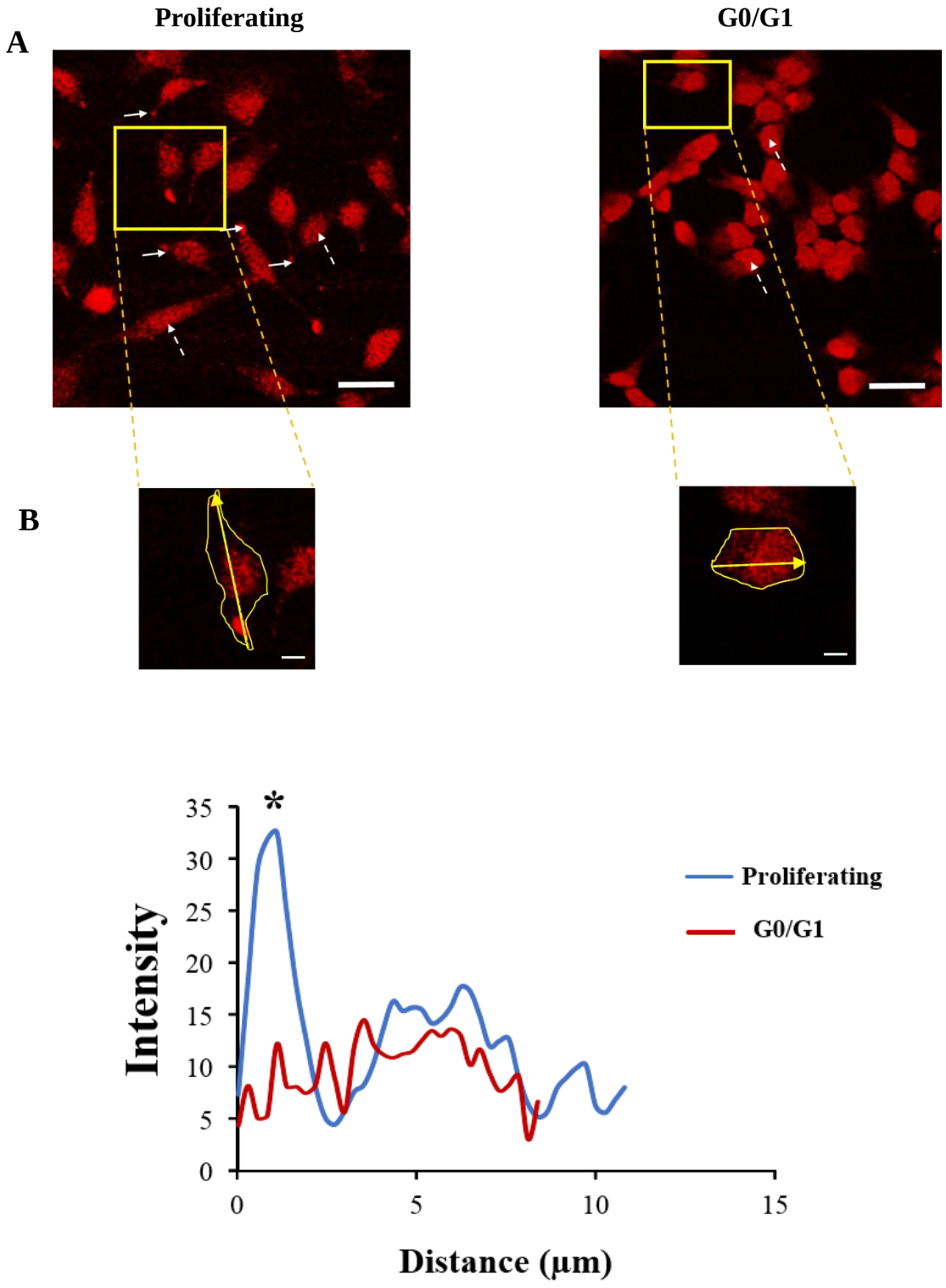

Figure 5.7 STIM1 expression and localisation in HeLa cells

HeLa cells were grown in 10% FCS medium (proliferating) or 0.1% FCS medium (G0/G1) for 4days. Cells were stained with anti-STIM1 primary antibody followed by Alexa Fluor 647 secondary antibody. **A)** Images were captured using laser scanning confocal

microscopy. In proliferating cells, STIM1 was present throughout the cell with slight higher expression in the nuclei (dashed arrows) and there was high occurrence STIM1 localisation into foci at the cell membrane (solid arrows). In G0/G1 cells, STIM1 shows similar expression profile however, there was no apparent areas of clustering. **B)** A line scan analysis of proliferating and G0/G1 cells. The path was done in a single cell through an axis (yellow arrow) to track the STIM1 expression profile. The line scan of proliferating cell (blue line) shows focus localisation of STIM1 (*) at cell membrane and STIM 1 expression throughout the cell with more expression in the cell nucleus, while the line scan of G0/G1 cell (red line) shows no focus localisation of STIM1 with a slightly lower STIM1 expression compared to proliferating. Line scan also shows that cell size decreased in G0/G1 cells compared to proliferating. Scale bars represent 10 μm. Images are representative of >10 images and were taken using an x63 objective. N=4.

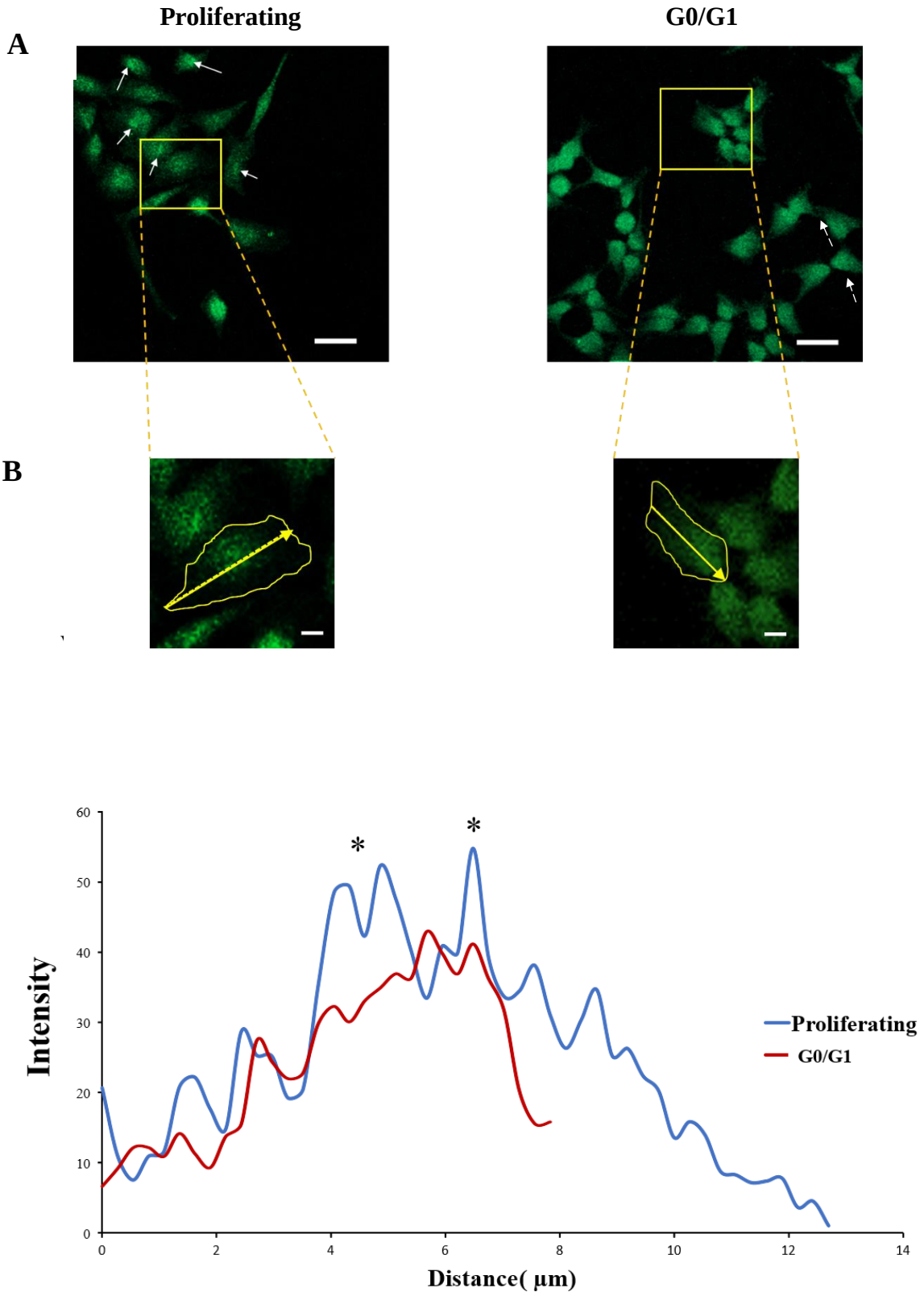

Figure 5.8 Orai1 expression and localisation in HeLa cells

HeLa cells were grown in 10% FCS medium (proliferating) or 0.1% FCS medium (G0/G1) for 4days. Cells were stained with anti-Orai1 primary antibody followed by Alexa Fluor

488 secondary antibody. **A)** Images were captured using laser scanning confocal microscopy. In proliferating cells, Orai1 was present throughout the cell and there were some examples of Orai1 clustering in the nuclei (solid arrows). In G0/G1 cells, Orai1 was present throughout the cell however, there were examples of cells that expressed higher levels of Orai1 in the cell nuclei (dashed arrows) which was diffuse with no apparent areas of clustering. **B)** A line scan analysis of proliferating and G0/G1 cells. The path was done in a single cell through an axis (yellow arrow) to track the Orai1 expression profile. The line scan of proliferating cell (blue line) shows Orai1 expression throughout the cell which is higher in the cell nucleus with occurrence of clustering (*), while the line scan of G0/G1 cell (red line) shows similar distribution of Orai1 expression as that of proliferating with no apparent clustering in the nucleus. Line scan also shows that cell size decreased in G0/G1 cells compared to proliferating. Scale bars represent 10 μm. Images are representative of >10 images and were taken using an x63 objective. N=4.

5.3.2 STIM1 and Orai1 localisation with cell cycle arrest in G0/G1 phase in NIH 3T3 cells

Immunofluorescence analysis of NIH 3T3 cells showed that STIM1 was clearly expressed in proliferating NIH 3T3 cells which was much higher in nuclei. There was high occurrence of localisation into foci near cell membrane (Figure 5.9.A). There was a similar expression pattern in G0/G1 cells (Figure 5.9), however, areas of foci were not observed.

For Orai1, as in HeLa cells, there was widespread expression of Orai1 throughout the cytoplasm and nuclei of proliferating NIH 3T3 cells and there was evidence of clustering in the nucleus (Figure 5.10.A). There was a similar expression pattern in G0/G1 cells though there was no occurrence of Orai1 clustering (Figure 5.10). The overall intensity of fluorescence of Orai1 was lower in G0/G1 cells compared to proliferating.

These changes in localisation of STIM1 and Orai1with cell cycle arrest in G0/G1 cells may alter their function and subsequently contribute to the observed reduction in SOCE response in G0/G1 NIH 3T3 cells (Section 4.2.2).

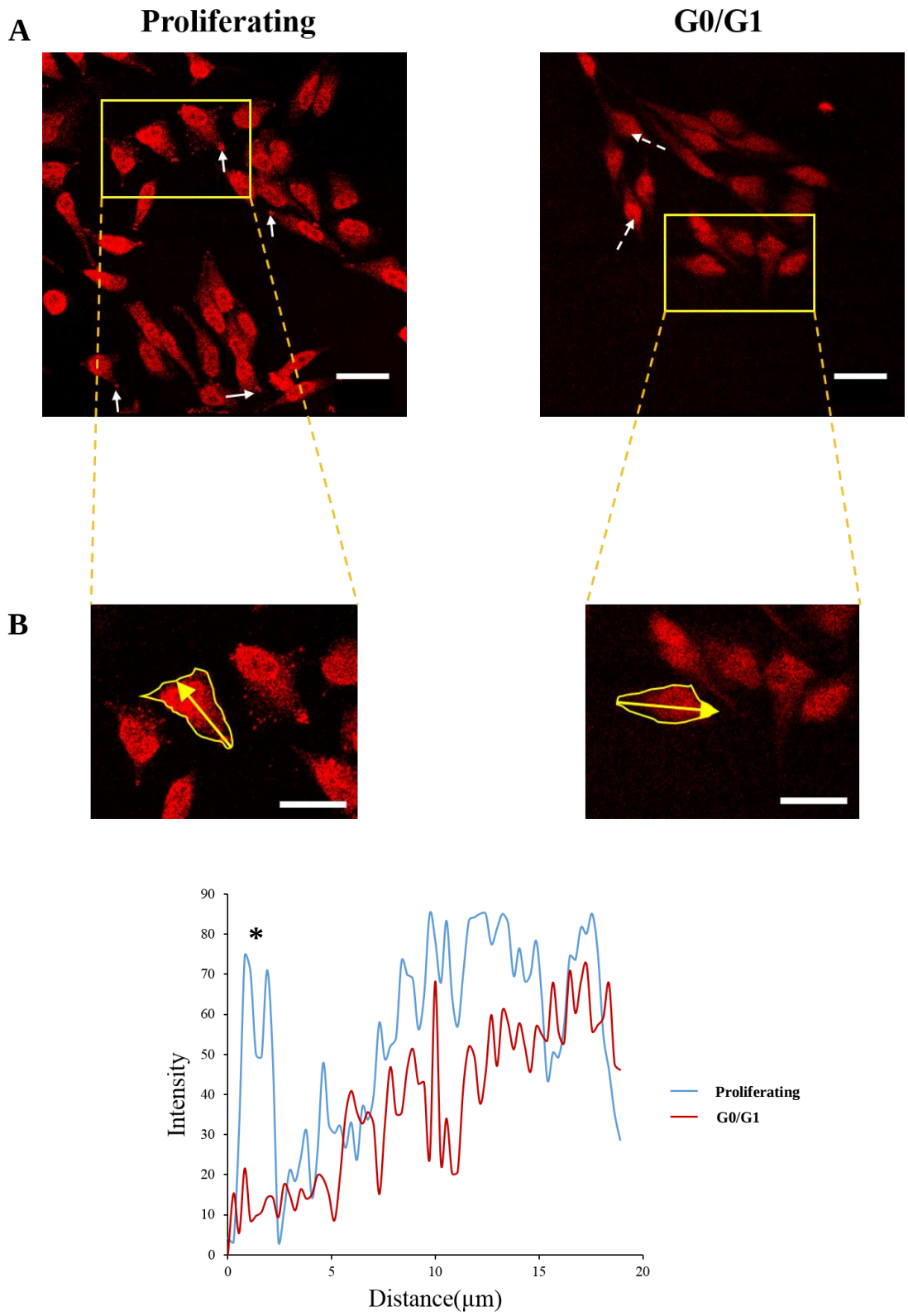

Figure 5.9 STIM1 expression and localisation in NIH 3T3 cells

NIH 3T3 cells were grown in 10% FCS medium (proliferating) or 0.1% FCS medium (G0/G1) for 2 days. Cells were stained with anti-STIM1 primary antibody followed by

Alexa Fluor 647 secondary antibody. **A)** Images were captured using laser scanning confocal microscopy. Proliferating cells shows high occurrence STIM1 localisation into foci at the cell membrane (solid arrows) and high diffuse STIM1 expression in the cell nucleus. In G0/G1 cells, STIM1 was present throughout the cell however, there were clear examples of cells that expressed higher levels of STIM1 in the cell nuclei (dashed arrows) with no apparent areas of clustering. **B)** A line scan analysis of proliferating and G0/G1 cells. The path was done in a single cell through an axis (yellow arrow) to track the STIM1 expression profile. The line scan of proliferating cell (blue line) shows focus localisation of STIM1 (*) at cell membrane and high STIM 1 expression in the cell nucleus. While the line scan of G0/G1 cell (red line) shows no focus localisation of STIM1 with high STIM1 expression in the cell nucleus compared to its cytoplasm. The overall STIM1 expression was somewhat lower in G0/G1 cells compared to proliferating. Scale bars represent 10 μm. Images are representative of >15 images and were taken using an x63 objective. N=3.

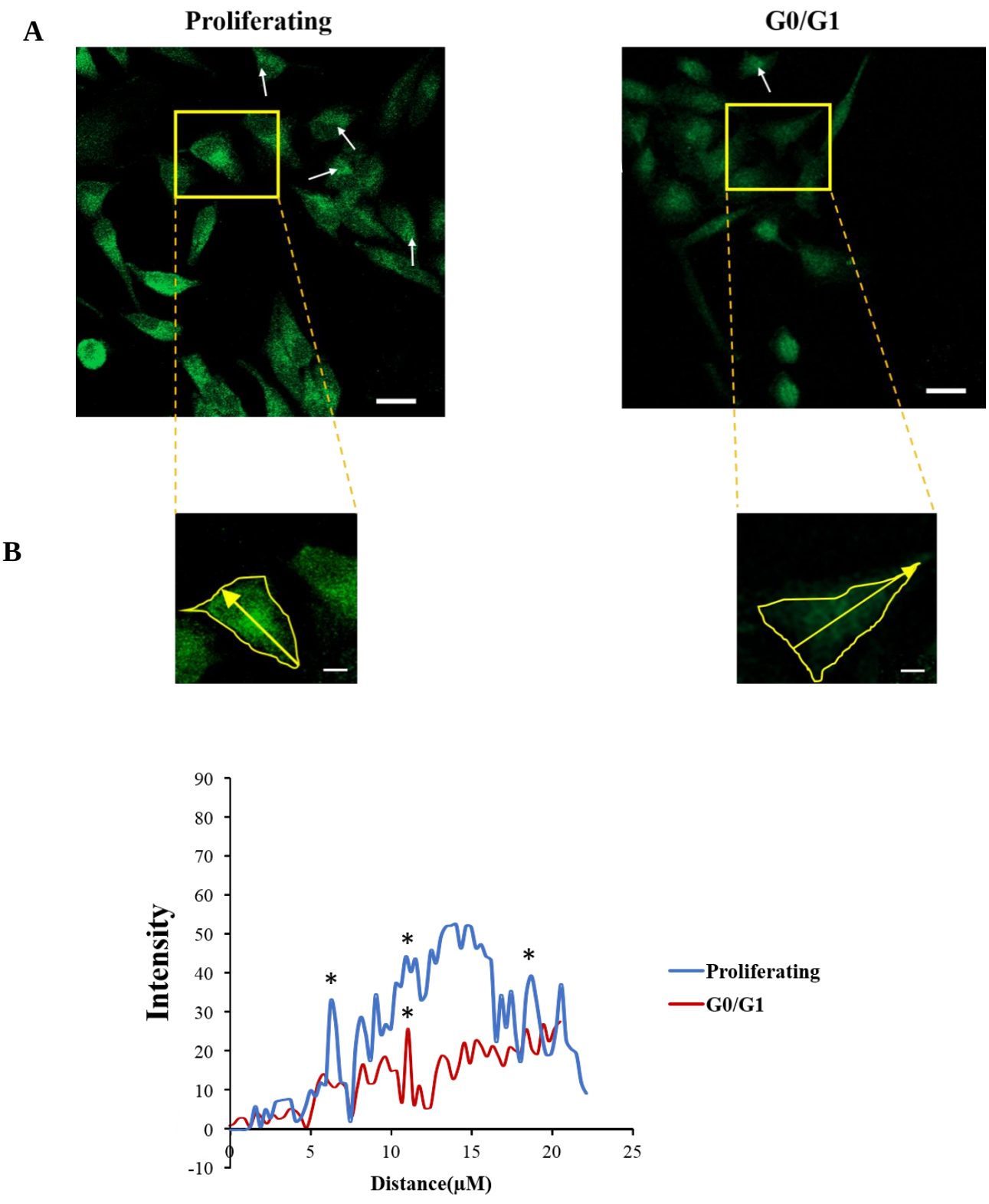

Figure 5.10 Orai1 expression and localisation in NIH 3T3 cells

NIH 3T3 cells were grown in 10% FCS medium (proliferating) or 0.1% FCS medium (G0/G1) for 4days. Cells were stained with anti-Orai primary antibody followed by Alexa Fluor 488 secondary antibody. **A)** Images were captured using laser scanning confocal

microscopy. In proliferating cells, Orai1 was present throughout the cell and there were some examples of Orai1 clustering in the nuclei (arrows). In G0/G1 cells, Orai1 was present throughout the cell with less apparent areas of clustering in the nucleus (arrows). **B)** A line scan analysis of proliferating and G0/G1 cells. The path was done in a single cell through an axis (yellow arrow) to track the Orai1 expression profile. The line scan of proliferating cell (blue line) shows low Orai1 expression in the cytoplasm throughout the cell with much more expression in the cell nucleus with areas of clustering (*). While the line scan of G0/G1 cell (red line) shows that Orai1 expression was decreased compared to proliferating and Orai1 clustering is much less. Line scan also shows that the cell size did not change in G0/G1 compared to proliferating. Scale bars represent 10 μm. Images are representative of >10 images and were taken using an x63 objective. N=3.

5.3.3 STIM1 and Orai1 localisation with serum starvation in hTERT RPE-1 cells

In hTERT RPE-1 cells, STIM1 and Orai1 expression was not detected in proliferating, D2 serum-starved or D4 serum-starved by immunofluorescence study (Figure 5.11 B and C).

For STIM1, this is unsurprising given that STIM1 expression was not detected in proliferating and most cases of D2 and D4 hTERT RPE-1 cells by western blots (Figure 5.5). However for Orai1, the anti- Orai1antibody used in the present study might be not suitable or not sensitive enough for the detection of Orai1in hTERT RPE-1 cells by immunofluorescence.

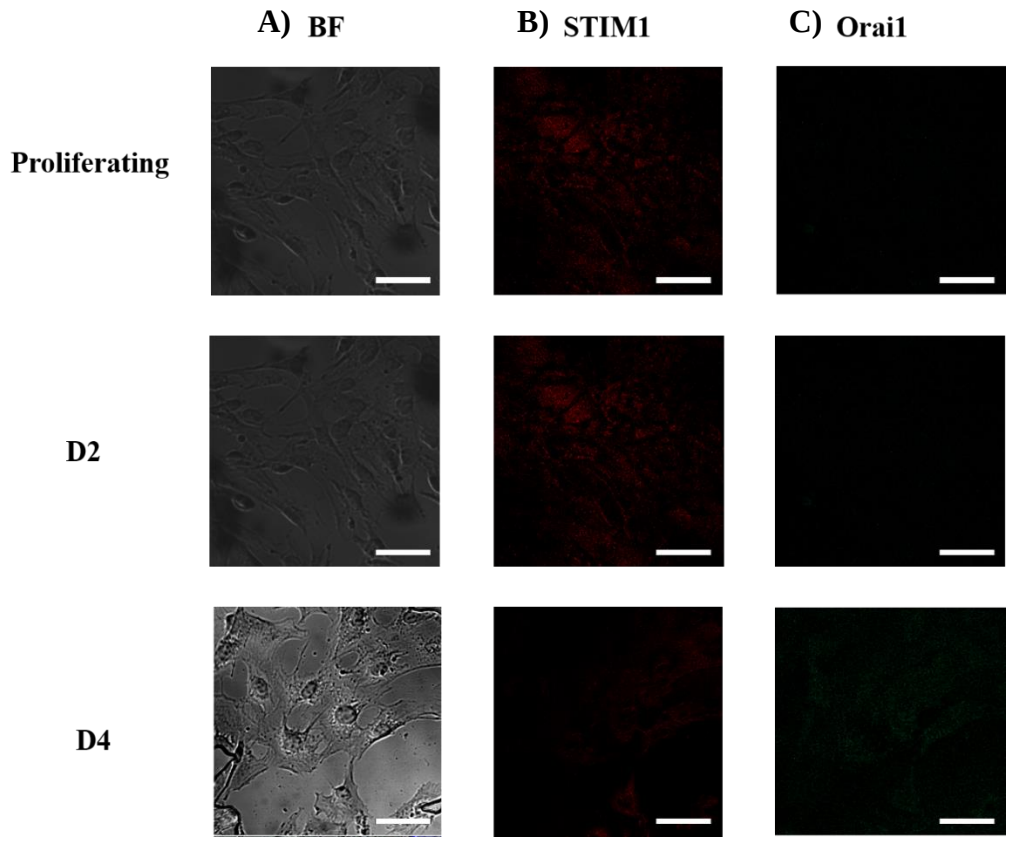

Figure 5.11 STIM1 and Orai1 immunofluorescent expression in hTERT RPE-1 cells
Proliferating (10% FCS) cells, D2 and D4 (0.1% FCS for 2 and 4 days respectively) cells were stained with anti-STIM1/anti-Orai primary antibodies followed by Alexa Fluor 647 / Alexa Fluor 488 secondary antibodies respectively. Images were captured using laser scanning confocal microscopy. **A)** BF (bright field) images show healthy cells. **B and C)** STIM1 and Orai1 were not detected by immunofluorescent staining. Scale bars represent 10 μm. Images are representative of >12 images and were taken using an x63 objective. N=4.

5.4 Discussion

Alterations of SOCE activity were observed with cell cycle arrest in G0/G1 phase in HeLa and NIH 3T3cells and with serum starvation in hTERT RPE-1 cells (Chapter 4).

The aim of the work presented in this chapter was to investigate the molecular basis underlying the observed alterations in SOCE by determining the level of expression and localisation SOCE proteins; STIM1 and Orai1.

The results show that STIM1 expression was significantly decreased in HeLa and NIH 3T3 cells with cell cycle arrest in G0/G1 phase consistent with a role for STIM1in arresting cell cycle in G0/G1 phase observed in other cell types. For example, knockdown of STIM1 significantly inhibited cell proliferation and arrested the cell cycle at the G0/G1 phase in hepatocellular carcinoma cell (Wu *et al.*, 2015), in hypopharyngeal carcinoma cells (Sun *et al.*, 2015) and in human glioblastoma cells (Li *et al.*, 2013) and results in cell cycle arrest in G1/S transition in cervical cancer SiHa cells (Chen *et al.*, 2016). Similarly, previous studies in this laboratory showed that STIM1 expression decreased when cells arrest in G0 like phase in differentiated N-type and S-type neuroblastoma cells, and this decrease was associated with SOCE down-regulation (Bell *et al.*, 2013; Whitworth, 2015).

Furthermore, in both HeLa and NIH 3T3 cells, the decrease in STIM1 expression (47.5% and 49.5 % respectively) is consistent with the previously observed down-regulation of SOCE (60% and 61% respectively) (Chapter 4) as STIM1 has been shown to play a role in SOCE (Liou *et al.*, 2005; Roos *et al.*, 2005; Zhang *et al.*, 2005) and the level of STIM1 expression has been extensively associated with extent of SOCE activity in many cell types. For example, SOCE down-regulation has been shown to be induced by STIM1 knockdown in HeLa cells (Liou *et al.*, 2005) endothelial cells (Abdullaev *et al.*, 2008), in N-type SH-SY5Y cells (Bell *et al.*, 2013), endothelial progenitor cells (Kuang *et al.*, 2010), SH-SY5Y cells, HEK293 cells, Jurkat T cells and Drosophila S2 cells (Roos *et al.*, 2005), as well as vascular smooth muscle cells (Takahashi *et al.*, 2007b; Aubart *et al.*, 2009; Potier *et al.*, 2009) and adipocytes (Graham *et al.*, 2009).

Taken together, these results indicate that a decrease in STIM1 expression underlies the SOCE down-regulation associated with cell cycle arrest in G0/G1 phase and suggesting a role for STIM1 in cell cycle arrest in G0/G1 phase in HeLa and NIH 3T3 cells. This will be further investigated later in serum starvation time course chapter.

Consistent with the changes in STIM1 expression, STIM1 localisation was altered when cells exit cell cycle and arrested in G0/G1 phase in HeLa and NIH 3T3 cells. There was clear evidence of STIM1 clustering in proliferating cells at the PM which disappeared in G0/G1 cells in both HeLa and NIH 3T3 cells. Consistent with this, it has been shown that STIM1 localisation was altered when cells arrest in G0 like phase during differentiation of N-type and S-type SH-SY5Y cells (Whitworth, 2015). STIM1 has been shown to redistribute to the PM and bind to Orai1 upon Ca^{2+} store depletion in sinoatrial node cells (Liu *et al.*, 2015), Xenopus oocytes (Courjaret and Machaca, 2014) and HEK293 cells (Fukushima *et al.*, 2012). These findings showed that STIM1 localisation has been intimately associated with Ca^{2+} store depletion and subsequent SOCE, indicating that the disappearance of STIM1 localisation may underlie the observed uncoupling of Ca^{2+} store depletion and SOCE associated with cell cycle arrest in G0/G1 phase in HeLa and NIH 3T3 cells.

Along with the role for STIM1 in SOCE, the level of Orai1 expression has been associated with SOCE. In this study, a decrease in Orai1 expression was associated with cell cycle arrest in G0/G1 phase in HeLa and NIH 3T3 and a down-regulation in SOCE.

A similar observation has been reported previously where Orai1 expression was observed to be down-regulated and associated with reduction in SOCE in N-type, S-type differentiating SH-SY5Y cells (arresting in G0 like phase) (Bell, 2011; Whitworth, 2015).

Orai1 protein is known to play role in cell cycle progression. Previous studies have demonstrated that Orai1 knockdown result in cell cycle arrest in G1/S transition cervical cancer SiHa cells (Chen *et al.*, 2016), in G0/G1 phase in ARPE-19 cells (Yang *et al.*, 2013), induced differentiation and cell cycle arrest in G0 like phase of N-type neuroblastoma cells and that cell cycle block in HEK293 cells induced by SOCE inhibition was associated with Orai1protein (Borowiec *et al.*, 2014).

Similarly, Orai1 protein is shown to play an important role in cell proliferation. Overexpression of Orai1induced a significant increase in cell proliferation rate in HEK293 and HeLa cells (Borowiec *et al.*, 2014) and Orai1 knockdown caused a dramatic decrease in proliferation rate of in HEK293 cells (El Boustany *et al.*, 2010), vascular smooth muscle cells (Potier *et al.*, 2009) and endothelial cells (Abdullaev *et al.*, 2008).

Similar to STIM1 protein, the observed decrease in Orai1 expression is consistent with the previously observed down-regulation of SOCE in this study, as Orai1 expression level has

been shown to be closely associated with SOCE activity. Orai1 knockdown causes reduction in SOCE in neural progenitor cells (Hao *et al.*, 2014), in differentiated N-type SH-SY5Y cells (Bell, 2011), acinar cells (Hong *et al.*, 2011), osteoclasts (Zhou *et al.*, 2011), HEK293 cells (Gwack *et al.*, 2007; Kawasaki *et al.*, 2010; Borowiec *et al.*, 2014), endothelial cells (Abdullaev *et al.*, 2008) and Jurkat T cells (Gwack *et al.*, 2007). Furthermore, Orai1 overexpression results in an increase in SOCE in HEK293 cells (Fukushima *et al.*, 2012), restores SOCE in differentiated N-type SH-SY5Y (Bell, 2011), in SCID T cells and fibroblasts (Gwack *et al.*, 2007).

Consistent with changes observed in Orai1 expression, Orai1 localisation was altered in HeLa and NIH 3T3 cells when cells arrested in G0/G1 phase. There was a dispersion of Orai1 clusters in the nuclei in proliferating cells which was mostly absent in G0/G1 cells. This observation was also observed in a previous study where Orai1 localisation was altered in neuroblastoma cells with differentiation (Whitworth, 2015).

Taken together this evidence suggests that the decrease in Orai1 expression underlies the SOCE down-regulation associated with cell cycle arrest in G0/G1 phase in HeLa and NIH 3T3 cells. Also, these observations indicate that Orai1 may play a role in cell cycle progression and cell proliferation in these cells.

In hTERT RPE-1 cells, however, STIM1expression was not detected in proliferating and most of serum starved cases by western blot and by immunofluorescence studies. It is possible the number of cells and/or the level of expression is presumably too low to be detected by the anti- STIM1 antibody used in this study.

By western blot, a band at a molecular weight just above the STIM1 molecular weight was occasionally observed using the anti-STIM1 antibody in serum starved hTERT RPE-1 cells. This increase in molecular weight suggested that there may be some sort of modification, such as phosphorylation or glycosylation which might affect STIM1 function and be responsible for the observed down-regulation of SOCE. Consistent with this observation, an increase in molecular weight has been previously observed to be associated with down-regulation in SOCE activity in neuroblastoma cells (Whitworth, 2015), STIM1 phosphorylation at multiple serine residues has been shown to inhibit SOCE by preventing puncta formation in endothelial cells (Sundivakkam *et al.*, 2013) and in HEK 293 cells (Smyth *et al.*, 2009).

Conversely, in other cell types, STIM1 phosphorylation plays a role in STIM1 activation during ER Ca^{2+} store depletion. For example, STIM1 phosphorylation plays a key role in conducting SOCE activation in human platelets (Lopez *et al.*, 2012) and in HEK293 cells (Pozo-Guisado *et al.*, 2010). It has been shown that STIM1 phosphorylation both activates and inactivates STIM1-dependent SOCE depending on the cell type, cell cycle phase, and the specific modified residue (Pozo-Guisado *et al.*, 2013).

Similarly, STIM1 has been shown to be glycosylated (Manji *et al.*, 2000; Dziadek and Johnstone, 2007), which can affect localisation of STIM1 to the PM (Williams *et al.*, 2002) and subsequently alter SOCE activity.

It is noteworthy that STIM1 has alternative isoforms; STIM1L and STIM1S that serve different functions. STIM1L has recently been recognised (Darbellay *et al.*, 2011) and has been shown to activate SOCE in cells lacking STIM1 (Sauc *et al.*, 2015). STIM1L has been shown to induce SOCE quicker than STIM1S, attributable to its association with Orai1 at rest rather than needing to migrate to bind Orai1 following store depletion like that of STIM1S (Darbellay *et al.*, 2011; Horinouchi *et al.*, 2012). Therefore, it is possible that SOCE in hTERT RPE-1 cells is mediated by STIM1L.

In summary, the results showed that hTERT RPE-1 cells may lack/or express a very low level of STIM1 and/or other isoforms of STIM1 or may have another STIM homologues; STIM2 that may responsible for the observed changes in SOCE with serum starvation.

Orai1 expression was slightly down-regulated in hTERT RPE-1 cells by ~14% and ~18.5 % in D2 and D4 of serum starvation compared to proliferating. Though these changes were not significant, it was consistent with the extent of down-regulation of SOCE which was ~ 13.5 % and 23.5 % (Section 4.2.3) confirming a role of Orai1in the process of SOCE in hTERT RPE-1cells.

While Orai1 expression was detected by western blot using anti- Orai1 antibody, the sensitivity of this antibody seems to be insufficient for the detection of Orai1in hTERT RPE-1 cells by immunofluorescence study (Figure 5.11).

The extent of the down-regulation of Orai1 expression (~ 68% and ~ 53%) in HeLa and NIH3T3 cells respectively could not be a direct effect of serum starvation as these decreases were far less and not significant in hTERT RPE-1 cells ~14% and ~18.5 % in D2 and D4 of serum starvation respectively. In addition, the extent of the down-regulation

of STIM1 was 47.5% and 53% in HeLa and NIH3T3 cells respectively. A previous study showed that no significant changes in either STIM1 or Orai1 expression levels were observed in SHSY-5Y and HSG cells under serum-free conditions (Sukumaran *et al.*, 2015). From that previous study (Sukumaran *et al.*, 2015) and since hTERT RPE-1 cells did not enter quiescent G0/G1 phase, these data imply that the down-regulation of SOCE proteins is associated with the cell cycle arrest in G0/G1 phase.

5.5 Conclusion

- A down regulation of STIM1 and Orai1 was observed in HeLa cells with cell cycle arrest in G0/G1 phase which possibly could explain the previously observed down-regulation of SOCE (Chapter 4).
- A down regulation of STIM1 and Orai1 was observed in NIH 3T3 cells with cell cycle arrest in G0/G1 phase indicating a role for these proteins in the previously observed down-regulation of SOCE (Chapter 4).
- Loss of STIM1 localisation at PM with cell cycle arrest in G0/G1 phase in both HeLa and NIH 3T3 cells might be responsible for the previously observed alterations in SOCE activity.
- In hTERT RPE-1 cells, Orai1 showed a slight decrease that was consistent to the slight down-regulation of SOCE previously observed (Chapter 4).
- Compared to hTERT RPE-1 cells, the alterations of Orai1 in HeLa and NIH 3T3 cells appeared to be attributed to cell cycle arrest and not serum starvation.

Chapter 6 Serum Starvation Time Course

6.1 Introduction

As previously shown in this study, serum starvation induced cell cycle arrest in G0/G1 phase in HeLa and NIH 3T3. Associated with the cell cycle arrest in G0/G1 phase, there was an uncoupling and a down-regulation of Ca^{2+} store release and SOCE and a decrease of the SOCE proteins STIM1 and Orai1.

For hTERT RPE-1 cells, serum starvation gave no increase in G0 cells, however, a down-regulation of Ca^{2+} store release and SOCE and changes of the SOCE proteins STIM1 and Orai1 were observed at day two and day four of the serum starvation time course.

The sequence of events occurring in the down regulation of SOCE and its proteins during serum starvation is not clear and therefore this chapter aims to investigate SOCE and SOCE proteins over a serum starvation time-course in the two cell lines; HeLa and NIH 3T3 where cells enter G0/G1 phase, and to compare these results with RPE-1 cells which don't enter G0/G1 upon starvation.

Throughout this chapter, the cells were grown in 10% FCS medium will be referred to as proliferating, whilst serum starved cells (0.01% FCS) will be referred to by the corresponding day of serum starvation time course.

6.2 Results - Changes in SOCE occurred in the first day of serum starvation time course

6.2.1 In HeLa cells

From D1 of the serum starvation time course, total Ca^{2+} store release (50.22± 2.16 FRUs) was significantly down-regulated compared to proliferating by ~33% (75.38 ± 2.08 FRUs) and total SOCE was also down-regulated by ~ 54% (207 ± 7.92 FRUs) compared to proliferating (451 ± 12.9 FRUs) (All $P < 0.0001$) (Figure 6.1.A). At D2, there was some recovery, where there was a significant down-regulation in total Ca^{2+} store release by ~ 23% (57.91 ± 2.824 FRUs) and in total SOCE by ~ 38 % (279.4 ± 11.35 FRUs) (All $P < 0.0001$) (Figure 6.1.A).

Total Ca^{2+} store release was further down-regulated in D3 by ~ 37% (47.42 ± 1.7FRUs), D4 by ~ 35% (48.8 ± 1.59 FRUs) and D5 by ~ 31% (51.76± 1.691FRUs) compared to proliferating (75.38 ± 2.08 FRUs) (All $P < 0.0001$). SOCE was also further down-regulated in D3 by 59.5%, (181.5 ± 5.61 FRUs), D4 by ~ 59 % (184.8 ± 5.51FRUs) and D5 by ~ 60% (180.7 ± 6.53 FRUs) compared to proliferating (451 ± 12.9 FRUs) (All $P < 0.0001$).

These results showed that serum starvation of HeLa cells induced changes in Ca^{2+} store release and SOCE in a multi-step manner, causing a down-regulation from D1 of serum starvation, some recovery at D2 then a further down-regulation at D3 after which the Ca^{2+} store release and SOCE were not further altered. This multi-step pattern correlates with the multi-step changes in the increase in percentage of G0 cells (Section 3.3.1, Figure 3.13).

These data were further confirmed by analysing maximal (as opposed to total) Ca^{2+} store release and maximal SOCE, using measurements of height of peak (HP) of Ca^{2+}-addback traces (method 2.8) (Figure 6.1.B). Maximal Ca^{2+} store release was significantly down-regulated at D1 by ~ 44% (0.18 ± 0.0058 FRUs), D2 by ~ 46% (0.17 ± 0.005FRUs), D3 by ~ 36% (0.21 ± 0.005FRUs), D4 by ~ 40% (0.19 ± 0.006FRUs) and D5 by ~ 38% (0.2 ± 0.006 FRUs) compared to proliferating (0.32 ± 0.008FRUs) (All $P < 0.0001$).

Consistent with the pattern of changes of total SOCE decrease, maximal SOCE was decreased in a multistep manner. Maximal SOCE was significantly down-regulated at D1 by ~33% (0.43 ± 0.013FRUs) compared to proliferating (0.64 ± 0.015 FRUs). At D2 there was some recovery where maximal SOCE was down regulated by ~17% (0.54 ± 0.017 FRUs) compared to proliferating (0.64 ± 0.015 FRUs). A D3 maximal SOCE was further down-regulated by ~34% (0.42 ± 0.009 FRUs) compared to proliferating and showed no further significant changes in D4 (0.403 ± 0.008 FRUs) and D5 (0.349 ± 0.009 FRUs) (All $P < 0.0001$) (Figure 6.1.B). Therefore both maximal Ca^{2+} store release and maximal SOCE were significantly reduced from the first day of serum starvation and remained down-regulated throughout the remainder of the five-day serum starvation time course.

Rate of rise (reflecting the speed of Ca^{2+} store release and activation of SOCE) and rate of decline (reflecting the speed of Ca^{2+} store emptying and deactivation of SOCE) of Ca^{2+}-addback traces were also analysed.

Rate of Ca^{2+} store release was significantly down-regulated from D1 by ~64 % (1.15 ± 0.5 $\times 10^{-3}$FRUs), D2 by ~ 65 % (1.14 ± 0.3 $\times 10^{-3}$FRUs), D3 by ~ 44.5 % (1.8 ± 0.4$\times 10^{-3}$

FRUs) , D4 by ~ 48% (1.68 ± 0.5×10^{-3}FRUs) and D5 by ~ 41% (0.92 ± 0.4 ×10^{-3} FRUs) compared to proliferating (3.25 ± 0.1 ×10^{-3}FRUs) (All P < 0.0001). This observation suggesting a decrease in of Ca^{2+} store capacity or decrease in TG sensitivity.

Rate of SOCE was also significantly down-regulated from D1 by ~27 % (5.75 ± 0.4×10^{-3} FRUs), D2 by ~ 35.5 % (5.08 ± 0.2×10^{-3} FRUs), D3 by ~ 37 % (4.99 ± 0.1 ×10^{-3} FRUs) , D4 by ~ 30% (5.5 ± 0.1×10^{-3}FRUs) and D5 by ~ 37.5 % (4.93 ± 0.2×10^{-3} FRUs) compared to proliferating (7.9± 0.4×10^{-3}FRUs) (All P < 0.0001) (Table 6.1).

Decline rate of Ca^{2+} store release was significantly increased at day four D4 by ~ 48 % (9.3 ± 1.24 × 10^{-5} FRUs) and at day five D5 by 91 % (11.26 ± 1.67 ×10^{-5} FRUs) compared to proliferating (5.897 ± 1.64×10^{-5} FRUs) (All P<0.05).

Decline rate of SOCE increased by 40%, 8%, 43 %, 39% in D1, D2, D3 and D4 respectively compared to proliferating, however the increase was not significant (P = 0.682). At D5 the decline rate of SOCE was significantly increased by ~54% (7.54 ± 2.06) compared to proliferating (4.82 ± 5.02) (P < 0.0001) (Table 6.1).

These findings suggest that serum starvation slows Ca^{2+} store release and increases the rate of emptying from the day one suggesting a decrease in Ca^{2+} store size or sensitivity to TG. Likewise, serum starvation slows the rate at which SOCE is activated from day one and increases rate of SOCE deactivation. Thus both Ca^{2+} store release and SOCE responses are smaller and shorter with serum starvation.

		Total All P <0.0001		Maximal All P <0.0001		ROR All P <0.0001		ROD All P <0.05	
		Values (FRUs)	**% change**	**Values (FRUs)**	**% change**	**Values ($\times 10^{-3}$ FRUs)**	**% change**	**Values ($\times 10^{-5}$ FRUs)**	**% change**
Ca^{2+} release	Proliferating	75.38±2.08	------	0.32 ± 0.008	------	3.25 ± 0.1	------	5.89 ± 1.16	------
	D1	50.22± 2.16	-33%	0.18± 0.005	-44 %	1.15 ± 0.5	-65 %	9.29 ± 1.84	58%
	D2	57.91± 2.82	-23%	0.17 ±0.005	-47%	1.14 ± 0.3	-65 %	8.53± 2.67	45%
	D3	47.42 ± 1.7	-37%	0.21 ± 0.005	-34%	1.8 ± 0.4	-44.5%	8.03 ± 1.65	36%
	D4	48.8 ± 1.59	-35%	0.19 ± 0.006	-40.5%	1.68 ± 0.5	-48 %	9.3 ± 1.24*	58%
	D5	51.76± 1.69	-31%	0.20± 0.006	-38%	0.92 ± 0.4	-72%	7.52 ± 2.06	28%
SOCE	Proliferating	451 ± 12.9	------	0.64 ± 0.015	------	7.9 ± 0.0004	------	4.82 ± 5.02	------
	D1	207 ± 7.929	-54%	0.43 ± 0.013	-32.5%	5.75 ± 0.0004	-27 %	6.83 ± 1.84	42%
	D2	279.4± 11.3	-38%	0.54 ± 0.017	-15.5 %	5.08 ± 0.0002	-35.5%	5.29 ± 2.67	10%
	D3	181.5± 5.61	-60%,	0.42± 0.009	-34 %,	4.99 ± 0.0001	-37%	7.03 ± 1.65	46%
	D4	184.8± 5.51	-59.2%	0.40 ± 0.008	-38%,	5.5 ± 0.0001	-29.5%	6.81 ± 1.24*	41%
	D5	180.7± 6.53	-60%	0.34± 0.009	-47 %	4.93 ± 0.0002	-37.5%	7.54 ± 2.06	56%

Table 6.1 Changes of Ca^{2+} signalling responses over five-day serum starvation in HeLa cells

The total response (area under the peak, AUP), maximal response (the height of peak, HOP), rate of rise (ROR) and rate of decline (ROD) for TG and $CaCl_2$

responses from calibrated fluorescence traces were calculated using Excel functions in a template spread sheet (Methodology chapter 2.8, figure 2.10) over five days of serum starvation. Data represented as means ± SEM. FRUs (fluorescence ratio unit). For proliferating cells n =228, for D1 n = 200, D2 n = 232, D3 n = 231, D4 n= 206 and D5 n= 167. N=5.

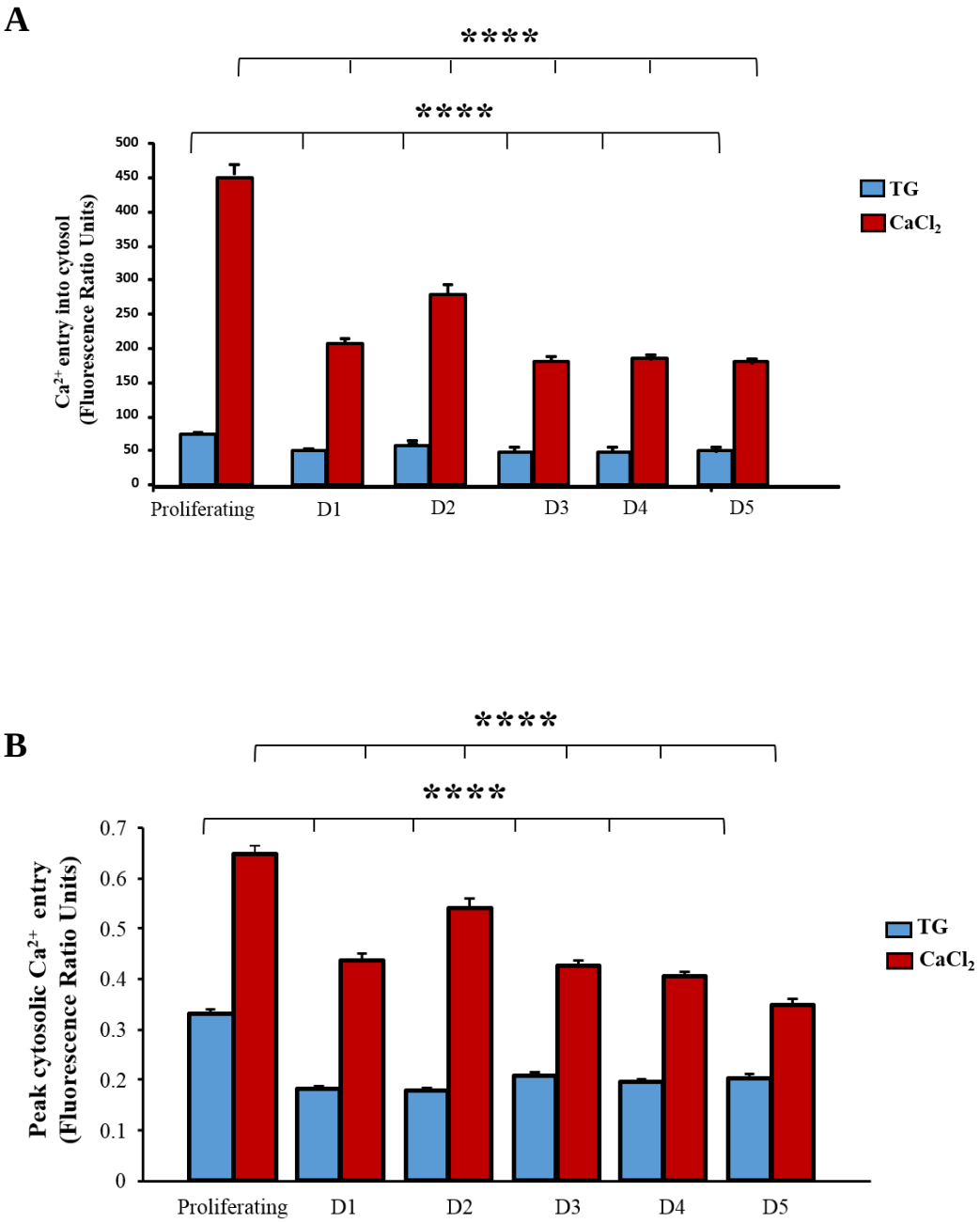

Figure 6.1 Serum starvation induces SOCE changes in a multi-step manner in HeLa cells

HeLa cells were grown in either 10% FCS medium (proliferating) or 0.1% FCS medium (starved) for five days. D1, D2, D3, D4 and D5 represent one day, two days, three days, four and five days of serum starvation. Graph shows mean of total Ca^{2+} entry into the cytosol following Ca^{2+} store release in response to stimulation with 200nM thapsigargin (TG) and subsequent SOCE following the addition of 2mM $CaCl_2$. Changes in

fluorescence ratio units (FRUs) reflect changes in [Ca2+]i. At D1, total Ca^{2+} store release was significantly down-regulated by 33.37% and total SOCE was down-regulated by 54.09% compared to proliferating (P <0.0001****). At D2, there was some recovery with total Ca^{2+} store release down-regulated by 23% and a significant down-regulation in SOCE by 38% compared to proliferating (P< 0.0001****). Comparing D2 to D1, there was a significant increase in total Ca^{2+} store release, P = 0.0356* and in total SOCE, P<0.0001****. Total Ca^{2+} store release was further down-regulated by 37%, 35% and 31% at D3, D4 and D5 respectively compared to proliferating (P < 0.0001****). SOCE was further down-regulated by 59%, 59% and 59 % at D3, D4 and D5 respectively compared to proliferating (P < 0.0001****). **B)** Maximal Ca^{2+} store release was significantly down-regulated by 44%, 45%, 36%, 40%, 38% in D1, D2, D3, D4 and D5 respectively compared to proliferating (P < 0.0001****). Maximal SOCE was down-regulated by 32%, 16%, 34%, 37%, 46 % in D1, D2, D3, D4 and D5 respectively compared to proliferating (P < 0.0001****). Error bars represent S.E.M. For proliferating cells n =228, for D1 n = 200, D2 n = 232, D3 n = 231, D4 n= 206 and D5 n= 167. N=5.

6.2.2 In NIH 3T3 cells

Ca^{2+} signalling changes were measured in NIH 3T3 cells over three day serum starvation time course as at day four of serum starvation cell viability was significantly decreased (Section 3.2.2 and 3.3.2).

At day one of serum starvation, an uncoupling of total Ca^{2+} store release and SOCE was observed. Total Ca^{2+} store release (40.2 ± 2.5) was not significantly different compared to proliferating (46.4 ± 2.20), (P= 0.1859) whilst total SOCE (60.43 ± 3.6 FRUs) was significantly down-regulated compared to proliferating (84.28 ± 3.82) by 28 % (P < 0.0001) (Figure 6.2.A).

At D2, total Ca^{2+} store release (10.55 ± 0.98) was significantly down-regulated by 77 % and at D3 (10.22 ± 1.15) by 78% compared to proliferating (46.4 ± 2.20) (All P < 0.0001). SOCE was further significantly down-regulated in D2 (32.49 ± 2.5) and D3 (32.94 ± 4.39) by 61.5 % and 61% compared to proliferating (84.28 ± 3.82) (All P < 0.0001) (Figure 6.2.A).

Thus an uncoupling of Ca^{2+} store release and SOCE occurs in the first day of serum starvation. From day two of serum starvation there is reduced Ca^{2+} store release and SOCE and these were coupled suggesting that either SOCE uncoupling is an early effect of serum starvation or that SOCE uncoupling is involved only in the initiation of entering the NIH 3T3 cells into quiescence but not in maintaining the quiescence state.

Similarly, at D1, maximal Ca^{2+} store release (0.15 ± 0.007 FRUs) was significantly up-regulated by ~ 26 % compared to proliferating (0.12 ± 0.004 FRUs) (P < 0.0001) and SOCE (0.17 ± 0.007 FRUs) was down-regulated by ~ 30 % compared to proliferating (0.24 ± 0.009 FRUs) (P < 0.0001). At D2 maximal Ca^{2+} store release (0.0428 ± 0.003 FRUs) was significantly down-regulated by 65 % and at D3 (0.045 ± 0.003 FRUs) by 62.5% compared to proliferating (0.12 ± 0.004 FRUs) (All P < 0.0001). Maximal SOCE was also down-regulated in D2 (0.15 ± 0.011 FRUs) and D3 (0.14 ± 0.011 FRUs) by 36.5 % and 40% compared to proliferating (0.24 ± 0.009 FRUs) (All P < 0.0001) (Figure 6.2.B).

At D1, rate of Ca^{2+} store release (0.81 ± 0.31×10^{-3} FRUs) was down-regulated by ~ 15.5%, at D2 (0.54±0.02×10^{-3} FRUs) by ~ 43.5% and at D3 (0.64 ± 0.04 ×10^{-3} FRUs) by ~ 33%

compared to proliferating ($0.968 \pm 0.047 \times 10^{-3}$ FRUs), however this down- regulation was not significant ($P > 0.05$) (Table 6.2).

Rate of SOCE was not significantly different at D1 ($4.69 \pm 0.32 \times 10^{-3}$ FRUs), D2 ($4.02 \pm 0.511 \times 10^{-3}$ FRUs) and D3 ($3.57 \pm 0.28 \times 10^{-3}$ FRUs) compared to proliferating ($4.85 \pm 0.39 \times 10^{-3}$ FRUs) ($P < 0.999$) (Table 6.2).

The increase in maximal Ca^{2+} release and rate of Ca^{2+} store release at D1 of the three-day serum starvation time course in conjunction with the previous observation of no change in store size suggests an increase in the sensitivity to TG as an initial response to serum starvation.

Decline rate of Ca^{2+} store release was slightly increased by ~ 12.5 % at D1, decreased by ~ 60% at D2 and increased again by ~ 22% at D3 compared to proliferating however this changes were not significant ($P = 0.976$) compared to proliferating. Decline rate of SOCE increased gradually over the 3-day serum starvation time course by ~ 32.59%, ~ 70.51% and ~ 93.9% in D1, D2 and D3 respectively compared to proliferating. The increase became significant at D3 ($P = 0.0139$) (Table 6.2). This observation indicates that serum starvation causes an increase in the speed of SOCE deactivation with subsequent smaller and shortened SOCE response.

These results show that SOCE was down- regulated from the first day in a gradual manner and reached its peak of down-regulation at day 2 which correlates with the changes in the G0 cells (Section 4.2.2, Figure 3.16).

		Total All P <0.0001		Maximal All P <0.0001		ROR All P > 0.05		ROD All P > 0.05	
		Values (FRUs)	**% changes**	**Values (FRUs)**	**% changes**	**Values ($\times 10^{-3}$ FRUs)**	**% changes**	**Values ($\times 10^{-5}$ FRUs)**	**% changes**
Ca^{2+} release	Proliferating	46.4 ± 2.20	------	0.12 ± 0.004	------	0.96± 0.047	------	13.35 ± 3.46	------
	D1	40.2 ± 2.5	-13%	0.15 ± 0.007	25%	0.81 ± 0.31	-15.5%	11.69 ± 4.85	12.5%
	D2	10.55±0.98	-77%	0.042 ± 0.003	-65%	0.54±0.02	-43.5%	5.22 ± 3.22	-61%
	D3	10.22±1.15	-78%	0.045 ± 0.003	-62.5%	0.64± 0.04	-33%	16.29 ± 5.39	22%
SOCE	Proliferating	84.28±3.82	------	0.24 ± 0.009	------	4.85 ± 0.39	------	1.7 ± 9.172	------
	D1	60.43 ± 3.6	-28%	0.17 ± 0.007	-30%	4.69 ± 0.32	-3%	2.52 ± 9.934	48%
	D2	32.49 ± 2.5	-61.5%	0.15 ± 0.011	-37.5%	4.02 ± 0.51	-17%	5.76 ± 6.489	239%
	D3	32.94±4.39	-61%	0.14 ± 0.011	-42%	3.57 ± 0.28	-26%	2.78 ± 8.35	64%

Table 6.2 Changes of Ca^{2+} signalling responses over 3-day serum starvation time course in NIH 3T3 cells

The total response (area under the peak, AUP), maximal response (the height of peak, HOP), rate of rise (ROR) and rate of decline (ROD) for TG and $CaCl_2$ responses from calibrated fluorescence traces were calculated using Excel functions in a template spread sheet (Methodology chapter 2.8, figure 2.10) over three days of serum starvation. Data represented as means ± SEM. FRUs (fluorescence ratio unit). For proliferating cells n =249, for D1 n = 198, D2 n = 128 and D3 n = 109, N=3.

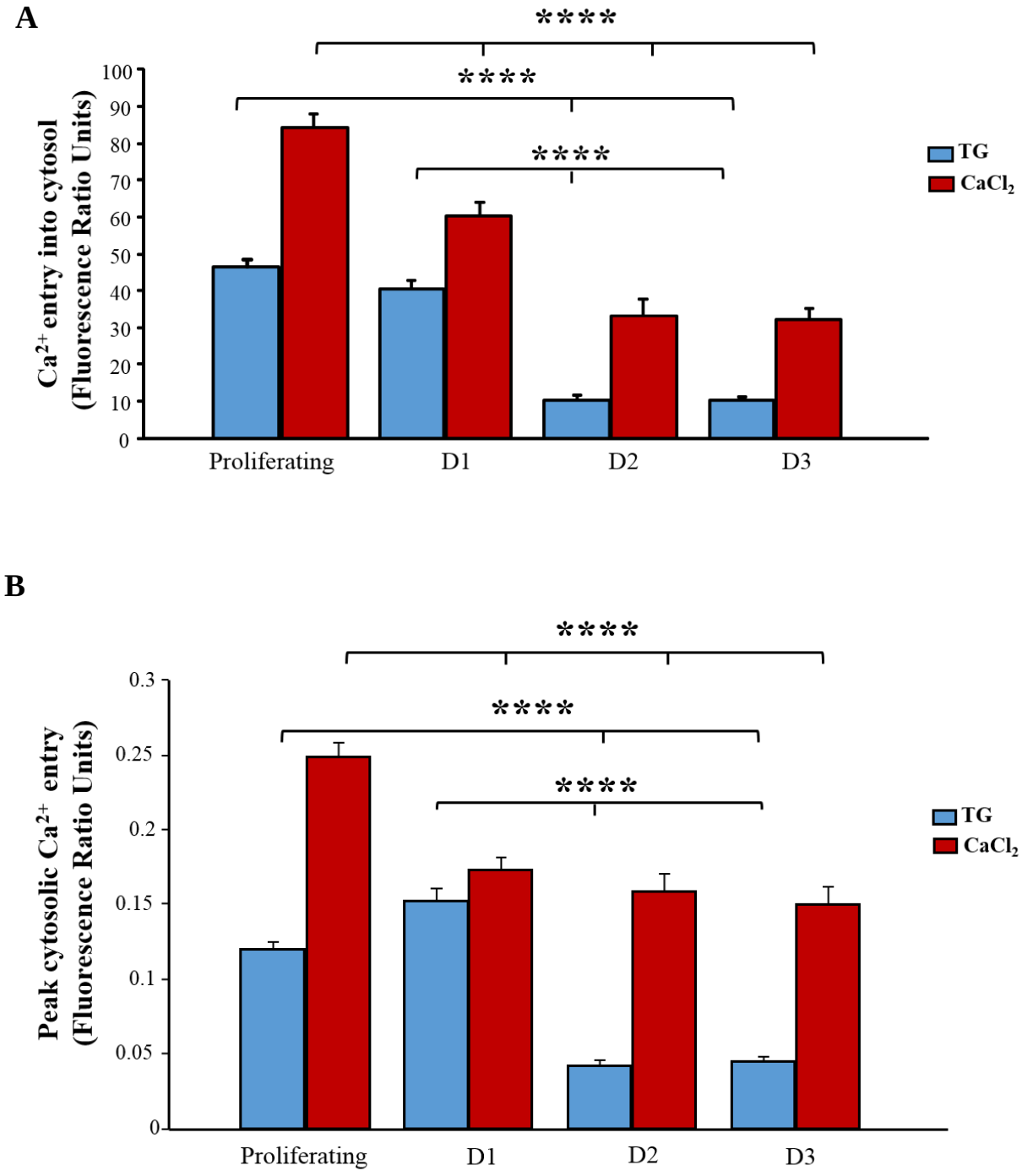

Figure 6.2 Serum starvation induces SOCE changes in a gradual manner in NIH 3T3 cells

NIH 3T3 cells were grown in either 10% FCS medium (proliferating) or 0.1% FCS medium (starved) for 3 days. D1, D2 and D3 represent one day, two days and three days of serum starvation. Graph shows mean of total Ca^{2+} entry into the cytosol following Ca^{2+}

store release in response to stimulation with 200nM thapsigargin (TG) and subsequent SOCE following the addition of 2mM $CaCl_2$ in proliferating and starved cells. Changes in fluorescence ratio units (FRUs) reflect changes in $[Ca^{2+}]_i$. Total Ca^{2+} store release was significantly down-regulated by 77% and 77% in D2 and D3 respectively compared to proliferating ($P < 0.0001$****). However, store release was not significantly different between proliferating and D1 cells, P= 0.1859. SOCE was significantly down-regulated by 28%, 61% and 60% in D1, D2 and D3 respectively compared to proliferating ($P < 0.0001$****). **B)** At D1, maximal Ca^{2+} store release was significantly up-regulated by ~ 26 % compared to proliferating, $P< 0.0001$****. At D2 and D3, maximal Ca^{2+} store release was significantly down-regulated by ~ 65% and ~ 62.5% respectively compared to proliferating (All $P < 0.0001$****). Maximal SOCE was down-regulated by ~ 30%, ~ 36% and ~ 39% in D1, D2 and D3 respectively compared to proliferating (All $P < 0.0001$****). Error bars represent S.E.M. For proliferating cells n =249, for D1 n = 198, D2 n = 128 and D3 n = 109, N=3.

6.2.3 In hTERT RPE-1 cells

Serum starvation induced significant down-regulation of total Ca^{2+} store release on D1 by ~ 28% (28.05 ± 1.76 FRUs), D2 by ~ 45%, (21.22 ± 0.9604 FRUs), D3 by ~ 45 % (21.26 ± 0.659 FRUs), D4 by ~ 40% (23.25±0.933FRUs) and D5 by ~37.5% (24.32±0.85FRUs), compared to proliferating (38.89 ± 1.05 FRUs) (All $P < 0.001$) (Figure 6.3.A). SOCE was also significantly down-regulated at D1 by ~ 21.5%, (47.98 ± 2.17 FRUs), D2 by ~ 13.5% (52.89 ± 1.643 FRUs), D3 by ~ 20.5 % (48.59 ± 2.57 FRUs), D4 by ~ 23.5% (46.58± 2.08) and D5 by ~ 21% (48.58± 4.08), compared to proliferating (61.21± 1.298 FRUs) (All $P < 0.05$) (Figure 6.3.A).

This data suggests either a reduction of store size or sensitivity to TG with subsequent reduction in SOCE occurring from day one of the five-day serum starvation time course.

These results also showed that there is an uncoupling of SOCE from Ca^{2+} store release from day two of serum starvation that was maintained over the starvation time course.

Consistent with the above results, maximal Ca^{2+} store release was significantly down-regulated in D1 by ~ 20% (0.14 ± 0.004 FRUs), D2 by ~ 40% (0.105 ± 0.007 FRUs), D3 by ~ 35.5 % (0.11 ± 0.003 FRUs), D4 by ~37.5% (0.11 ± 0.004 FRUs) and D5by ~ 42 % (0.101 ± 0.003 FRUs) compared to proliferating (0.175 ± 0.004 FRUs) (All $P < 0.001$) (Figure 6.3.B). Maximal SOCE was also significantly down-regulated at D1 by ~ 30% (0.28 ± 0.006 FRUs), D2 by ~ 37% (0.25± 0.005 FRUs), D3 by ~ 35.5 % (0.26 ± 0.008 FRUs), D4 by ~ 43% (0.23± 0.009 FRUs) and D5 by ~ 35% (0.26± 0.01FRUs) compared to proliferating (0.40 ± 0.008 FRUs) (All $P < 0.01$) (Figure 6.3.B).

Rate of Ca^{2+} store release was not significantly different over the five day serum starvation time course compared to proliferating ($P > 0.05$). D1 (1.79 ± 0.09 $\times 10^{-5}$ FRUs), D2 (2.11 ± 0.25 $\times 10^{-5}$ FRUs), D3 (1.84 ± 0.077 $\times 10^{-5}$), D4 (2.01±0.26 $\times 10^{-5}$ FRUs) and D5 (1.91±0.35 $\times 10^{-5}$ FRUs). Rate of SOCE was significantly decreased in D2 by ~ 36% (4.39 ± 0.32$\times 10^{-3}$FRUs), D3 by ~ 32% (4.25 ± 0.21$\times 10^{-3}$ FRUs), D4 by ~ 28% (4.601±0.15 × 10^{-3} FRUs) and D5 by ~ 37% (4.32±0.13 × 10^{-3} FRUs) compared to proliferating (6.86 ± 0.14× 10^{-3} FRUs) ($P < 0.01$) (Table 6.3).

Decline rate of Ca^{2+} store release and SOCE was not significantly changed over the five day serum starvation time course (All $P > 0.05$) (Table 6.3).

		Total		Maximal		ROR		ROD	
		Values (FRUs)	**% change**	**Values (FRUs)**	**% change**	**Values (×10^{-3} FRUs)**	**% change**	**Values (×10^{-5} FRUs)**	**% change**
Ca^{2+}release	Proliferating	38.89±1.05	------	0.175±0.004	------	1.84 ± 0.08	------	20.95 ± 7.5	------
	D1	28.05±1.76***	-28%	0.14±0.004***	-20%	1.79 ± 0.09	-2.5%	23.2 ± 4.27	10.5%
	D2	21.2± 0.96***	-45%	0.10±0.007***	-43%	2.11 ± 0.25	14.5%	14.15 ± 10.08	-32%
	D3	21.26±0.65***	-45%	0.11±0.003***	-37%	1.84 ± 0.077	0	13.23 ± 9.07	-36%
	D4	23.25±0.93***	-40%	0.11±0.004***	-37.5%	2.01±0.26	9%	17.51± 5.08	-16.5%
	D5	24.32±0.85***	-37.5%	0.10±0.003***	-42%	1.91±0.35	4%	20.43± 4.1	-2%
SOCE	Proliferating	61.21±1.29	------	0.40 ± 0.008	------	6.86 ± 0.14	------	133.7 ± 11.94	------
	D1	47.98±2.17*	-21.5%	0.28 ± 0.006**	-30%	6.12 ± 0.37	-10%	108.9 ± 15.46	-18%
	D2	52.89±1.64*	-13.5%	0.25± 0.005**	-38%	4.39 ± 0.32**	-36%	86.27 ± 9.07	-35%
	D3	48.59 ± 2.57*	-20.5 %	0.26 ± 0.008**	-35%	4.25 ± 0.21**	-38%	91.6 ± 15.31	-31%
	D4	46.58±2.08*	-23.5%	0.23± 0.009**	-43%	4.6±0.15**	-33%	90.42±10.06	-32%
	D5	48.58±4.08*	- 21%	0.26± 0.01**	-35%	4.32±0.13**	-37%	97.22±11.21	-27%

Table 6.3 Changes of Ca^{2+} signalling responses over five-day serum starvation time course in hTERT RPE-1 cells

The total response (area under the peak, AUP), maximal response (the height of peak, HOP), rate of rise (ROR) and rate of decline (ROD) for TG and $CaCl_2$ responses from calibrated fluorescence traces were calculated using Excel functions in a template spread sheet (Methodology chapter 2.8, figure 2.10) over three days of serum starvation. Data represented as means ± SEM. FRUs (fluorescence ratio unit) $P< 0.05$ *, $P < 0.01$**, $P < 0.001$***. For proliferating cells n =338, for D1 n = 211, D2 n = 195 and D3 n = 196, N=3. For D4 and D5 N=2.

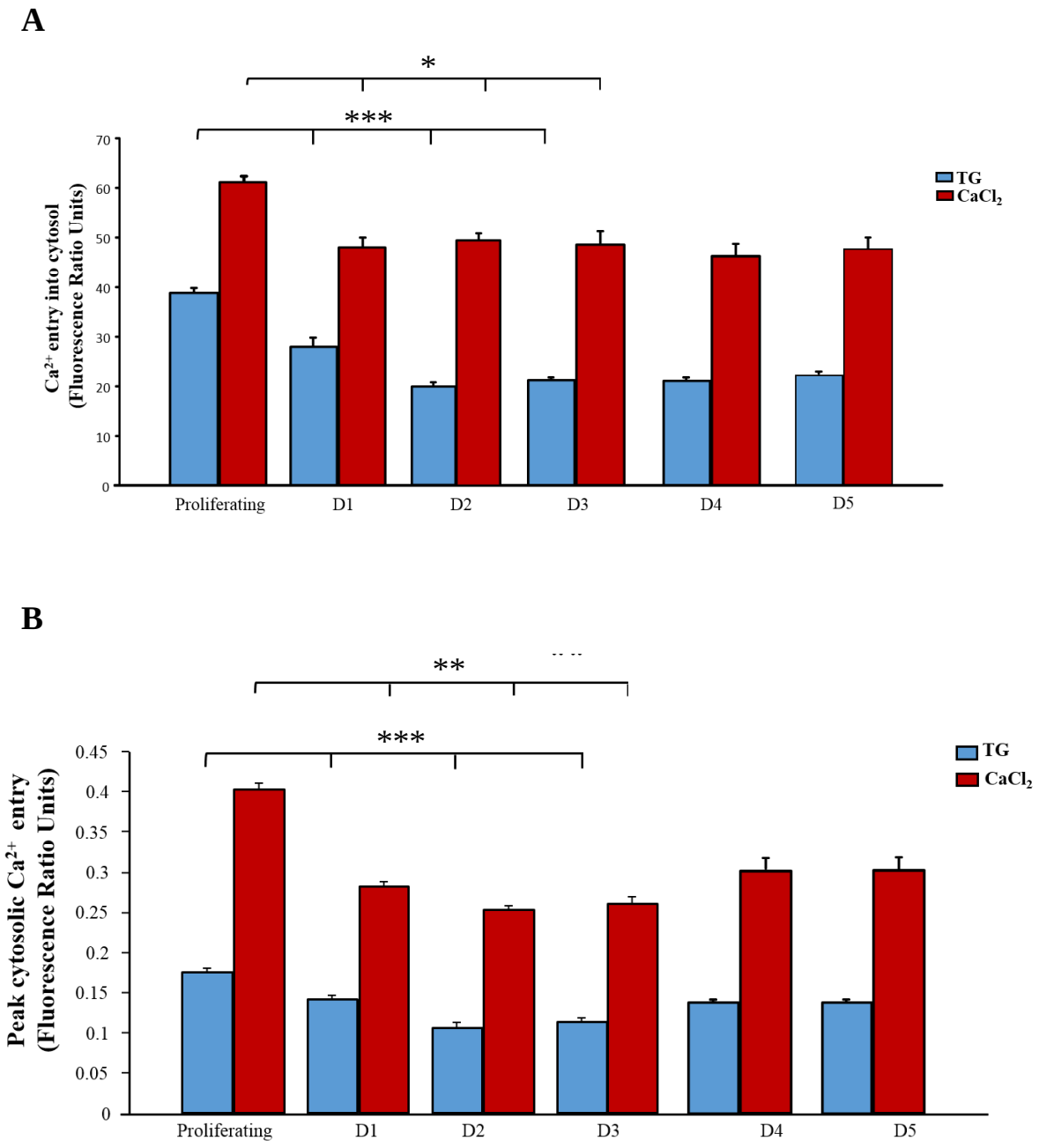

Figure 6.3 Serum starvation induces SOCE changes from first day in hTERT RPE-1 cells

hTERT RPE-1 cells were grown in either 10% FCS medium (proliferating) or 0.1% FCS medium (starved) for 3 days. D1, D2 and D3 represent one day, two days and three days of serum starvation. Graph shows mean of total Ca^{2+} entry into the cytosol following Ca^{2+} store release in response to stimulation with 200nM thapsigargin (TG) and subsequent SOCE following the addition of 2mM $CaCl_2$ in proliferating and starved cells. Fluorescence ratio units (FRUs) represent a change in $[Ca^{2+}]_i$. Total Ca^{2+} store release was

significantly down-regulated by ~ 28%, ~ 458% ~ 45%, ~40% and ~ 37.5% in D1, D2, D3, D4 and D5 respectively compared to proliferating (All $P < 0.001$***). SOCE was also significantly down-regulated by ~ 21.5%, ~13.5%, ~ 20.5 %, 23.5% and 21% in D1, D2, D3, D4 and D5 respectively compared to proliferating (All $P < 0.05$*). **B)** Maximal Ca^{2+} store release was significantly down-regulated by ~ 20%, ~40% and ~ 35.5%, 37.5 and 42% in D1, D2, D3,D4 and D5 respectively compared to proliferating (All $P < 0.001$***). Maximal SOCE was down-regulated by ~ 30%, ~37% 35.5%, 43% and35% in D1, D2, D3, D4 and D5 respectively compared to proliferating (All $P < 0.01$**). Error bars represent S.E.M. For proliferating cells n =338, for D1 n = 211, D2 n = 195 and D3 n = 196, N=3. For D4 and D5 N=2.

6.3 Results - Changes in SOCE proteins expression occurred from the first day of serum starvation time course

As seen above, SOCE became down-regulated from the first day of serum starvation. In order to determine any changes in STIM1and Orai1 protein expression associated with the observed changes in SOCE, cells were grown in 10% FCS medium or 0.1% FCS medium (starved) for four days for HeLa and RPE-1 cells and three days for NIH 3T3 cells and then western blots were performed on protein extracted from proliferating and starved cells (Methods 2.6).

6.3.1 In HeLa cells

STIM1 was expressed before and over the 5-day serum starvation time course in HeLa cells as determined by a band detected at 84kDa by an anti-STIM1 antibody (Figure 6.4.A). Blots were re-probed with β-actin, used as a loading control, and STIM1 levels were expressed as a ratio of β-actin in order to quantify changes in band intensity (Figure 6.4.B).

STIM1 protein expression was significantly decreased by~ 53%, ~ 34.5%, ~39%, ~49% and ~60.5% on D1, D2,D3,D4 and D5 respectively compared to proliferating ($P < 0.01$**).

Similarly, Orai1 was expressed in both proliferating and starved cells as determined by a band detected between 37 and 50 kDa by an anti- Orai1 antibody (Figure 6.5.A). Blots were re-probed with β-actin, used as a loading control, and Orai1 was expressed as a ratio of β-actin in order to quantify changes in band intensity (Figure 6.5.B).

Orai1 protein expression was significantly decreased in D1, D2 and D3 by ~ 36%, ~ 42%, ~ 29% respectively compared to proliferating ($P <0.05$), at D4 and D5 Orai1 was further decrease by ~ 68.5% and ~ 66% respectively compared to proliferating ($P < 0.01$). This down-regulation would possible contribute to the dampened SOCE observed in day three and day four of serum starvation time course in HeLa cells (Chapter 3).

Orai1 expression showed a triple band in proliferating and over the serum starvation time course. The upper, middle and lower (Figure 6.5.C) Orai1 band were analysed individually. Orai1 expression showed the same pattern as that of whole band analysis where it was significantly decreased from the first day of serum starvation, show some

recovery at D2 and D3 however it is still significantly decreased compared to proliferating cells ($P < 0.05$). In D4 and D5, there was a further decrease in Orai1 expression compared to proliferating ($P < 0.01$).

These results showed that there was a parallel relation between SOCE and STIM1 changes (Figure 6.6.A) whereas Orai1 expression was inversely correlated to the changes in G0 cells (Figure 6.6.B).

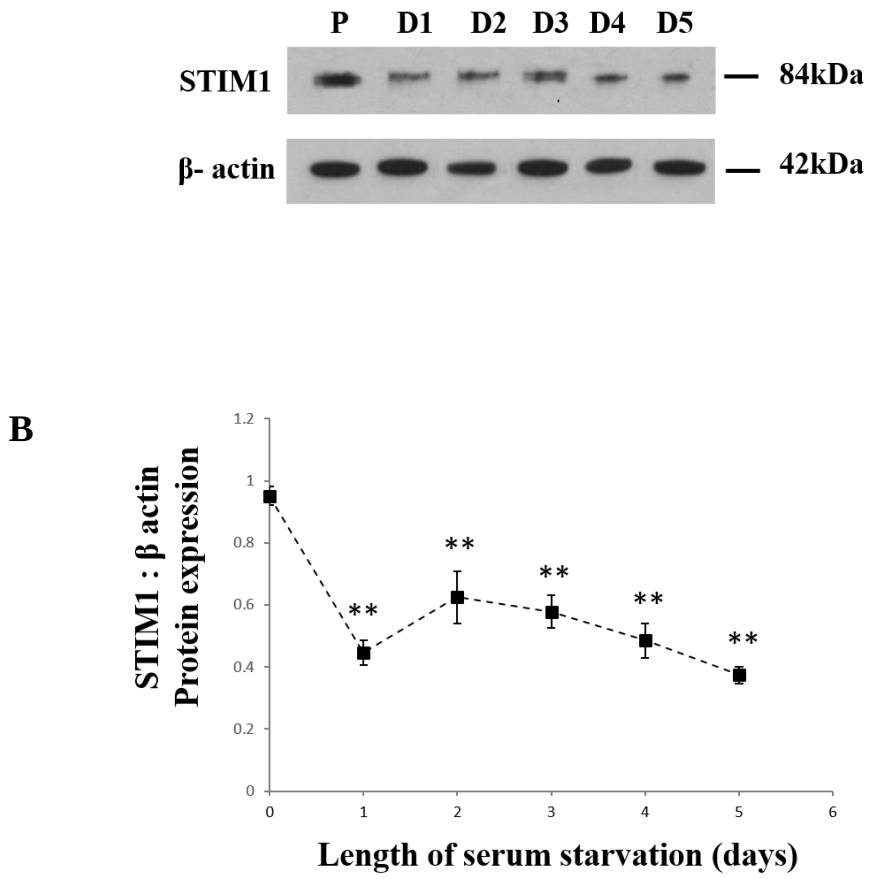

Figure 6.4 STIM1 expression was decreased from first day of serum starvation in HeLa cells

HeLa cells were grown in 10% FCS medium (proliferating) or 0.1% FCS medium (starved) for 5 days. Blots were probed with anti-STIM1 antibody which detected a band at 84 kDa or β- actin antibody which was used as a loading control and detected a band at 42 kDa. **A)** STIM1 was expressed in proliferating (P) and starved cell populations D1, D2, D3, D4 and D5. Blots were re-probed with anti-β-actin antibody (42kDa), used as a loading control. **B)** Quantitative measurements of bands were performed using densitometry (ImageJ software, Methods 2.6.9) where STIM1 was expressed as a ratio of β-actin. There was a significant decrease in STIM1 expression from day one of the serum starvation time-course by ~ 53% ($P < 0.01$**). STIM1 expression was also decreased by ~ 34.5%, ~39%, ~49% and ~60.5% in D2,D3,D4 and D5 respectively compared to proliferating ($P < 0.01$**). N = 5.

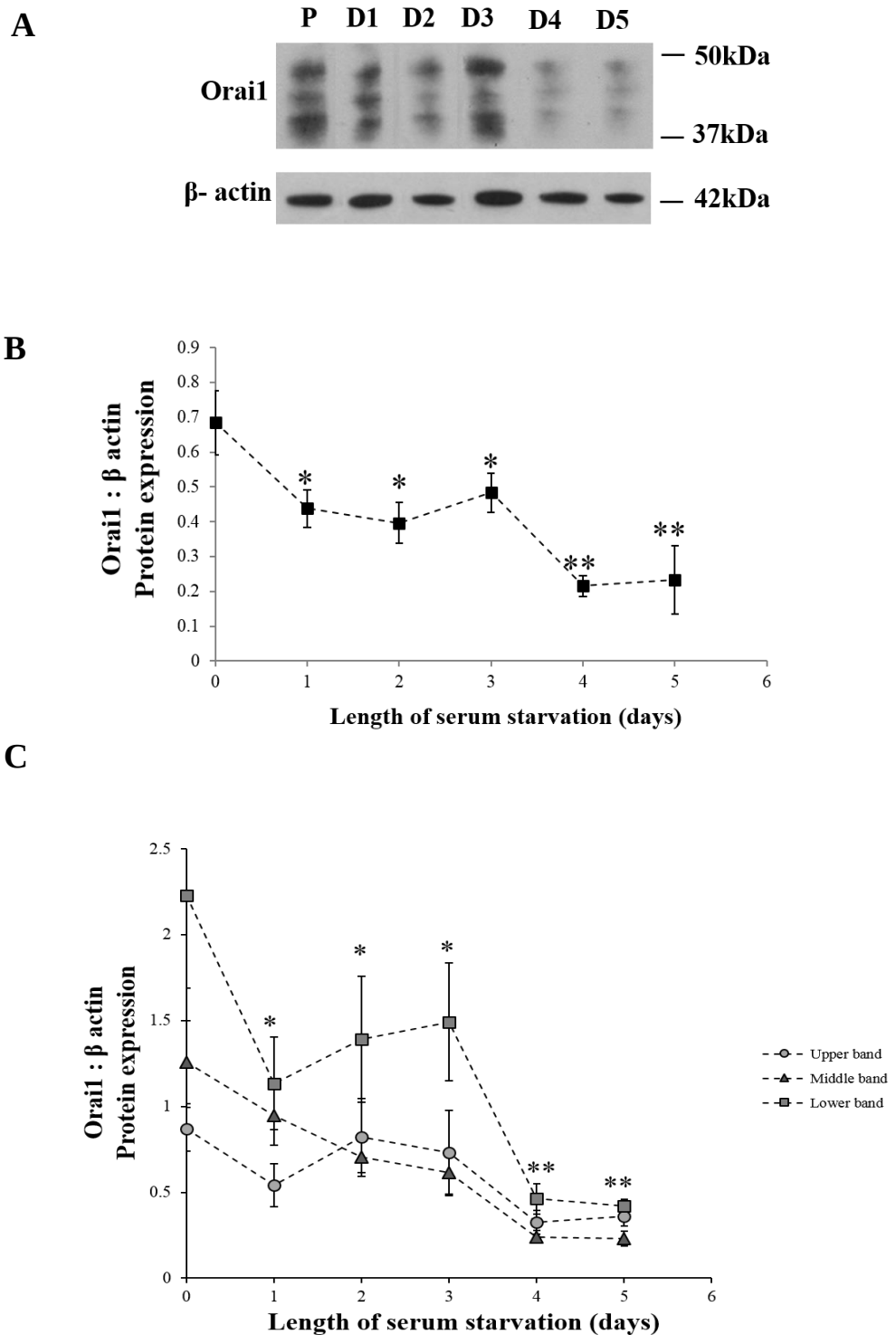

Figure 6.5 Orai1 expression was decreased from first day of serum starvation in HeLa cells

HeLa cells were grown in 10% FCS medium (proliferating) or 0.1% FCS medium (starved) for 5 days. Blots were probed with anti-Orai1 antibody which detected a band between 37 and 50 kDa or β- actin antibody which was used as a loading control and

detected a band at 42 kDa. **A**) Orai1 was expressed in proliferating (P) and starved cell populations D1, D2, D3, D4 and D5. **B**) Quantitative measurements of bands were performed using densitometry (ImageJ software, Methods 2.6.9) where Orai1 was expressed as a ratio of β-actin. There was a significant decrease in Orai1 expression in D1, D2 and D3 by ~ 36%, ~ 42%, ~ 29% respectively compared to proliferating ($P < 0.05$*), at D4 and D5 Orai1 was further decrease by ~ 68.5% and ~ 66% respectively compared to proliferating ($P < 0.01$**). **C)** Quantitative analysis of upper, middle and lower Orai1 bands. Orai1 expression showed the same pattern as that of whole band analysis (B). Orai1 expression was significantly decreased from the first day of serum starvation, show some recovery at D2 and D3 however it is still significantly decreased compared to proliferating cells ($P < 0.05$*). In D4 and D5, there was a further decrease in Orai1 expression compared to proliferating ($P < 0.01$**). N=4.

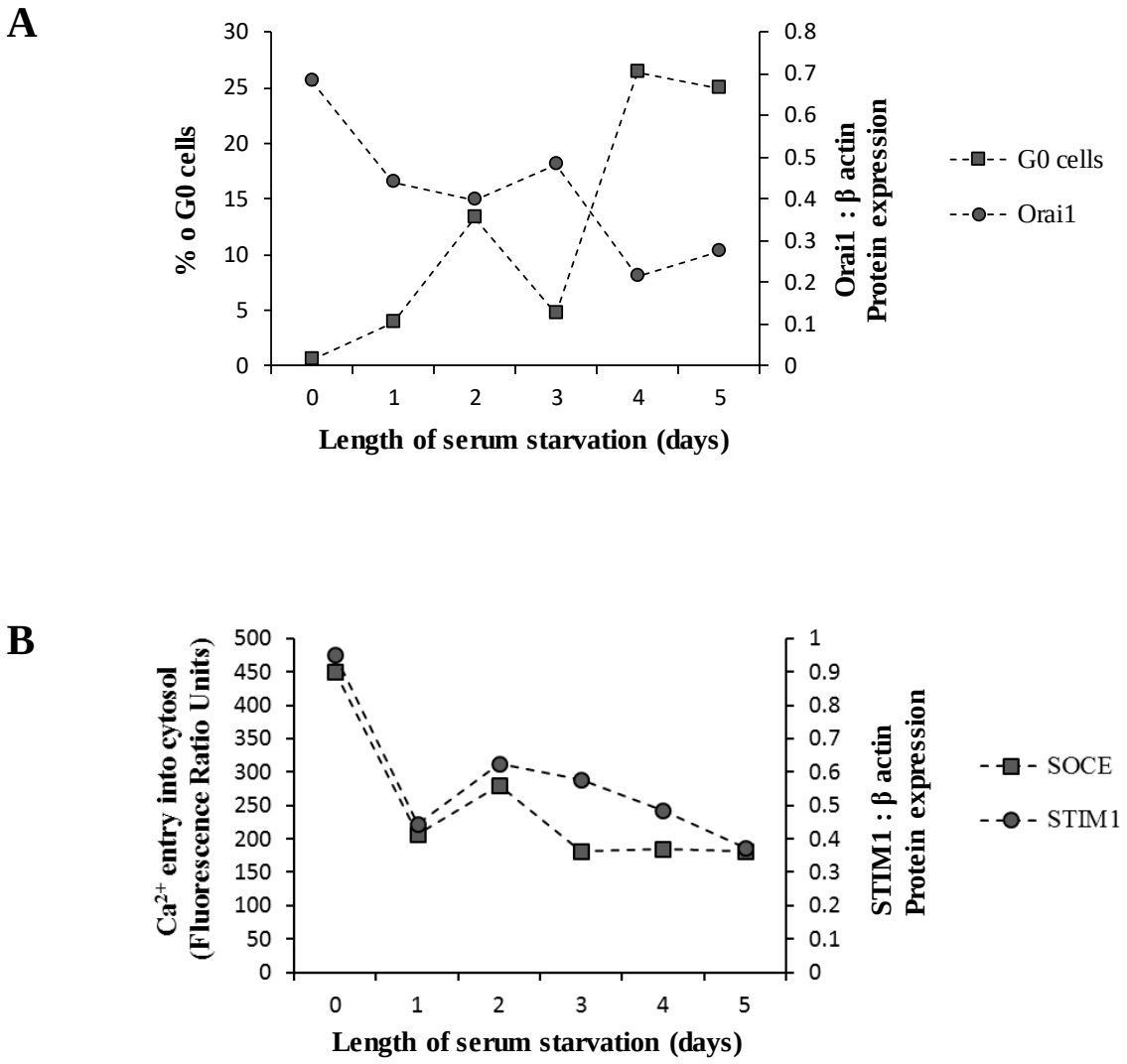

Figure 6.6 A comparison between changes in STIM1 and Orai1 in relation to SOCE and percentage of G0 cell respectively in HeLa cells

6.3.2 In NIH 3T3 cells

As seen in HeLa cells, STIM1 was also expressed before and over the three day serum starvation time course in NIH 3T3 cells as determined by a band detected at 84kDa by an anti-STIM1 antibody (Figure 6.7.A). Blots were re-probed with β-actin and STIM1 was expressed as a ratio of β-actin which showed that STIM1 protein expression was decreased from the first day by 29% compared to proliferating. This decrease was consistent with the down-regulation of SOCE which was 28% at day one (Section 6.2.2). At D2 and D3, STIM1 expression was significantly decreased by ~49.5% and ~54.5% respectively compared to proliferating ($P = 0.0243$) (Figure 6.7.B). The extent of down-regulation of SOCE was ~60% and ~61% in day two and day three of serum starvation time course respectively (Figure 6.2.A). The changes observed in SOCE are consistent with those seen in STIM1 expression and again confirm that STIM1 is involved in the process of SOCE in NIH 3T3 cells.

The relationship between Orai1 expression and SOCE following serum starvation was also investigated in NIH 3T3 cells.

Orai1 was expressed before and over the three day serum starvation time course in NIH 3T3 cells as determined by a band detected between 37 and 50 kDa by an anti- Orai1 antibody (Figure 6.8.A). Blots were re-probed with β-actin, used as a loading control, and Orai1 was expressed as a ratio of β-actin in order to quantify changes in band intensity (Figure 6.8.B).

Orai1 protein expression was significantly decreased by ~68.5%, ~53% and ~47% in day one, day two and day three of serum starvation time course compared to proliferating ($P < 0.05$). Thus the observed increase in percentage of G0 cells at D1and D2 with serum starvation in NIH 3T3 cells (Section 3.3.2) suggests that Orai1 down-regulation as being more influential in this than expression levels of STIM1, which were only slightly altered at D1.

As observed previously, Orai1 expression appeared in two distinct molecular masses in proliferating and over the 3-day serum starvation time course. The upper and lower Orai1 band were analysed individually (Figure 6.8.C). Consistent with the previous data showed in chapter 5, the upper band showed significant down-regulation of Orai1expression in D1, D2 and D3 cells compared to proliferating ($P < 0.01$**), while the lower band showed no

significant changes compared to proliferating ($P > 0.05$). This again may suggest that the activity Orai1 may exist in two different states in NIH 3T3 cells.

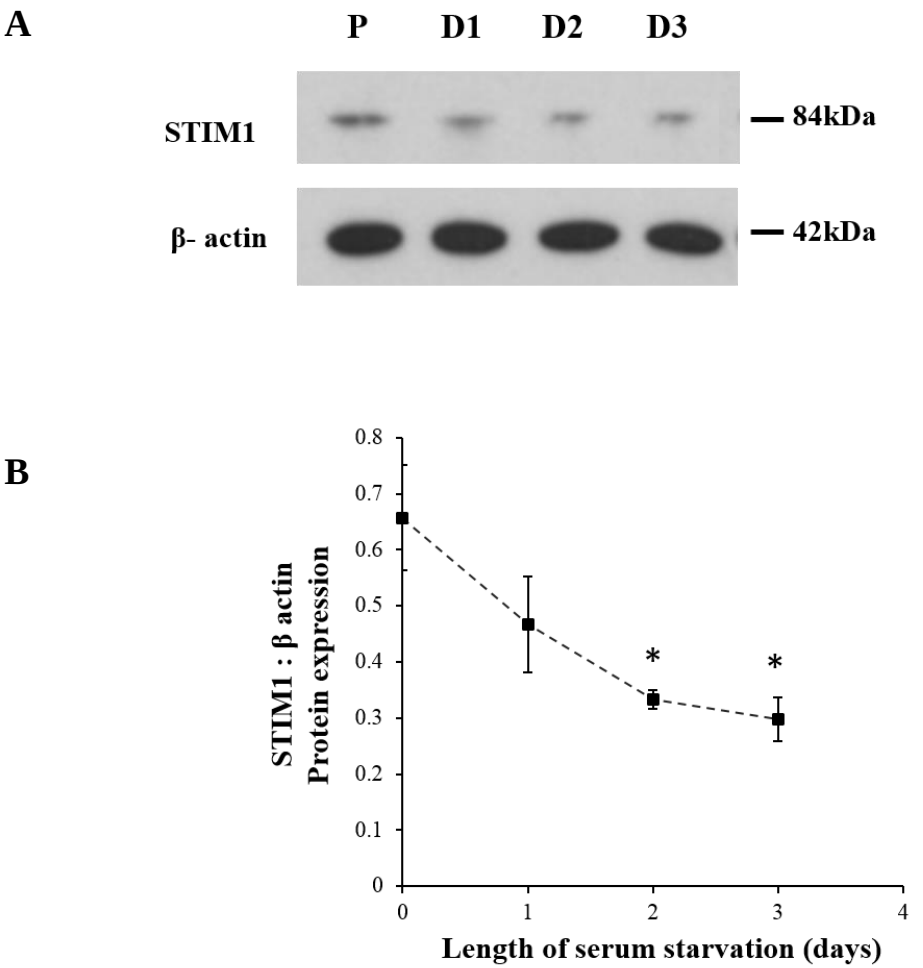

Figure 6.7 STIM1 expression was significantly decreased from day two of serum starvation in NIH 3T3 cells

NIH 3T3 cells were grown in 10% FCS medium (proliferating) or 0.1% FCS medium (starved) for three days. Blots were probed with anti-STIM1 antibody which detected a band at 84 kDa or β- actin antibody which was used as a loading control and detected a band at 42 kDa. **A**) STIM1 was expressed in both proliferating (P) and starved cell populations; D1, D2 and D3. **B**) Quantitative measurements of bands were performed using densitometry (ImageJ software, Methods 2.6.9) where STIM1 was expressed as a ratio of β-actin. There was a significant decrease in STIM1 expression by ~ 49.5% and ~ 54.5% in D2 and D3 respectively compared to proliferating.

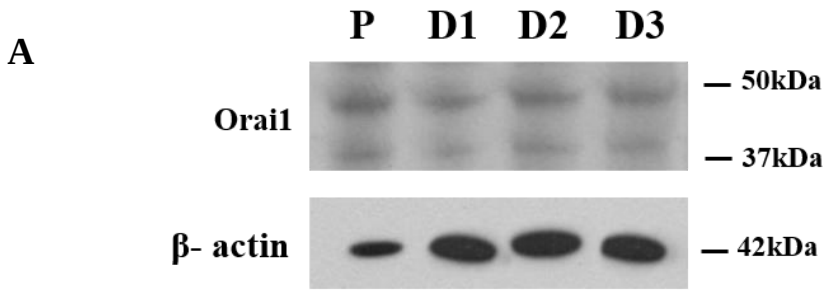

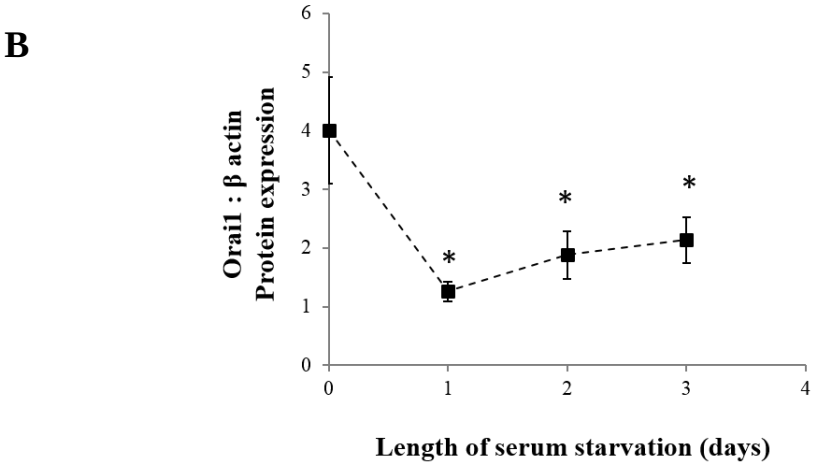

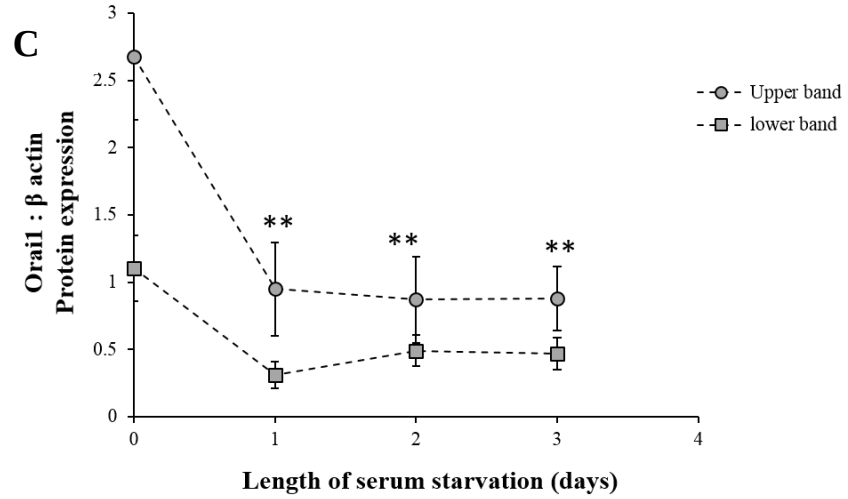

Figure 6.8 Orai1 expression was decreased from the first day of serum starvation time course in NIH 3T3 cells

NIH 3T3 cells were grown in 10% FCS medium (proliferating) or 0.1% FCS medium (starved) for 3days. Blots were probed with anti-Orai1 antibody which detected a band between 37 and 50 kDa or β- actin antibody which was used as a loading control and detected a band at 42 kDa. **A**) Orai1 was expressed in proliferating (P) and starved cell populations D1, D2 and D3. **B**) Quantitative measurements of bands were performed using densitometry (ImageJ software, Methods 2.6.9) where Orai1 was expressed as a ratio of β-actin. There was a significant decrease in Orai1 expression in D1 ($P < 0.01$), D2 and D3 ($P < 0.05$) by ~ 70%, ~ 53%, ~ 46.5% respectively compared to proliferating. **C)** Quantitative analysis of upper and lower Orai1 bands. Orai1 expression was significantly decreased in D1, D2 and D3 cells compared to proliferating ($P < 0.01$**). Whilst lower Orai1 bands showed no significant changes compared to proliferating ($P > 0.05$) cells. N=3.

6.3.3 In hTERT RPE-1 cells

As previously observed in hTERT RPE-1 cells, STIM1 was not expressed in proliferating cells and at D1 of serum starvation time course. From D2 of the serum starvation time course, two patterns of STIM1 expression were observed. Generally, there was no STIM1 expression (Figure 6.9.A) and in others, STIM1 was slightly expressed at a higher molecular weight, as determined by a slight upward band shift (Figure 6.9.B) detected just above 84kDa by an anti-STIM1 antibody. Blots were re-probed with β-actin, used as a loading control.

These results confirmed the previously observed expression of STIM1 in hTERT RPE-1 which suggested that these cells might lack or have level of STIM1 protein too low to be detected. In addition, the occasionally noticed upshifted band which may indicate phosphorylation of STIM1 or the presence of a different cross-reacting isoform or some other posttranslational modifications that could alter STIM1 function.

Orai1 was expressed before and over the 5-day serum starvation time course in hTERT RPE-1 cells as determined by a band detected between 37 and 50 kDa by an anti- Orai1 antibody (Figure 6.10.A). Blots were re-probed with β-actin, used as a loading control, and Orai1 was expressed as a ratio of β-actin which showed a decrease in Orai1 expression by 12%, 19%, 17%, 17% and 14% in D1,D2,D3,D4 and D5 of serum starvation time course compared to proliferating ($P > 0.05$) (Figure 6.10.B). These slight decreases of Orai1 expression correlate with the observed slight down-regulation of SOCE consistent with the role of Orai1 in SOCE.

Orai1 expression showed a double band in proliferating and over the serum starvation time course. The upper and lower (Figure 6.10.C) Orai1 band were analysed individually. This showed the same pattern as that of whole band analysis where there was a slight non-significant decrease in Orai1 expression over serum starvation time course compared to proliferating.

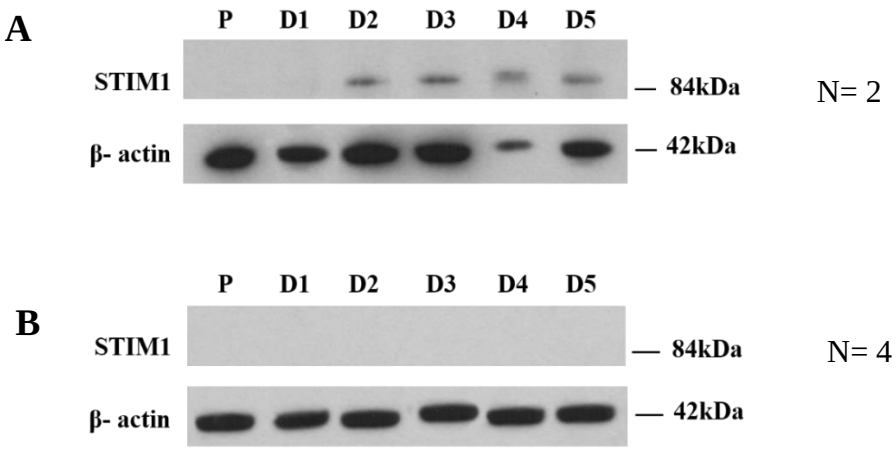

Figure 6.9 STIM1 expression with five-day serum starvation time course in hTERT RPE-1 cells

Western blots were performed on protein extracted from hTERT RPE-1 cells following growing in 10% FCS (proliferating = P) or 0.1% FCS for 5 days. Blots were probed with anti-STIM1 antibody which detected a band at 84 kDa or β- actin antibody which was used as a loading control and detected a band at 42 kDa. **A**) STIM1 expression was not detected in proliferating (P) and D1 cells while there was a very low STIM1 expression in D2, D3, D4 and D5. **B)** STIM1 expression was not detected in proliferating (P) cells D1, D2, D3, D4 and D5. N=6.

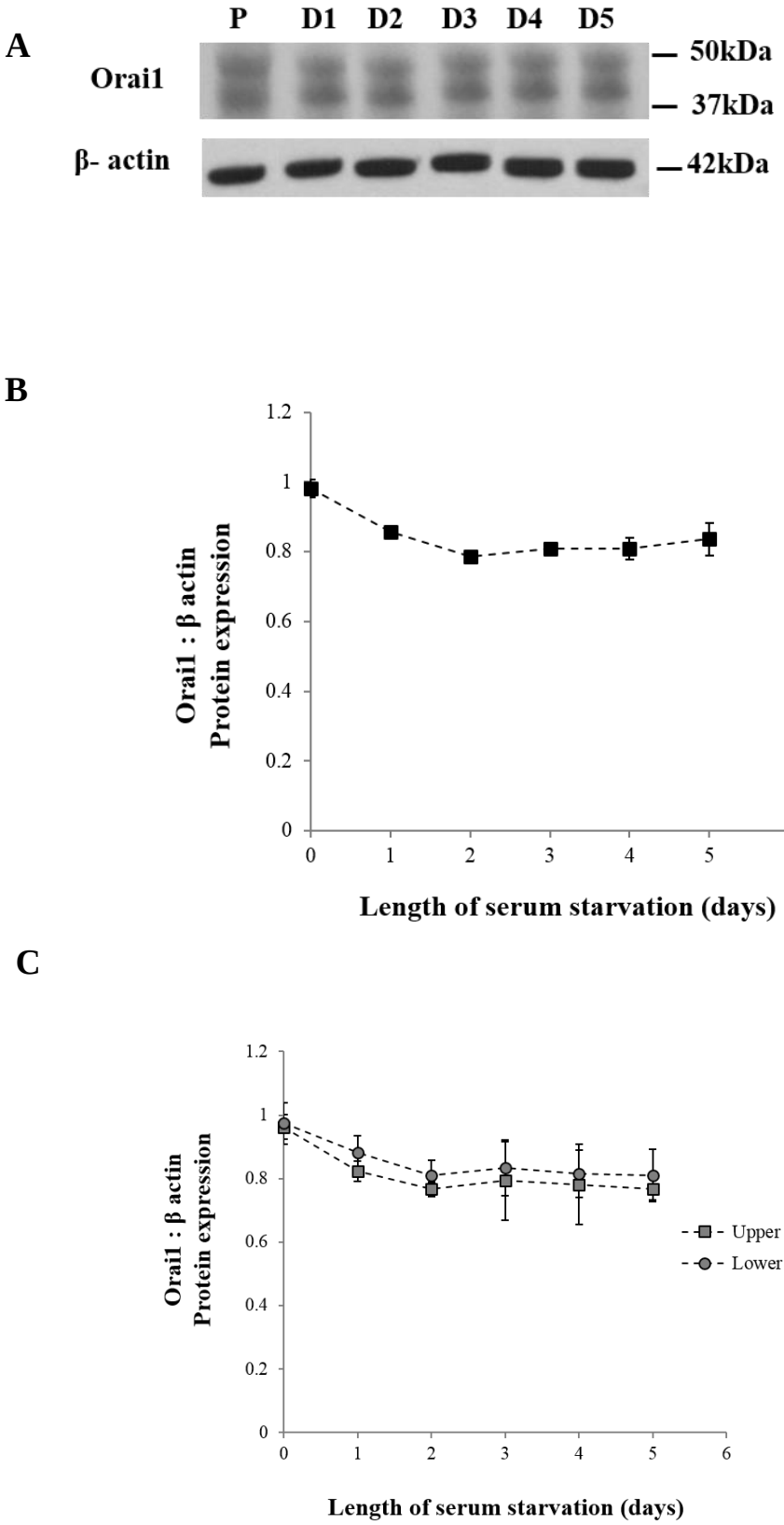

Figure 6.10 Orai1 expression was decreased from the first day of serum starvation time course in hTERT RPE-1 cells

hTERT RPE-1 cells were grown in 10% FCS medium (proliferating) or 0.1% FCS medium (starved) for 5 days. Blots were probed with anti-Orai1 antibody which detected a band between 37 and 50 kDa or β- actin antibody which was used as a loading control and detected a band at 42 kDa. **A**) Orai1 was expressed in proliferating (P) and starved cell populations D1, D2, D3, D4 and D5. **B**) Quantitative measurements of bands were performed using densitometry (ImageJ software, Methods 2.6.9) where Orai1 was expressed as a ratio of β-actin. There was no significant changes in Orai1 expression over the 5-day serum starvation time course compared to proliferating ($P > 0.05$). **C)** Quantitative analysis of upper and lower Orai1 bands. Orai1 expression showed the same pattern as that of whole band analysis (B). There was no significant differences in Orai1 expression over the 5-day serum starvation time course compared to proliferating ($P > 0.05$). N=4.

6.4 Discussion

In the present study, serum starvation induced cell cycle arrest in G0/G1 phase in HeLa and NIH 3T3 but not in hTERT RPE-1 cells. Associated with the cell cycle arrest in G0/G1 phase, there was an uncoupling and a down-regulation of Ca^{2+} store release and SOCE and a decrease of the SOCE proteins STIM1 and Orai1. hTERT RPE-1 cells showed no changes in cell cycle progression, however, a down-regulation of Ca^{2+} store release and SOCE and slight alterations of the SOCE proteins; STIM1 and Orai1 were detected at day 2 and day 4 of the serum starvation time course.

The sequence of the down regulation of SOCE and its proteins over serum starvation time course has not been previously determined and therefore this chapter aimed to investigate SOCE and SOCE proteins over a serum starvation time-course in HeLa, NIH 3T3 and RPE-1 cells to determine whether down regulation of SOCE and its proteins occur as a consequence of G0/G1 arrest or are involved in triggering it.

Interestingly, the sequence of changes in SOCE and its protein over the serum starvation time course was informative in that they occur before cell cycle arrest rather than after and therefore imply roles for STIM1 and Orai1 in SOCE and cell cycle arrest in G0/G1 phase.

An uncoupling of Ca^{2+} store release and SOCE was observed from the first day of serum starvation in HeLa cells. Both Ca^{2+} store release and SOCE was down-regulated, however, the down-regulation of Ca^{2+} store release was ~ 34% whilst that of SOCE was ~ 55%. This uncoupling was observed throughout the 5-day serum starvation time course with no alterations in its extent. An uncoupling of SOCE from Ca^{2+} store release with down-regulation of SOCE has been previously observed in N-type neuroblastoma cells from the first day when the cells were induced to be differentiated (arrested in G0 like phase) by 7-days 9cRA treatment (Whitworth, 2015) which was also maintained throughout the treatment. These observations suggest that the uncoupling might be needed to induce and maintain the cell cycle arrest in G0/G1 phase in HeLa cells.

The sequences of SOCE down-regulation was somewhat different in NIH 3T3 cells, an uncoupling of Ca^{2+} store release and SOCE was observed from first day of serum starvation however, the extent of Ca^{2+} store release was not significantly altered and SOCE was down-regulated by ~ 28%. A similar observation has been previously shown in RBL cells, where 24 hours serum starvation induced uncoupling of SOCE from Ca^{2+} store

release with a down-regulation only of SOCE (Bodding, 2001). At day two, both Ca^{2+} store release and SOCE were markedly down regulated by ~ 77% and ~ 62% respectively and the extent of uncoupling was obviously decreased.

Taken together, these results suggest that uncoupling with the marked down-regulation of SOCE might be required for induction of cell cycle arrest in G0/G1 phase.

Interestingly, hTERT RPE-1 cells also showed an uncoupling of SOCE from Ca^{2+} store release though it was different from that observed in HeLa and NIH 3T3 cells. The uncoupling here occurred at day two of serum starvation and the extent of down-regulation in Ca^{2+} store release (~ 45%) was more than that of SOCE (~ 20%). The extent of this uncoupling was not altered over the five-day serum starvation time course.

These results showed that serum starvation induced uncoupling of Ca^{2+} store release and SOCE in a cell-type specific way and suggest that uncoupling of SOCE from Ca^{2+} store release plays different roles in various cell types.

STIM1 and Orai1 were down-regulated in HeLa cells from the first day of serum starvation. The manner of down-regulation was a multistep manner with an interesting correlation of STIM1 changes to SOCE changes (Figure 6.6.A) where STIM1 was down-regulated from day one of serum starvation, then showed some recovery at day two then a further decrease at day three. Orai1 expression appeared to correlate with the changes in G0 cells (Figure 6.6.B). There was a decrease in Orai1 expression from the first day that correlates with the increase in G0 cells, then some recovery at day 3 that correlate with some decrease in G0 cells, and finally at day four, a decrease in Orai1 expression correlating with the increase in G0 cells.

In NIH 3T3 cells, STIM1 and Orai1 were down-regulated in a gradual manner. As in HeLa cells, down-regulation of STIM1 expression was consistent with the down-regulation of SOCE. At day one STIM1 was down-regulated by 29% consistent with the down-regulation of SOCE which was 28%. At D2 and D3, the decrease in STIM1 expression was ~ 49.5% and ~54.5% respectively consistent with extent of down-regulation of SOCE (~ 60% and ~61 respectively) (Figure 6.2.A). Similar to the observed relation between Orai1 and the percentage of G0 cells in HeLa, Orai1 expression in NIH 3T3 cells showed a robust decrease at day one with no further significant changes at day two and day three. This robust decrease coincided to the robust increase in G0 cells (from ~3% to ~ 39%) observed at day one (Section 3.3.2).

These findings correspond with the previously discussed changes in percentage of G0 cells and SOCE and provide further evidence to support a multistep cell cycle arrest response in HeLa cells and a gradual response in NIH 3T3 cells. In addition, these results reveal that both STIM1 and Orai1 form an element of SOCE in proliferating HeLa and NIH 3T3 cells and that the decrease in Orai1 expression observed with serum starvation is a key enabling step in arresting cells in G0/G1 phase. Orai1 therefore appeared to play a direct role in cell cycle arrest in G0/G1 phase. This is in contrast to STIM1, which does not seem to have a direct role in the cell cycle progression in HeLa and NIH 3T3 cells.

The role of STIM1 and Orai1 in SOCE has been discussed in chapter 5, where STIM1 has been shown to form the molecular basis of SOCE (Liou *et al.*, 2005; Roos *et al.*, 2005; Zhang *et al.*, 2005) and the level of STIM1 expression has been extensively associated with extent of SOCE activity in many cell types. For example, in HeLa cells (Liou *et al.*, 2005), endothelial cells (Abdullaev *et al.*, 2008), in N-type SH-SY5Y cells (Bell *et al.*, 2013), endothelial progenitor cells (Kuang *et al.*, 2010), SH-SY5Y cells, HEK293 cells, Jurkat T cells and Drosophila S2 cells (Roos *et al.*, 2005), as well as vascular smooth muscle cells (Takahashi *et al.*, 2007b; Aubart *et al.*, 2009; Potier *et al.*, 2009) and adipocytes (Graham *et al.*, 2009).

Similarly, Orai1 knockdown causes reduction in SOCE in neural progenitor cells (Hao *et al.*, 2014), in differentiated N-type SH-SY5Y cells (Bell, 2011), acinar cells (Hong *et al.*, 2011), osteoclasts (Zhou *et al.*, 2011), HEK293 cells (Gwack *et al.*, 2007; Kawasaki *et al.*, 2010; Borowiec *et al.*, 2014), endothelial cells (Abdullaev *et al.*, 2008) and Jurkat T cells (Gwack *et al.*, 2007). Furthermore, Orai1 overexpression results in an increase in SOCE in HEK293 cells (Fukushima *et al.*, 2012), restores SOCE in differentiated N-type SH-SY5Y (Bell, 2011), in SCID T cells and fibroblasts (Gwack *et al.*, 2007).

In hTERT RPE-1 cells, STIM1 protein was not expressed at day one of serum starvation which is similar to proliferating cells. However, from day two, an upshifted band at a molecular weight just above the STIM1 molecular weight was occasionally observed using the anti-STIM1 antibody. This increase in molecular weight suggesting that there may be some sort of modification, such as phosphorylation or glycosylation which might affect STIM1 function and be responsible for the observed down-regulation of SOCE. Consistent with this observation, as discussed in chapter 5, an increase in molecular weight has been previously observed to be associated with down-regulation in SOCE activity in

neuroblastoma cells (Whitworth, 2015), while STIM1 phosphorylation has been observed to inhibit SOCE in endothelial cells (Sundivakkam *et al.*, 2013) and in HEK 293 cells (Smyth *et al.*, 2009). Likewise, STIM1 might be glycosylated (Manji *et al.*, 2000; Dziadek and Johnstone, 2007), that may affect localisation of STIM1 to the PM (Williams *et al.*, 2002) and subsequently alter SOCE activity.

In addition, STIM1 has alternative isoforms; STIM1L and STIM1S that serves different function. STIM1L has recently been recognised (Darbellay *et al.*, 2011) and has been shown to activate SOCE in cells lacking STIM1 (Horinouchi *et al.*, 2012; Sauc *et al.*, 2015).

Furthermore, STIM2; the other STIM homologues has been found to induce store independent Ca^{2+} entry (Parvez *et al.*, 2008) and activate SOCE as it responds to a smaller decreases in ER $[Ca^{2+}]_i$ than STIM1 (Brandman *et al.*, 2007). STIM2 knockdown reduces basal $[Ca^{2+}]_i$ and overexpression increases basal $[Ca^{2+}]_i$ (Brandman *et al.*, 2007) and also inhibits SOCE (Soboloff *et al.*, 2006b). In addition knockdown of STIM2 in HeLa cells caused a reduction in SOCE (Liou *et al.*, 2005) but has also been shown to have no effect in Jurkat T cells (Roos *et al.*, 2005).

In summary, the results showed that hTERT RPE-1 cells may lack/or express a very low level of STIM1 and/or other isoforms of STIM1 or may have another STIM homologues; STIM2 that may responsible for the observed uncoupling and down-regulation SOCE activity with five-day serum starvation time course.

In hTERT RPE-1 cells, Orai1 showed a slight down-regulation from the first day of serum starvation that corresponded to the observed slight down-regulation of SOCE consistent with a possible role for Ora1 in the regulation of SOCE.

6.5 Conclusions

- An uncoupling of SOCE from Ca^{2+} store release with the marked down-regulation of SOCE occurred from first day of serum starvation in both HeLa and NIH 3T3 cells suggesting that inhibition of SOCE might be involved in triggering cell cycle arrest in G0/G1 phase.
- Serum starvation induced a down-regulation of SOCE and its protein, STIM1 and Orai1 in a multistep manner in HeLa cells that correlated to the multistep manner increase of G0 cells previously observed.
- Serum starvation induced a down-regulation of SOCE and its protein, STIM1 and Orai1 in a gradual manner in NIH 3T3 cells that correlated to the gradual increase of G0 cells previously observed.
- STIM1 and Orai1 proteins appeared to play a key role in SOCE in both HeLa and NIH 3T3 cells.
- Unlike STIM1, Orai1 seemed to be a positive regulator of cell cycle progression in HeLa cells.
- In hTERT RPE-1 cells, serum starvation induced a slight corresponding down-regulation of SOCE and Orai1 that may indicate a role for Orai1 in alterations of SOCE in these cells.

Part II - Results - Cell Cycle Re-entry

Chapter 7 Morphology and Flow cytometry

7.1 Introduction

As previously discussed, serum starvation induced cell cycle arrest in quiescent G0/G1 phase in HeLa and NIH 3H3 and this arrest was determined morphologically and by flow cytometry. Cells arrested in G0/G1 phase at day four of serum starvation for HeLa cells and at day two for NIH 3T3 cells. This arrest was determined by a significant decrease in total and mitotic cell number with normal viability, an increase in G0 cells and a decrease in S/G2/M cells. However, in hTERT RPE-1 cells, serum starvation did not induce cell cycle arrest as no changes were observed either morphologically or by flow cytometry analysis.

It has been demonstrated that cell cycle arrest in quiescent G0/G1 phase is defined as a reversible growth/proliferation arrest (Coller *et al.*, 2006; Daignan-Fornier and Sagot, 2011; Cheung and Rando, 2013).

Therefore, the aim of this chapter was to determine the reversibility of the induced cell cycle arrest by adding the serum back to the G0/G1 HeLa and NIH 3T3 cells and define this both morphologically and by flow cytometry.

As hTERT RPE-1 cells showed no morphological differences or cell cycle arrest with serum starvation (Section 3.2.3 and 3.3.3), there was no need to perform serum add-back with these cells.

Throughout this part of thesis (Part II cell cycle re-entry), HeLa, NIH 3T3 and hTERT RPE-1 cells (10% FCS) will be referred to as proliferating whilst G0/G1 cells in HeLa and NIH 3T3 cells and serum starved hTERT RPE-1 (0.1% FCS) will be referred to as D4D0, D2D0 and D2D0 respectively. The cells induced by serum add-back will be referred to as D4D1, D4D2, and D4D3 for HeLa and as D2D1 and D2D2 for NIH 3T3 and hTERT RPE-1 cells as the first letter (D) referred to days of starvation and the last letter (D) referred to days of serum add-back.

7.2 Results – Morphological changes

As described previously, cell viability, total and mitotic cell number and cell diameter were determined to investigate cell proliferation status and cell cycle progression.

7.2.1 Serum add-back induced cell proliferation in HeLa cells

Serum starvation induced cell cycle arrest in G0/G1 phase in HeLa cells was characterised by a decrease in total and mitotic cell number and cell diameter (Section 3.2.1).

Morphological changes were observed over the three day time-course of serum add-back to determine the reversibility of the previously observed changes. Proliferating (10% FCS) cells or G0/G1 (0.1% FCS) cells were grown for four days. After four days, serum was added back to G0/G1 cells; both proliferating and G0/G1 cells were grown in 10% FCS medium for further three days.

D4D0 (control) cells (0.1% FCS) were grown in clusters and characterised by elongated angular cell bodies; cells in interphase. Mitotic cells (spherical cells) can hardly be seen (Figure 7.1). From the first day of serum add-back (D4D1), mitotic cells could be seen and an increase in their number was observed over the serum add-back time course (Figure 7.1). There was a significant increase in percentage of mitotic cell number from day two; D4D2 (10.4±0.92%) and D4D3 (11.2±0.81%) compared to G0/G1 cells (D4D0) (1.7 ± 0.55%) (All $P < 0.01$) that was not significantly different compared to proliferating (10.51 ± 0.41%) ($P > 0.05$) (Figure 7.2.A and Table 7.1).

Similarly, total cell count showed that serum add-back induced cell proliferation in G0/G1 HeLa cells. This is clearly shown in figure 7.1 where confluency increased gradually from the first day of serum add-back (D4D1) and became much higher in D4D3 cells compared to D4D0 cells. This was also demonstrated by comparing the cell counts for D4D0 (0.1% FCS for 3days); 12.8×10^3 cells/ml and D4D3 cells (10 % FCS for 3days); 41.6×10^3 cells/ml where cells were seeded at the same density prior to the 3-day treatment (Figure 7.3). These findings showed that serum add-back induced cell proliferation which indicates that G0/G1 cells re-entered the cell cycle and restored normal proliferation status.

Cell diameter has been shown to be decreased with cell cycle arrest in G0/G1 cells (Section 3.2.1). Here, with serum add- back, cell diameter was significantly increased at

D4D2 by 17.5% (15.9± 1. 06μm) and D4D3 by 22% (16.52 ± 1.03μm) (All $P < 0.001$) compared to D4D0 (control) (13.5± 1.1μm). By day two of serum add-back the cell diameter was not significantly different compared to proliferating (17.21±1.1 μm) ($P>0.05$) (Figure 7.2.B and Table 7.1).

Cell viability was also determined using trypan blue stain. Cell viability showed significant increase at D4D2 by 42% (94.24±5.29 %) ($P = 0.0435$) and D4D3 by 36% (89.9 ± 8.35%) ($P = 0.0469$) compared to D4D0 (control) (66.18 ± 4.51) (Figure 7.2.C and Table 7.1).

These results indicate that 2-day serum add-back was enough to induce quiescent G0/G1 HeLa cells to re-enter the cell cycle and proliferate.

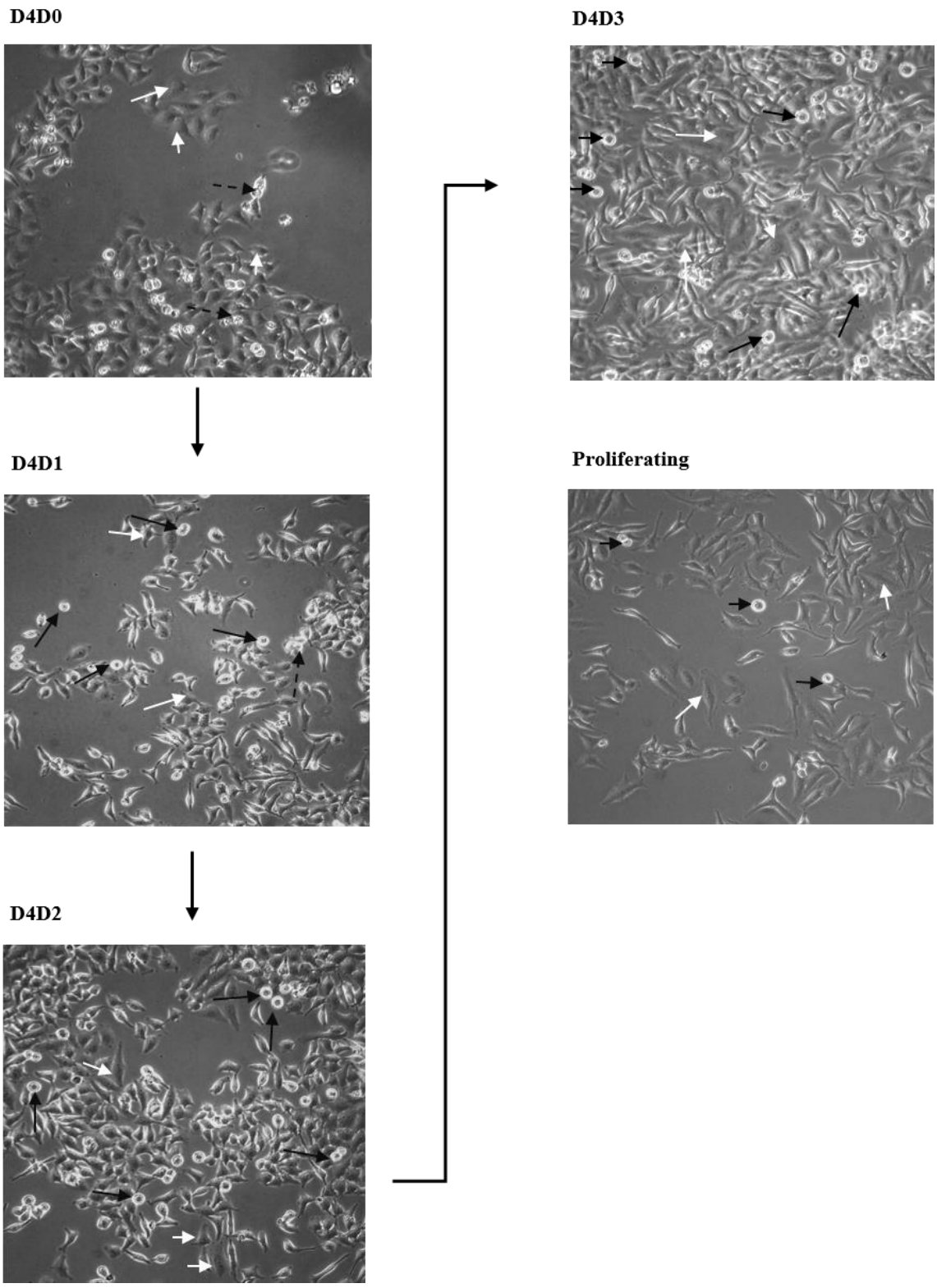

Figure 7.1 Serum add-back to G0/G1 HeLa cells induced cell cycle re-entry and cell proliferation

HeLa cells were grown in 10% FCS medium (proliferating) or 0.1% FCS medium for four days to induce cell cycle arrest in G0/G1 phase (D4D0). After four days, serum was added

back to G0/G1 cells; both proliferating and G0/G1 cells were grown in 10% FCS medium for a further 3 days. D4D0, D4D1, D4D2, D4D3 represent four days of serum starvation followed by zero day, one day, two days and three days of serum add-back. In D4D0 cells, most cells are in interphase i.e. flattened cells with angular shaped bodies (white arrows) that grew in clusters with no appearance of any mitotic (spherical) cells. From day one of serum add-back (D4D1), the mitotic cells (solid black arrows) appear and gradually increases in number with an obvious increase in cell confluency. In D4D2 and D4D3, mitotic cells markedly increase in number and cells in interphase show increase in diameter, and cells show no differences compared to proliferating. Cell confluency became far higher in D4D3 cells compared to D4D0 cells. Dashed black arrows represent debris. Images are representative of >15 images. Scale bars represent 50μm.

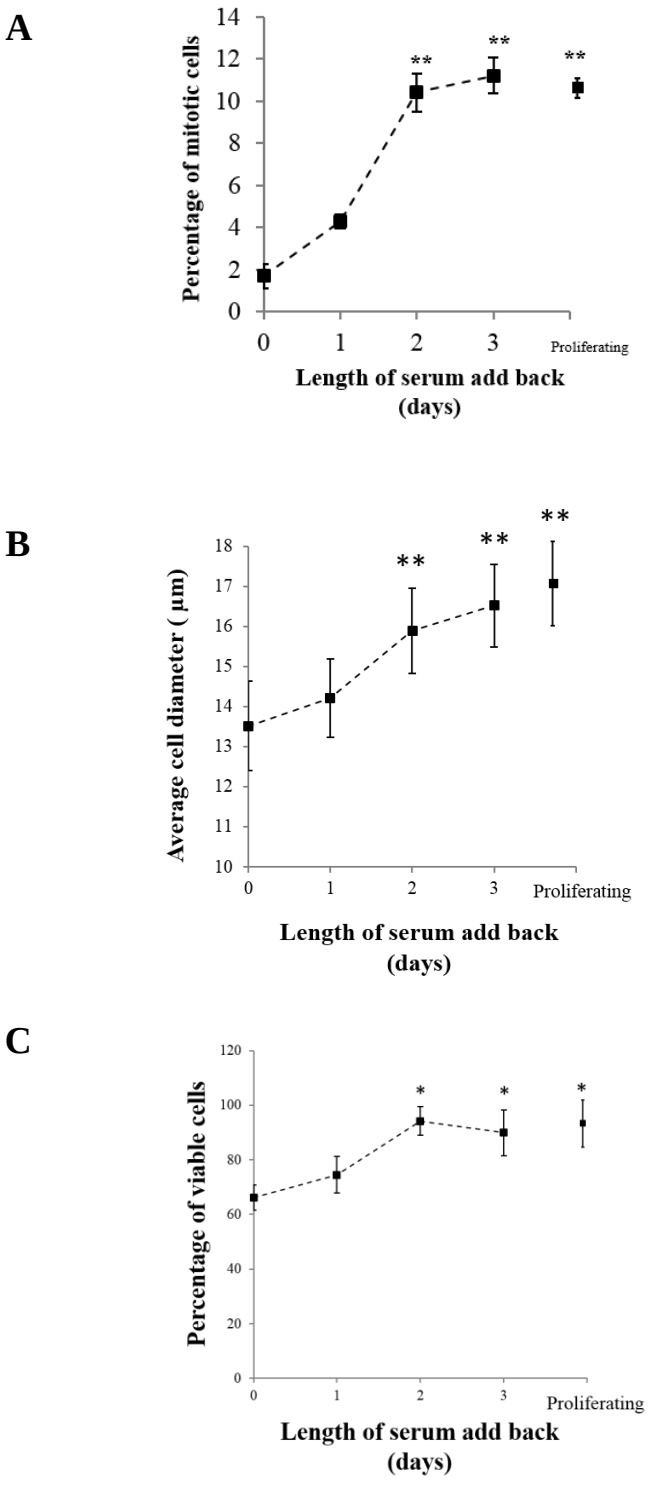

Figure 7.2 Serum add-back to G0/G1 HeLa cells restored proliferating growth characteristics

G0/G1 HeLa cells were stimulated by increasing the FCS from 0.1 % to 10% in culture medium for three days. **A)** Mitotic cells were counted and expressed as a percentage of the total cell population. Mitotic cells were significantly increased by ~ 511% and ~ 559%

(All P <0.01) in day two and day three of serum add-back respectively compared to day zero (control cells). **B)** Cell diameter was significantly increased by ~ 17.5% and ~ 22% (All P <0.01) in day two and day three of serum add-back respectively compared to day zero (control cells). **C)** Cell viability was detected by trypan blue stain (Method 2.4) cell viability show slight significant increase at day two and day three of serum add-back compared to day zero ($P < 0.05$). Error bars represent S.E.M. N=4.

	Mitotic cells (%)	Cell diameter (μm)	Cell viability (%)
D4D0 (control)	1.7±0.55	13.5±1.10	66.18±4.51
D4D1	4.3±0.342 (P= 0.6032)	14.21±0.97 (P=0.1329)	74.53±6.75 (P= 0.7264)
D4D2	10.4± 0.923 (P < 0.01)	15.9±1.06 (P < 0.01)	94.24± 5.29 (P=0.04351)
D4D3	11.2 ± 0.81 (P < 0.01)	16.52±1.03 (P < 0.01)	89.9± 8.35 (P = 0.0469)
Proliferating	10.51± 0.41 (P < 0.01)	17.21 ± 1.1 (P < 0.01)	93.06± 7.22 (P = 0.0462)

Table 7.1 Growth characteristics changes of HeLa cells over the three-day serum add-back time course

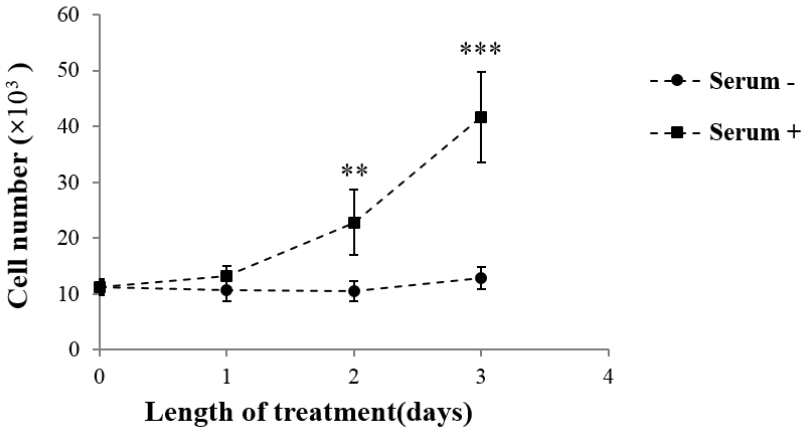

Figure 7.3 Serum add-back induced cell proliferation in G0/G1 HeLa cells

G0/G1 HeLa cells were stimulated by increasing the FCS from 0.1 % to 10% in culture medium for three days. Quantification of cells/ml culture medium was done by Cellometer (Method 2.4). Day 0; D4D0 cells, n=4 (11.2×10^3 cells/ml), D4D0 cells n=4 (11.2×10^3 cells/ml). Day 1; D4D0 cells, n=6 (107×10^3 cells/ml), D4D1 cells n=6 (13.1×10^3 cells/ml), P=0.392. Day 2; D4D0 cells, n=4 (10.4×10^3cells/ml), D4D2 cells, n=3 (22.8×10^3cells/ml), P<0.01**. Day 3; D4D0 cells, n=6 (12.8×10^3 cells/ml), D4D3 cells n=4 (41.6×10^3cells/ml), P < 0.001***.

7.2.2 Serum add-back induced cell proliferation in NIH 3T3 cells

Serum starvation induced cell cycle arrest in G0/G1 phase in NIH 3T3 cells was associated with a decrease in total and mitotic cell number (Section 3.2.2).

Similar to HeLa cells, morphological changes were observed with serum add-back to determine the reversibility of the previously observed changes as an indicator of re-entry into the cell cycle. Proliferating (10% FCS) cells or D2D0 (G0/G1) cells (0.1% FCS) were grown for two days. After two days, serum was added back to D2D0 cells; both proliferating and D2D0cells were grown in 10% FCS medium for further two days.

D2D0 (control) cells (0.1% FCS) were characterised by cells in interphase with elongated angular cell bodies. Mitotic (spherical) cells can hardly be seen (Figure 7.4). From the first day of serum add-back (D2D1), the mitotic cells could clearly be detected (Figure 7.4). There was a significant increase in percentage of mitotic cell number in D2D1 (9.4±0.82%) and D2D2 (12.4±0.76%) compared to D2D0 (0.5 ± 0.15%) (All $P < 0.001$) that was not significantly different compared to proliferating (10.9 ± 0.38%) ($P > 0.05$) (Figure 7.5.A and Table 7.2). Consistent with the previous observation, total cell count showed that serum add-back induced cell proliferation in G0/G1 NIH 3T3 cells. This is shown clearly in figure 7.4 where confluency increased gradually from the first day of serum add-back (D2D1) compared to D2D0 cells. In addition, this was observed by comparing cell counts for D2D0; 0.1% FCS for 2days (2.7×10^3) and D2D2 cells; 10 % FCS for 2 days (51×10^3) where cells were seeded at the same density prior to the two-day treatment (Figure 7.6). The increase in mitotic and total cell number indicates that serum add-back induced G0/G1 NIH 3T3 cells to enter the cell cycle and resume proliferation.

In contrast to HeLa cells, there was no significant changes detected in cell diameter over the 2 day serum add-back ($P > 0.05$) which was not also significantly different compared to proliferating ($P > 0.05$) suggesting that cell diameter cannot be an indicative for cell cycle arrest in NIH 3T3 cells (Figure 7.5.B and Table 7.2).

With serum add-back, cell viability showed no significant changes over the two-day serum add-back ($P > 0.05$) (Table 7.2).

The results showed that quiescent G0/G1 NIH 3T3 cells were induced to re-enter the cell cycle after one day of serum add-back.

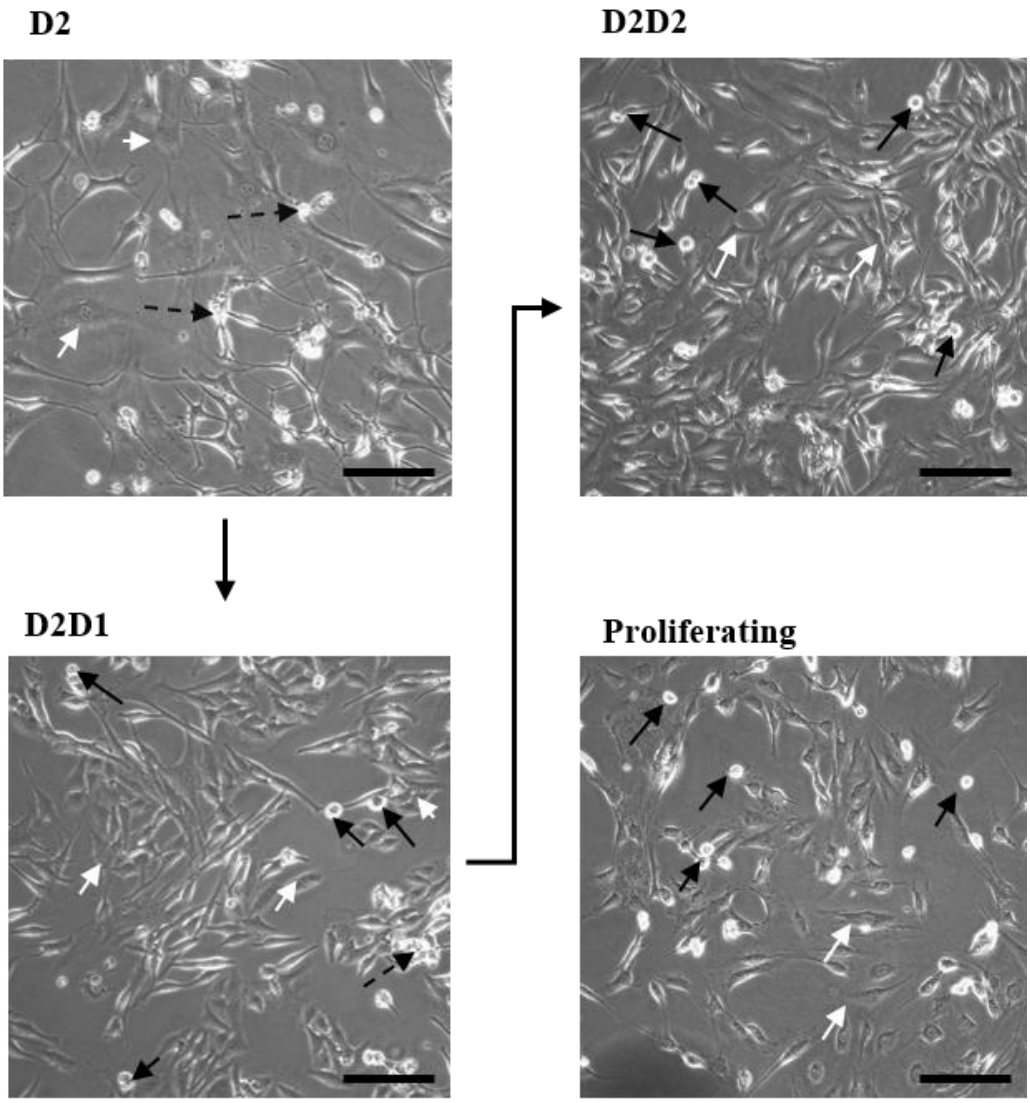

Figure 7.4 Serum add-back to G0/G1 NIH 3T3 cells induced cell cycle re-entry and cell proliferation

NIH 3T3 cells were grown in 10% FCS medium (proliferating) or 0.1% FCS medium for 2 days to induce cell cycle arrest in G0/G1 phase. After 2 days, serum was added back to G0/G1 cells; both proliferating and G0/G1 cells were further grown in 10% FCS medium for 2 days. D2D0, D2D1, D2D2 represent two days of serum starvation followed by zero day, one day and two days of serum add-back. In D2D0 cells, almost cells are in interphase; flattened cells with angular shaped bodies (white arrows) with no appearance of any mitotic cells (spherical cells). From day one of serum add-back (D2D1), the mitotic cells (solid black arrows) appears and gradually increases in number. In D2D2 mitotic cells markedly increase in number and cells show no differences compared to proliferating.

Cell confluency increases in D2D1 and D2D2 compared to proliferating. Dashed black arrows represent debris. Images are representative of >15 images. Scale bars represent 50µm.

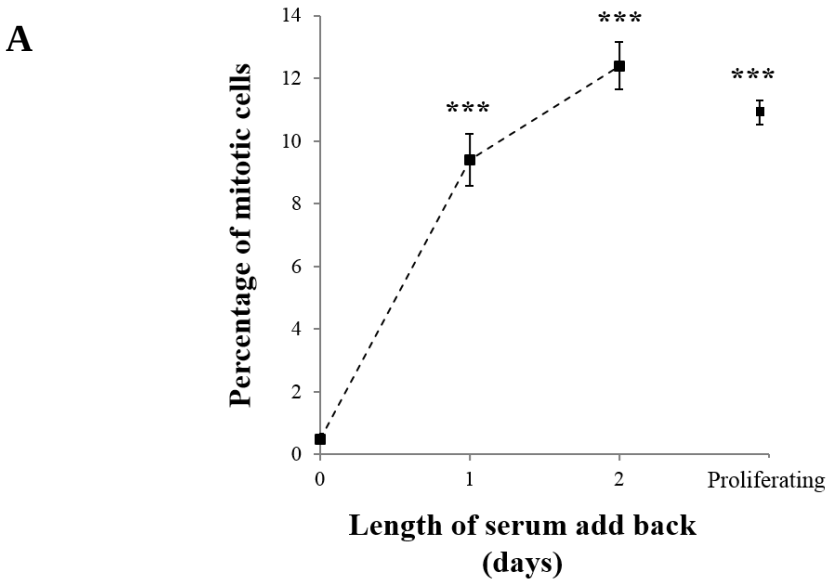

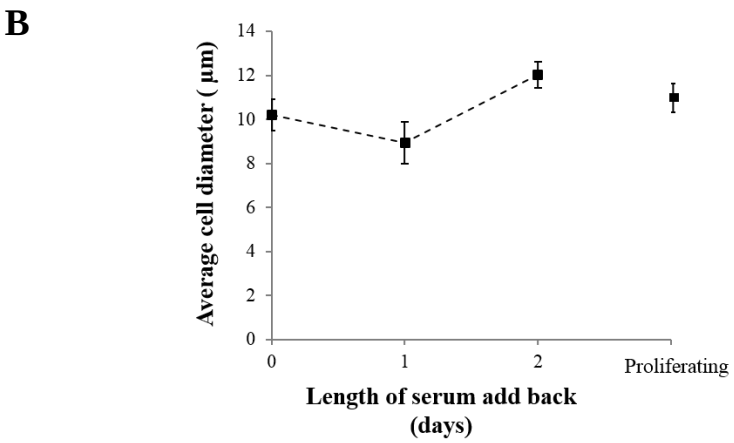

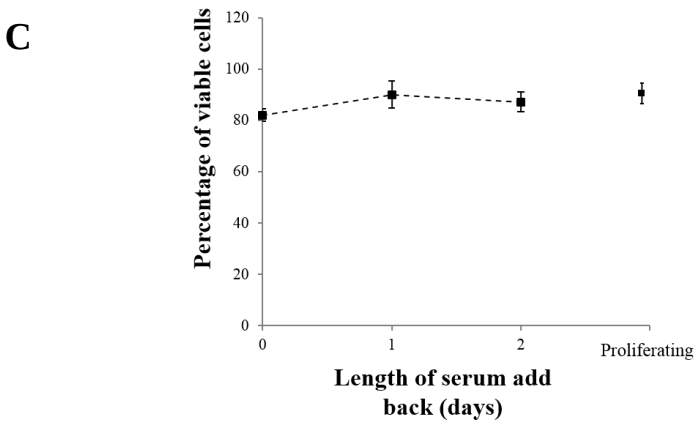

Figure 7.5 Serum add-back to G0/G1 NIH 3T3 cells restored proliferating growth characteristics

G0/G1 NIH 3T3 cells were stimulated by increasing the FCS from 0.1 % to 10% in culture medium for 2 days. **A)** Mitotic cells were counted and expressed as a percentage of the total cell population. Mitotic cells were significantly increased in day one and day two of serum add-back compared to day zero (control cells) (all $P < 0.001$). There was no significant differences in mitotic cell number from day one of serum add-back compared to proliferating ($P > 0.05$). **B)** Cell diameter was not significantly different over the 2-day serum add-back compared to day zero ($P > 0.05$). **C)** Cell viability was detected by trypan blue stain (Method 2.4) cell viability was not significantly different over the 2-day serum add-back compared to day zero ($P > 0.05$). Both cell diameter and viability were not significantly different over the 2-day serum add-back compared to proliferating. Error bars represent S.E.M. N=3.

	Mitotic cells (%) (All P< 0.001)	Cell diameter (µm) (All P > 0.05)	Cell viability (%) (All P > 0.05)
D2D0 (control)	2.5±0.45	10.21±0.72	66.03± 2.48
D2D1	9.4±0.82	8.94±0.95	85.98± 5.34
D2D2	12.4± 0.76	12.01±0.57	87.14± 3.84
Proliferating	10.9± 0.38	11.63±0.62	89.01± 3.84

Table 7.2 Growth characteristics changes of NIH 3T3 cells over two-day serum add-back time course

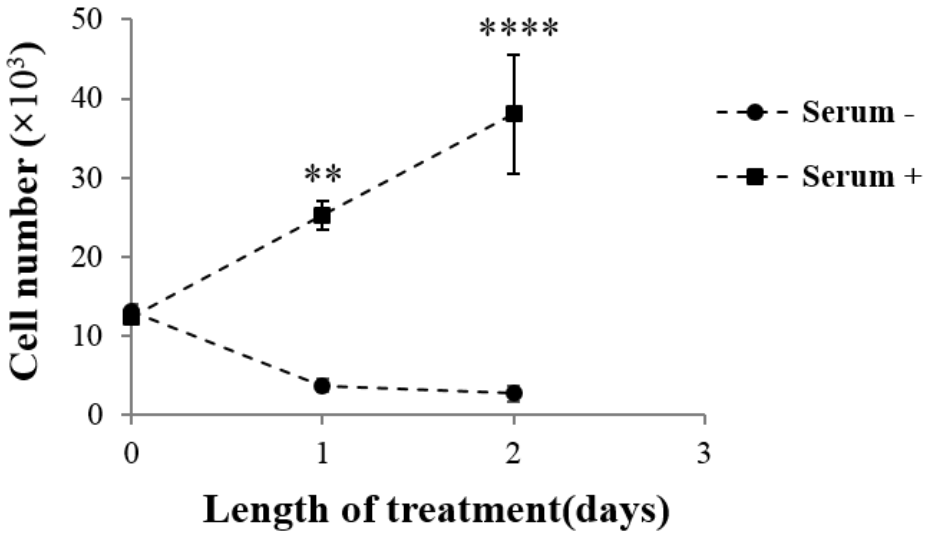

Figure 7.6 Serum add-back induced cell proliferation in G0/G1 NIH 3T3 cells

G0/G1 NIH 3T3 cells were induced by increasing the FCS from 0.1 % to 10% in culture medium for two days. Quantification of cells/ml culture medium was done by Cellometer (Method 2.4). Day 0; D4D0 cells, n=4 (13.2×10^3 cells/ml), D4D0 cells n=4 (13.2×10^3 cells/ml). Day 1; D4D0 cells, n=4 (3.7×10^3 cells/ml), D4D1 cells n=4 (25.2×10^3 cells/ml),

P<0.01**. Day 2; D4D0 cells, n=4 (2.7 $\times 10^3$cells/ml), D4D2 cells, n=5 (51$\times 10^3$cells/ml), P < 0.0001****.

7.3 Results- Flow cytometry

7.3.1 The proportion of G0, G1 and S/G2/M subpopulations was restored after two days of serum add-back in HeLa cells

HeLa cells were grown in 10% FCS medium (proliferating) or 0.1% FCS medium for four days (D4D0) the point at which the percentage of G0 cells was significantly increased. After four days, serum was added back to D4 cells for three days (D4D3).

The percentage of viable cells increased throughout the serum add-back time course. At D4D1 by ~50% (61.2±3.01%, P = 0.1588), D4D2 by ~ 87.5% (75.16±10.22, P = 0.0461) and D4D3 by ~117.5% (87.3±9.79, P = 0.0382) compared to D4D0 (control) (40.1±4.44 %) (Figure 7.3 and Figure 7.2). From day two of serum add-back the viability status was not significantly different compared to proliferating cells (82.3±13.25, P = 0.3684) (Figure 7.7 and Table 7.3).

Cell cycle analysis by flow cytometry showed that serum add-back to the G0/G1 cells significantly decreases the percentage of G0 cells and brings it back to the proliferating levels. The percentage of G0 cells decreased at D4D2 by ~68.5% (7.86 ± 3.97 %, P = 0.031) and D4D3 by ~90% (2.9±0.91%, P = 0.0282) compared to D4D0 (25.0 3± 9.6 %). The percentage of G0 was not significantly different at D4D2 compared to proliferating (1.5±0.51, P = 0.3564) (Figure 7.8 and Figure 7.9) highlighting the reversibility of the quiescent G0/G1 state induced by serum starvation.

Similarly, serum add-back restored the proliferating level of the S/G2/M percentage from the first day. The percentage of S/G2/M cells was significantly increased in D4D1 by ~171% (25.1 ± 6.53%, P = 0.0016), D4D2 by ~146% (22.8 ± 3.42, P = 0.0031) and D4D3by~122% (20.63 ± 3.21, P = 0.0085) compared to D4D0 (control) (9.26 ± 0.913) (Figure 7.8 and Figure 7.9). Compared to proliferating (23.7±0.775), the percentage of S/G2/M cells was not significantly different in D4D1 (P = 0.9842) (Table 7.3).

The percentage of G1 cells showed a slight increase in over the 3-day serum add-back time-course peaked at D4D3 (76.83±12.34) compared to D4D0 (control) by~15% (65.96±12.69) however the increase was not significant (P > 0.05) (Table 7.3).

These results revealed that serum add-back restored the proliferating level of the percentage of G0, G1 and S/G2/M subpopulations of HeLa cells indicating that the serum starvation induced cell cycle arrest in G0/G1 phase was reversible.

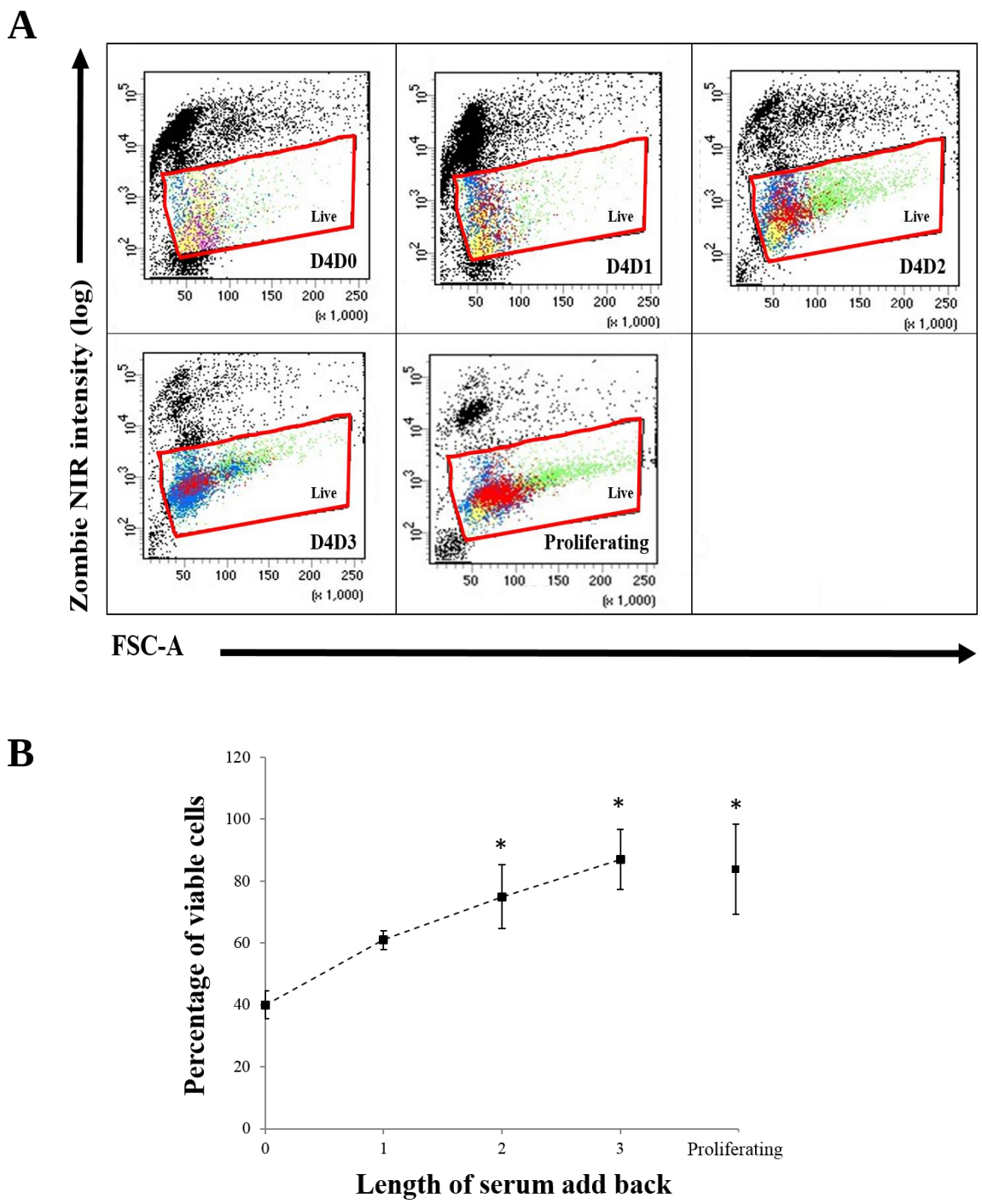

Figure 7.7 Serum add-back restored viability of G0/G1 HeLa cells

HeLa cells were grown in 10% FCS medium (proliferating) or 0.1% FCS medium for 4 days (D4). After 4 days, serum was added back to starved cells (D4); both proliferating and D4 cells were grown in 10% FCS medium for further 3 days **A)** Dot plots of flow cytometric analysis performed on HeLa cells stained with viability stain; Zombie NIR.

D4D0, D4D1, D4D2, D4D3 represent four days of serum starvation followed by zero day, one day, two days and three days of serum add-back. FSC-A represents forwards scatter area. Each dot appearing on the dot plot represents a single cell. The proportion of viable cells were detected by Flow cytometry based on strength of fluorescence signal. The dot plots showing distribution of two cell populations represents the —dead cells (black dots outside live gate; red box) that exhibit significant Zombie NIR fluorescence signal, and live cells (coloured dots within the live gate, colour code is shown in the next figure; Figure 7.8) which do not. The distribution of viable cells appeared to be increased in D4D1, D4D2 and D4D3 compared to D4D0 (control). Compared to proliferating, the 3-day serum add-back appear to restore the distribution of viable cell. **B)** Graph shows quantitative measurements of the proportion of live cells as a percentage of total HeLa cells population. The percentage of viable cells was increased by ~ 50% ($P = 0.1588$), ~ 87.5% ($P= 0.0461$) and ~ 117.5% ($P = 0.0382$) in D4D1, D4D2 and D4D3 compared to D4D0 (control). There was no significant difference in the percentage of viable cells in D4D2; $P = 0.3684$ and D4D3; $P = 0.9789$ compared to proliferating. n= 10,000. N= 3.

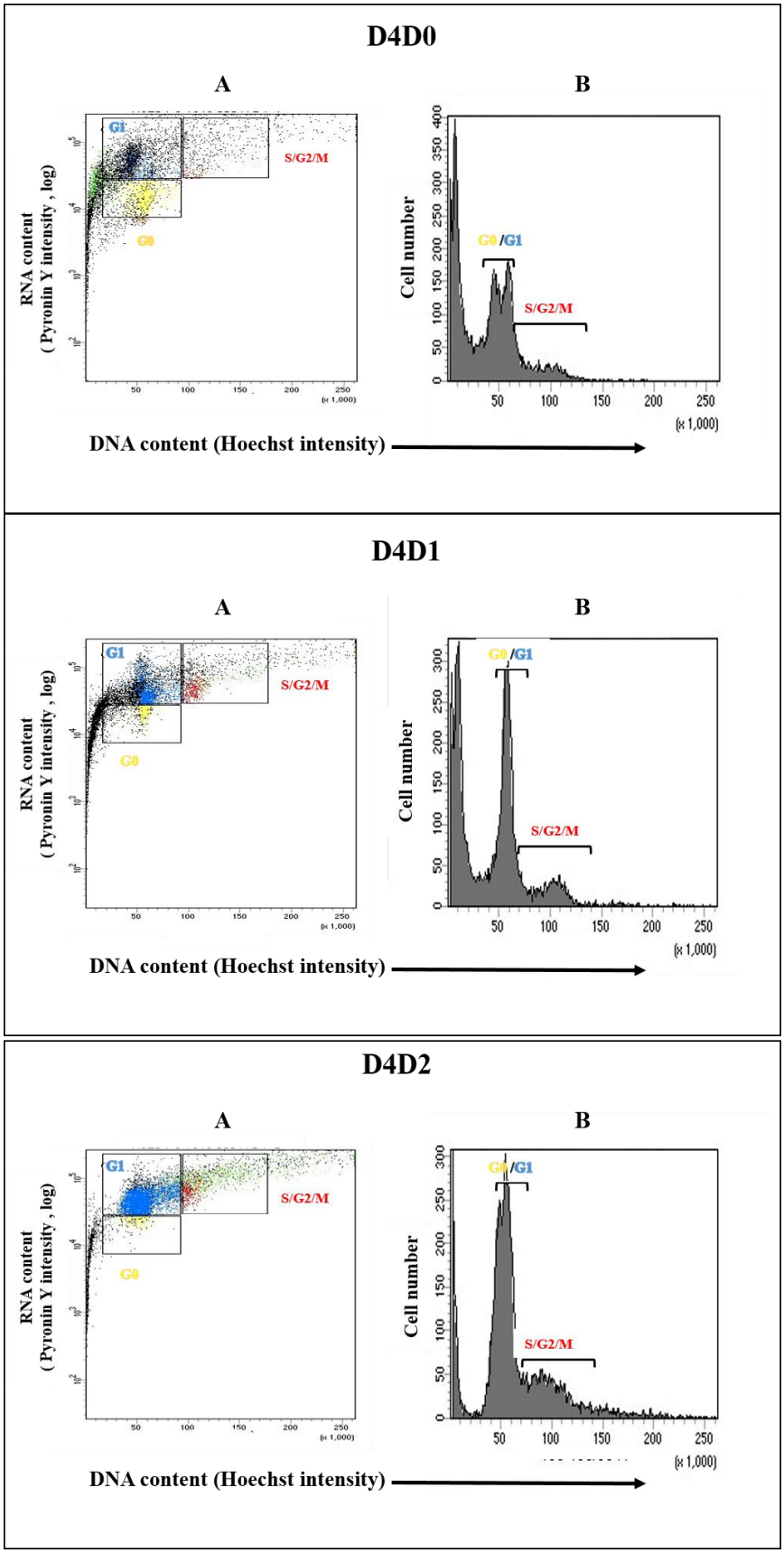
D4D0
A
B
G1
S/G2/M
G0
RNA content
(Pyronin Y intensity , log)
Cell number
G0 /G1
S/G2/M
(x 1,000)
DNA content (Hoechst intensity)
D4D1
A
B
G1
S/G2/M
G0
RNA content
(Pyronin Y intensity , log)
Cell number
G0 /G1
S/G2/M
(x 1,000)
DNA content (Hoechst intensity)
D4D2
A
B
G1
S/G2/M
G0
RNA content
(Pyronin Y intensity , log)
Cell number
G0 /G1
S/G2/M
(x 1,000)
DNA content (Hoechst intensity)

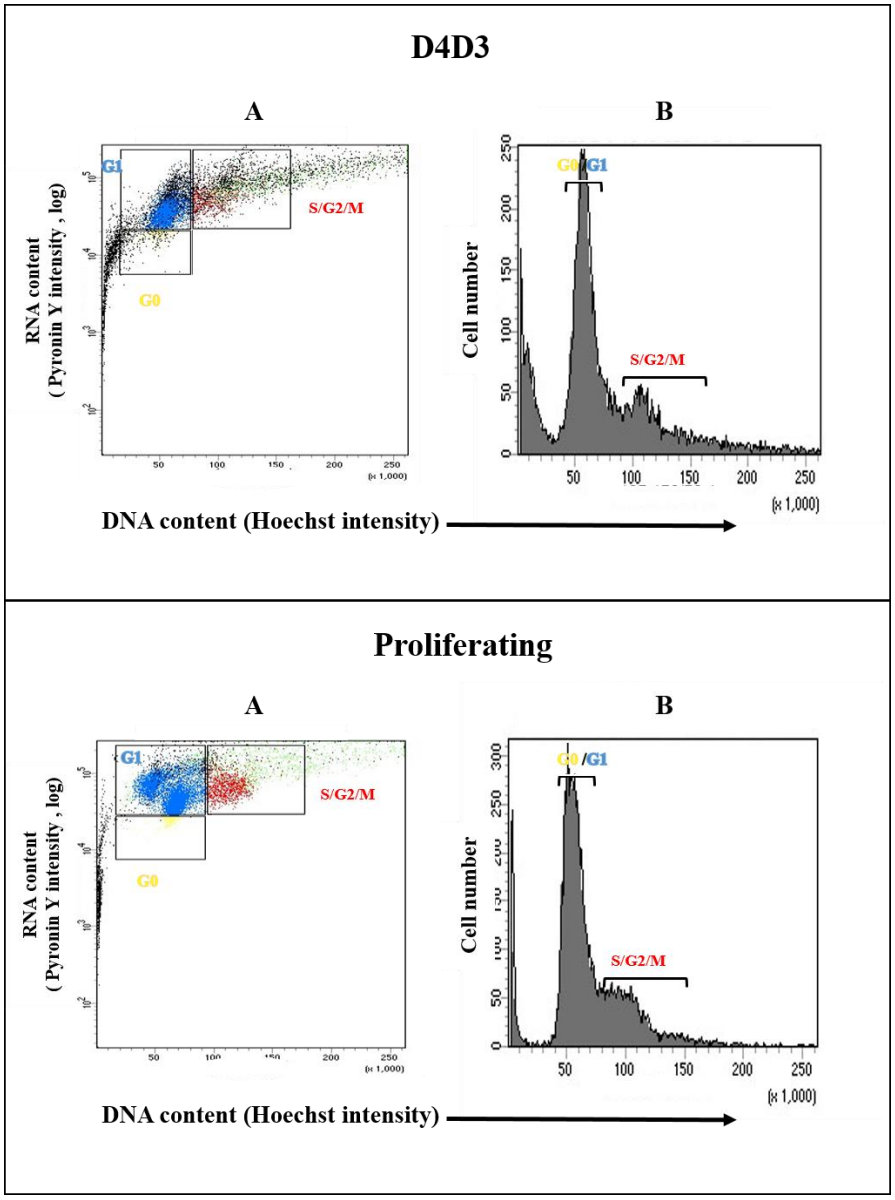

Figure 7.8 Serum add-back time-course restored the proportion of S/G2/M, G1 and G0 subpopulations in HeLa cells

HeLa cells were grown in 10% FCS medium (proliferating) or 0.1% FCS medium for four days (D4). After four days, serum was added back to starved cells (D4); both proliferating and D4 cells were grown in 10% FCS medium for further 3 days **A)** Flow cytometry plots of HeLa cells stained with viability stain; Zombie NIR, DNA stain; Hoechst and RNA stain; Pyronin Y. Dead cells were excluded from the whole cell population (Figure 7.7). The proportions of cells in S phase, G2 phase and M phase (S/G2/M), cells in G1 phase and cells in G0 phase were detected by Flow cytometry based on DNA and RNA contents

using FACsDIVA software. Cells were classed G1 if they exhibited single DNA content and were RNA positive (blue dots), cells were classed S/G2/M if they exhibited double DNA content and were RNA positive (red dots) and cells were classed G0 if they exhibited single DNA content and were RNA negative (yellow). Each dot represents a single cell. A difference in distribution of dots in S/G2/M (red), G1 (blue) and G0 (yellow) gates is obvious over the 3-day serum add-back time-course. The extent of S/G2/M cells and G1 cells appear to be increased in D4D1, D4D2 and D4D3 while the extent of G0 cells appear to be decreased compared to D4D0 (control). Compared to proliferating, the 3-day serum add-back appear to restore the proportion of S/G2/M , G1 and G0 subpopulations in starved HeLa cells. **B)** Histogram of HeLa cells stained with Hoechst stain showing DNA content distribution. There is an increase in cell number of both G0/G1 and S/G2/M in D4D1, D4D2 and D4D3 compared to D4D0 (control). Compared to proliferating, the three day serum add-back appear to restore cell number of both G0/G1 and S/G2/M. n= 10,000. N=3.

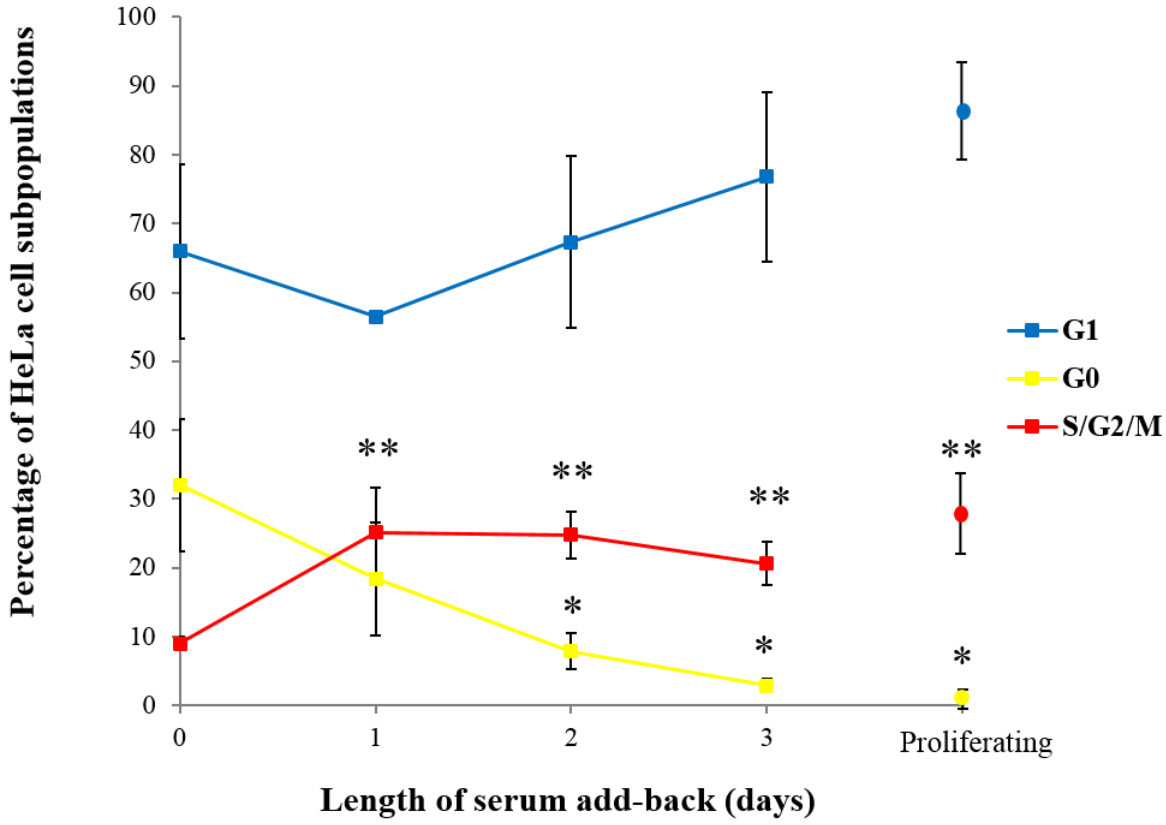

Figure 7.9 Quantitative measurements of the proportion of S/G2/M and G0 or G1 subpopulations with three-day serum add-back course in HeLa cells

HeLa cells were grown in 10% FCS medium (proliferating) or 0.1% FCS medium for 4 days. After 4 days, serum was added back to starved cells; both proliferating and starved cells were grown in 10% FCS medium for further 3 days The proportion of S/G2/M, G1 and G0 cell subpopulations was determined as a percentage of the total HeLa viable cell population. Cells were stained with viability stain; Zombie NIR, DNA stain; Hoechst and RNA stain; Pyronin Y. Dead cells were excluded from the whole cell population. The proportion of S/G2/M, G1 and G0 cell subpopulations were calculated by Flow cytometry depending on DNA and RNA contents using FACsDIVA software. Cells were classed G1 if they exhibited single DNA content and were RNA positive, cells were classed S/G2/M if they exhibited double DNA content and were RNA positive while cells were classed G0 if they exhibited single DNA content and were RNA negative. Quantitative measurements of

the proportions of G0 and S/G2/M cells were significantly changed with the 3-day serum add-back course. The percentage of G0 cells was decreased by ~ 43%, ~ 68% and ~ 90% in day one, day two and day three of serum add-back time course respectively compared to day zero (control) however the decrease was significant from day two ($P = 0.031$*). There was no significant difference in the percentage of G0 cells in day three ($P = 0.3564$) compared to proliferating (1.533 ± 0.516 %). The percentage of S/G2/M cells was increased by ~ 171 %, ~ 146 % and ~ 122 % in day one, day two and day three of serum add-back time course respectively compared to day zero (control) (All $P < 0.01$**). There was no significant difference in the percentage of S/G2/M cells from day one of serum add-back compared to proliferating ($P > 0.05$). There were no significant changes in the percentage of G1 cells over the 3-day serum add-back time-course compared to day zero ($P > 0.05$). n= 10,000. N=4.

	Viability cells (%)	G0 cells (%)	G1 cells (%) (All P > 0.0.5	S/G2/M cells (%)
D4D0 (control)	40.1±4.44	25.03± 9.6	65.96±12.69	9.26 ± 0.913
D4D1	61.2±3.01 P =0.1588	18.39±8.25 P = 0.532	56.5±0.834	25.1 ± 6.53 P = 0.0016
D4D2	75.16±10.22 P = 0.0461	7.86±2.57 P =0.03102	68.33±12.39	22.8 ± 3.42 P = 0.0031
D4D3	87.3±9.79 P = 0.0382	2.9±0.91 P=0.0282	76.83±12.34	20.63 ± 3.21 P = 0.0085
Proliferating	82.3±13.25 P= 0.0421	1.5±0.51 P = 0.0236	74.7±8.13	23.7±0.77 P = 0.003

Table 7.3 Summary of flow cytometry data of HeLa cells viability and subpopulations over the three-day serum add-back time course (means ± SEM)

7.3.2 The proportion of G0, G1 and S/G2/M subpopulations was restored after two days of serum add-back in NIH 3T3 cells

NIH 3T3 cells were grown in 10% FCS medium (proliferating) or 0.1% FCS medium for two days (D2D0) the point at which the percentage of G0 cells was significantly increased. After two days, serum was added-back to D2 cells for two days (D2D2).

Flow cytometry analysis showed that the percentage of viable cells was increased gradually with serum add-back. At D2D1 by ~30% (63.93 ± 7.68%) and at D2D2 by ~ 41 % (69.07 ± 3.66) in D2D1, D2D2 compared to D2D0 (49.03 ± 4.20%) however the increase was not significant, ($P > 0.05$) (Figure 7.10).

Consistent with restoration of cell proliferation status observed morphologically, the percentage of G0 cells was significantly decreased in D2D1 by 56% (20.13±5.895, $P = 0.0245$) and D2D2 by 77% (10.6 ± 5.288, $P = 0.0098$) compared to control D2D0 (45.73 ± 4.09) (Table 7.4). The percentage of G0 cells in D2D2 was not significantly different compared to proliferating (8.1±3.31) ($P > 0.999$) (Figure 7.11 and Figure 7.12).

Corresponding to the restoration of the percentage of G0 cells, the percentage of G1cells was significantly increased in D2D1 by ~ 60% (60.7 ± 3.81 %, $P = 0.0074$) and D2D2 by~93% (73.73±5.45, $P = 0.0094$) compared to control D2D0 (38.13 ± 1.65%) (Table 7.4). Also, the percentage of G1 cells in D2D2 showed no significant difference compared to proliferating (75.83± 1.72) ($P > 0.999$) (Figure 7.11 and Figure 7.12).

Likewise, the percentage of S/G2/M (+ve) cells was increased in D2D1 by~38% (16.9± 0.80) D2D2 (14.8± 0.89) compared to control D2D0 (12.3± 0.60) however, this increase was not significant ($P >0.05$). The S/G2/M (-ve) cells nearly disappeared with serum add-back. At D2D1 (2.2 ± 2.1%), and D2D2 (0.86 ± 0.62%) compared to D2D0 (3.83 ± 1.36) ($P > 0.05$) (Figure 7.11 and Figure 7.12 and Table 7.4).

The changes in the percentage of both S/G2/M subgroups were not significant, however, the percentage of S/G2/M (+ve) cells increased gradually back to the proliferating level and the percentage of S/G2/M (-ve) cells decreased gradually and nearly disappears by D2D2.

These results showed that serum add-back induced cell proliferation and cell cycle re-entry in G0/G1 cells from the first day and restored the full proliferating level of the percentage of G0, G1 and S/G2/M subpopulations from day two. This clearly denotes that the serum starvation induced cell cycle arrest in G0/G1 phase was reversible.

.

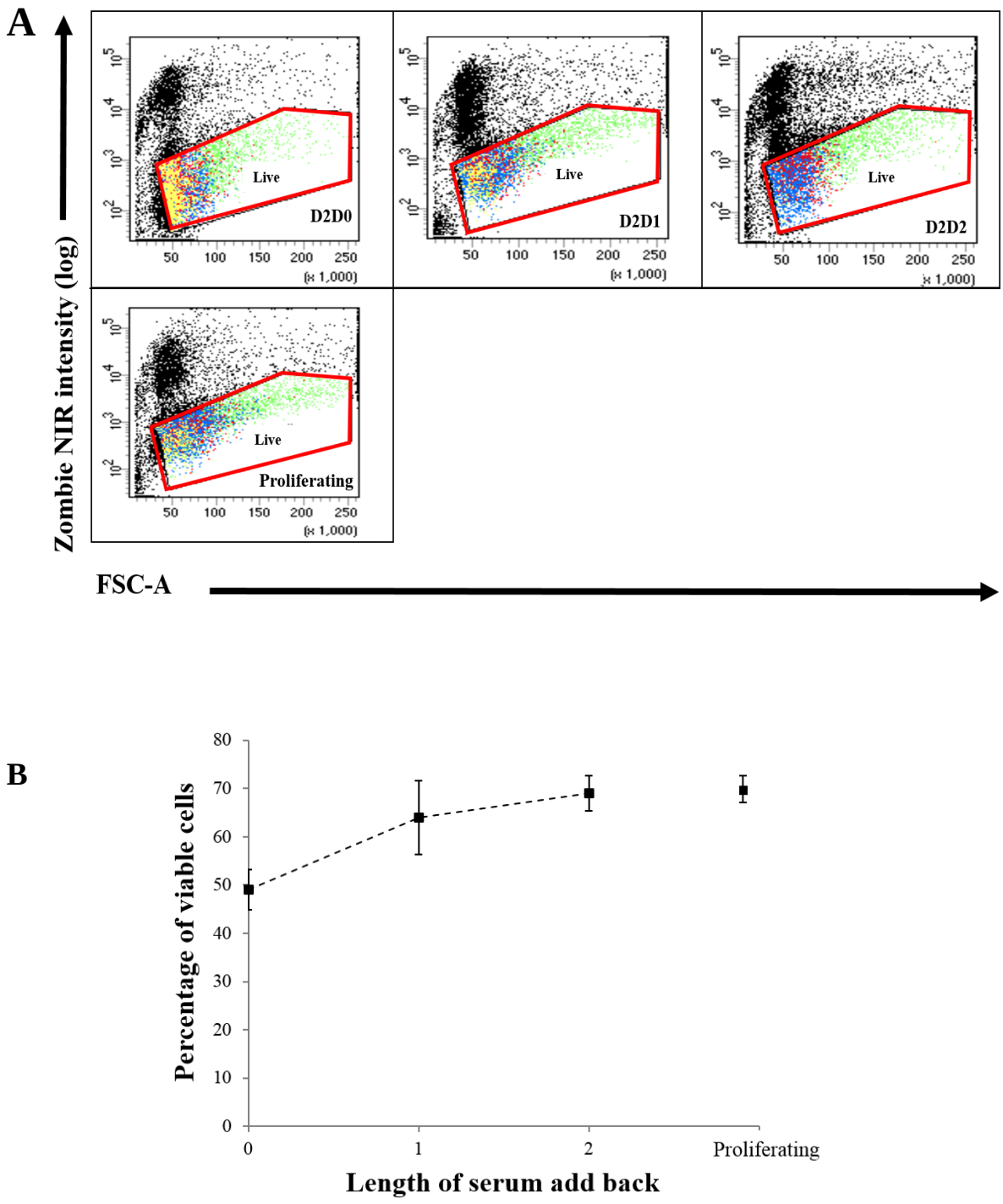

Figure 7.10 Serum add-back restored viability of G0/G1 NIH 3T3 cells

NIH 3T3 cells were grown in 10% FCS medium (proliferating) or 0.1% FCS medium for 2 days (D4). After 2 days, serum was added back to starved cells (D2); both proliferating and D2 cells were grown in 10% FCS medium for further 2 days **A)** Dot plots of flow cytometric analysis performed on NIH 3T3 cells stained with viability stain; Zombie NIR. D2D0, D2day one, D2D2 represent Two days of serum starvation followed by zero day, one day and two days of serum add-back. FSC-A represents forwards scatter area. Each dot appearing on the dot plot represents a single cell. The proportion of viable cells were detected by Flow cytometry based on strength of fluorescence signal. The dot plots showing distribution of two cell populations represents the —dead cells (black dots outside live gate; red box) that exhibit significant Zombie NIR fluorescence signal, and live cells (coloured dots within the live gate, colour code is shown in the next figure; Figure 7.11) which do not. The distribution of viable cells appeared to be increased in D2D1 and D2D2 compared to D2D0 (control). **B)** Graph shows quantitative measurements of the proportion of live cells as a percentage of total NIH 3T3 cells population. The percentage of viable cells was increased by 30 % and 41 in D2D1, D2D2 compared to D2D0 (control) however the increase was not significant ($P > 0.05$). n= 10,000. N= 3.

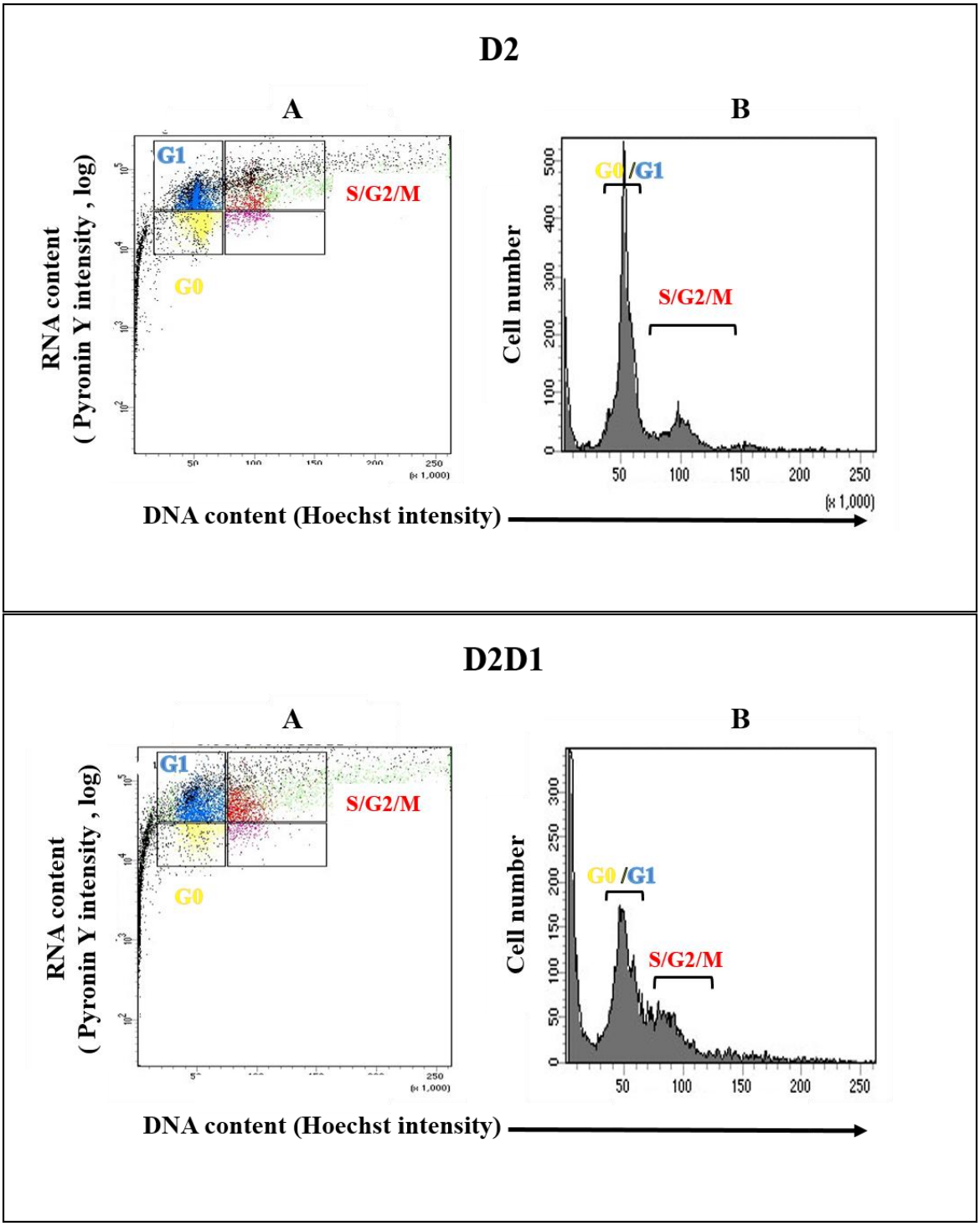
D2
A
B
G1
S/G2/M
G0
RNA content
(Pyronin Y intensity , log)
G0 /G1
S/G2/M
Cell number
(x 1,000)
DNA content (Hoechst intensity)
D2D1
A
B
G1
S/G2/M
G0
RNA content
(Pyronin Y intensity , log)
G0 /G1
S/G2/M
Cell number
DNA content (Hoechst intensity)

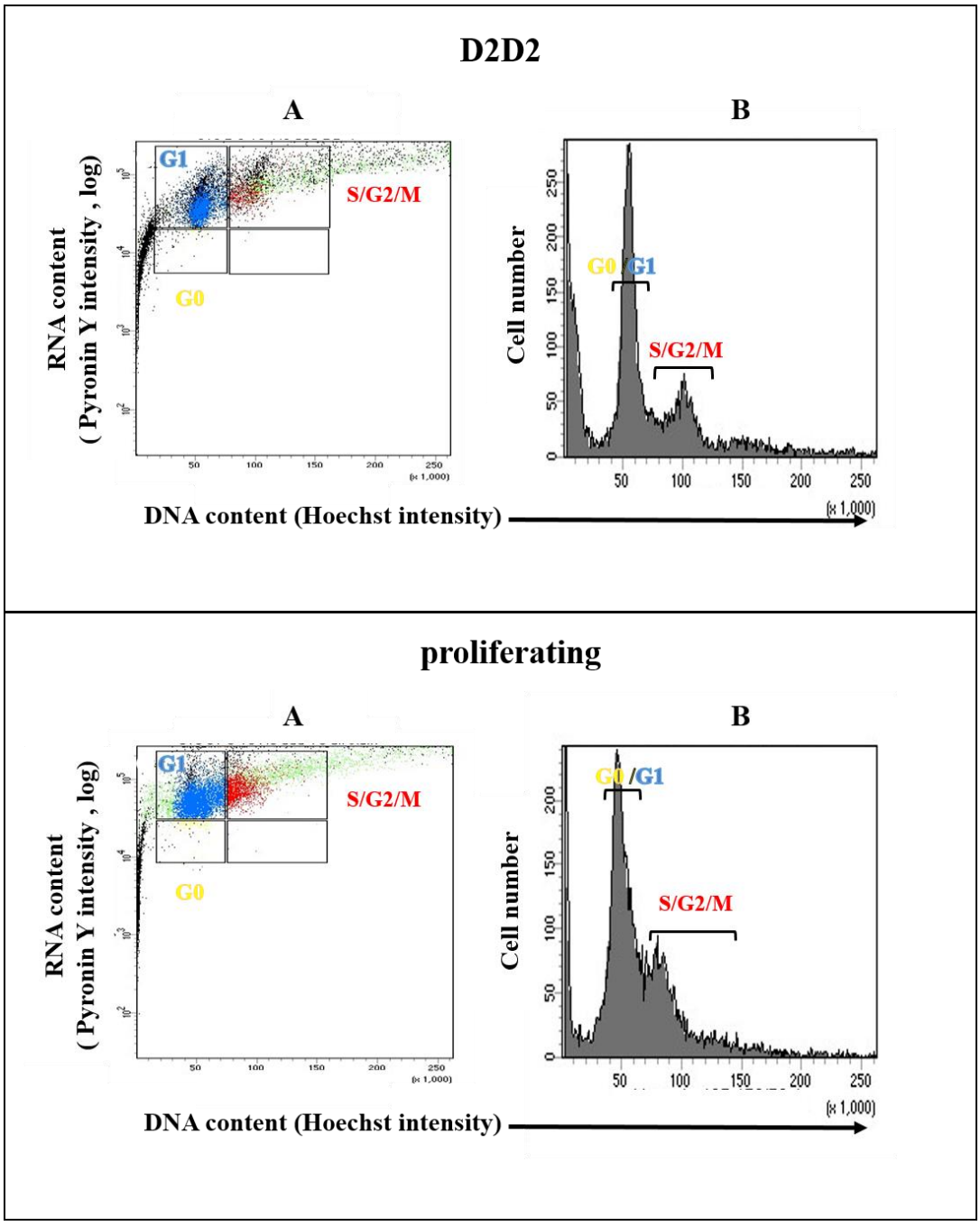

Figure 7.11 Serum add-back time-course restored the proportion of S/G2/M, G1 and G0 subpopulations in NIH 3T3 cells

NIH 3T3 cells were grown in 10% FCS medium (proliferating) or 0.1% FCS medium for two days (D2). After two days, serum was added back to starved cells (D2); both proliferating and D2 cells were grown in 10% FCS medium for further two days **A)** Flow cytometry plots of

NIH 3T3 cells stained with viability stain; Zombie NIR, DNA stain; Hoechst and RNA stain; Pyronin Y. Dead cells were excluded from the whole cell population (see fig.1). The proportions of cells in S phase, G2 phase and M phase (S/G2/M), cells in G1 phase and cells in G0 phase were detected by Flow cytometry based on DNA and RNA contents using FACsDIVA software. Cells were classed G1 if they exhibited single DNA content and were RNA positive (blue dots), cells were classed S/G2/M (+ve) if they exhibited double DNA content and were RNA positive (red dots), cells were classed S/G2/M (-ve) if they exhibited double DNA content and were RNA negative (pink dots) and cells were classed G0 if they exhibited single DNA content and were RNA negative (yellow dots). Each dot represents a single cell. A difference in distribution of dots in S/G2/M (+ve) (red), S/G2/M (-ve) (pink), G1 (blue) and G0 (yellow) gates is obvious over the 2-day serum add-back time-course. The extent of S/G2/M (+ve) cells and G1 cells appear to be increased in D2day one and D2D2 while the extent of G0 cells and S/G2/M (-ve) appear to be decreased compared to D2D0 (control). Comparing to proliferating, the 2-day serum add-back appear to restore the proportion of S/G2/M (+ve), S/G2/M (-ve), G1 and G0 subpopulations in starved NIH 3T3 cells. B) Histogram of NIH 3T3 cells stained with Hoechst stain showing DNA content distribution. There is an increase in cell number of both G0/G1 and S/G2/M in D2day one, and D2D2 compared to D2D0 (control). Comparing to proliferating, the 2-day serum add-back appear to restore cell number of both G0/G1 and S/G2/M. n= 10,000. N=3.

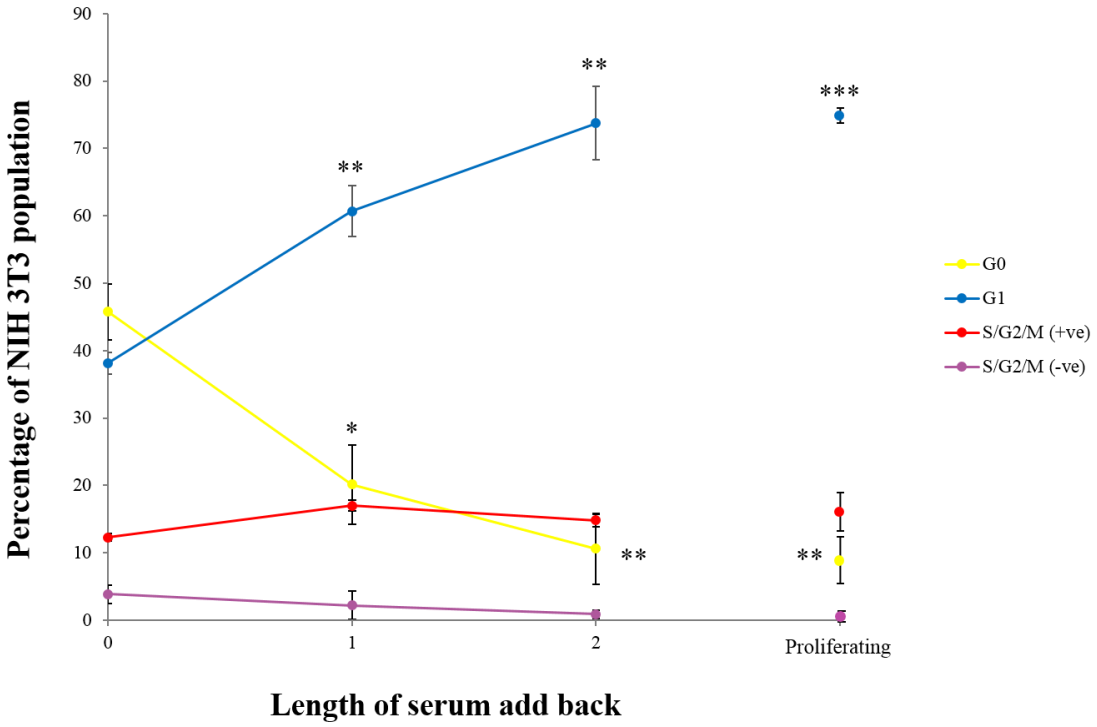

Figure 7.12 Quantitative measurements of the proportion of S/G2/M and G0 or G1 subpopulations with two-day serum add-back course in NIH 3T3 cells

NIH 3T3 cells were grown in 10% FCS medium (proliferating) or 0.1% FCS medium for 2 days (starved). After 2 days, serum was added back to starved cells; both proliferating and starved cells were grown in 10% FCS medium for further 2 days. The proportion of S/G2/M, G1 and G0 cell subpopulations was determined as a percentage of the total NIH 3T3 viable cell population. Cells were stained with viability stain; Zombie NIR, DNA stain; Hoechst and RNA stain; Pyronin Y. Dead cells were excluded from the whole cell population. The proportion of S/G2/M, G1 and G0 cell subpopulations were calculated by Flow cytometry depending on DNA and RNA contents using FACsDIVA software. Cells were classed G1 if they exhibited single DNA content and were RNA positive, cells were classed S/G2/M (+ve) if they exhibited double DNA content and were RNA positive, cells were classed S/G2/M (-

ve) if they exhibited double DNA content and were RNA negative while cells were classed G0 if they exhibited single DNA content and were RNA negative. Quantitative measurements of the proportions of G0 and G1 cells were significantly changed with 2-day serum add-back. The percentage of G0 cells was significantly decreased by ~ 55 % and ~ 76.82% in day one and day two of serum add-back respectively compared to day zero (control) ($P > 0.05$. There was no significant difference in the percentage of G0 cells in day one ($P = 0.7371$) and day two ($P = 0.9848$) compared to proliferating. The percentage of G1 cells was significantly increased by ~ 59 % and ~93% in day one and day two of serum add-back respectively compared to day zero (control)(All $P < 0.01$). There was no significant difference in the percentage of G1 cells in day two of serum add-back ($P = 0.9716$) compared to proliferating. The percentage of S/G2/M (+ve) cells was increased by ~ 37 % and ~ 20 % in day one and day two of serum add-back respectively compared to day zero (control) however the increase was not significant ($P > 0.05$). The percentage of S/G2/M (-ve) cells was not significantly decreased by 42.60 % and 77.38 % in day one and day two of serum add-back respectively compared to day zero (control) ($P > 0.05$). There was no significant difference in the percentages of both S/G2/M (+ve) and S/G2/M (-ve) in day one and day two of serum add-back compared to proliferating ($P > 0.999$). n= 10,000. N=4.

	Viability (%)	G0 cells (%)	G1 cells (%)	S/G2/M (+ve) cells (%)	S/G2/M (-ve) cells (%)
D2D0	49.03 ± 4.205	45.73 ± 4.099.	38.13 ± 1.65	12.3± 0.60	3.83 ± 1.36
D2D1	63.93 ± 7.684 P > 0.05	20.13±5.895 P = 0.0245	60.7 ± 3.811 P = 0.0074	16.9± 0.80 P > 0.05	2.2 ± 2.1 P > 0.05
D2D2	69.07 ± 3.663 P > 0.05	10.6 ± 5.288 P = 0.0098	73.73±5.45 P = 0.0094	14.8±0.89 P > 0.05	0.86 ± 0.62 P > 0.05
Proliferating	66.21±2.6 P > 0.05	8.1±3.31 P = 0.0085	75.83 ± 1.72 P = 0.0024	15.93±2.85 P > 0.05	0 P > 0.05

Table 7.4 Summary of flow cytometry data of NIH 3T3 cells viability and subpopulations over the two-day serum add-back time course

7.4 Discussion

The quiescent G0/G1 state has been defined as a temporary and reversible absence of proliferation (Coller *et al.*, 2006; Daignan-Fornier and Sagot, 2011; Cheung and Rando, 2013). In this study (Chapter 3), serum starvation induced cell cycle arrest in G0/G1 phase in HeLa and NIH 3T3 cells was determined morphologically and by flow cytometry analysis.

For HeLa cells, four-day serum starvation caused a significant decrease in total and mitotic cell number with normal viability, a decrease in cell diameter, an increase in G0/G1cells to 93% (~26% in G0 and 67% in G1 phase). For NIH 3T3 cells, two-day serum starvation caused a significant decrease in total and mitotic cell number with reserved viability, a significant increase in G0/G1 cells to ~ 92 % (~54% in G0 and 38% in G1 phase).

The aim of this chapter was to determine the reversibility of the induced cell cycle arrest by adding the serum back to the G0/G1 HeLa and NIH 3T3 cells and define this both morphologically and by flow cytometry.

For hTERT RPE-1 cells, serum starvation did not affect cell cycle progression as there were no changes observed either morphologically or by flow cytometry. Therefore, there was no need to measure morphological or cell cycle changes with serum add-back.

Serum add-back induced an increase in total cell number as well as mitotic cell number from day one of treatment in HeLa and NIH 3T3 cells (Figure 7.1 and Figure 7.4). In HeLa cells, total cell number was increased from 11.2 $\times 10^3$cells/ml in D4D0 to 22.8 $\times 10^3$cells/ml in D4D2 and 41.6 $\times 10^3$cells/ml in D4D3 (Figure 7.3). In NIH 3T3 cells, total cell number increased from 13.2$\times 10^3$ cells/ml in D2D0 to 25$\times 10^3$cells/ml in D2D1 and 51$\times 10^3$cells/ml in D2D2 (Figure 7.6). This data clearly indicate that serum add-back induced cell proliferation and cell cycle resumption in G0/G1 cells in both HeLa and NIH 3T3 cells.

To investigate cell viability, trypan blue stain was used. Data showed that cell viability was increased by ~ 42% in D4D2 HeLa cells compared to D4D0 cells ($P < 0.05$) (Figure 7.2) and by ~ 32% in D2D2 compared to D4D0 cells in NIH 3T3 cells ($P > 0.05$).

The increase in cell viability further confirms the resumption of cell proliferation in HeLa and NIH 3T3 cells.

Cell diameter showed a significant increase and was restored to the proliferating level in HeLa cells from day two of serum add-back, however, in NIH 3T3 cells, there was no significant changes in cell diameter with cell cycle arrest or with cell cycle re-entry suggesting that cell diameter could be an indicator for cell cycle arrest in G0/G1 phase in HeLa cells but not in NIH 3T3 cells.

Flow cytometry experiments measuring the cellular DNA and RNA content were also performed to further analyse cell cycle and to separate G0 and G1 cells (Shapiro, 1981; Darzynkiewicz *et al.*, 2011) as G0 cells were identified as the population with single DNA content and an RNA content lower than that in cells in S and G2/M phases (Crissman *et al.*, 1985; Lemons *et al.*, 2010).

Dead cells were excluded first by flow cytometry using a fluorescent viability dye; Zombie NIR (Figure 7.7 and Figure 7.10) which confirmed the data previously obtained using trypan blue stain. Serum add-back increased cell viability from day two in HeLa cells by ~ 87.5%, and from day one in NIH3T3 cells by ~ 30%. This again indicates that serum add-back induced cell proliferation that causes increase in number of viable cells (Tableand Table).

Flow cytometry cell cycle analysis revealed that, in HeLa cells, the percentage G0 cells decreased from the first day of serum add-back (~18.5%) and became significantly lower at D4D2 (~ 4%) compared to D4D0 (~25%) cells and not significant compared to proliferating level (1.5%). Consistently, a marked significant increase in S/G2/M cells was observed at D4D1 (~ 25%) compared to D4D0 (~ 5%) with no significant difference compared to proliferating level (~ 24%).

Similarly, in NIH 3T3 cells, G0 cells decreased significantly with serum add-back from the first day. Percentage of G0 cells decreased from ~ 54% in D2D0 to ~ 20% in D2D1 and further decreased to ~ 10% in D2D2 (not significantly different to proliferating cells at ~ 8%). A corresponding increase in G1 and S/G2/M cells was also observed where G1 and S/G2/M cells increased from ~ 38% and ~ 12% in D2D0 to ~ 60 % and ~ 15% in D2D1 respectively that was not significant compared to proliferating cells (~ 75% and ~16%) respectively.

Serum starvation-induced cell cycle arrest followed by serum add-back has been extensively used in cell cycle research (Zetterberg and Larsson, 1985; Pardee, 1992; Kerkhoff and Rapp, 1997; Xiong *et al.*, 2012; Lemos et al., 2007; Kothapalli et al., 2008; Van Rechem et al., 2010; Xiong et al., 2012). In this chapter, data clearly revealed that the obtained serum starvation induced cell cycle arrest in G0/G1 phase was reversible by serum add-back. On the basis of these results, serum add-back experiments will be used in order to study Ca^{2+} signalling when cells re- enter the cell cycle and this data is presented in subsequent chapters.

7.5 Conclusions

Serum add-back to G0/G1 cells induced cell proliferation and cell cycle re-entry in both HeLa and NIH 3T3 cells indicating that the previously induced G0/G1 cell cycle arrest was reversible.

Chapter 8 Store-Operated Ca^{2+} Entry (SOCE)

8.1 Introduction

As previously discussed, serum starvation of HeLa and NIH 3T3 cells induces cell cycle arrest in G0/G1 phase associated with an uncoupling and a down regulation of Ca^{2+} store release and SOCE. Serum add-back induced cells arrested in G0/G1 phase to re-enter the cell cycle and restored the proliferating percentage of G0 cells in both HeLa and NIH 3T3 cells. The aim of this chapter was to identify Ca^{2+} signalling changes with adding the serum back to G0/G1 cells in order to investigate Ca^{2+} signalling associated with cell cycle re-entry.

As there was alterations in Ca^{2+} signalling with serum starvation in hTERT RPE-1 cells, Ca^{2+} signalling changes with adding the serum back to the serum starved cells were also investigated. This determination of Ca^{2+} signalling with serum add-back in hTERT RPE-1 cells, which don't enter G0/G1 upon starvation gives the opportunity to assess the contribution of cell cycle re-entry in Ca^{2+} signalling changes in other cell types which do go into G0/G1 upon starvation; HeLa and NIH 3T3 cells.

8.2 Results - SOCE

8.2.1 SOCE was not restored with cell cycle re-entry in HeLa cells

Proliferating (10% FCS) cells or G0/G1 (0.1% FCS) cells were grown for four days; the point at which the percentage of G0 cells was significantly increased (Section 3.3.1). After four days, serum was added back to G0/G1 cells; both proliferating and G0/G1 cells were grown in 10% FCS medium for further three days.

Ca^{2+}-addback traces of changes in fura-2 fluorescence ratio showed differences in the level of SOCE responses in D4D3 cells compared to D4D0 cells (Figure 8.1.A). These differences may reflect the serum add-back induced restoration of the proliferating profile of proportion of S/G2/M, G1 and G0 subpopulations; cells exist in different cell cycle phases and therefore give a mixed pattern of Ca^{2+} responses compared to D4D0 cells that are synchronised; ~ 93% of cells were in G0/G1 phase (Section 3.3.1) and thus giving similar SOCE responses.

The traces also showed that both store depletion in response to TG addition (200nM) and subsequent Ca^{2+} entry following the addition of Ca^{2+} (2mM) were not restored in D4D3 cells compared to proliferating cells (Figure 8.1.B).

At day two of the serum add-back time course (D4D2), total Ca^{2+} store release (46.61 ± 1.10 FRUs) was not different compared to D4D0 cells (47.42 ± 1.703 FRUs), whilst total SOCE was significantly down-regulated by ~ 25% (135.42 ± 9.85 FRUs) compared to D4D0 cells (181.5± 5.61 FRUs) ($P < 0.05$). In D4D3 cells total Ca^{2+} store release was increased by 18% (55.78 ± 2.73 FRUs) compared to D4D0 level ($P > 0.05$) similarly, SOCE at D4D3 (201.79 ± 8.31 FRUs) was slightly increased by 11% above the D4D0 level ($P = 0.444$). These results showed that both total Ca^{2+} store release and SOCE were not restored after 3-day serum add-back to proliferating levels (All $P<0.0001$), however there was a slight increase in both Ca^{2+} store release and SOCE which might be explained by serum add-back causing partial recovery of the Ca^{2+} signalling responses (Figure 8.2.A and Table 8.1).

Consistent with this, maximal Ca^{2+} store release was not significantly different in D4D1 (0.205 ± 0.004), D4D2 (0.22 ± 0.003 FRUs) and D4D3 cells (0.19± 0.006) compared to D4D0 (0.32 ± 0.0055 FRUs) ($P > 0.05\%$). Compared to proliferating (0.61 ± 0.008), maximal Ca^{2+} store release was not restored over the 3-day serum add-back time course (All $P < 0.0001$) (Figure 8.2.B and Table 8.2).

Maximal SOCE was significantly down-regulated in D4D2 by ~ 25 % (0.3199 ± 0.0146 FRUs) compared to D4D0 (0.4264 ± 0.0098 FRUs) ($P < 0.05$). There was no significant difference in maximal SOCE of D4D1 (0.39 ± 0.01) and D4D3 cells (0.43± 0.014) compared to D4D0. Compared to proliferating (0.64 ± 0.01), maximal SOCE was not restored over the 3-day serum add-back time course (All $P < 0.0001$) (Figure 8.2.B and Table 8.2).

The effect of serum add-back and cell cycle re-entry on rate of rise and rate decline of TG and $CaCl_2$ responses were also determined (Method 2.8). Rate of Ca^{2+} store release was significantly down-regulated by ~ 44% in D4D2 ($1.066 \pm 0.034 \times 10^{-3}$ FRUs) compared to D4D0 ($1.806 \pm 0.044 \times 10^{-3}$ FRUs) $P = 0.0232$. There were no significant changes in rate of Ca^{2+} store release D4D1 (0.61± 0.054) and D4D3 cells (0.32 ± 0.031) compared to D4D0 ($P = 0.4666$). Compared to proliferating (3.25± 0.105), rate of Ca^{2+} store release was not restored over the 3-day serum add-back time course, (All $P < 0.0001$). There was no significant change

in rate of SOCE over the three-day serum add-back time course compared to D4D0 ($P > 0.05$). In D4D1 ($5.32 \pm 0.15 \times 10^{-3}$ FRUs), D4D2 ($5.72 \pm 0.52 \times 10^{-3}$ FRUs) and D4D3 ($5.70 \pm 0.18 \times 10^{-3}$ FRUs) compared to D4D0 ($4.99 \pm 0.14 \times 10^{-3}$ FRUs) (All $P > 0.05$) (Table 8.2). Subsequently, compared to proliferating ($7.9 \pm 0.4 \times 10^{-3}$ FRUs), rate of SOCE was not restored over the three-day serum add-back time course (All $P < 0.0001$).

Decline rate of Ca^{2+} store release decreased in D4D2 by 51% ($5.54 \pm 5.38 \times 10^{-5}$ FRUs) and D4D3 by 41% ($5.75 \pm 1.96 \times 10^{-5}$ FRUs) compared to D4D0 ($11.4 \pm 12.4 \times 10^{-5}$ FRUs) however this decrease was not significant ($P > 0.05$) (Table 8.1). There was no significant difference in decline rate of Ca^{2+} store release over the 3-day serum add-back time course compared to proliferating. (All $P > 0.999$). Decline rate of SOCE was decreased in D4D3 by 22% ($3.32 \pm 1.01 \times 10^{-5}$ FRUs) compared to D4D0 ($10.41 \pm 1.24 \times 10^{-5}$ FRUs) ($P < 0.05$). Decline rate of SOCE was restored in D4D3 compared to proliferating (All $P > 0.999$) (Table 8.2).

The present results reveal that down-regulation of Ca^{2+} store release and SOCE associated with cell cycle arrest in G0/G1 phase were not restored with cell cycle re-entry by three days of serum add-back.

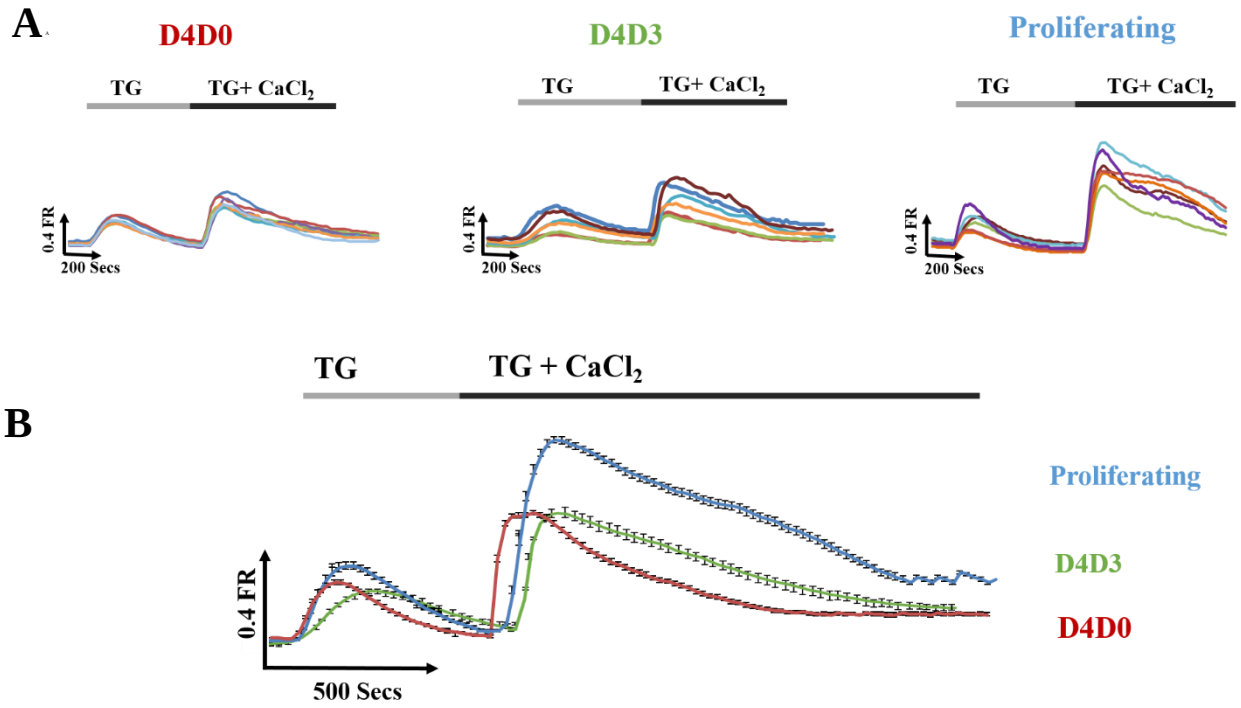

Figure 8.1 Ca^{2+} signalling traces of HeLa cells with serum add-back

HeLa cells were grown in 10% FCS medium (proliferating) or 0.1% FCS medium for 4 days (D4D0). After 4 days, serum was added back to G0/G1 cells for three days (D4D3).TG represents the addition of the SERCA inhibitor thapsigargin to induce Ca^{2+} store release and $CaCl_2$ represents Ca^{2+} addition to the Ca^{2+} free buffer to induce SOCE. **(A)** Typical Ca^{2+}-addback traces from 6 individual cells within one experiment in proliferating (blue), D4 cells (red) and D4D3 (green) show differences in level of Ca^{2+} responses in proliferating and D4D3 compared to D4 cells. **(B)** Typical Ca^{2+} addback traces from proliferating (blue), D4 cells (red) and D4D3 (green). Traces represent an average from 80 cells ± S.E.M from one experiment. Fura-2 fluorescence was measured at excitation wavelengths of 340 nm and 380 nm and an emission wavelength of 510 nm, with changes in fluorescence ratio (FR) reflect changes in $[Ca^{2+}]_i$. Addition of thapsigargin (TG, first peak) caused increase in FR in proliferating and starved cells indicating increase in $[Ca^{2+}]_i$ as Ca^{2+} is depleted from ER stores. Following Ca^{2+} addback ($CaCl_2$, second peak) an increase in FR occurred, as Ca^{2+} enters the cytosol via SOCE to replenish depleted stores. Both Ca^{2+} store release and SOCE responses appear to be not restored over the three-day serum add-back time course compared to proliferating cells.

		Total		Maximal	
		Values (FRUs)	**% change**	**Values (FRUs)**	**% change**
Ca^{2+}store release	D4D0 (control)	47.42±1.703	-----	0.32±0.005	-----
	D4D1	42.1±1.9 P > 0.999	-11%	0.20±0.004 P > 0.05	-37%
	D4D2	46.61±1.10 P > 0.999	-1.5%	0.22±0.003 P > 0.05	-31%
	D4D3	55.78 ± 2.73 P > 0.999	18%	0.19± 0.006 P > 0.05	-40%
	Proliferating	70±3.1	-----	0.61±0.001	-----
SOCE	D4D0 (control)	181.5± 5.61	-----	0.426 ± 0.0098	-----
	D4D1	198.1±5.6 P > 0.05	9%	0.39 ± 0.01 P > 0.05	-7%
	D4D2	135.4± 9.85 P < 0.05	-25%	0.3199±0.014 P < 0.05	-26%
	D4D3	201.7 ± 8.31 P > 0.05	11%	0.43± 0.014 P > 0.05	2%
	Proliferating	457±12.5	-----	0.64±0.008	-----

Table 8.1Summary of quantifications of total and maximum Ca^{2+} store release and SOCE responses with cell cycle re-entry in HeLa cells

The total response (area under the peak, AUP), maximal response (the height of peak, HOP), for TG and $CaCl_2$ responses from calibrated fluorescence traces were calculated using Excel

functions in a template spread sheet (Methodology chapter 2.8, figure 2.10) over three days of serum add-back . Data represented as means ± SEM. FRUs (fluorescence ratio unit). For proliferating cells n =228, for D4D0 n = 231, D4D1 n = 299, D4D2 n = 214 and D4D3 n= 270, N=4.

		ROR (FRUs (All P > 0.05)		ROD (FRUs× 10^{-5}) (All P > 0.999)	
		Values (×10^{-3} FRUs)	**% change**	**Values (×10^{-5} FRUs)**	**% change**
Ca^{2+}store release	D4D0 (Control)	1.80±0.044	-------	11.4±12.4	-------
	D4D1	2.31± 0.054	28%	11.59±12.4	-1.5%
	D4D2	1.06± 0.034 P = 0.0232	-44%	5.54±5.38	-51%
	D4D3	1.76± 0.031 P= 0.4666	-5%	5.75±1.96	-49%
	Proliferating	2.25±0.1	-------	5.89±0.11	-------
SOCE	D4D0 (control)	4.99 ± 0.14 P = 0.9331	-------	10.41±1.24	-------
	D4D1	5.32± 0.150 P = 0.5047	6%	13.58±0.72	30%
	D4D2	5.72± 0.52	14%	10.03±0.53	-3%
	D4D3	5.70± 0.18	14%	3.32±1.52	-68%
	Proliferating	7.9 ± 0.4	-------	8.89±1.01	-------

Table 8.2 Summary of quantifications ROR and ROD of Ca^{2+} store release and SOCE responses with cell cycle re-entry in HeLa cells

The rate of rise (ROR) and rate of decline (ROD) for TG and $CaCl_2$ responses from calibrated fluorescence traces were calculated using Excel functions in a template spread sheet (Methodology chapter 2.8, figure 2.10) over three days of serum add-back . Data represented as means ± SEM. FRUs (fluorescence ratio unit). For proliferating cells n =228, for D4D0 n = 231, D4D1 n = 299, D4D2 n = 214 and D4D3 n= 270, N=4.

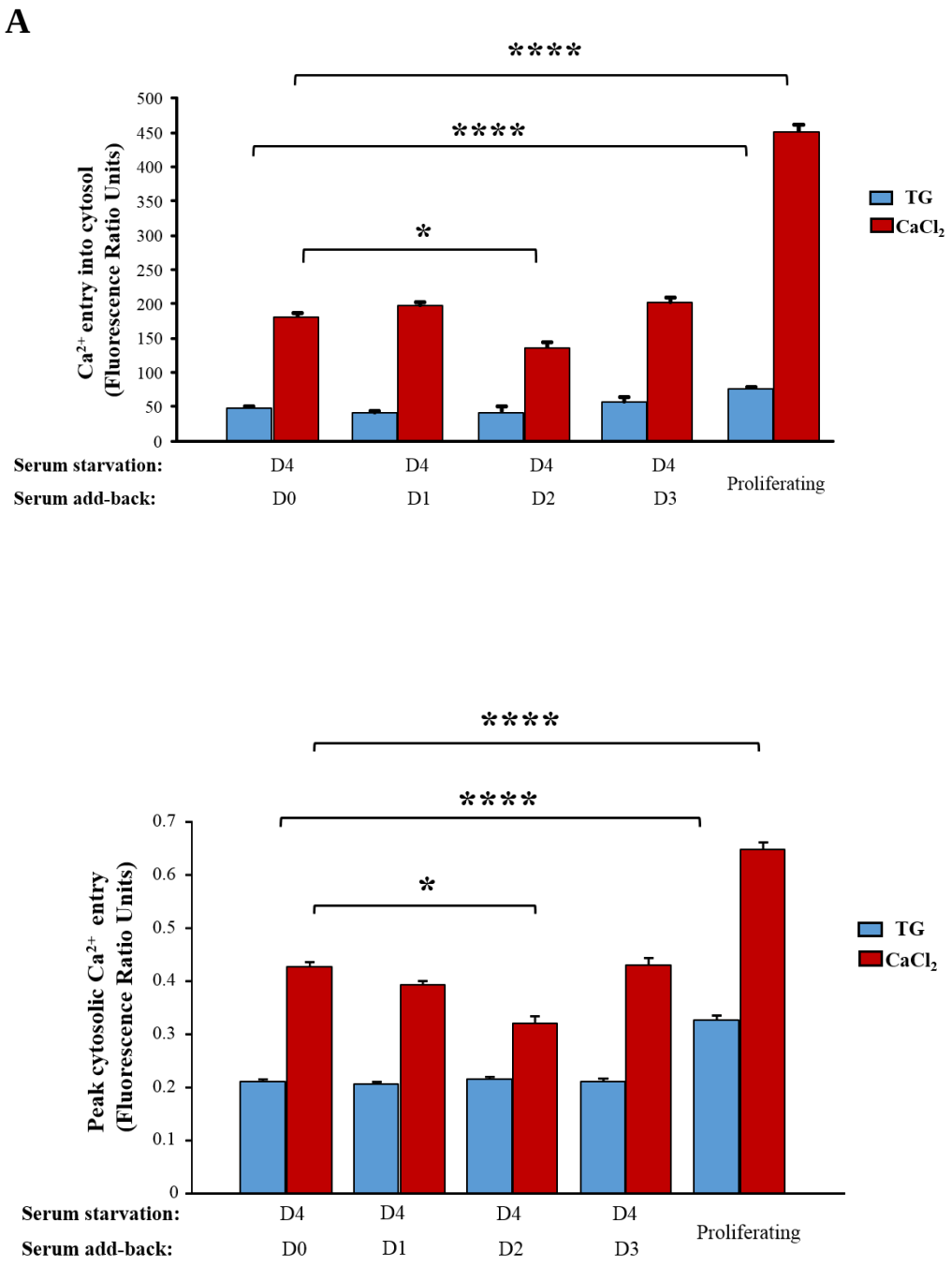

Figure 8.2 Ca^{2+} responses were not restored with cell cycle re-entry in HeLa cells

HeLa cells were grown in 10% FCS medium (proliferating) or 0.1% FCS medium for four days (D4). After four days, serum was added back to starved cells (D4); both proliferating and D4 cells were growing in 10% FCS medium for further three days. **A)** Graph shows mean of total Ca^{2+} entry into the cytosol following Ca^{2+} store release in response to stimulation with

200nM thapsigargin (TG) and subsequent SOCE following the addition of 2mM $CaCl_2$. Changes in fluorescence ratio units (FRUs) reflect changes in $[Ca^{2+}]_i$. Total Ca^{2+} store release was not significantly altered over 3-day serum add-back time course (P = 0.998). However, SOCE was significantly down-regulated by 25.38 % at day two of the serum add-back time course (D4D2) compared to D4D0 (P < 0.0001****). By day three of the serum add-back time course (D4D3) SOCE was increased back to the G0/G1 level (D4D0) (P = 0.444). Both total Ca^{2+} store release and SOCE were not restored after 3-day serum add-back course to proliferating levels (All P<0.0001****). **B)** Graph shows mean of maximal store release in response to TG addition and maximal SOCE after adding Ca^{2+}. Maximal Ca^{2+} store release was not significantly altered over 3-day serum add-back time course (P > 0.999). Compared to proliferating, maximal Ca^{2+} store release was not restored over the 3-day serum add-back time course (All P < 0.0001****). Maximal SOCE was significantly down-regulated by ~ 24.9 % in D4D2 compared to D4D0 (P = 0.0001****). Compared to proliferating, maximal SOCE was not restored over the 3-day serum add-back time course, all P < 0.0001****. Error bars represent S.E.M. For proliferating cells n =228, for D4D0 n = 231, D4D1 n = 299, D4D2 n = 214 and D4D3 n= 270, N=4.

8.2.2 SOCE was restored with cell cycle re-entry in NIH 3T3 cells

Proliferating (10% FCS) cells or G0/G1 (0.1% FCS) cells were grown for two days; the point at which the percentage of G0 cells was significantly increased (Section 3.3.2). After two days, serum was added back to G0/G1 cells and both proliferating and G0/G1 cells were grown in 10% FCS medium for further two days.

As observed in HeLa cells, Ca^{2+}-addback traces from D2D0, D2D2 and proliferating NIH 3T3 cells indicated that the dissimilarities in levels of Ca^{2+} responses in proliferating cells were restored in D2D2 cells compared to D2D0 cells (Figure 8.3.A). This may reflect the previously observed resuming of cell cycle with serum add-back, therefore cells in different cell cycle phases generating varying Ca^{2+} responses. The traces also showed that both store depletion in response to TG addition (200nM) and subsequent Ca^{2+} entry following the addition of Ca^{2+} (2mM) were restored in D2D2 cells compared to proliferating cells (Figure 8.3.B).

Total Ca^{2+} store release was significantly upregulated in D2D1 by ~73% (98.13 ± 4.03 FRUs) and in D2D2 by ~70% (96.29 ± 6.93 FRUs) compared to D2D0 (56.71 ± 3.48 FRUs) ($P < 0.0001$). Compared to proliferating (102.62 ± 3.66 FRUs) total Ca^{2+} store release was restored after one-day serum add-back D2D1 ($P > 0.05$) (Figure 8.4.A). Total SOCE was significantly upregulated by ~ 50 % in D2D1 (213.71 ± 7.05 FRUs) and ~ 61% in D2D2 (229.9 ± 22.1 FRUs) compared to D2D0 (142.17 ± 7.98 FRUs) (All $P < 0.0001$). Compared to proliferating (236.82 ± 9.15 FRUs) total SOCE was restored after one-day serum add-back D2D1 ($P > 0.05$) (Figure 8.4.A and Tabl3 8.3).

Consistent with this, maximal Ca^{2+} store release was significantly upregulated in D2D1 by~41% (0.26± 0.007FRUs) and in D2D2 by ~36.5% (0.25 ± 0.003 FRUs) compared to D2D0 (0.18 ± 0.009 FRUs) ($P < 0.0001$). Compared to proliferating (0.26 ± 0.008 FRUs) maximal Ca^{2+} store release was restored after one-day serum add-back D2D1 ($P > 0.999$) (Figure 8.4.B). Maximal SOCE was also significantly upregulated by ~ 19 % in D2D1 (0.55 ± 0.01 FRUs) and ~ 30% in D2D2 (0.60± 0.02 FRUs) compared to D2D0 (0.46± 0.01 FRUs) (All $P < 0.0001$). Compared to proliferating (0.60 ± 0.01 FRUs) maximal SOCE was restored after one-day serum add-back D2D1 ($P > 0.999$) (Figure 8.4.B and Table 8.3).

Rate of Ca^{2+} store release was significantly increased in D2D1 by ~65% ($1.03 \pm 0.03 \times 10^{-3}$ FRUs) and in D2D2 by ~42% (1.12 ± 0.04 FRUs) compared to D2D0 (0.63 ± 0.02 FRUs) ($P < 0.05$). Compared to proliferating (0.97 ± 0.05 FRUs) rate Ca^{2+} store release was restored after one-day serum add-back D2D1 ($P > 0.999$). Rate of SOCE was not significantly different in D2D1 (2.8 ± 0.6 FRUs) and in D2D2 (3.1± 0.13 FRUs) compared to D2D0 (3.2± 0.09 FRUs) (All $P > 0.999$) (Table 8.3). This observation indicates that cell cycle re-entry restored the efficiency of Ca^{2+} store release.

Both decline rate of Ca^{2+} store release and SOCE were not significantly altered over the 2-day serum add-back time course (All $P > 0.0999$) (Table 8.3).

The present results revealed, in contrast to HeLa cells, that overall Ca^{2+} store release and SOCE were restored with cell cycle re-entry in NIH 3T3 cells.

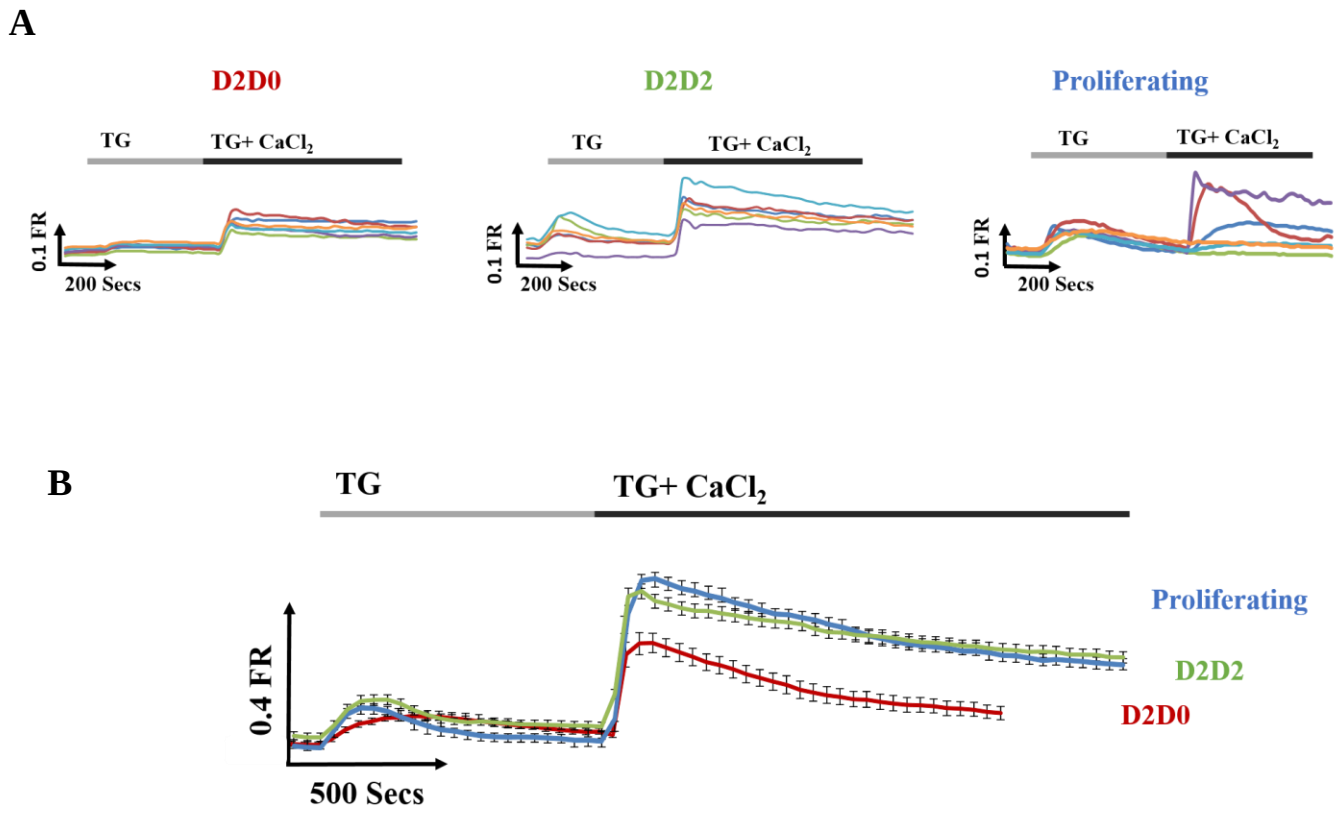

Figure 8.3 SOCE traces with cell cycle re-entry in NIH 3T3 cells

NIH 3T3 cells were grown in 10% FCS medium (proliferating) or 0.1% FCS medium for 2 days (D2D0). After 2 days, both proliferating and D2D0 cells were grown in 10% FCS for further 2 days. TG represents the addition of the SERCA inhibitor thapsigargin to induce Ca^{2+} store release and $CaCl_2$ represents Ca^{2+} addition to the Ca^{2+} free buffer to induce SOCE. **(A)** Typical Ca^{2+}-addback traces from 6 individual cells within one experiment in proliferating (blue), D2 cells (red) and D2D2 (green) show variability in Ca^{2+} responses in proliferating and D2D2 compared to D2 cells. **(B)** Mean Ca^{2+} addback traces from proliferating (blue), D2D0 cells (red) and D2D2 (green). Traces represent an average from 60 cells ± S.E.M from one experiment. Fura-2 fluorescence was measured at excitation wavelengths of 340 nm and 380 nm and an emission wavelength of 510 nm, with changes in fluorescence ratio (FR) reflect changes in $[Ca^{2+}]_i$. Addition of thapsigargin (TG, first peak) caused increase in FR in proliferating and starved cells indicating increase in $[Ca^{2+}]_i$ as Ca^{2+} is depleted from ER stores. Following Ca^{2+} addback ($CaCl_2$, second peak) an increase in FR occurred, as Ca^{2+} enters the

cytosol via SOCE to replenish depleted stores. Both Ca^{2+} store release and SOCE responses appear to be restored over the two-day serum add-back time course compared to proliferating cells. For proliferating cells n = 130, for D2D0 n = 101, D2D1 n = 179, D2D2 n = 188, N=4.

		Total (P < 0.0001)		Maximal (P < 0.0001)		ROR		ROD (P > 0.05)	
		Values(FRUs)	**% change**	**Values(FRUs)**	**% change**	**Values($\times 10^{-3}$ FRUs)**	**% change**	**Values ($\times 10^{-5}$ FRUs)**	**% change**
Ca^{2+}store release	D2D0	56.71±3.48	-----	0.18±0.009	-----	0.63 ± 0.02	-----	6.71 ± 1.27	-----
	D2D1	98.13±4.03	73%	0.26±0.007	44%	1.03 ± 0.03 P < 0.05	63%	8.91± 0.91	33%
	D2D2	96.29±6.93	70%	0.25±0.003	39%	1.12± 0.04 P < 0.05	78%	12.01±1.4	79%
	Proliferating	102.6±3.66	81%	0.26±0.008	44%	0.97 ± 0.05	54%	12.5±2.6	86%
SOCE	D2D0	142.1±7.98	-----	0.46± 0.01	-----	3.2± 0.09	-----	4.72±1.01	-----
	D2D1	213.7±7.05	50%	0.55 ± 0.01	20%	2.8 ± 0.6 P > 0.999	-12.5%	2.65±0.93	-44%
	D2D2	229.9±22.1	62%	0.60± 0.02	30%	3.1± 0.13 P > 0.999	-3%	2.24±0.85	-53%
	Proliferating	236.8±9.15	66%	0.60 ± 0.01	30%	3.57± 0.11	-12%	2.23±1.02	-53%

Table 8.3 Summary of quantifications of Ca^{2+} store release and SOCE responses in NIH 3T3 cells with cell cycle re-entry

The total response (area under the peak, AUP), maximal response (the height of peak, HOP), rate of rise (ROR) and rate of decline (ROD) for TG and $CaCl_2$ responses from calibrated fluorescence traces were calculated using Excel functions in a template spread

sheet (Methodology chapter 2.8, figure 2.10) over two days of serum add-back . Data represented as means ± SEM. FRUs (fluorescence ratio unit).

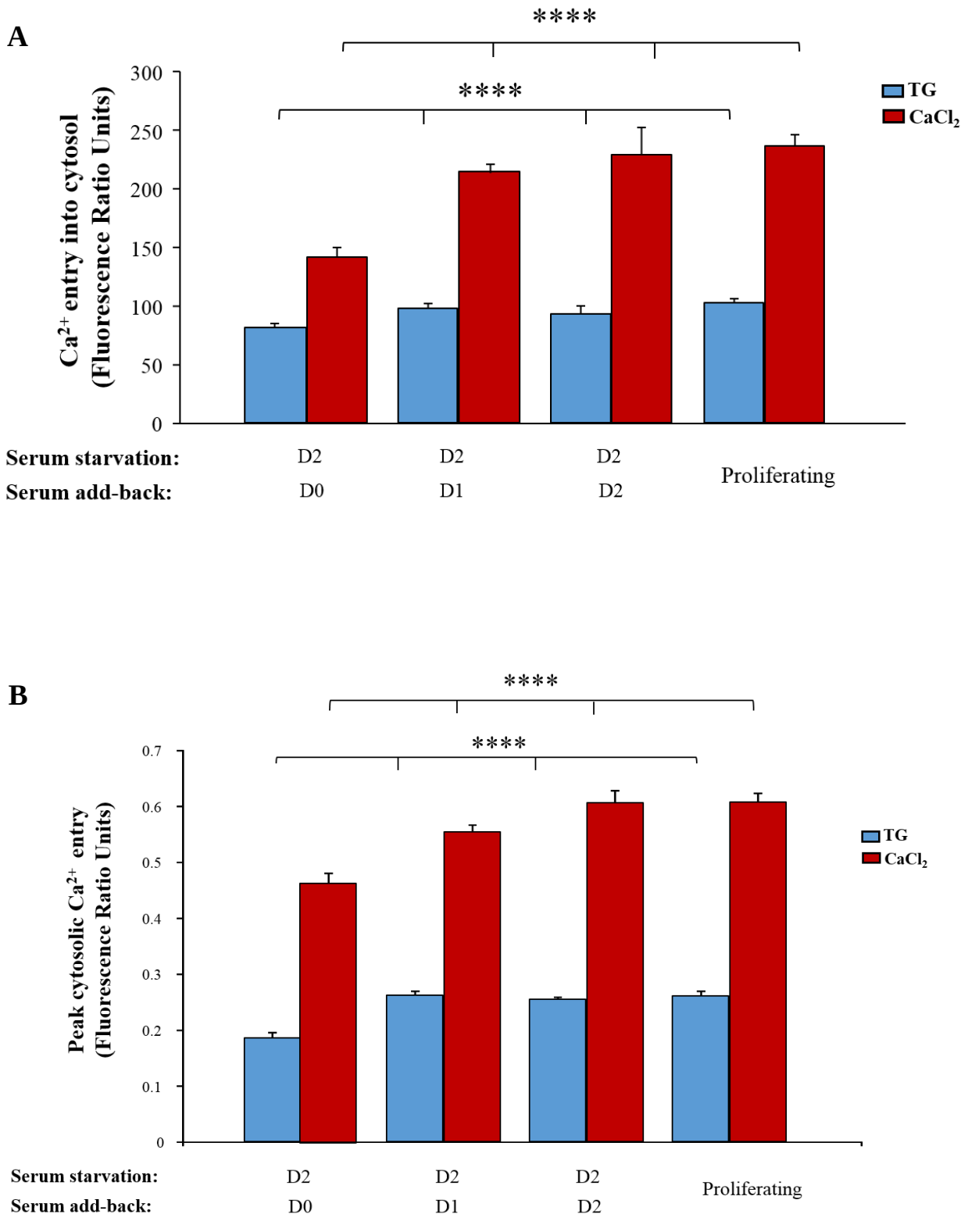

Figure 8.4 Ca^{2+} responses were restored with cell cycle re-entry in NIH 3T3 cells

NIH 3T3 cells were grown in 10% FCS medium (proliferating) or 0.1% FCS medium for 2 days (D2D0). After 2 days, serum was added back to D2D0 cells; both proliferating and D2D0 cells were growing in 10% FCS medium for further 2 days. Changes in fluorescence ratio units (FRUs) reflect changes in $[Ca^{2+}]_i$ following Ca^{2+} store release in response to stimulation with 200nM thapsigargin (TG) and subsequent SOCE following the addition of 2mM $CaCl_2$. **A)** Graph shows mean of total store release in response to TG addition and maximal SOCE after adding Ca^{2+}. D2D0, D2D1, D2D2 represent two days of serum starvation followed by zero day, one day and two days of serum add-back. Total Ca^{2+} store release was significantly upregulated by ~ 73% and ~ 70% in D2D1 and D2D2 respectively compared to D2D0. Total SOCE was significantly upregulated by ~ 50 % and ~ 61% in D2D1 and D2D2 compared to D2D0 (All $P < 0.0001$****). Compared to proliferating, both total Ca^{2+} store release and SOCE were restored after one-day serum add-back time course D2D1; $P > 0.999$. **B)** Maximal Ca^{2+} store release was significantly upregulated by ~ 41% and ~ 58% in D2D1 and D2D2 compared respectively to D2D0 ($P < 0.0001$****). Compared to proliferating, maximal Ca^{2+} store release restored after one day serum add-back time course, all $P > 0.999$. Maximal SOCE was significantly upregulated by ~ 19% and 30% in D2D1 and D2D2 compared to D2D0 ($P < 0.0001$****). Compared to proliferating, maximal SOCE was restored over the 2-day serum add-back time course, $P = 0.7351$. Error bars represent S.E.M. For proliferating cells n = 130, for D2D0 n = 101, D2D1 n = 179, D2D2 n = 188, N=4.

8.2.3 SOCE was restored with serum add-back in hTERT RPE-1 cells

In this study, serum starvation of hTERT RPE-1 cells did not affect cell cycle progression, and so consequently did not induce cell cycle arrest in G0/G1 phase (Section 3.3.3), however, Ca^{2+} signalling responses were altered in response to serum starvation (Section 4.2.3). Therefore, Ca^{2+} signalling changes were further investigated with adding the serum back to serum-starved RPE-1 cells in order to detect the reversibility of serum starvation induced Ca^{2+} signalling changes.

Typical Ca^{2+}-addback traces from 6 individual cells within one experiment were chosen randomly to show various profiles of single cell Ca^{2+} signals (Figure 8.5. A). Ca^{2+}-addback traces from D2D0, D2D2 and proliferating hTERT RPE-1 cells were similar and showed variances in Ca^{2+} responses. This is not surprising giving that the hTERT RPE-1 cells were not synchronised either with serum starvation or with serum add-back.

Mean Ca^{2+}-addback traces from D2D0, D2D2 and proliferating cells indicated that both Ca^{2+} store release in response to TG addition (200nM) and SOCE following the addition of $CaCl_2$ (2mM) appeared to be upregulated in D2D2 cells compared to D2D0 cells and restored compared to proliferating cells (Figure 8.3.B).

In order to quantify Ca^{2+} entry into the cell cytosol the area from under TG and $CaCl_2$ responses were calculated from calibrated fluorescence traces (Method 2.8). Area under peak (AUP) was presented in graphs as mean ± SEM of n determinations.

Total Ca^{2+} store release was significantly up regulated in D2D1 cells by ~ 43% (37.76 ± 2.765 FRUs) and D2D2 by ~ 45% (38.27 ± 7.367 FRUs) respectively compared to D2D0 (26.35 ± 4.18 FRUs) ($P<0.001$). Compared to proliferating cells (39.12 ± 2.13 FRUs), Ca^{2+} store release was restored after 1 day of serum add-back ($P > 0.05$) (Figure 8.6.A). Total SOCE was also significantly up-regulated up regulated in D2D1 by 18.5% (57.5 ± 10.2 FRUs) and D2D2 by 21% (58.7 ± 8.61 FRUs) compared to D2D0 (48.4 ± 6.351 FRUs), ($P <0.05$). Compared to proliferating cells (66.43 ± 2.19 FRUs), there was significant difference at D2D1 and D2D2 ($P > 0.05$) (Figure 8.6.A and Table 8.4).

Consistent with the upregulation and restoration of total Ca^{2+} store release and SOCE, maximal Ca^{2+} store release was significantly up-regulated in D2D1 cells by 32% (0.175 ±

0.012FRUs) and D2D2 by 58% (0.209 ± 0.007 FRUs) respectively compared to D2D0 (0.132 ± 0.008 FRUs) ($P<0.001$).Compared to proliferating cells (0.20 ± 0.008 FRUs), maximal Ca^{2+} store release was restored after the first day of the serum add-back time course ($P > 0.05$). (Figure 8.6.B and Table 8.4).

Maximal SOCE was significantly upregulated in D2D1 cells by ~8% (0.25 ± 0.022FRUs) and D2D2 by ~51% (0.349 ± 0.013 FRUs) respectively compared to D2D0 (0.230 ± 0.016 FRUs), however, it was only significant in D2D2 ($P<0.001$). Compared to proliferating cells (0.20 ± 0.008 FRUs), maximal SOCE was restored after day 2 of the serum add-back time course ($P > 0.05$) (Figure 8.6.B and Table 8.4).

Rate of Ca^{2+} store release showed no significant differences over the 2-day serum add-back time course. In D2D1 cells ($1.83\pm0.054\times10^{-3}$ FRUs) and D2D2 ($1.62\pm0.062 \times 10^{-3}$ FRUs) compared to D2D0 ($1.975\pm 0.048 \times10^{-3}$ FRUs) ($P >0.05$) (Table 8.4). Rate of SOCE was upregulated D2D1 cells by ~16% ($5.51\pm 0.056 \times10^{-3}$ FRUs) and D2D2 by ~13%($5.38 \pm 0.11\times10^{-3}$FRUs) respectively compared to D2D0 ($4.75 \pm 0.175 \times 10^{-3}$ FRUs) however this upregulation was not significant. ($P > 0.05$). Compared to proliferating cells ($6.079 \pm 0.146\times10^{-3}$ FRUs), rate of SOCE was not significantly different over the 2-day serum add-back time course ($P > 0.05$) (Table 8.4).

Decline rate of Ca^{2+} store release was not significantly changed over the 2-day serum add-back time course. In D2D1 cells ($12.005\pm 4.43 \times10^{-5}$ FRUs) and D2D2 ($17.91\pm7.26 \times10^{-5}$ FRUs) compared to D2D0 ($26.16 \pm 4.24 \times10^{-5}$ FRUs) ($P >0.05$) (Table 8.4). Decline rate SOCE was significantly increased in D2D1 cells by ~53% ($143.70 \pm 8.17\times10^{-5}$ FRUs) and D2D2 by ~60% ($150.12 \pm 10.81\times10^{-5}$FRUs) compared to D2D0 ($93.50\pm 7.26 \times10^{-5}$ FRUs) ($P < 0.05$). Compared to proliferating cells ($170.1 \pm 0.9.1\times10^{-5}$ FRUs), decline rate of SOCE was not significantly different over the two-day serum add-back time course ($P > 0.05$) (Table 8.4).

In summary, the results showed that total Ca^{2+} store release and SOCE were restored from the first day of serum add-back in hTERT RPE-1 cells.

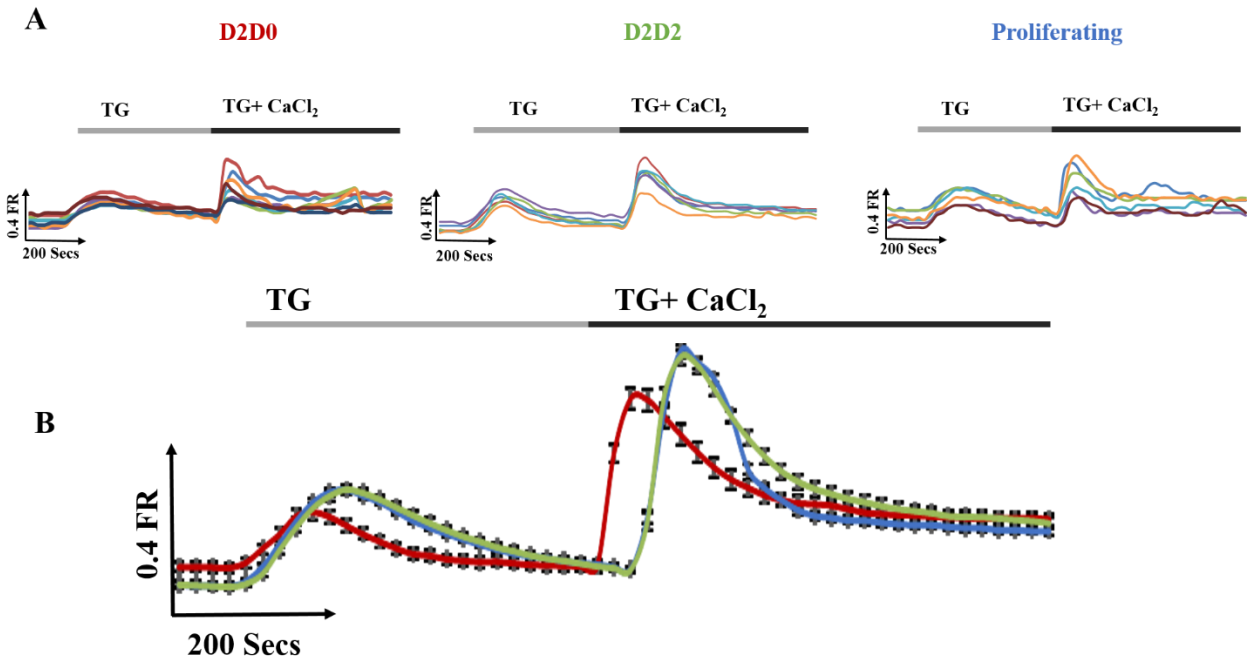

Figure 8.5 SOCE serum add-back traces of hTERT RPE-1 cells

RPE-1 cells were grown in 10% FCS medium (proliferating) or 0.1% FCS medium for 2 days (D2D0). After 2 days both proliferating and D2D0 cells were grown in 10% FCS for further 2 days.TG represents the addition of the SERCA inhibitor thapsigargin to induce Ca^{2+} store release and $CaCl_2$ represents Ca^{2+} addition to the Ca^{2+} free buffer to induce SOCE. **(A)** Typical Ca^{2+}-addback traces from 6 individual cells within one experiment in proliferating (blue), D2D0 cells (red) and D2D2 (green) show variability in Ca^{2+} responses in proliferating and D2D2 compared to D2 cells. **(B)** Mean Ca^{2+} addback traces from proliferating (blue), D2D0 cells (red) and D2D2 (green). Traces represent an average from 100 cells ± S.E.M from one experiment. Fura-2 fluorescence was measured at excitation wavelengths of 340 nm and 380 nm and an emission wavelength of 510 nm, with changes in fluorescence ratio (FR) reflect changes in $[Ca^{2+}]_i$. Addition of thapsigargin (TG, first peak) caused increase in FR in proliferating and starved cells indicating increase in $[Ca^{2+}]_i$ as Ca^{2+} is depleted from ER stores. Following Ca^{2+} addback ($CaCl_2$, second peak) an increase in FR occurred, as Ca^{2+} enters the cytosol via SOCE to replenish depleted stores. Both Ca^{2+} store release and SOCE responses

appear to be restored over the two-day serum add-back time course compared to proliferating cells.

		Total		Maximal		ROR (All P > 0.05)		ROD	
		Values (FRUs)	**% change**	**Values (FRUs)**	**% change**	**Values ($\times 10^{-3}$FRUs)**	**% change**	**Values ($\times 10^{-5}$ FRUs)**	**% change**
Store release	D2D0 (Control)	26.35± 4.18	------	0.132±0.008	------	1.975±0.048	------	26.16 ± 4.24	------
	D2D1	37.7 ± 2.76 P < 0.001	43%	0.17±0.012 P < 0.001	29%	1.83±0.054	-7%	12.00± 4.43 P >0.05	-54%
	D2D2	38.27±7.36 P < 0.001	45%	0.20±0.007 P < 0.001	52%	1.62±0.062	-17%	17.91±7.26 P > 0.05	-31%
	Proliferating	39.12±2.13	48.6%	0.20 ± 0.00	52%	1.8±0.08	-6.5%	26.16±4.24	-20%
SOCE	D2D0 (Control)	48.4±6.351	------	0.23±0.01	------	4.75 ± 0.175	------	93.50±7.26	------
	D2D1	57.5±10.26 P <0.05	18.5%	0.25± 0.022 P = 0.0743	8%	5.51± 0.056	16%	143.7±8.17 P < 0.05	53%
	D2D2	58.7 ± 8.61 P <0.05	21%	0.34±0.013 P < 0.001	48%	5.38 ± 0.11	13%	150.1±10.8 P < 0.05	60%
	Proliferating	57.43±0.19	18.5 %	0.20± 0.008	13%	6.079±0.146	27%	170.1±0.91	81%

Table 8.4 Summary of quantifications of Ca^{2+} store release and SOCE responses in hTERT RPE-1cells with serum add-back

The total response (area under the peak, AUP), maximal response (the height of peak, HOP), rate of rise (ROR) and rate of decline (ROD) for TG and $CaCl_2$ responses from calibrated fluorescence traces were calculated using Excel functions in a template spread sheet (Methodology chapter 2.8, figure 2.10) over two days of serum add-back . Data represented as means ± SEM. FRUs (fluorescence ratio unit). For proliferating cells n = 281, for D2D0 n = 145, D2D1 n = 122 and D2D2 n = 127, N=4.

A

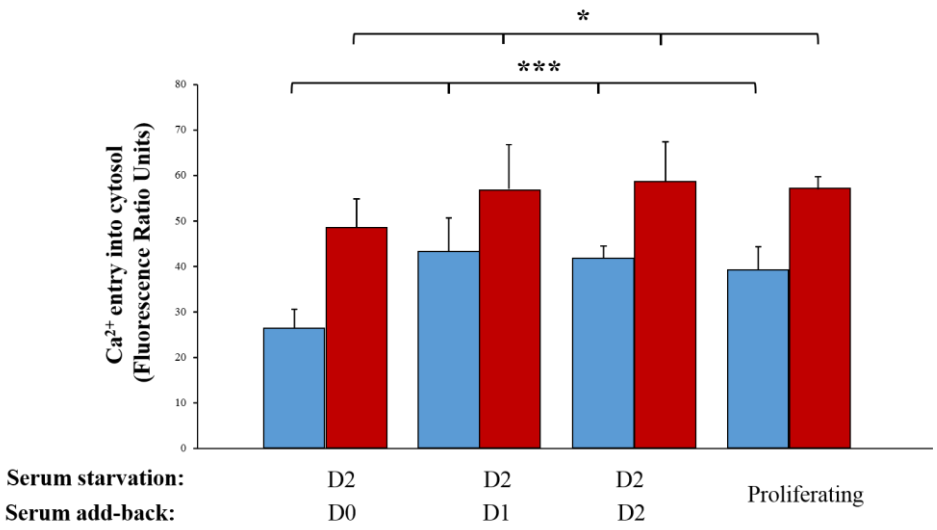

B

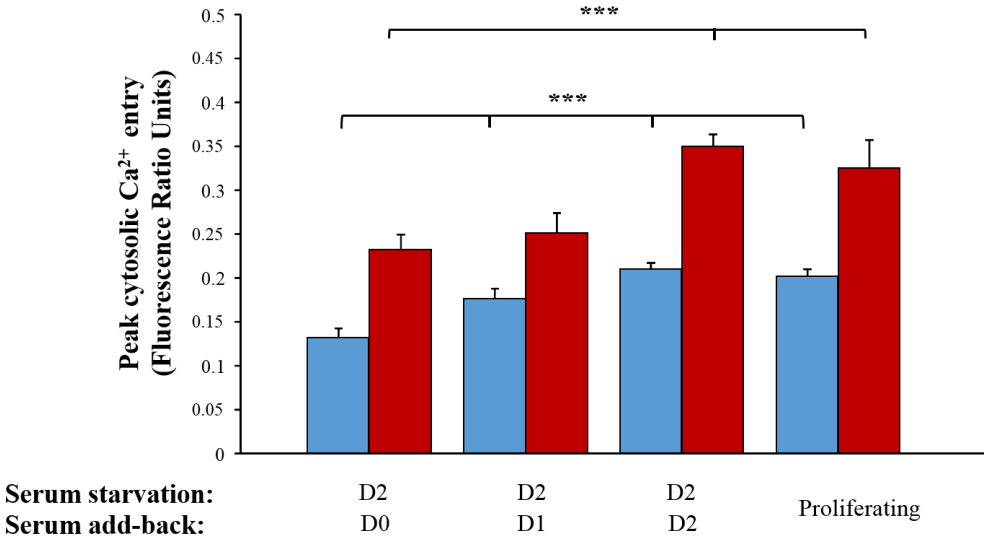

Figure 8.6 Ca^{2+} responses were restored with serum add-back in hTERT RPE-1 cells

hTERT RPE-1 cells were grown in 10% FCS medium (proliferating) or 0.1% FCS medium for 2 days (D2). After 2 days, serum was added back to starved cells (D2); both proliferating and D2 cells were growing in 10% FCS medium for further 2 days. **A)** Graph shows means of total Ca^{2+} entry into the cytosol following Ca^{2+} store release in response to stimulation with 200nM thapsigargin (TG) and subsequent SOCE following the addition of

2mM $CaCl_2$. Changes in fluorescence ratio units (FRUs) reflect changes in $[Ca^{2+}]_i$. Total Ca^{2+} store release was significantly increased in D2D1 and D2D2 cells by ~ 45% and ~ 43%compared to D2D0, all P < 0.001***. SOCE were significantly reduced in D2D2 cells by ~ 26.5% compared to D2D0, P <0.05*. Both total Ca^{2+} store release and SOCE were restored with serum add-back compared to proliferating. **B)** Graph shows means of maximal Ca^{2+} store release and maximal SOCE. Maximal Ca^{2+} store release was significantly increased from first day of serum add-back time course compared to D2D0 (control starved cells), P<0.001***. Whilst maximal SOCE was significantly increased from second day of serum add-back time course, P<0.001***. Error bars represent S.E.M. For proliferating cells n = 281, for D2D0 n = 145, D2D1 n = 122 and D2D2 n = 127, N=4.

8.3 Discussion

Serum starvation-induced cell cycle arrest in G0/G1 in HeLa and NIH 3T3 cells was observed to be associated with an uncoupling and a down regulation of Ca^{2+} store release and SOCE. G0/G1 cells were induced to re-enter the cell cycle by serum add-back and restored the proliferating percentage of G0 cells in both HeLa and NIH 3T3 cells. In contrast, in hTERT RPE-1 cells, serum starvation did not induce cell cycle arrest in G0/G1 phase (Section 3.3.3), however, a slight down regulation of Ca^{2+} store release and SOCE were observed (Section 4.2.3). The aim of the work presented in this chapter was to identify the Ca^{2+} signalling changes with cell cycle re-entry in HeLa and NIH 3T3 cells and to determine the effect of serum add-back on Ca^{2+} signalling in serum starved hTERT RPE-1 cells, allowing a subsequent comparison to HeLa and NIH 3T3 in order to determine the extent of contribution of cell cycle re-entry to the observed Ca^{2+} signalling changes.

The results show that Ca^{2+} store release and SOCE in HeLa cells were not restored from G0/G1 levels to the proliferating levels with cell cycle re-entry even with the extension of serum add-back for one more day after full restoration of proliferating percentage of G0 cells. (Figure 8.2). This result indicates that HeLa cells might not need Ca^{2+} or need very low level of Ca^{2+} entry to re-enter cell cycle and resume proliferation. SOCE, possibly, was not restored as a result of non-restoration of Ca^{2+} store release or it might be an underlying molecular mechanisms cause non restoration of SOCE, therefore, STIM1 and Orai1 proteins will be investigated with cell cycle re-entry in the next chapter.

Non-restoration of Ca^{2+} store release suggests that an irreversible change in the capacity of the Ca^{2+} store or in sensitivity to TG occurred with cell cycle arrested in G0/G1 phase or they might need a longer duration of serum add-back to be restored.

It is noteworthy that there was a significant uncoupling between Ca^{2+} store release and SOCE with a down-regulation of SOCE at day two (D4D2) of serum add-back compared to G0/G1 cells (D4D0) in HeLa cells that might be explained by the observation that there was a significant increase in number of cells in S to G2/M transition (Chapter 7) at which the SOCE is known to be down-regulated and uncoupled to Ca^{2+} store release (Chen *et al.*, 2016).

Compared to HeLa cells, Ca^{2+} signalling responses with cell cycle re-entry were different in NIH 3T3 cells, both Ca^{2+} store release and SOCE were coupled and restored from G0/G1 levels to the proliferating levels after one day of serum add-back. This result reveals an extensive association between cell cycle progression and SOCE in NIH 3T3 cells. A similar result was observed in RBL cells, where cell cycle re-entry was associated with restoration of the reduction in I_{CRAC} occurred following cell cycle block in G0/G1 phase by serum-free treatment (Bodding, 2001).

Ca^{2+} signals are known to play a major role in cell cycle progression and cell proliferation. Previous studies have clearly shown that SOCE controls cell growth and proliferation in several cell types. For example, SOCE down-regulation reduced cell proliferation in non-small cell lung adenocarcinoma cells (Ay *et al.*, 2015), FSH-stimulated ovarian cancer cells (Tao *et al.*, 2013) and human metastatic melanoma cell lines (Umemura *et al.*, 2014).

However, in other cell types, blocking SOCE by knocking down STIM1 has no effect on cell proliferation in human metastatic renal cellular carcinoma (Dragoni *et al.*, 2014), human umbilical vein endothelial cells (HUVEC) (Antigny *et al.*, 2012), HEK293 cells (El Boustany *et al.*, 2010), human myoblasts (Darbellay *et al.*, 2009), as well as vascular smooth muscle cells (Li *et al.*, 2008).

In addition, it has been previously demonstrated that the degree of cellular transformation determines the requirement for extracellular Ca^{2+} for cell proliferation (Boynton, 1988; Whitfield, 1992; Capiod, 2013).

Further evidence consistent with the progression of cell cycle without restoration of SOCE is that HeLa cells have been shown to be insensitive to external Ca^{2+} and proliferate normally in the absence of external Ca^{2+} and subsequently with no Ca^{2+} entry for at least three days with no decrease in cell viability (Borowiec *et al.*, 2014) and this also was observed in HEK293 cells and human hepatoma cell line Huh-7 (Borowiec *et al.*, 2014) in addition to transformed human fibroblasts (Boynton *et al.*, 1977; Takuwa *et al.*, 1993). Taken together, these results imply an uncoupling between cell proliferation and Ca^{2+} entry in cancer HeLa cells whilst in precancerous NIH 3T3 cells they are coupled.

In hTERT RPE-1 cells, there was an up-regulation of Ca^{2+} store release and SOCE by 43% and 18.5% respectively after one day serum add-back which restored the normal levels of Ca^{2+} response indicating that the down- regulation observed with serum starvation was reversible.

The observed up-regulation and restoration of SOCE in NIH 3T3 cells could not be a direct effect of serum add-back : Firstly, SOCE in HeLa cells was not restored with serum add-back; Secondly, the extension of the up-regulation of SOCE (50%) with cell cycle re-entry in NIH 3T3 cells was far higher than that with serum add-back in hTERT RPE-1 cells (18.5%) showing that there is a greater contribution of cell cycle re-entry in up-regulation of SOCE in NIH 3T3 cells.

It is important to remark that, in NIH 3T3 cells, SOCE was fully restored after one day of serum add-back before the full restoration of the proliferating percentage of G0 cells which was restored after two days of serum add-back (Figure 7.12) suggesting that SOCE might be involved in triggering cell cycle re-entry in these cells.

The difference in Ca^{2+} responses to cell cycle re-entry between HeLa and NIH3T3 cells suggests that there may be underlying differences in the expression of SOCE proteins. Therefore expression of the SOCE proteins STIM1 and Orai1 were investigated with cell cycle re-entry (Chapter 9) to determine any changes in expression that may underlie the observed changes in SOCE.

8.4 Conclusions

- In HeLa cells, SOCE was not restored with cell cycle re-entry suggesting that SOCE has no role in HeLa cells proliferation.
- Compared to hTERT RPE-1 cells, the restoration of SOCE with serum add-back in NIH 3T3 cells could strongly be associated to cell cycle re-entry.
- In NIH 3T3 cells, SOCE was fully restored after one day of serum add-back preceding the full restoration cell cycle progression suggesting that SOCE might have a role in resuming cell cycle progression and cell proliferation.

Chapter 9 Store-Operated Ca^{2+} Entry Proteins

9.1 Introduction

In the present study, cell cycle arrest in G0/G1 phase in HeLa and NIH 3T3 cells was associated with an uncoupling and down regulation of Ca^{2+} store release and SOCE and a significant down-regulation of SOCE proteins STIM1and Orai1. In the previous chapter, results showed that Ca^{2+} store release and SOCE were restored in NIH 3T3 cells with cell cycle re-entry but not in HeLa cells. In hTERT RPE-1 cells, serum starvation induced a down regulation of Ca^{2+} store release and SOCE and a slight down-regulation of SOCE protein Orai1, also, serum add-back restored the observed changes in Ca^{2+} store release and SOCE observed with serum-starvation.

This chapter aimed to investigate the expression of SOCE associated proteins with cell cycle re-entry in HeLa and NIH 3T3 cells and with serum add-back in hTERT RPE-1 cells.

9.2 Results- STIM1 and Orai1 expression

Western blots were performed on protein extracted from HeLa, NIH 3T3, hTERT RPE-1 cells in order to determine expression levels of STIM1 and Orai1.

9.2.1 STIM1 and Orai1 expression with cell cycle re-entry in HeLa cells

SOCE was not restored in HeLa cells following three days of serum add-back (Section 4.2.1). In order to determine any changes in STIM1and Orai1 protein expression associated with this observation, HeLa cells were grown in 10% FCS medium (proliferating) or 0.1% FCS medium for four days D4D0 (G0/G1). After four days, serum was added back to D4D0; both proliferating and D4D0 cells were grown in 10% FCS medium for further three days.

STIM1 was expressed over the three day serum add-back time course in HeLa cells as determined by a band detected at 84kDa by an anti-STIM1 antibody (Figure 9.1.A). Blots were re-probed with β-actin, used as a loading control, and STIM1 was expressed as a ratio of β-actin in order to quantify changes in band intensity (Figure 9.1.B).

STIM1 protein expression was not significantly changed (i.e. remained down-regulated) over the 3-day serum add-back time course compared to D4D0 (control) cells ($P = 0.0953$) indicating that STIM1 expression is not induced with cell cycle re-entry which is consistent with the involvement of STIM1 in the process of SOCE in HeLa cells.

Orai1 was expressed over the three day serum add-back time course in HeLa cells as determined by a band detected between 37 and 50 kDa by an anti- Orai1 antibody (Figure 9.2.A). Orai1 was expressed as a ratio of β-actin, which revealed that Orai1 protein expression was increased from first day of serum add-back by ~211% compared to D4D0 (Control) and remained upregulated by ~128 % and ~207 % in D4D2 and D4D3 respectively compared to D4D0 cells ($P = 0.0043$). In D4D2, there was a drop in Orai1 expression compared to D4D1 however it was also significantly increased compared to D4D0 cells ($P < 0.01$). Interestingly, this drop in Orai1 expression coincided with the observed decrease in SOCE at day 2 of serum add-back further confirming a role of Orai1 in SOCE in HeLa cells. From the first day of serum add-back, Orai1expression was not significantly different compared to proliferating ($P > 0.999$) (Figure 9.2.B).

As previously observed in HeLa cells, Orai1 was expressed in three distinct molecular masses. Analysis of the three masses individually showed that Orai1 was expressed in a same pattern as that of whole band analysis where Orai1 expression was significantly increased from the first day of serum-add-back and remain increased in D4D3 compared to D4D0 cells ($P=0.0067$). As previously detected, in D4D2, there was a drop in Orai1 expression compared to D4D1 however it was also significantly increased compared to D4D0 cells ($P = 0.0237$). Compared to proliferating, Orai1 expression was restored with cell cycle re-entry ($P > 0.999$) (Figure 9.2.C).

These results suggest that unlike STIM1, Orai1 protein may play a role in cell cycle progression and cell proliferation in HeLa cells.

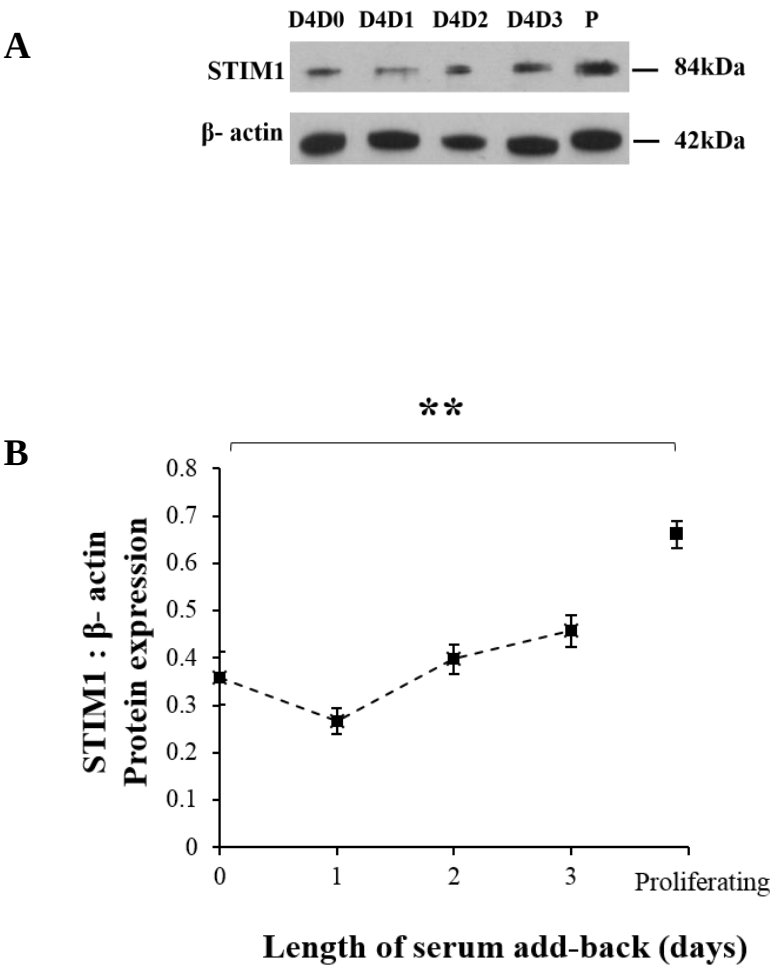

Figure 9.1 STIM1 expression was not restored with cell cycle re-entry in HeLa cells
HeLa cells were grown in 10% FCS medium (proliferating) or 0.1% FCS medium for 4 days (D4). After 4 days, serum was added back to starved cells (D4D0); both proliferating and D4 cells were grown in 10% FCS medium for further 3 days. D4D0, D4D1, D4D2, D4D3 represent four days of serum starvation followed by zero day, one day, two days and three days of serum add-back. Blots were probed with anti-STIM1 antibody which detected a band at 84 kDa or β- actin antibody which was used as a loading control and detected a band at between 42 kDa. **A**) STIM1 was expressed in all cell populations; D4D0, D4D1, D4D2, D4D3 and proliferating. **B**) Quantitative measurements of bands were performed using densitometry (ImageJ software, Methods 2.6.9) where STIM1 was expressed as a ratio of β-actin. There was no significant changes in STIM1 expression over the 3-day serum add-back. Compared to proliferating, the STIM1 expression is still significantly lower ($P = 0.0031$). N=4.

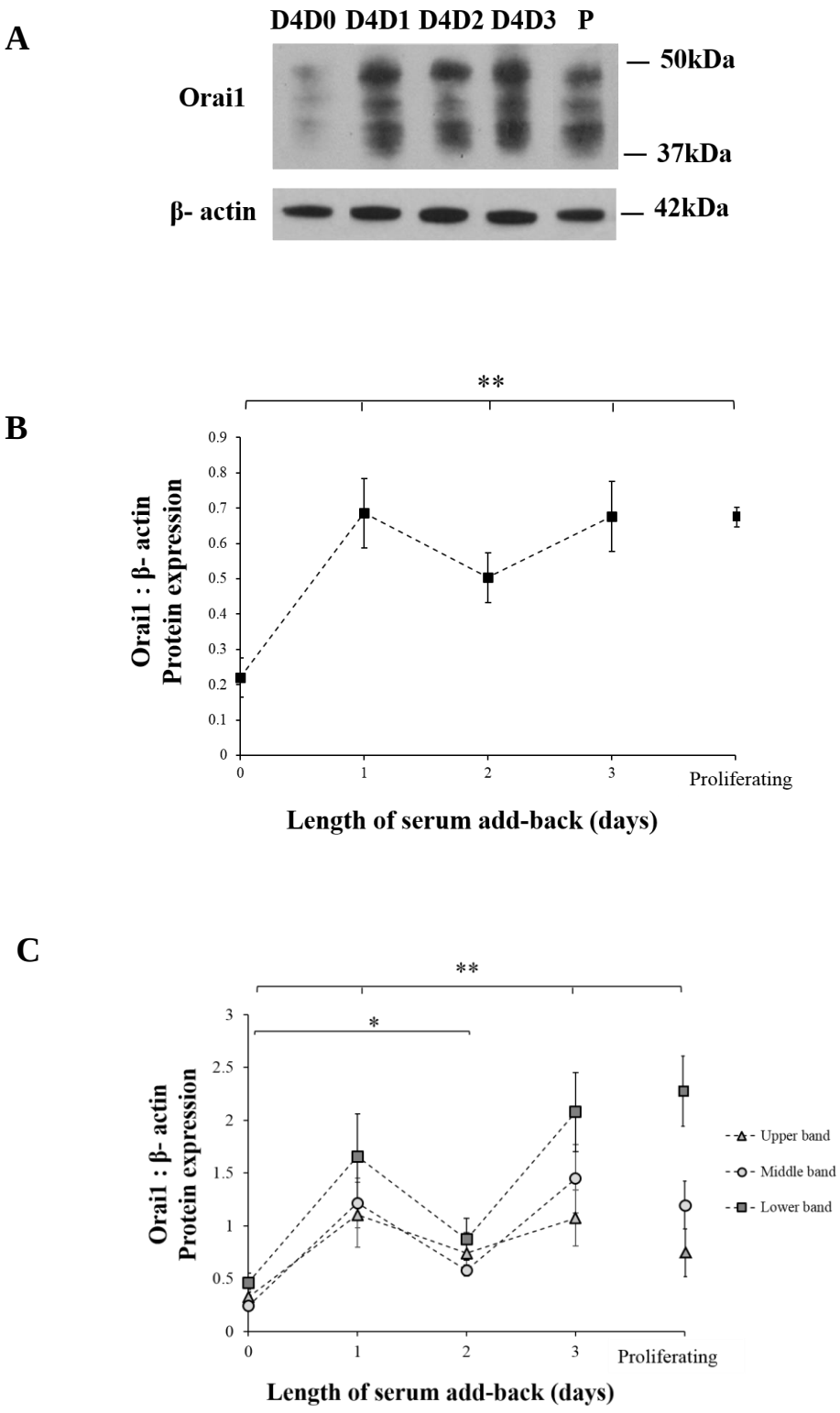

Figure 9.2 Orai1 expression was restored with cell cycle re-entry in HeLa cells

HeLa cells were grown in 10% FCS medium (proliferating) or 0.1% FCS medium for 4 days (D4). After 4 days, serum was added back to starved cells (D4); both proliferating and D4 cells were grown in 10% FCS medium for further 3 days. D4D0, D4D1, D4D2,

D4D3 represent four days of serum starvation followed by zero day, one day, two days and three days of serum add-back. Blots were probed with anti-Orai1 antibody which detected 3 bands at between 37 and 50 kDa. **A**) Orai1 was expressed in all cell populations; D4D0, D4D1, D4D2, D4D3 and proliferating. Blots were re-probed with anti-β-actin antibody (42kDa), used as a loading control. **B**) Quantitative measurements of bands were performed using densitometry (ImageJ software, Methods 2.6.9) where Orai1 was expressed as a ratio of β-actin. From first day, there was a significant increase in Orai1 expression by ~211% compared to D4D0 (Control).In D4D2 and D4D3 Orai1 expression was also increased by ~128 % and ~207 % respectively compared to D4D0 cells ($P = 0.0043$) and was not significantly different compared to proliferating($P > 0.999$). **C)** Quantitative analysis of upper, middle and lower Orai1 bands. Orai1 expression showed the same pattern as that of whole band analysis (B). Orai1 expression was significantly increased from the first day of serum-add-back and remain increased in D4D3 compared to D4D0 cells (P=0.0067**). In D4D2, there was a drop in Orai1 expression compared to D4D1 however it was also significantly increased compared to D4D0 cells ($P = 0.0237$*). Compared to proliferating, Orai1 expression was restored with cell cycle re-entry ($P > 0.999$). N=4.

9.2.2 STIM1 and Orai1 expression with cell cycle re-entry in NIH 3T3 cells

NIH 3T3 cells were grown in 10% FCS medium (proliferating) or 0.1% FCS medium for 2 days (D2D0) After 2 days, serum was added back to D2D0 cells for 2 days (D2D2).

STIM1 was expressed over the two day serum add-back time course in NIH 3T3 cells as determined by a band detected at 84kDa by an anti-STIM1 antibody (Figure 9.3.A). In contrast to HeLa cells, STIM1 protein expression was significantly increased by ~ 90.5% and ~ 95.5% in D2D1 and D2D2 of serum add-back time course respectively compared to D2D0 cells ($P = 0.0240$), and was not significantly different compared to proliferating ($P = 0.0835$) (Figure 9.3.B). Thus the STIM1 expression was restored with cell cycle re-entry which would likely contribute to the restored SOCE observed in NIH 3T3 cells with cell cycle re-entry and suggest again that STIM1 is involved in the process of SOCE in NIH 3T3 cells.

Similarly, Orai1 was expressed over the two day serum add-back time course in NIH 3T3 cells as determined by a double band detected between 37 and 50 kDa by an anti- Orai1 antibody (Figure 9.4.A). Blots were re-probed with β-actin, used as a loading control, and Orai1 was expressed as a ratio of β-actin which showed that Orai1 protein expression was significantly increased by ~73.5% and ~83% in D2D1 and D2D2 of serum add-back time course respectively compared to D2D0 cells ($P = 0.0062$), and was not significantly different compared to proliferating ($P > 0.999$) (Figure 9.4.B). These results are consistent with a role of Orai1 in SOCE and cell cycle progression.

As observed previously, Orai1 was expressed in a double band in NIH 3T3 cells. The upper and lower Orai1 band (Figure 5.4.C) were analysed individually. The upper band showed a significant increase in Orai1expression in D2D1 and D2D2 cells by ~195.5% and ~194% compared to proliferating ($P < 0.01$) whereas the lower band showed no significant difference in Orai1 expression in over the two day serum add-back time course compared to D2D0 cells ($P=0.0784$). This would again confirm that Orai1exists in two different states in NIH 3T3 cells.

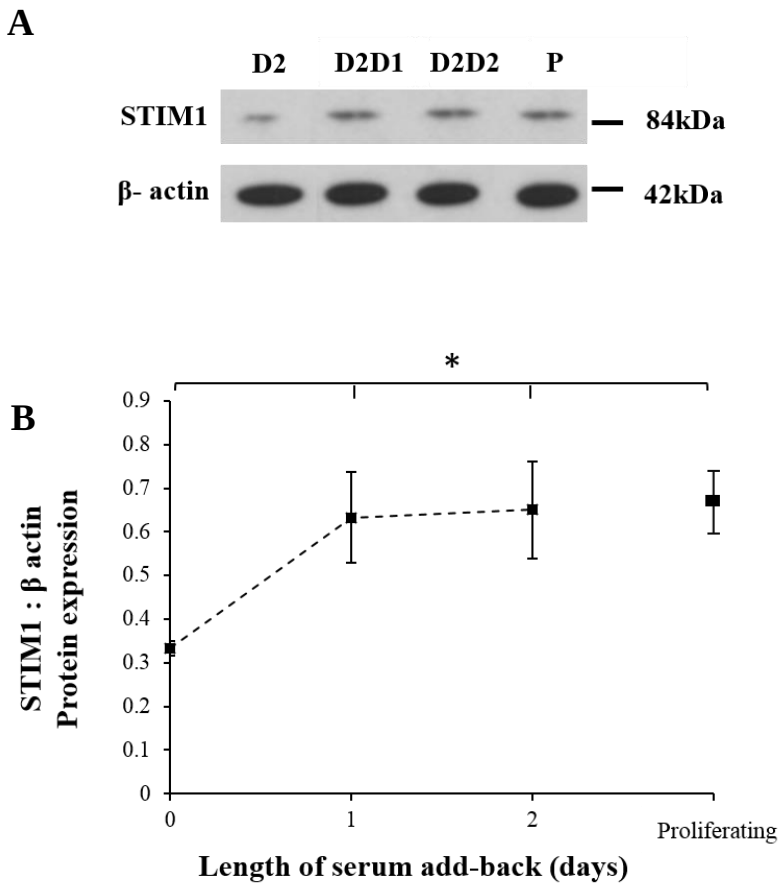

Figure 9.3 STIM1 expression was restored with cell cycle re-entry in NIH 3T3 cells
NIH 3T3 cells were grown in 10% FCS medium (proliferating) or 0.1% FCS medium (G0/G1) for 2 days. Blots were probed with anti-STIM1 antibody which detected a band at 84 kDa or β- actin antibody which was used as a loading control and detected a band at 42 kDa. **A**) STIM1 was expressed in all cell populations; D2D0, D2D1, D2D2 and proliferating. **B**) Quantitative measurements of bands were performed using densitometry (ImageJ software, Methods 2.6.9) where STIM1 was expressed as a ratio of β-actin. From first day, there was a significant increase in STIM1 expression by ~90.5% compared to D2D0 (Control) ($P = 0.0240$) and was not significantly different compared to proliferating ($P = 0.0853$). $N = 3$.

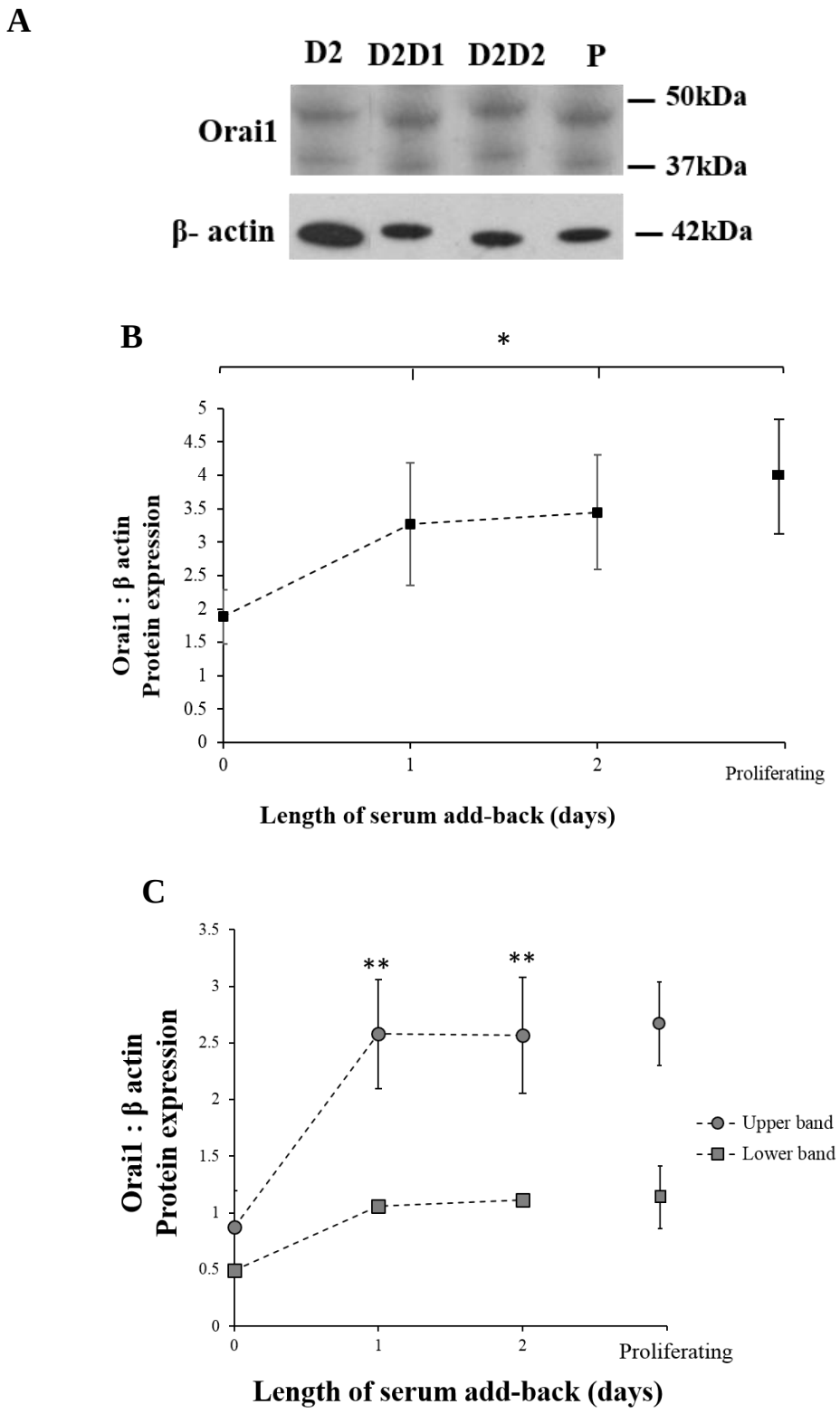

Figure 9.4 Orai1 expression was restored with cell cycle re-entry in NIH 3T3 cells

Western blots were performed on protein extracted from NIH 3T3 cells following growing for 2 days in 10% FCS (proliferating = P) or 0.1% FCS (G0/G1). Blots were probed with anti-Orai1 antibody which detected a band between 37 and 50 kDa or β- actin antibody

which was used as a loading control and detected a band at 42 kDa. **A**) Orai1 was expressed in all cell populations; D2D0, D2D1, D2D2 and proliferating. **B**) Quantitative measurements of bands were performed using densitometry (ImageJ software, Methods 2.6.9) where Orai1 was expressed as a ratio of β-actin. There was a significant increase in Orai1 expression by ~73.5% compared to D2D0 (Control) ($P = 0.0026$*) and was not significantly different compared to proliferating ($P > 0.9999$). **C)** Quantitative analysis of upper and lower Orai1 bands. Orai1 expression was significantly up-regulated in D2D1 and D2D2 cells compared to D2D0 ($P < 0.01$**). Whilst lower Orai1 bands showed no significant difference compared to D2D0 ($P=0.0784$) cells. N=3.

9.2.3 STIM1 and Orai1 expression with serum add-back in hTERT RPE-1 cells

As previously showed in chapter 5, Orai1 protein expression was slightly down-regulated with serum starvation, also, in chapter 7, SOCE changes were restored with serum add-back in hTERT RPE-1 cells. Therefore, STIM1and Orai1 protein expression was further determined with serum add-back by western blotting on protein extracted from proliferating (10% FCS), D2D0 (0.1% FCS for 2 days), D2D1 and D2D2 (0.1% FCS for 2 days and 10% FCS for 1 and 2 days respectively).

As observed previously, STIM1 protein expression showed two scenarios in D2D0 and D2D1 where most blots (N =4) showed no STIM1 expression (Figure 9.5.A) but one case showed slight STIM1 expression at a higher molecular weight as determined by a slight upward band shift detected just above 84kDa by an anti-STIM1 antibody (Figure 9.5.B). However in all blots of D2D2 and proliferating cells STIM1 was not expressed (Figure 9.5.A and B).

Orai1 was expressed over the two day serum add-back time course in hTERT RPE-1 cells as determined by a double band detected between 37 and 50 kDa by an anti-Orai1 antibody (Figure 9.6.A). Orai1 protein expression as a ratio of β-actin was increased by ~8.5% and ~17 % in D2D1 and D2D2 of serum add-back time course respectively compared to D2D0 cells, however this increase was not significant (P = 0.0841) (Figure 9.6.B).

As seen before, Orai1 expression showed a double band in proliferating and over serum add-back time course. The upper and lower Orai1 bands (Figure 9.6.C) were analysed individually. This showed the same pattern as that of whole band analysis where there was no significant different in Orai1 expression inD2D1 and D2D2 compared to D2D0.

Orai1 expression level in D2D2 was similar to that of proliferating cells indicating that Orai1 expression reverts to the proliferating level with serum add-back which could contribute to observed restoration of SOCE. In addition, the extent of SOCE up-regulation was ~21% in D2D2 of a serum add-back time course (Figure 8.6.A). The changes observed in SOCE are similar to those seen in Orai1 expression and further suggest that Orai1 is involved in the process of SOCE in hTERT RPE-1 cells.

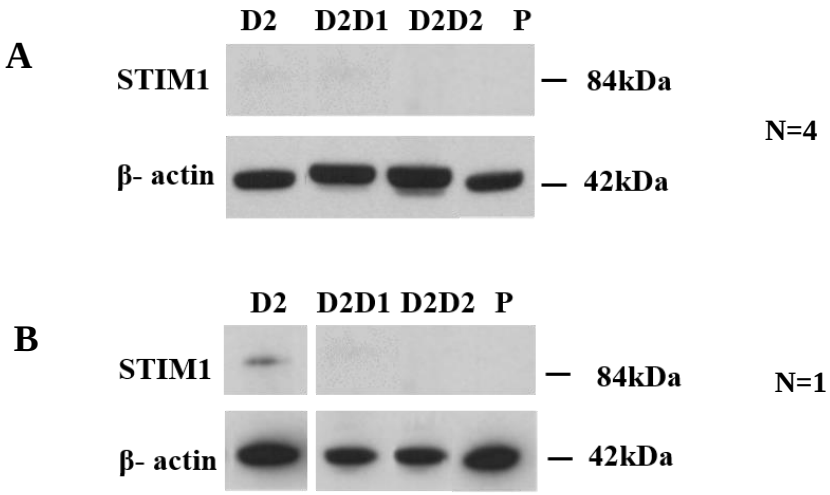

Figure 9.5 STIM1 expression with serum add-back in hTERT RPE-1 cells

Western blots were performed on protein extracted from hTERT RPE-1 cells following growing in 10% FCS (proliferating = P) or 0.1% FCS for 2 days (D2) and for 4 days (D4). Blots were probed with anti-STIM1 antibody which detected a band at 84 kDa or β- actin antibody which was used as a loading control and detected a band at 42 kDa. **A**) STIM1 expression was not detected in D2D0, D2D1, D2D2 and proliferating (P) cells **B)** STIM1 expression was not detected in D2D2 and proliferating (P) while there was a very low STIM1 expression in D2D0 and D2D1. N=5.

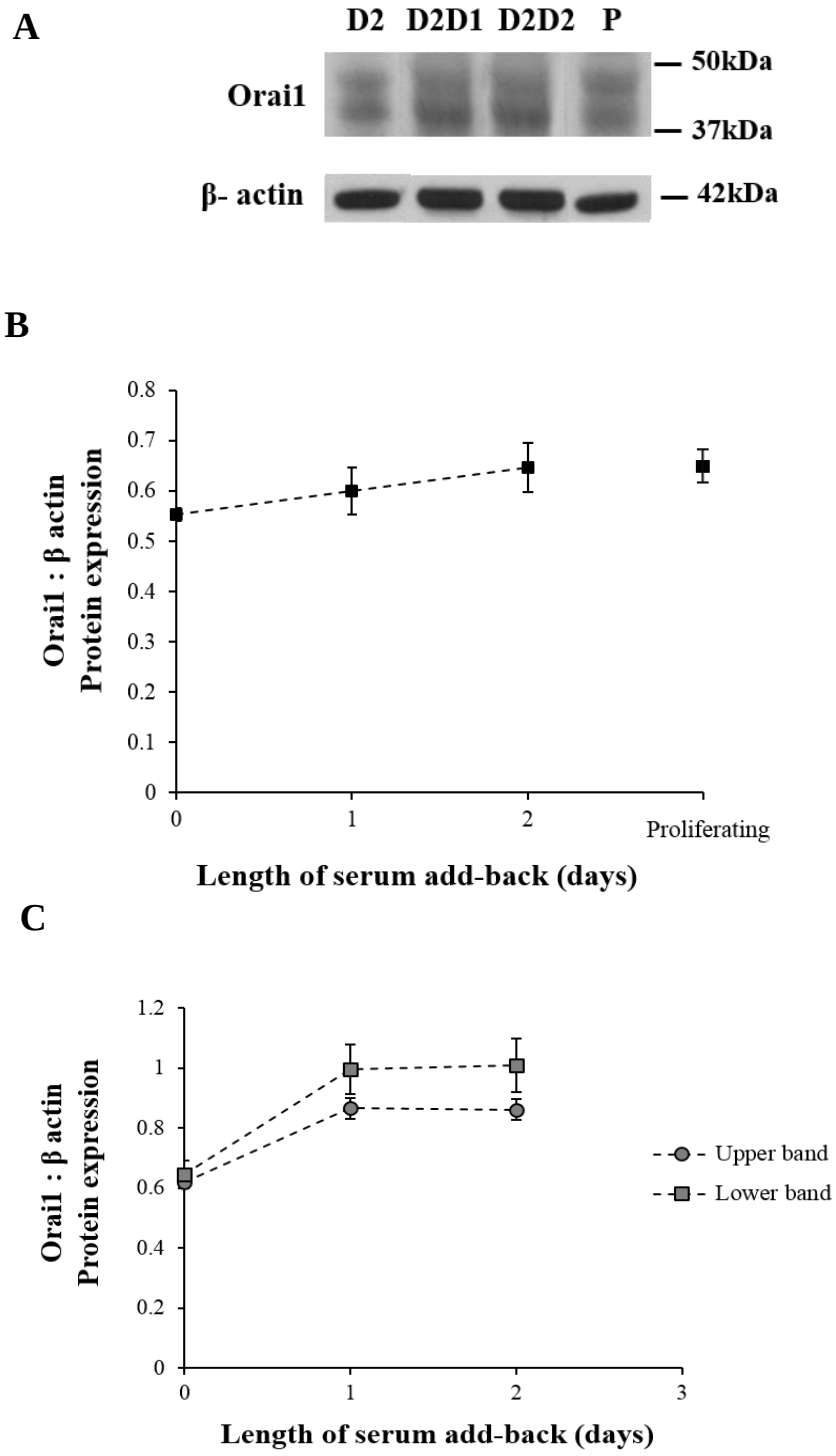

Figure 9.6 Orai1 expression with serum add-back in hTERT RPE-1 cells

Western blots were performed on protein extracted from hTERT RPE-1 cells following growing in 10% FCS (proliferating = P) or 0.1% FCS for 2 days (D2) and for 4 days (D4). Blots were probed with anti-Orai1 antibody which detected a band between 37 and 50 kDa or β- actin antibody which was used as a loading control and detected a band at 42 kDa. **A**) Orai1 was expressed in all cell populations; D2D0, D2D1, D2D2 and proliferating. **B**)

Quantitative measurements of bands were performed using densitometry (ImageJ software, Methods 2.6.9) where Orai1 was expressed as a ratio of β-actin. There was an increase in Orai1 expression in D2D1 and D2D2 cells compared to D2D0, however this increase was not significant. ($P > 0.05$). **C)** Quantitative analysis of upper and lower Orai1 bands. Orai1 expression showed the same pattern as that of whole band analysis (B). There was no significant differences in Orai1 expression in D2D1 and D2D2 cells compared to D2D0 ($P > 0.05$). N=4.

9.3 Results- STIM1 and Orai1 localisation

Localisation of SOCE proteins were also investigated with serum-back in the 3 cell types, HeLa, NIH 3T3 and hTERT RPE-1 cells by immunofluorescent analysis. Fixed cells were stained with either anti-STIM1 primary antibody or anti-Orai1 primary antibody followed by Alexa Fluor 647 secondary antibody or Alexa Fluor 488 secondary antibody respectively. Cells then were examined and images were taken by laser scanning confocal microscopy using an x63 objective (Method 2.7).

9.3.1 STIM1 and Orai1 localisation with cell cycle re-entry in HeLa cells

There was widespread expression of STIM1 throughout the cytoplasm in both D4D0 and D4D3 cells however, there was a clear evidence of localisation into foci near cell membrane (Figure 9.7.A) in D4D3 cells that was not observed in D4D0 cells (Figure 9.7.A and B.).

The overall intensity of fluorescence of STIM1 was not different in D4D3 cells compared to D4D0 (Figure 9.7.B) consistent with the extent of expression (Section 9.2.1). Though there was restoration of localisation of STIM1 with cell cycle re-entry, the STIM1 expression was not restored which might explain the observed non restoration of SOCE in HeLa cells (Section 8.2.1).i.e. although localisation changed by D4D3, overall levels remain too low to restore SOCE

Orai1 was also expressed throughout the cytoplasm and nuclei of D4D0 and D4D3 cells with some examples of clustering in the nucleus in D4D3 cells (Figure 9.8.A and B). These clusters were not observed in D4D0 indicating that Orai1 expression was altered with cell cycle re-entry. In addition, these clusters were previously observed in proliferating cells (Figure 5.8).

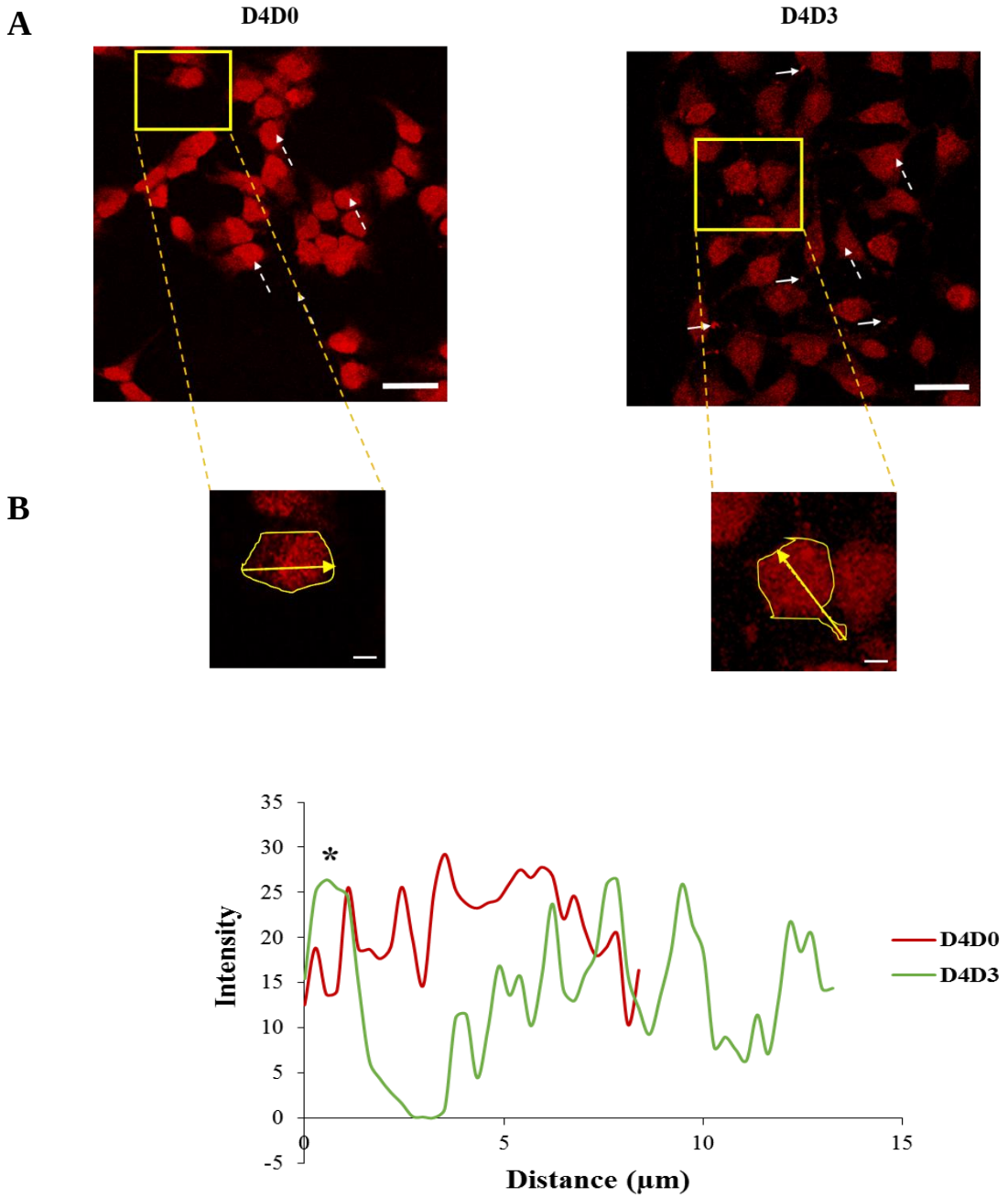

Figure 9.7 Restoration of STIM1 expression profile with cell cycle re-entry in HeLa cells

HeLa cells were grown in 10% FCS medium (proliferating) or 0.1% FCS medium for 4 days (D4). After 4 days, serum was added back to starved cells for 3 days (D4D3). Cells were stained with anti-STIM1 primary antibody followed by Alexa Fluor 647 secondary antibody. **A)** Images were captured using laser scanning confocal microscopy. In D4D0 cells**,** STIM1 was present throughout the cell however, the level of expression is higher in the cell nuclei (dashed arrows) with no apparent areas of clustering. In D4D3 cells, STIM1

was present throughout the cell and there was high occurrence STIM1 localisation into foci at the cell membrane (solid arrows). **B)** A line scan analysis of D4D0 and D4D3 cells. The path was done in a single cell through the longest axis (yellow arrow) to track the STIM1 expression profile. The line scan of D4D0 cell (red line) shows no focus localisation of STIM1 with clear high STIM1 expression in the cell nucleus. The line scan of D4D3 cell (green line) shows restoration of focus localisation of STIM1 (*) at cell membrane. Scale bars represent 10 μm. Images are representative of >10 images and were taken using an x63 objective. N=3.

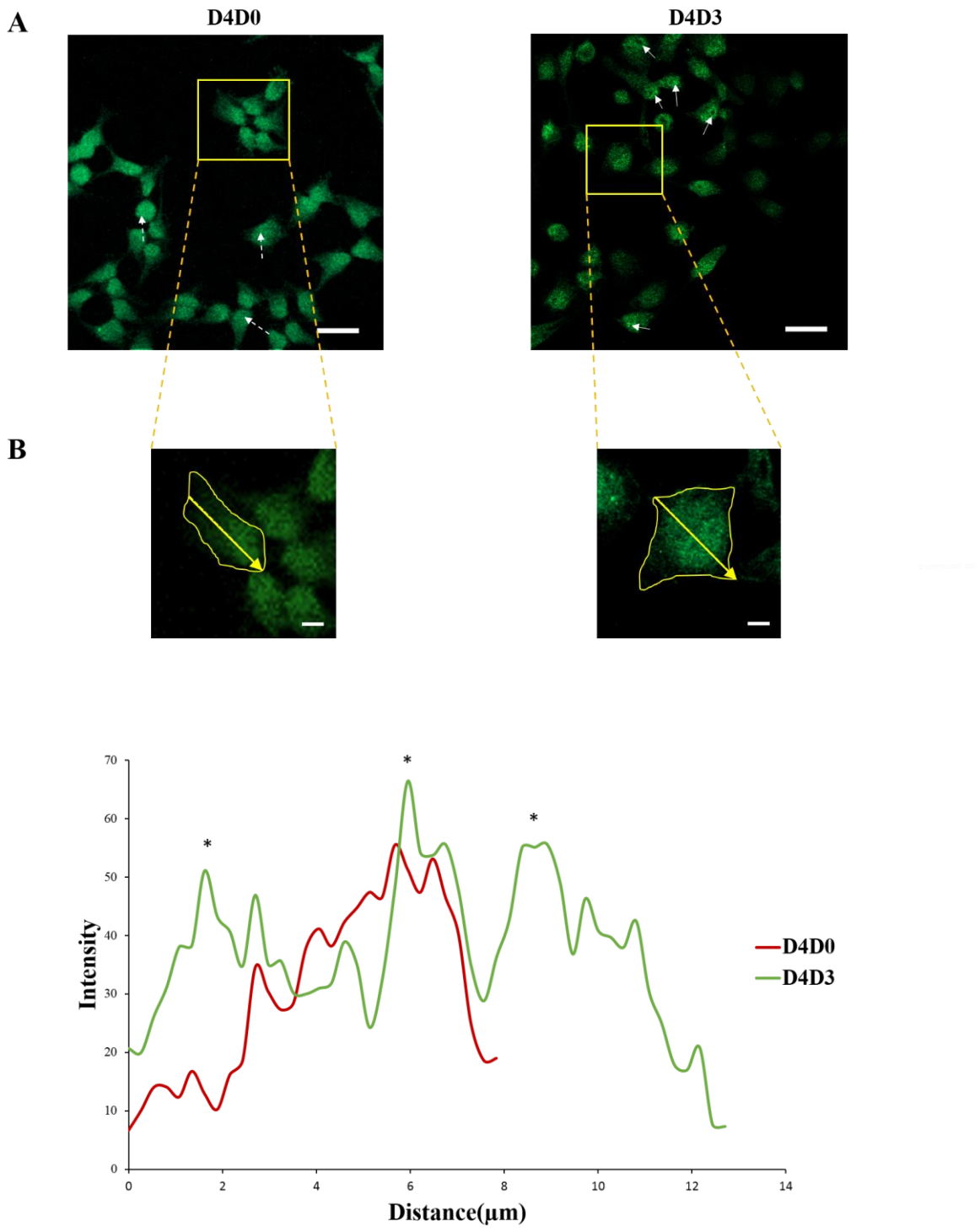

Figure 9.8 Restoration of Orai1 expression profile with cell cycle re-entry in HeLa cells

HeLa cells were grown in 10% FCS medium (proliferating) or 0.1% FCS medium for 4 days (D4). After 4 days, serum was added back to starved cells for 3 days (D4D3). Cells were stained with anti-Orai1 primary antibody followed by Alexa Fluor 488 secondary antibody. **A)** Images were captured using laser scanning confocal microscopy. In D4D0

cells, Orai1 was present throughout the cell however, the level of expression is almost diffuse in the cell nuclei (dashed arrows) with no apparent areas of clustering. In D4D3 cells, Orai1 was present throughout the cell and there was some examples of Orai1 clustering in the cell nuclei (solid arrows). **B)** A line scan analysis of D4D0 and D4D3 cells. The path was done in a single cell through an axis (yellow arrow) to track the Orai1 expression profile. The line scan of D4D0 cell (red line) shows no clustering of Orai1 in the cell nucleus. The line scan of D4D3 cell (green line) shows some Oria1 clustering in the nuclei (*). Scale bars represent 10 μm. Images are representative of >15 images and were taken using an x63 objective. N=3.

9.3.2 STIM1 and Orai1 localisation with cell cycle re-entry in NIH 3T3 cells

Similar to HeLa cells, STIM1 was expressed throughout the cytoplasm in both D2D0 and D2D2 cells. In D2D2, STIM1 showed obvious examples of localisation into foci near cell membrane (Figure 9.7) similar to that of proliferating cells (Figure 9.9.A), these foci were not observed in D4D0 cells (Figure 9.9.A and B).

As seen in STIM1, Orai1 was expressed throughout the cytoplasm and nuclei of D2D0 and D2D2 cells. Orai1 expression in D2D2 (Figure 9.10.A.B) was similar to that in proliferating cells (Figure 5.10.A) showed some localisation into clusters in cell nucleus which was not seen in D4D0 indicating that Orai1 expression was altered with cell cycle re-entry.

These results revealed that both STIM1 and Orai1 localisation were restored with cell cycle re-entry consistent with the observed restoration of its expression and with observed restoration of SOCE upon cell cycle re-entry.

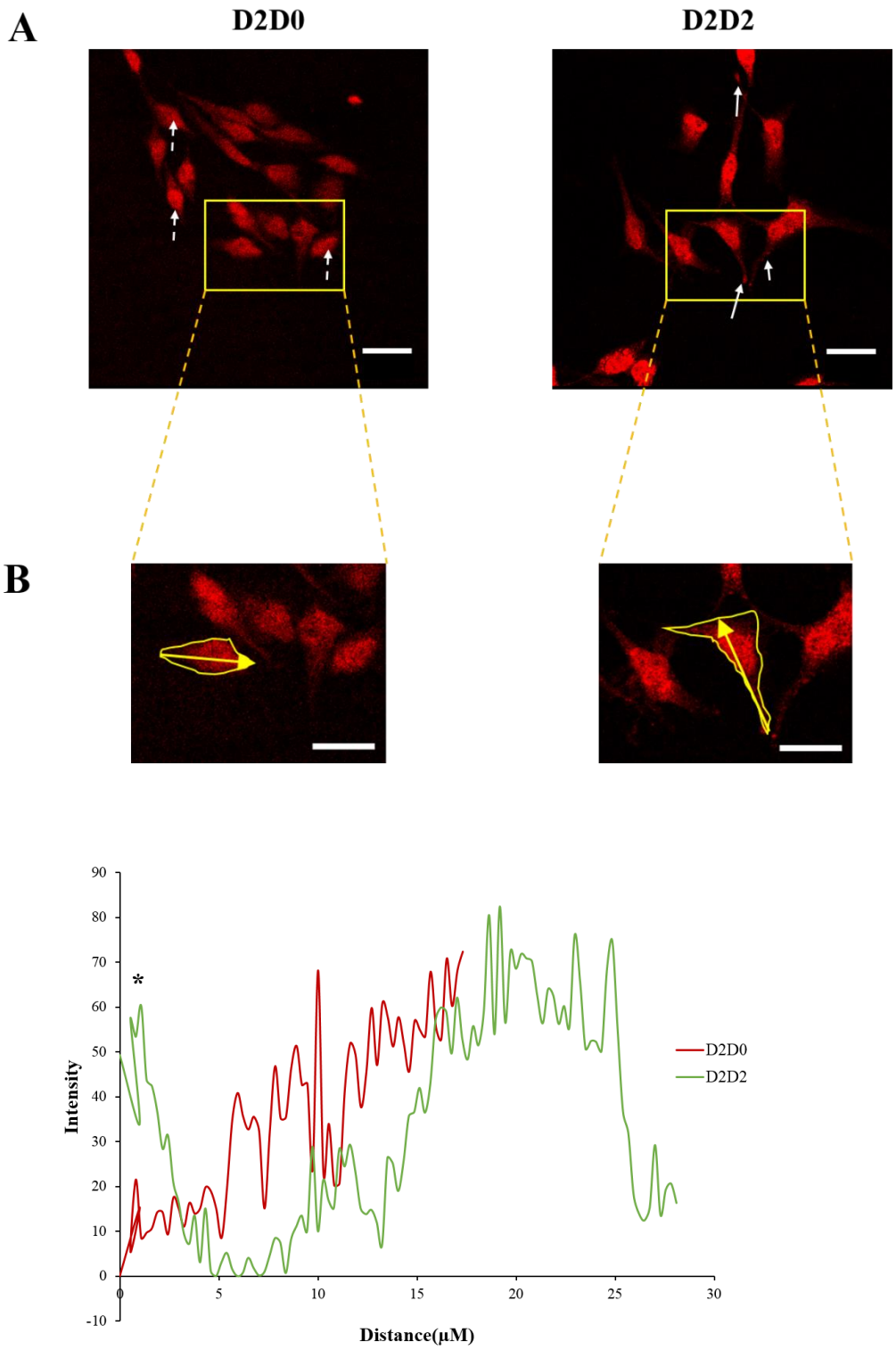

Figure 9.9 Restoration of STIM1 expression profile with cell cycle re-entry in NIH 3T3 cells

NIH 3T3 cells were grown in 10% FCS medium (proliferating) or 0.1% FCS medium for 2 days (D2D0). After 2 days, serum was added back to D2D0 cells for 2 days (D2D2). Cells were stained with anti-STIM1 primary antibody followed by Alexa Fluor 647 secondary

antibody. **A)** Images were captured using laser scanning confocal microscopy. In D2D0 cells, STIM1 was present throughout the cell however, STIM1 expression was higher in the cell nuclei (dashed arrows) with no apparent areas of clustering. In D2D2 cells, STIM1 was present throughout the cell and there was high occurrence STIM1 localisation into foci at the cell membrane (solid arrows). **B)** A line scan analysis of D4D0 and D4D3 cells. The path was done in a single cell through an axis (yellow arrow) to track the STIM1 expression profile. The line scan of D2D0 cell (red line) shows no focus localisation of STIM1. The line scan of D2D2 cell (green line) shows restoration of focus localisation of STIM1 (*) at cell membrane. Scale bars represent 10 μm. Images are representative of >12 images and were taken using an x63 objective. N=3.

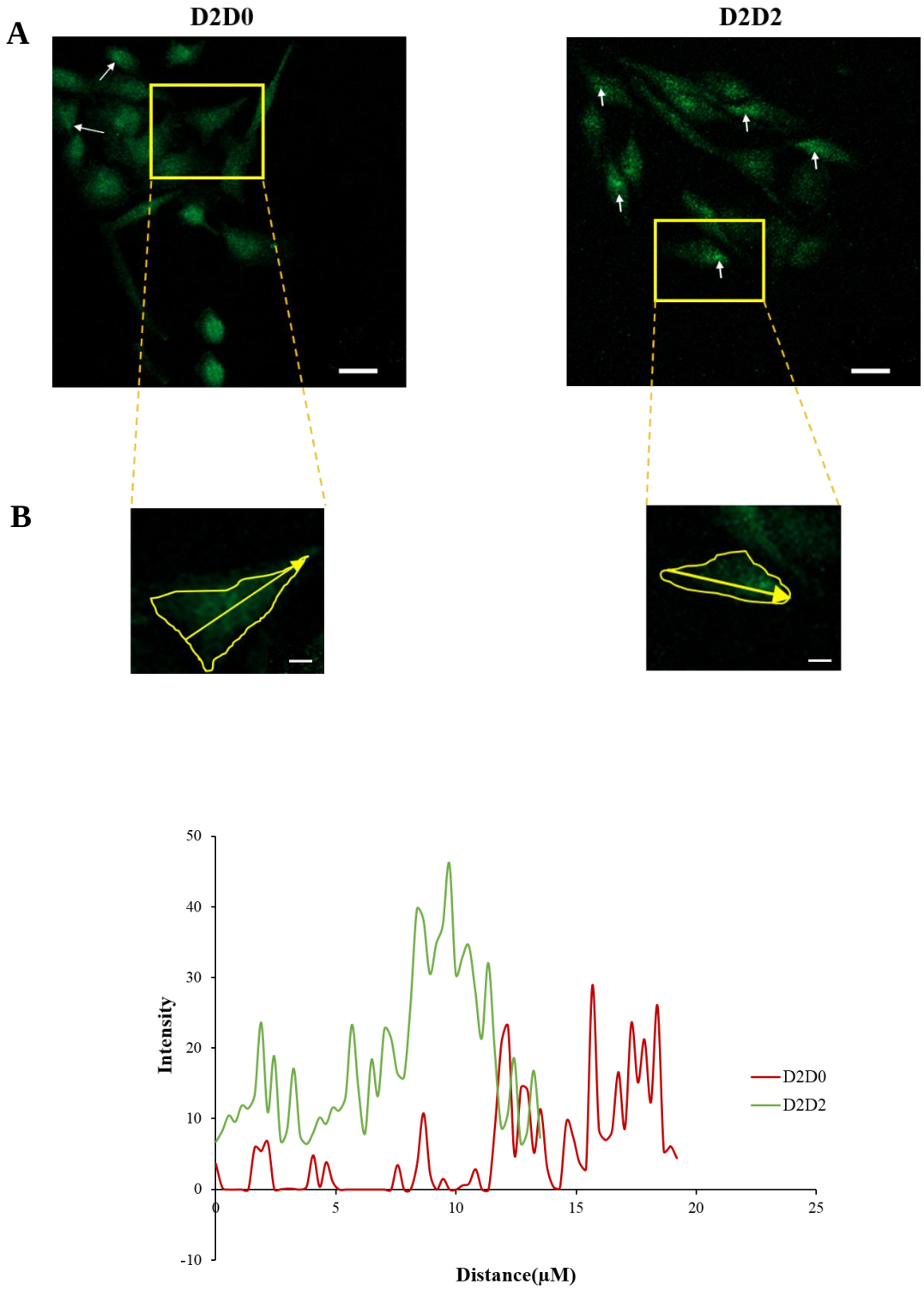

Figure 9.10 Restoration of Orai1 expression profile with cell cycle re-entry in NIH 3T3 cells

NIH 3T3 cells were grown in 10% FCS medium (proliferating) or 0.1% FCS medium for 2 days (D2D0). After 2 days, serum was added back to D2D0 cells for 2 days (D2D2). Cells

were stained with anti-Orai1 primary antibody followed by Alexa Fluor 488 secondary antibody. **A)** Images were captured using laser scanning confocal microscopy. In D2D0 cells, Orai1 was expressed throughout the cell which appear to be lower than that of D2D2 with less areas of clustering (arrows). In D2D2 cells, Orai1 was present throughout the cell and there were clear examples of Orai1 clustering in the cell nuclei (arrows). **B)** A line scan analysis of D2D0 and D2D2 cells. The path was done in a single cell through an axis (yellow arrow) to track the Orai1 expression profile. The line scan of D2D0 cell (red line) shows low Orai1 expression throughout the cell nucleus. The line scan of D2D2 cell (green line) shows high level of Orai1 expression. Scale bars represent 10 μm. Images are representative of >15 images and were taken using an x63 objective. N=4.

9.3.3 STIM1 and Orai1 localisation with serum starvation in hTERT RPE-1 cells

In this chapter, western blot results (Section 9.2.3) showed that STIM1 was not expressed in proliferating and D2D2 hTERT RPE-1 cells. In addition, STIM1 and Orai1 expression was not detected in proliferating and serum starved hTERT RPE-1 cells by immunofluorescence studies (Section 5.2.3).

Here, immunofluorescence staining was done to detect STIM1 and Orai1localisation in D2D0 and D2D2 hTERT RPE-1 cells which showed that STIM1 and Orai1 was not detected either with serum starvation or with serum add-back (Figure 9.11 B and C).

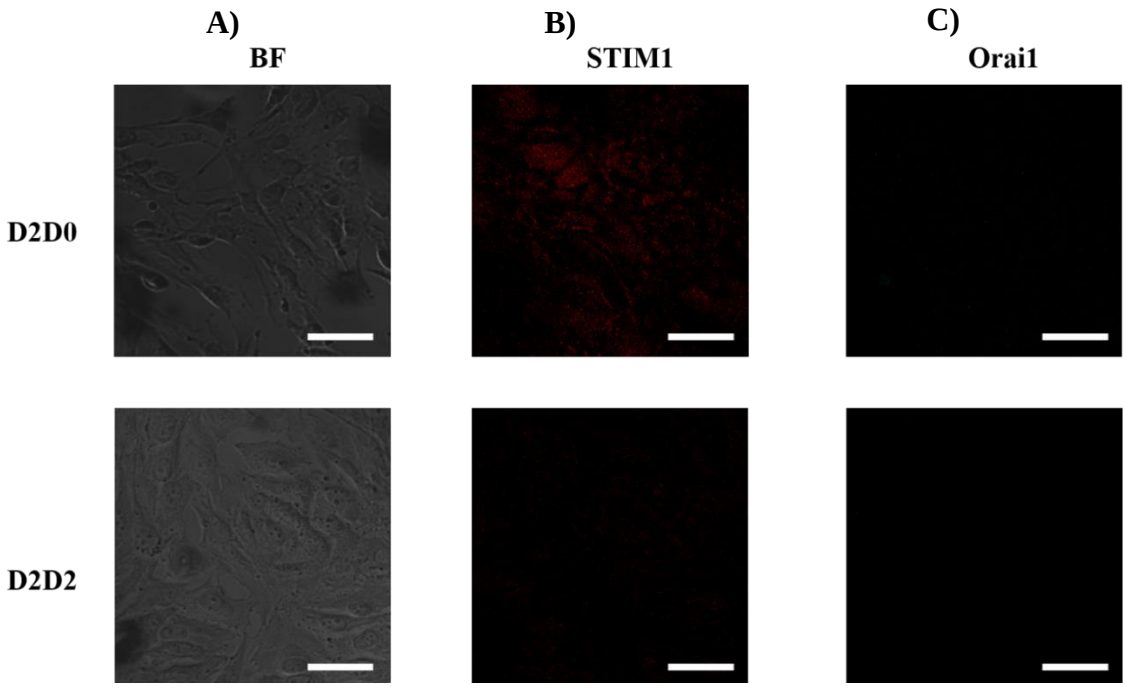

Figure 9.11 STIM1 and Orai1 expression were not detected in hTERT RPE-1 cells by immunofluorescent studies

D2D0 (0.1% FCS) cells and D2D2 (2 days 0.1% FCS followed by 2 days10% FCS) cells were stained with anti-STIM1/anti-Orai primary antibodies followed by Alexa Fluor 647 / Alexa Fluor 488 secondary antibodies respectively. Images were captured using laser scanning confocal microscopy. **A)** BF (bright field) images show healthy cells. **B and C)** STIM1 and Orai1 were not detected by immunofluorescent staining. Scale bars represent 10 μm. Images are representative of >12 images and were taken using an x63 objective. N=4.

9.4 Discussion

As previously showed, cell cycle arrest in G0/G1 phase in HeLa and NIH 3T3 cells was associated with a an uncoupling and a down regulation of Ca^{2+} store release and SOCE and a significant down-regulation of SOCE proteins; STIM1and Orai1. The reversibility of Ca^{2+} signalling with cell cycle re-entry was investigated in the previous chapter and revealed that Ca^{2+} store release and SOCE were restored in NIH 3T3 cells but not in HeLa cells. In hTERT RPE-1 cells, serum starvation did not induce cell cycle arrest however it induced a down regulation of Ca^{2+} store release and SOCE and a slight down-regulation of the SOCE protein Orai1.With serum add-back the observed down-regulation of Ca^{2+} signalling was restored.

Therefore, the aim of the work presented in this chapter was to determine the reversibility of expression of SOCE proteins with cell cycle re-entry in HeLa and NIH 3T3 cells and with serum add-back in hTERT RPE-1 cells.

Serum add-back for 3 days to G0/G1 HeLa cells did not restore the proliferating level of STIM1 expression which remained down-regulated. This is consistent with the level of SOCE in G0/G1 HeLa cells with 3-day serum add-back time course which also was not restored following treatment (Section 8.2.1). As previously discussed (Discussion 5.4), it has been demonstrated that STIM1 has a role in SOCE (Liou *et al.*, 2005; Roos *et al.*, 2005; Zhang *et al.*, 2005) and that level of STIM1 expression has been tightly associated with extent of SOCE activity in many cell types. For example, SOCE down-regulation has been shown to be induced by STIM1 knockdown in HeLa cells (Liou *et al.*, 2005), endothelial cells (Abdullaev *et al.*, 2008), in N-type SH-SY5Y cells (Bell *et al.*, 2013), endothelial progenitor cells (Kuang *et al.*, 2010), SH-SY5Y cells, HEK293 cells, Jurkat T cells and Drosophila S2 cells (Roos *et al.*, 2005), as well as vascular smooth muscle cells (Takahashi *et al.*, 2007b; Aubart *et al.*, 2009; Potier *et al.*, 2009) and adipocytes (Graham *et al.*, 2009).

These results also showed that STIM1 expression was uncoupled from cell cycle progression and cell proliferation. Indeed, knocking down of STIM1 caused dramatic reduction in SOCE with no alteration in cell proliferation in many cell types, such as human myoblasts (Darbellay *et al.*, 2009), HEK293 cells (El Boustany *et al.*, 2010), vascular smooth muscle (Li *et al.*, 2008) and human umbilical vein endothelial cells

(HUVEC) derived cell line (Antigny *et al.*, 2012). Furthermore, silencing STIM1 did not affect cell proliferation rate and cell cycle distribution while SOCE was greatly decreased in human metastatic renal cellular carcinoma (Dragoni *et al.*, 2014) and LNCaP (Dubois *et al.*, 2014).

The mechanism underlying the non-restoration of STIM1 protein expression with serum add-back is not clear. One possibility that the protein need a longer duration of serum add-back to recover or it may be irreversibly down regulated but still functioning as SOCE still operates but at much reduced levels.

Taken together, these results along with previous studies again confirm a role of STIM1 in SOCE and suggested strongly that, in several cell models, such as HeLa cells, STIM1 expression and cell proliferation are uncoupled.

In contrast to HeLa cells, proliferating level of STIM1 expression was restored in G0/G1 NIH 3T3 cells from the first day of serum add-back. This is consistent with the restoration of SOCE in G0/G1 NIH 3T3 following one day of serum add-back (Section 8.2.2). These results confirm the role and the close association of STIM1 expression and SOCE as previously discussed.

Also the restoration of STIM1 expression was coincident with the marked decrease in G0 cells percentage and cell cycle re-entry, however, the full restoration of proliferating STIM1 expression level preceded the full restoration of proliferating G0 cell percentage which occurred at day 2 of serum add-back suggesting a role of STIM1 in inducing cell cycle progression in NIH 3T3 cells. The role of STIM1 in cell cycle progression and cell proliferation has also been discussed (Discussion 5.4) where, knockdown of STIM1 significantly inhibited cell proliferation and arrested the cell cycle at the G0/G1 phase in hepatocellular carcinoma cell (Wu *et al.*, 2015), in hypopharyngeal carcinoma cells (Sun *et al.*, 2015) and in human glioblastoma cells (Li *et al.*, 2013) and results in cell cycle arrest in G1/S transition in cervical cancer SiHa cells (Chen *et al.*, 2016).

The results showed that Orai1expression increased and reverted back to its proliferating level from the first day of serum-add-back in both G0/G1 HeLa and G0/G1 NIH 3T3 cells. This finding is associated with the observed decrease in percentage of G0 cells and cell cycle re-entry and preceded the full restoration of proliferating level of G0 cells (Section 7.2.1) suggesting an increased expression of Orai1 might possibly drive G0/G1 HeLa and G0/G1 NIH 3T3 cells toward cell cycle re-entry and proliferation.

This result is consistent with a previous study where Orai1 overexpression induced a significant increase in cell proliferation rate in HEK293 and HeLa cells (Borowiec *et al.*, 2014).

Consistent with the above results, previous studies have demonstrated that Orai1 knockdown results in cell cycle arrest in G1/S transition in cervical cancer SiHa cells (Chen *et al.*, 2016), in G0/G1 phase in ARPE-19 cells (Yang *et al.*, 2013), induced differentiation and cell cycle arrest in G0 like phase of N-type neuroblastoma cells (Bell *et al.*, 2013) and that cell cycle block in HEK293 cells induced by SOCE inhibition was associated with Orai1 protein (Borowiec *et al.*, 2014). Furthermore, Orai1 knockdown caused a dramatic decrease in proliferation rate of in HEK293 cells (El Boustany *et al.*, 2010), vascular smooth muscle cells (Potier *et al.*, 2009) and endothelial cells (Abdullaev *et al.*, 2008).

It is worth mentioning that the observed up-regulation and restoration of Orai1 expression in NIH 3T3 cells with cell cycle re-entry was accompanied by a restoration of SOCE consistent with the involvement of this protein in the SOCE pathway as previously discussed (discussion 5.4). However, in HeLa cells, the observed up-regulation and restoration of Orai1 expression with cell cycle re-entry was not accompanied by restoration of SOCE which could be explained by the observation that STIM1 expression was not restored and remained down-regulated.

These results suggest that unlike STIM1, the up-regulation in Orai1 may be directly involved in the induction of cell cycle progression and cell proliferation that is observed following serum add-back.

In hTERT RPE-1 cells, similar to the previous findings (Section 5.2.3), STIM1expression was not detected in D2D2 and proliferating and most of D2D0 and D2D1 cases by western blot and in all conditions by immunofluorescence studies. Possibly, the number of cells and/or the level of expression is presumably too low to be detected by the anti- STIM1 antibody used in this study.

Occasionally, in D2D0 and D2D1, there was an increase in the molecular weight of STIM1 suggesting that there may be some sort of modification, such as phosphorylation or glycosylation taking place that might affect STIM1 function thereby contributing to dampened SOCE (discussion 5.4), this slight upshifted STIM1 band disappeared in most

of D2D1 and all D2D2 suggesting that STIM1 expression reverts back to its proliferating state.

The results in this chapter, confirm the previous observations in chapter 5, that hTERT RPE-1 cells may lack/or express a very low level of STIM1 and/or other isoforms of STIM1 may contribute to the observed changes in SOCE.

The data also showed that, in hTERT RPE-1 cells, Orai1 expression was slightly upregulated by ~8.5% and ~17 % in D2D1 and D2D2 of serum add-back compared to proliferating. Though these changes were not significant, it was consistent with the extent of up-regulation of SOCE which was ~ 8 % and 21 % (Section 9.2.3).

Taken together, the data suggest that the restoration of SOCE activity with serum add-back could be driven predominantly by Orai1in hTERT RPE-1cells as the expression of STIM1 is very low and occasionally altered.

The results revealed that STIM1 and Orai1 localisation reverted back when cells re-enter the cell cycle in HeLa and NIH 3T3 cells. The STIM1 clustering at the PM and Orai1 clustering in cell nucleus that was previously observed in proliferating cells and disappeared in G0/G1 cells re-appeared with cell cycle re-entry in D4D3 HeLa cells and D2D2 NIH 3T3 cells.

This observation was in consistent with previous studies which reported that STIM1 and Orai1 localize and bind in zebrafish embryos during cell division (Chan *et al.*, 2016), and that STIM1 and Orai1 localisation was altered when cells arrested in G0 like phase with differentiation of N-type and S-type SH-SY5Y cells (Whitworth, 2015). Furthermore, STIM1 has been shown to redistribute to the PM and bind to Orai1 upon Ca^{2+} store depletion in sinoatrial node cells (Liu *et al.*, 2015), Xenopus oocytes (Courjaret and Machaca, 2014) and HEK293 cells (Fukushima *et al.*, 2012).

These findings highlight the importance of STIM1 and Orai1 localisation in cell cycle progression and SOCE activity in HeLa and NIH 3T3 cells.

Again it is important to remark that, though the STIM1 localisation was restored with cell cycle re-entry in HeLa cells, STIM1expression was not restored leaving SOCE activity dampened.

In summary, in HeLa cells, STIM1 does not appear to be required for cell cycle re-entry whilst Orai1, in addition to its role in SOCE, may have another role by acting as a positive regulator of cell cycle progression and cell proliferation. Additional roles of Orai1 have been previously reported. Orai1 has been shown to control cell proliferation in HEK293 and HeLa cells and that this process is probably independent of ICRAC (Borowiec *et al.*, 2014) to regulate expression of Na^+/Ca^{2+} exchanger type 1 (NCX1) and plasma membrane Ca^{2+} pump isoform 1 (PMCA1) (Baryshnikov *et al.*, 2009) and have a role in vascular remodelling (Beech, 2012).

In NIH 3T3 cells, both SOCE proteins; STIM1 and Orai1 were remodelled with cell cycle arrest in G0/G1 and cell cycle re-entry suggesting a role of these proteins in cell cycle progression and cell proliferation. Further investigations of the role of STIM1and Orai1 on cell cycle progression in NIH 3T3 cells could be done by knocking down and overexpressing these proteins.

9.5 Conclusions

- Restoration of Orai1 only was observed in HeLa cells with cell cycle re-entry suggesting that Orai1 might have a positive role in cell cycle progression and cell proliferation.
- In contrast, STIM1 was not restored with cell cycle re-entry in HeLa cells indicating that persistently low STIM1 might be responsible for the previously observed non-restoration of SOCE with cell cycle re-entry (Chapter 8)
- Restoration of both STIM1 and Orai1 was observed in NIH 3T3 cells with cell cycle re-entry implying a role of these proteins in the previously observed restoration of SOCE with cell cycle re-entry (Chapter 8) and suggesting a role of these proteins in cell cycle progression and cell proliferation.
- Compared to hTERT RPE-1 cells, the alterations of Orai1protein in HeLa and NIH 3T3 cells appeared to be attributed to cell re-entry and not serum add-back.
- In hTERT RPE-1cells Orai1 appeared to play a role in SOCE.

Chapter 10 Final Discussion

10.1 Summary of findings in relevance to objectives

The aim of this study was to investigate the remodelling of Ca^{2+} signalling when cells enter and exit a quiescent G0/G1 phase in a comparison between the aggressive cancerous HeLa and pre-cancerous NIH 3T3 cell lines and an immortalised but non-cancerous hTERT RPE-1 cells.

Serum starvation is a well-known experimental method to induce cell cycle arrest in the quiescent G0/G1 phase in mammalian cells (Langan and Chou, 2011; Xiong et al., 2012). Previous studies have shown differences in the duration of serum starvation (1-3 days) used to induce cell cycle arrest in G0/G1 phase (Nishikura and Murray, 1987; Matsumura et al., 1990; Kerkhoff and Rapp, 1997; Kues et al., 2000; Bodding, 2001; Cooper, 2003; Tani et al., 2007; Kim et al., 2008; Xiong et al., 2012) (Chapter 3 discussion). No studies extended the period of serum starvation beyond the 2-3 days reported in the literature. Furthermore, all reported literature only used the DNA content as a method to identify the G0/G1 arrest in the HeLa and NIH 3T3 cells with serum starvation, no previous studies used both DNA and RNA content to separate G0 from G1 cells.

The first objective of this research therefor was to investigate and observe the cellular changes associated with serum starvation for five days morphologically and by flow cytometry in order to determine the minimum time of serum starvation required to reach cell cycle arrest in quiescent G0/G1 phase. As discussed above the flow cytometry analysis of DNA and RNA content had not been previously used in this type of investigation. This is one novel contribution of this current research.

Morphologically, the results showed that total and mitotic cell number were significantly reduced at day four of serum starvation in HeLa cells and at day two in NIH 3T3 cells whilst in RPE-1 cells no changes were observed up to five days of serum starvation (Figures 3.2, 3.5 and 3.8).

By flow cytometry, HeLa cells showed an increase in percentage of G0 cells in a multi-step manner which peaked and became significant at day four of serum starvation (Figure 3.13 and table 10.1). For NIH 3T3 cells, percentages of G0 cells increased significantly in

a gradual manner which peaked at day two of serum starvation (Figure 3.16 and table 10.1). In hTERT RPE-1 cell there was no alteration in cell subpopulations in response to serum starvation indicating that serum starvation did not induce cell cycle arrest in hTERT RPE-1cells (Figure 3.19 and table 10.1). The non-alteration in cell cycle progression in hTERT RPE-1 cells was expected since these cells are used as control for other cell types; HeLa and NIH 3T3 cells (Chapter 3 discussion)

On the basis of these findings, the minimum required duration of serum starvation to arrest HeLa cells and NIH 3T3 cells in G0/G1 phase is found to be four days and two days respectively. In addition, these findings enabled the use of hTERT RPE-1 cells as a control for HeLa and NIH 3T3 cells in order to investigate Ca^{2+} signalling responses that were specific to cell cycle arrest in G0/G1 phase.

Ca^{2+} is a ubiquitous intracellular second messenger that controls a diverse range of cellular processes (Berridge *et al*., 2000; Bootman *et al*., 2001). Ca^{2+} release from the endoplasmic reticulum and the subsequent Ca^{2+} entry; SOCE, is one of the major pathways that plays a key role in cell cycle progression, cell proliferation, and cell division (Bootman *et al.*, 2001; Targos *et al.*, 2005). Recently, remodelling of SOCE has been shown to contribute to cancer hallmarks such as uncontrolled cellular proliferation, migration as well as resistance to cell death (Bergmeier *et al.*, 2013). The uncontrolled proliferation has been linked to the ability of cancer cells to evade cellular mechanisms that induce cell cycle arrest (Hainaut and Plymoth, 2013). Nonetheless, SOCE remodelling during cell cycle arrest in quiescent G0/G1 phase has been poorly investigated.

The second objective of this study was to characterise SOCE and SOCE protein remodelling with cell cycle arrest in G0/G1 phase in HeLa and NIH 3T3 cells and to compare these findings to hTERT RPE-1 cells which do not enter G0/G1 during serum starvation.

SOCE was characterised in HeLa, NIH 3T3 and hTERT RPE-1 cells by measuring changes in intracellular Ca^{2+} in fura-2 loaded cells (Chapter 4).

The down-regulation of SOCE was observed with cell cycle arrest in quiescent G0/G1 in HeLa and NIH 3T3 that occurred to a greater extent (~ 60% and ~ 61% respectively) compared to that in hTERT RPE-1 cells during serum starvation (~18%) (Table 10.1). This provides a clear evidence that SOCE is remodelled (i.e. down-regulated) during quiescent G0/G1 phase in HeLa and NIH 3T3 cells.

It has been previously observed that serum starvation induced G0/G1 arrest in RBL cells was associated with SOCE down-regulation. However, as discussed earlier in Chapter 4, Bodding (2001) attributed this down-regulation to cell cycle arrest while Tani (2007) attributed the SOCE down-regulation to serum starvation and not cell cycle arrest. From the investigation carried out in the current research, it has been shown that this response could be attributed to a great extent to cell cycle arrest in G0/G1 phase and to a lesser extent to serum starvation.

In addition, the alteration in Ca^{2+} signalling responses with G0/G1 cell cycle arrest was different between cancerous HeLa cells and precancerous NIH 3T3 cells. In HeLa cells, an uncoupling of SOCE from Ca^{2+} store release with marked down-regulation of SOCE was observed. While in NIH 3T3 cells there was a marked down-regulation of SOCE which was still coupled to Ca^{2+} store release. This observation suggests that the mechanisms underlying the down-regulation of SOCE might be different between cancerous and precancerous cells or it might be cell type specific.

The impact of arresting cells in quiescent G0/G1 phase on the level of STIM1and Orai1 expression and localisation has not been investigated previously in HeLa and NIH 3T3 cells.

In this study, the level of expression of the two key Ca^{2+} signalling proteins, STIM1and Orai1 was measured by western blot with cell cycle arrested quiescent G0/G1 phase in HeLa and NIH 3T3 cells and with serum starved in hTERT RPE-1 cells (Table 10.1). In both HeLa and NIH 3T3 cells, STIM1 (Figure 5.1 and 5.3 respectively) and Orai1 (Figure 5.2 and 5.4 respectively) became down-regulated with cell cycle arrest in quiescent G0/G1 phase. In hTERT RPE-1 cells, expression of STIM1 was not detected (Figure 5.5) whilst Orai1 showed slight down-regulation with serum starvation (Figure 5.6). The extent of remodelling (i.e. down-regulation) of Orai1 expression occurred to a greater extent in HeLa and NIH3T3 cells (68% and 53%) respectively than that in hTERT RPE-1 cells (~16%) revealing a clear contribution of cell cycle arrest in this remodelling (Table 10.1). This is consistent with the observation in a previous study (Sukumaran *et al.*, 2015) which showed that no significant changes in either STIM1 or Orai1 expression levels were observed in SHSY-5Y and HSG cells under serum-free conditions. Hence, the remodelling of SOCE proteins is mostly attributed to cell cycle arrest in G0/G1 phase.

An investigation of changes of SOCE and its proteins over the serum starvation time course was done (chapter 6) which revealed that, in HeLa cells, the changes in SOCE, STIM1 and Orai1 occurred in a multistep manner closely correlated to the multistep manner increase of G0 cells. Furthermore, there was a parallel relation between SOCE and STIM1 changes (Figure 6.6.A) whereas Orai1 expression was inversely correlated to the changes in G0 cells (Figure 6.6.B). Similarly, in NIH 3T3 cells, the changes in SOCE, STIM1 and Orai1 over the serum starvation time course occurred gradually and peaked at day two which was closely related to the gradual increase in G0 cell that also peaked at day two.

These findings show the close relation between the remodelling of SOCE and the increase in the percentage of G0 cells and also highlight the essential role of Orai1 in cell cycle progression in HeLa and NIH 3T3 cells. Furthermore, these results contribute to the large body of evidence of role for STIM1and Orai1 in SOCE in HeLa and NIH 3T3 cells.

A fundamental part of studying Ca^{2+} signalling in quiescent G0/G1 cells is to investigate the reversibility of this phase.

Therefore, the third objective was to stimulate quiescent G0/G1 HeLa and NIH 3T3 cells by adding the serum back and define the response both morphologically and by flow cytometry.

Morphologically, serum add-back induced an increase in total cell number as well as mitotic cell number from day one of treatment and restored cell proliferation status from day two in HeLa and NIH 3T3 cells (Figure 7.1and Figure 7.4.C).

Flow cytometry results revealed that the percentage of G0 cells reverted back to proliferating levels when serum was added back for 2 days to the quiescent G0/G1 cells in both HeLa and NIH 3T3 cells (Figure 7.9, 7.12 and Table 10.2). These findings indicate that serum add-back induced cell proliferation and cell cycle resumption in in both HeLa and NIH 3T3 G0/G1 cells.

Bodding (2001) and Tani (2007) have shown that SOCE down-regulation with serum starvation and cell cycle arrest in G0/G1 phase was reversible when the arrested RBL cells were induced to enter the cell cycle by serum add-back. No previous investigations of the remodelling of the SOCE portions with cell cycle re-entry were reported.

The fourth objective was to investigate the remodelling of SOCE and its proteins when cells re-enter the cell cycle.

Ca^{2+} signals with cell cycle re-entry were different between HeLa and NIH 3T3 cells (Table 10.2). Cell cycle re-entry of HeLa cells did not affect Ca^{2+} store release and SOCE which remained dampened (Figure 8.2). While in NIH 3T3 cells, Ca^{2+} store release and SOCE were up-regulated and restored to their proliferating levels (Figure 8.4 and Table 10.2). These observations indicate that SOCE has a role in cell cycle progression in precancerous NIH 3T3 cell but not in cancerous HeLa cells.

From previous findings STIM1 and Orai1 appear to have similar roles in SOCE down-regulation with cell cycle arrest. However, in HeLa cells, Orai1 appears to have an additional role in cell proliferation and cell cycle progression (Section 6.3.1 and Figure 9.2). This conclusion was based on the observation that restoration of Orai1 alone was associated with cell cycle re-entry and resumption of cell proliferation in HeLa cells (Section 9.2.1 and Figure 9.2). In contrast, STIM1 did not revert with cell cycle re-entry (Section 9.2.1 and Figure 9.1) arguing against an additional role for STIM1 in regulating the cell cycle, however, strongly confirming its role in SOCE which remained dampened with resuming cell cycle. This conclusion suggests that Orai1 might be a target for drug therapy of aggressive cancer disease like HeLa cells.

Additional roles of Orai1 has been previously reported. Orai1 has been shown to control cell proliferation in HEK293 and HeLa cells and that this process is probably independent of ICRAC (Borowiec *et al.*, 2014), regulate expression of Na^{+} /Ca^{2+} exchanger type 1 (NCX1) and plasma membrane Ca^{2+} pump isoform 1 (PMCA1) (Bergmeier *et al.*, 2013) and It has also been reported to have a role in vascular remodelling (Beech, 2012).

In NIH 3T3 cells, both STIM1 and Orai1 appear to have a role in cell cycle progression and cell proliferation. This could be concluded from the observations that the expression of both proteins reverted to its proliferating level from the first day of serum-add-back (Section 9.2.2, Figures 9.3 and Figure 9.4) prior to the full restoration of proliferating level of G0 cells which occurred after two days of serum add-back (Result 7.3.2). This conclusion could be further investigated by knocking down the STIM1and Orai1 in NIH 3T3 cells and analysing the effects of each on cell cycle progression.

	G0/G1 HeLa cells	G0/G1 NIH 3T3 cells	Starved hTERT RPE-1 cells
Cell diameter	- 15%	00	00
Mitotic cell number	- 90%	- 95%	00
G0 cells number	26%	52%	00
Ca^{2+} store release	-35%	-77%	- 45%
SOCE	- 60%	- 61%	-18%
STIM1	- 47.5%	- 49.5%	**
Orai1	- 68%	-53%	-16%

Table 10.1 Summary of percentage changes of findings in G0/G1 HeLa, G0/G1 NIH 3T3 and serum starved hTERT RPE-1 cells compared to proliferating

** STIM1 protein was not/barely detected in hTERT RPE-1 cells by western blot and IF (Figure 5.5 and 5.11).

	HeLa cells	NIH 3T3 cells	hTERT RPE-1 cells
Cell diameter	Restored	N/C	N/C
Mitotic cell number	Restored	Restored	N/C
G0 cells number	Restored	Restored	N/C
Ca^{2+} store release	Not restored	Restored	Restored
SOCE	Not restored	Restored	Restored
STIM1	Not restored	Restored	**
Orai1	Restored	Restored	Restored

Table 10.2 Summary of findings with serum add-back to G0/G1 HeLa, G0/G1 NIH 3T3 and serum starved hTERT RPE-1 cells

** STIM1 was not/barely detected in hTERT RPE-1 cells by western blot and IF (Figure 9.5 and 9.11).

10.2 Contribution of research

This study investigated remodelling of SOCE and its proteins when cells enter and exit a quiescent G0/G1 phase and contributes novel findings in a number of areas including:

1. Identification of the percentage of G0 cells in quiescent G0/G1 arrest. All reported literature only utilised the DNA content to identify the G0/G1 arrest from S, G2 and M cells in the HeLa and NIH 3T3 cells, no previous studies use both DNA and RNA content in order to separate G0 from G1 cells in HeLa and NIH 3T3 cells (Chapter 3). This more rigorous approach might have significant impact on determination of contribution of G0 cells in regulation of various mechanisms during G0/G1 phase such regulation of expression of different proteins (e.g. p53) or gene expression.
2. This research extended the investigations of the down-regulation of the SOCE associated with the cell arrest in G0/G1. From the findings of this research, it has been shown that the down-regulation of SOCE associated with cell cycle arrest in G0/G1 phase induced by serum starvation can be attributed to a greater extent to cell cycle arrest in G0/G1 phase and to a lesser extent to serum starvation (Chapter 4 discussion).
3. This research is pioneering in investigating the remodelling of the SOCE proteins; STIM1 and Orai1 during cell cycle arrest in G0/G1 phase in HeLa and NIH 3T3 cells. The results show that these proteins were decreased with cell cycle arrest in G0/G1 phase (Chapter 5).
4. The present study confirms a recent research finding that serum starvation per se does not alter Orai1 expression (Sukumaran *et al*., 2015) and suggested that the remodelling of Orai1 is mostly attributed to cell cycle arrest in G0/G1 phase. (Chapter 5).
5. An inverse correlation between percentage of G0 cells and level of expression of Orai1expression has been shown in the both HeLa and NIH 3T3 cells (but more clearly) in HeLa cells. This result suggests that Orai1 may be used as a target for drug therapy of aggressive cancer disease like HeLa cells (Chapter 6)
6. Previous research reported the remodelling of SOCE with serum add-back (Bodding, 2001; and Tani, 2007). No previous research investigated the remodelling of SOCE proteins, STIM1 and ORAi1 with cell cycle re-entry and

serum add-back. The present study showed that remodelling of SOCE and its proteins, STIM1 and Orai1is different in cancerous HeLa cells and precancerous NIH 3T3 cells with cell cycle re-entry (chapter 8 and 9).

10.3 Limitations

The work presented in this research was limited in time and resources in a number of ways:

1. One limitation of the SOCE measurements in cells arrested in G0 phase is they are measured using all cells in interphase (it is not possible to determine which cells are in G0/G1 prior to recording Ca^{2+} changes). It remains unclear therefore whether G0 cells have a fully down-regulated SOCE pathway (with the measured SOCE being a property of the contaminating cells in G1, S or G2 phases) or whether a SOCE pathway may still be present and functioning in G0 cells, albeit at a decreased level.
2. In HeLa cells, cell cycle arrest caused a down-regulation of STIM1 which did not revert back to its proliferation level with cell cycle re-entry and even with 3 days of serum add-back. It would be interesting to determine whether or not this down-regulation is permanently irreversible by monitoring STIM1 expression for a longer duration of serum add-back. This can be included for further research.
3. In NIH 3T3 cells, both STIM1 and Orai1 reverted back with cell cycle re-entry. Due to time limits, the role of STIM1 and Orai1 in cell cycle progression in NIH 3T3 cells were not investigated, but future studies of knocking down or overexpressing each protein and looking at its effects on cell cycle progression would be valuable
4. In hTERT RPE-1 cells, STIM1 and Orai1 were not detected by immunofluorescence staining. The cell fixation was only carried out using PFA due to time limitations. Future work could be to investigate alternative fixation methods (e.g. methanol) Furthermore, other STIM1/Orai1 antibodies could have also been tried. This could be a subject for further research.

10.4 Further research

This study is relevant to the ongoing research efforts to understanding the Ca^{2+} signalling remodelling involved in cancerous diseases. Any progress or development in this research area could be valuable in enhancing such efforts.

- The key results from this study have revealed that SOCE and expression of STIM1and Orai1 remodelling was different between cancer HeLa cells and precancerous NIH 3T3 cells with cell cycle arrest in G0/G1 phase following serum starvation and with cell cycle re-entry by serum add-back in HeLa and NIH 3T3 cells.

  Repeating this research using a more diverse array of cancerous and non-cancerous cell types would give a greater understanding of cell-type specific remodelling of SOCE and its proteins; STIM1 and Orai1 when cells exit and re-enter the cell cycle which could offer new therapeutic possibilities that target regulation of the cell cycle; e.g. cancer.

- An inverse correlation between Orai1 expression and percentage of G0 cells was observed in this study in HeLa cells. This correlation could represent a positive role of Orai1 for cell cycle progression. It would be interesting to investigate this further by manipulating Orai1 protein expression in HeLa cells which might induce G0/G1 cell cycle arrest. In addition, this finding could be also investigated in other cell types which could elucidate a universal role for Orai l in cell cycle progression.
- This study showed that SOCE didn't revert to its normal levels in HeLa cells with resumption of proliferation after three days of serum add-back. The rate of proliferation as well as the level of Ca^{2+} could show some changes if the period of investigation extended to more than three days. This deserves further investigation.
- This thesis demonstrated that STIM1 and Orai1 proteins expression was closely associated with cell cycle progression in NIH 3T3 cells. Further investigation of the role of STIM1and Orai1 in cell cycle progression in NIH 3T3 cells by manipulating its expression is needed.

10.5 Final remarks

Uncontrolled proliferation is a hallmark of cancer cells. Ca^{2+} signalling plays a key role in controlling cell proliferation and cell cycle progression (Bootman *et al*., 2001; Carafoli, 2002; Berridge *et al*., 2003). Recently many reports have suggested that intracellular Ca^{2+} remodelling might be critically contributing to various forms of cancer. Therefore, a series of studies set out to investigate a number of therapeutic possibilities involving Ca^{2+} signalling against cancer (Roderick and Cook, 2008; Stewart *et al.*, 2015). The main considerations in cancer treatment are inhibition of proliferation, induction of differentiation and induction of apoptosis (Bergner and Huber, 2008). Understanding changes involved in the switch from proliferation to quiescence are therefore essential in the treatment of cancer diseases. Furthermore, identification of Ca^{2+} signalling during reverse processes i.e from quiescence to proliferation could contribute to understand the mechanisms governing tumour dormancy. Thus might provide promising targets for early prevention of cancer by inhibition of growth of malignant dormant tumours and cancer stem cells (Almog, 2013).

The results obtained in this thesis have revealed that SOCE and its proteins; STIM1 and Orai1 are remodelled when cells enter quiescent G0/G1 phase and in the reverse process where G0/G1 cells are induced to proliferate again.

The findings contribute to the understanding of the remodelling of SOCE with cell cycle progression in cancer and precancerous cells which may provide potential strategies for cancer. Further understanding of the remodelling of Orai1 and STIM1 proteins in the switch from proliferation to quiescence in various cell types is still required.

Chapter 11 References

Abdullaev, I.F., Bisaillon, J.M., Potier, M., Gonzalez, J.C., Motiani, R.K. and Trebak, M. (2008) 'Stim1 and Orai1 Mediate CRAC Currents and Store-Operated Calcium Entry Important for Endothelial Cell Proliferation', *Circulation Research*, 103(11), pp. 1289-U185.

Alicia, S., Angelica, Z., Carlos, S., Alfonso, S. and Vaca, L. (2008) 'STIM1 converts TRPC1 from a receptor-operated to a store-operated channel: Moving TRPC1 in and out of lipid rafts', *Cell Calcium*, 44(5), pp. 479-491.

Almog, N. (2013) 'Genes and Regulatory Pathways Involved in Persistence of Dormant Micro-tumors', in Enderling, H., Almog, N. and Hlatky, L. (eds.) *Systems Biology of Tumor Dormancy*. pp. 3-17.

Altman, S.A., Randers, L. and Rao, G. (1993) 'Comparison of trypan blue-dye exclusion and fluorometric assays for mammalian-cell viability determinations', *Biotechnology Progress*, 9(6), pp. 671-674.

Andreeff, M., Darzynkiewicz, Z., Sharpless, T.K., Clarkson, B.D. and Melamed, M.R. (1980) 'Discrimination of human-leukemia subtypes by flow cytometric analysis of cellular DNA and RNA', *Blood*, 55(2), pp. 282-293.

Antigny, F., Girardin, N. and Frieden, M. (2012) 'Transient Receptor Potential Canonical Channels Are Required for in Vitro Endothelial Tube Formation', *Journal of Biological Chemistry*, 287(8), pp. 5917-5927.

Arredouani, A., Yu, F., Sun, L. and Machaca, K. (2010) 'Regulation of store-operated Ca^{2+} entry during the cell cycle', *Journal of Cell Science*, 123(13), pp. 2155-2162.

Aubart, F.C., Sassi, Y., Coulombe, A., Mougenot, N., Vrignaud, C., Leprince, P., Lechat, P., Lompre, A.M. and Hulot, J.S. (2009) 'RNA Interference Targeting STIM1 Suppresses Vascular Smooth Muscle Cell Proliferation and Neointima Formation in the Rat', *Molecular Therapy*, 17(3), pp. 455-462.

Ay, A.S., Benzerdjeb, N., Sevestre, H., Ahidouch, A. and Ouadid-Ahidouch, H. (2015) 'Orai3 Constitutes a Native Store-Operated Calcium Entry That Regulates Non Small Cell Lung Adenocarcinoma Cell Proliferation (vol 8, e72889, 2013)', *Plos One*, 10(4).

Baba, Y., Hayashit, K., Fujii, Y., Mizushima, A., Watarai, H., Wakamori, M., Numaga, T., Mori, Y., Iino, M., Hikida, M. and Kurosaki, T. (2006) 'Coupling of STIM1 to store-operated Ca^{2+} entry through its constitutive and inducible movement in the endoplasmic reticulum', *Proceedings of the National Academy of Sciences of the United States of America*, 103(45), pp. 16704-16709.

Baryshnikov, S.G., Pulina, M.V., Zulian, A., Linde, C.I. and Golovina, V.A. (2009) 'Orai1, a critical component of store-operated Ca2+ entry, is functionally associated with Na^{+}/Ca^{2+} exchanger and plasma membrane Ca2+ pump in proliferating human arterial myocytes', *American Journal of Physiology-Cell Physiology*, 297(5), pp. C1103-C1112.

Beech, D.J. (2012) 'Orai1 calcium channels in the vasculature', *Pflugers Archiv-European Journal of Physiology*, 463(5), pp. 635-647.

Bell, N. (2011) Calcium signalling and differentiation in neuroblastoma cells. *Institute of Cell and Molecular Biosciences.* PhD thesis. Newcastle University.

Bell, N., Hann, V., Redfern, C.P.F. and Cheek, T.R. (2013) 'Store-operated Ca^{2+} entry in proliferating and retinoic acid-differentiated N- and S-type neuroblastoma cells', *Biochimica Et Biophysica Acta-Molecular Cell Research*, 1833(3), pp. 643-651.

Bergmeier, W., Weidinger, C., Zee, I. and Feske, S. (2013) 'Emerging roles of store-operated Ca^{2+} entry through STIM and ORAI proteins in immunity, hemostasis and cancer', *Channels*, 7(5), pp. 379-391.

Bergner, A. and Huber, R.M. (2008) 'Regulation of the Endoplasmic Reticulum Ca2+-Store in Cancer', *Anti-Cancer Agents in Medicinal Chemistry*, 8(7), pp. 705-709.

Berna-Erro, A., Redondo, P.C. and Rosado, J.A. (2012) 'Store-Operated Ca^{2+} Entry', in Islam, M.S. (ed.) *Calcium Signaling*. pp. 349-382.

Berridge, M., Lipp, P. and Bootman, M. (1999) 'Primer - Calcium signalling', *Current Biology*, 9(5), pp. R157-R159.

Berridge, M.J. (2009) 'Inositol trisphosphate and calcium signalling mechanisms', *Biochimica Et Biophysica Acta-Molecular Cell Research*, 1793(6), pp. 933-940.

Berridge, M.J., Bootman, M.D. and Lipp, P. (1998) 'Calcium - a life and death signal', *Nature*, 395(6703), pp. 645-648.

Berridge, M.J., Bootman, M.D. and Roderick, H.L. (2003) 'Calcium signalling: Dynamics, homeostasis and remodelling', *Nature Reviews Molecular Cell Biology*, 4(7), pp. 517-529.

Berridge, M.J., Lipp, P. and Bootman, M.D. (2000) 'The versatility and universality of calcium signalling', *Nature Reviews Molecular Cell Biology*, 1(1), pp. 11-21.

Bird, G.S., DeHaven, W.I., Smyth, J.T. and Putney, J.W. (2008) 'Methods for studying store-operated calcium entry', *Methods*, 46(3), pp. 204-212.

Bodding, M. (2001) 'Reduced store-operated Ca^{2+} currents in rat basophilic leukaemia cells cultured under serum-free conditions', *Cell Calcium*, 30(2), pp. 141-150.

Bootman, M.D., Collins, T.J., Mackenzie, L., Roderick, H.L., Berridge, M.J. and Peppiatt, C.M. (2002) '2-Aminoethoxydiphenyl borate (2-APB) is a reliable blocker of store-operated Ca^{2+} entry but an inconsistent inhibitor of InsP(3)-induced Ca2+ release', *Faseb Journal*, 16(10).

Bootman, M.D., Collins, T.J., Peppiatt, C.M., Prothero, L.S., MacKenzie, L., De Smet, P., Travers, M., Tovey, S.C., Seo, J.T., Berridge, M.J., Ciccolini, F. and Lipp, P. (2001) 'Calcium signalling - an overview', *Seminars in Cell & Developmental Biology*, 12(1), pp. 3-10.

Borowiec, A.S., Bidaux, G., Tacine, R., Dubar, P., Pigat, N., Delcourt, P., Mignen, O. and Capiod, T. (2014) 'Are Orail and Orai3 channels more important than calcium influx for cell proliferation?', *Biochimica Et Biophysica Acta-Molecular Cell Research*, 1843(2), pp. 464-472.

Boynton, A.L. (1988) 'Calcium and epithelial-cell proliferation', *Mineral and Electrolyte Metabolism*, 14(1), pp. 86-94.

Boynton, A.L., Whitfield, J.F., Isaacs, R.J. and Tremblay, R.G. (1977) 'Different extracellular calcium requirements for proliferation of nonneoplastic, preneoplastic, and neoplastic mouse cells', *Cancer Research*, 37(8), pp. 2657-2661.

Brandman, O., Liou, J., Park, W.S. and Meyer, T. (2007) 'STIM2 is a feedback regulator that stabilizes basal cytosolic and endoplasmic reticulum Ca^{2+} levels', *Cell*, 131(7), pp. 1327-1339.

Breitwieser, G.E. and Gama, L. (2001) 'Calcium-sensing receptor activation induces intracellular calcium oscillations', *American Journal of Physiology-Cell Physiology*, 280(6), pp. C1412-C1421.

Brown, A.M., Riddoch, F.C., Robson, A., Redfern, C.P.F. and Cheek, T.R. (2005) 'Mechanistic and functional changes in Ca^{2+} entry after retinoic acid-induced differentiation of neuroblastoma cells', *Biochemical Journal*, 388, pp. 941-948.

Campisi, J. (2000) 'Cancer, aging and cellular senescence', *In Vivo*, 14(1), pp. 183-188.

Capiod, T. (2013) 'The Need for Calcium Channels in Cell Proliferation', *Recent Patents on Anti-Cancer Drug Discovery*, 8(1), pp. 4-17.

Chan, C.M., Aw, J.T.M., Webb, S.E. and Miller, A.L. (2016) 'SOCE proteins, STIM1 and Orai1, are localized to the cleavage furrow during cytokinesis of the first and second cell division cycles in zebrafish embryos', *Zygote*, 24(6), pp. 880-889.

Chen, Y.F., Chen, Y.T., Chiu, W.T. and Shen, M.R. (2013) 'Remodeling of calcium signaling in tumor progression', *Journal of Biomedical Science*, 20.

Chen, Y.W., Chen, Y.F., Chen, Y.T., Chiu, W.T. and Shen, M.R. (2016) 'The STIM1-Orai1 pathway of store-operated Ca^{2+} entry controls the checkpoint in cell cycle G1/S transition', *Scientific Reports*, 6.

Cheung, T.H. and Rando, T.A. (2013) 'Molecular regulation of stem cell quiescence', *Nature Reviews Molecular Cell Biology*, 14(6), pp. 329-340.

Clapham, D.E. (2007) 'Calcium signaling', *Cell*, 131(6), pp. 1047-1058.

Coller, H.A., Sang, L.Y. and Roberts, J.M. (2006) 'A new description of cellular quiescence', *Plos Biology*, 4(3), pp. 329-349.

Cooper, S. (2003) 'Reappraisal of serum starvation, the restriction point, G0, and G1 phase arrest points', *Faseb Journal*, 17(3), pp. 333-340.

Courjaret, R. and Machaca, K. (2014) 'Mid-range Ca^{2+} signalling mediated by functional coupling between store-operated Ca2+ entry and IP3-dependent Ca2+ release', *Nature Communications*, 5.

Crissman, H.A., Darzynkiewicz, Z., Tobey, R.A. and Steinkamp, J.A. (1985) 'Correlated measurements of DNA,RNA and protein in individual cells by flow-cytometry ', *Science*, 228(4705), pp. 1321-1324.

Cumming, G., Fidler, F. and Vaux, D.L. (2007) 'Error bars in experimental biology', *Journal of Cell Biology*, 177(1), pp. 7-11.

Daignan-Fornier, B. and Sagot, I. (2011) 'Proliferation/quiescence: the controversial "aller-retour"', *Cell Division*, 6.

Darbellay, B., Arnaudeau, S., Bader, C.R., Konig, S. and Bernheim, L. (2011) 'STIM1L is a new actin-binding splice variant involved in fast repetitive Ca2+ release', *Journal of Cell Biology*, 194(2), pp. 335-346.

Darbellay, B., Arnaudeau, S., Konig, S., Jousset, H., Bader, C., Demaurex, N. and Bernheim, L. (2009) 'STIM1-and Orai1-dependent Store-operated Calcium Entry Regulates Human Myoblast Differentiation', *Journal of Biological Chemistry*, 284(8), pp. 5370-5380.

Darzynkiewicz, Z., Traganos, F., Zhao, H., Halicka, H.D. and Li, J.W. (2011) 'Cytometry of DNA Replication and RNA Synthesis: Historical Perspective and Recent Advances Based on "Click Chemistry"', *Cytometry Part A*, 79A(5), pp. 328-337.

DeHaven, W.I., Jones, B.F., Petranka, J.G., Smyth, J.T., Tomita, T., Bird, G.S. and Putney, J.W. (2009) 'TRPC channels function independently of STIM1 and Orai1', *Journal of Physiology-London*, 587(10), pp. 2275-2298.

DeHaven, W.I., Smyth, J.T., Boyles, R.R. and Putney, J.W. (2007) 'Calcium inhibition and calcium potentiation of Orai1, Orai2, and Orai3 calcium release-activated calcium channels', *Journal of Biological Chemistry*, 282(24), pp. 17548-17556.

Demuro, A., Penna, A., Safrina, O., Yeromin, A.V., Amcheslavsky, A., Cahalan, M.D. and Parker, I. (2011) 'Subunit stoichiometry of human Orai1 and Orai3 channels in closed and open states', *Proceedings of the National Academy of Sciences of the United States of America*, 108(43), pp. 17832-17837.

Divirgilio, F., Fasolato, C. and Steinberg, T.H. (1988a) 'Inhibitors of membrane-transport system for organic-anions block fura-2 excretion from pc12 and n2a cells ', *Biochemical Journal*, 256(3), pp. 959-963.

Divirgilio, F., Steinberg, T.H. and Silverstein, S.C. (1990) 'Inhibition of fura-2 sequestration and secretion with organic anion transport blockers ', *Cell Calcium*, 11(2-3), pp. 57-&.

Divirgilio, F., Steinberg, T.H., Swanson, J.A. and Silverstein, S.C. (1988b) 'Fura-2 secretion and sequestration in macrophages - a blocker of organic anion transport reveals that these processes occur via a membrane-transport system for organic-anions ', *Journal of Immunology*, 140(3), pp. 915-920.

Donohue, P.J., Feng, S.L.Y., Alberts, G.F., Guo, Y., Peifley, K.A., Hsu, D.K.W. and Winkles, J.A. (1996) 'Fibroblast growth factor-1 stimulation of quiescent NIH 3T3 cells increases G/T mismatch-binding protein expression', *Biochemical Journal*, 319, pp. 9-12.

Dragoni, S., Turin, I., Laforenza, U., Potenza, D.M., Bottino, C., Glasnov, T.N., Prestia, M., Ferulli, F., Saitta, A., Mosca, A., Guerra, G., Rosti, V., Luinetti, O., Ganini, C., Porta, C., Pedrazzoli, P., Tanzi, F., Montagna, D. and Moccia, F. (2014) 'Store-Operated Ca2+ Entry Does Not Control Proliferation in Primary Cultures of Human Metastatic Renal Cellular Carcinoma', *Biomed Research International*.

Dubois, C., Vanden Abeele, F., Lehen'kyi, V., Gkika, D., Guarmit, B., Lepage, G., Slomianny, C., Borowiec, A.S., Bidaux, G., Benahmed, M., Shuba, Y. and Prevarskaya, N. (2014) 'Remodeling of Channel-Forming ORAI Proteins Determines an Oncogenic Switch in Prostate Cancer', *Cancer Cell*, 26(1), pp. 19-32.

Dziadek, M.A. and Johnstone, L.S. (2007) 'Biochemical properties and cellular localisation of STIM proteins', *Cell Calcium*, 42(2), pp. 123-132.

El Boustany, C., Katsogiannou, M., Delcourt, P., Dewailly, E., Prevarskaya, N., Borowiec, A.S. and Capiod, T. (2010) 'Differential roles of STIM1, STIM2 and Orai1 in the control of cell proliferation and SOCE amplitude in HEK293 cells', *Cell Calcium*, 47(4), pp. 350-359.

Feske, S., Gwack, Y., Prakriya, M., Srikanth, S., Puppel, S.H., Tanasa, B., Hogan, P.G., Lewis, R.S., Daly, M. and Rao, A. (2006) 'A mutation in Orai1 causes immune deficiency by abrogating CRAC channel function', *Nature*, 441(7090), pp. 179-185.

Frischauf, I., Fahrner, M., Jardin, I. and Romanin, C. (2016) 'The STIM1: Orai Interaction', in Rosado, J.A. (ed.) *Calcium Entry Pathways in Non-Excitable Cells*. pp. 25-46.

Fukushima, M., Tomita, T., Janoshazi, A. and Putney, J.W. (2012) 'Alternative translation initiation gives rise to two isoforms of Orai1 with distinct plasma membrane mobilities', *Journal of Cell Science*, 125(18), pp. 4354-4361.

Graham, S.J.L., Black, M.J., Soboloff, J., Gill, D.L., Dziadek, M.A. and Johnstone, L.S. (2009) 'Stim1, an endoplasmic reticulum Ca2+ sensor, negatively regulates 3T3-L1 pre-adipocyte differentiation', *Differentiation*, 77(3), pp. 239-247.

Greig, R.G., Koestler, T.P., Trainer, D.L., Corwin, S.P., Miles, L., Kline, T., Sweet, R., Yokoyama, S. and Poste, G. (1985) 'Tumorigenic and metastatic properties of normal and ras-transfected nih/3t3 cells ', *Proceedings of the National Academy of Sciences of the United States of America*, 82(11), pp. 3698-3701.

Groigno, L. and Whitaker, M. (1998) 'An anaphase calcium signal controls chromosome disjunction in early sea urchin embryos', *Cell*, 92(2), pp. 193-204.

Grynkiewicz, G., Poenie, M. and Tsien, R.Y. (1985) 'A new generation of Ca-2+ indicators with greatly improved fluorescence properties ', *Journal of Biological Chemistry*, 260(6), pp. 3440-3450.

Gwack, Y., Srikanth, S., Feske, S., Cruz-Guilloty, F., Oh-hora, M., Neems, D.S., Hogan, P.G. and Rao, A. (2007) 'Biochemical and functional characterization of Orai proteins', *Journal of Biological Chemistry*, 282(22), pp. 16232-16243.

Hainaut, P. and Plymoth, A. (2013) 'Targeting the hallmarks of cancer: towards a rational approach to next-generation cancer therapy', *Current Opinion in Oncology*, 25(1), pp. 50-51.

Hanahan, D. and Weinberg, R.A. (2000) 'The hallmarks of cancer', *Cell*, 100(1), pp. 57-70.

Hao, B.X., Lu, Y.Y., Wang, Q., Guo, W.J., Cheung, K.H. and Yue, J.B. (2014) 'Role of STIM1 in survival and neural differentiation of mouse embryonic stem cells independent of Orai1-mediated Ca2+ entry', *Stem Cell Research*, 12(2), pp. 452-466.

Hartwell, L.H. and Weinert, T.A. (1989) 'Checkpoints - controls that ensure the order of cell-cycle events ', *Science*, 246(4930), pp. 629-634.

Hayflick, L. and Moorhead, P.S. (1961) 'The serial cultivation of human diploid cell strains.', *Exp. Cell Res*, 25, pp. 585-621.

Hazelton, B., Mitchell, B. and Tupper, J. (1979) 'Calcium, magnesium, and growth-control in the wi-38 human fibroblast cell ', *Journal of Cell Biology*, 83(2), pp. 487-498.

Hodeify, R., Selvaraj, S., Wen, J., Arredouani, A., Hubrack, S., Dib, M., Al-Thani, S.N., McGraw, T. and Machaca, K. (2015) 'A STIM1-dependent 'trafficking trap'

mechanism regulates Orai1 plasma membrane residence and Ca2+ influx levels', *Journal of Cell Science*, 128(16), pp. 3143-3154.

Hogan, P.G., Lewis, R.S. and Rao, A. (2010) 'Molecular Basis of Calcium Signaling in Lymphocytes: STIM and ORAI', in Paul, W.E., Littman, D.R. and Yokoyama, W.M. (eds.) *Annual Review of Immunology, Vol 28*. pp. 491-533.

Hong, J.H., Li, Q., Kim, M.S., Shin, D.M., Feske, S., Birnbaumer, L., Cheng, K.T., Ambudkar, I.S. and Muallem, S. (2011) 'Polarized but Differential Localization and Recruitment of STIM1, Orai1 and TRPC Channels in Secretory Cells', *Traffic*, 12(2), pp. 232-245.

Hoover, P.J. and Lewis, R.S. (2011) 'Stoichiometric requirements for trapping and gating of Ca^{2+} release-activated Ca^{2+} (CRAC) channels by stromal interaction molecule 1 (STIM1)', *Proceedings of the National Academy of Sciences of the United States of America*, 108(32), pp. 13299-13304.

Horinouchi, T., Higashi, T., Higa, T., Terada, K., Mai, Y., Aoyagi, H., Hatate, C., Nepal, P., Horiguchi, M., Harada, T. and Miwa, S. (2012) 'Different binding property of STIM1 and its novel splice variant STIM1L to Orai1, TRPC3, and TRPC6 channels', *Biochemical and Biophysical Research Communications*, 428(2), pp. 252-258.

Hoyt, MA., Totis, L., Roberts, BT. (1991) ' Saccharomyces-cerevisiae genes required for cell-cycle arrest in response to loss of microtubule function', *Cell*, 66 (3), pp. 507-517.

Huang, G.N., Zeng, W.Z., Kim, J.Y., Yuan, J.P., Han, L.H., Muallem, S. and Worley, P.F. (2006) 'STIM1 carboxyl-terminus activates native SOC, I-crac and TRPC1 channels', *Nature Cell Biology*, 8(9), pp. 1003-U96.

Izant, J.G. (1983) 'The role of calcium-ions during mitosis - calcium participates in the anaphase trigger ', *Chromosoma*, 88(1), pp. 1-10.

Jardin, I., Salido, G.M. and Rosado, J.A. (2008) 'Role of lipid rafts in the interaction between hTRPC1, Orai1 and STIM1', *Channels*, 2(6), pp. 401-403.

Jiang, X.R., Jimenez, G., Chang, E., Frolkis, M., Kusler, B., Sage, M., Beeche, M., Bodnar, A.G., Wahl, G.M., Tlsty, T.D. and Chiu, C.P. (1999) 'Telomerase expression in human somatic cells does not induce changes associated with a transformed phenotype', *Nature Genetics*, 21(1), pp. 111-114.

Kahl, C.R. and Means, A.R. (2003) 'Regulation of cell cycle progression by calcium/calmodulin-dependent pathways', *Endocrine Reviews*, 24(6), pp. 719-736.

Kawasaki, T., Lange, I. and Feske, S. (2009) 'A minimal regulatory domain in the C terminus of STIM1 binds to and activates ORAI1 CRAC channels', *Biochemical and Biophysical Research Communications*, 385(1), pp. 49-54.

Kawasaki, T., Ueyama, T., Lange, I., Feske, S. and Saito, N. (2010) 'Protein Kinase C-induced Phosphorylation of Orai1 Regulates the Intracellular Ca2+ Level via the Store-operated Ca2+ Channel', *Journal of Biological Chemistry*, 285(33), pp. 25720-25730.

Kerker, M., Vandilla, M.A., Brunsting, A., Kratohvil, J.P., Hsu, P., Wang, D.S., Gray, J.W. and Langlois, R.G. (1982) 'Is the central dogma of flow-cytometry true - that fluorescence intensity is proportional to cellular dye content ', *Cytometry*, 3(2), pp. 71-78.

Kerkhoff, E. and Rapp, U.R. (1997) 'Induction of cell proliferation in quiescent NIH 3T3 cells by oncogenic c-Raf-1', *Molecular and Cellular Biology*, 17(5), pp. 2576-2586.

Kim, J., Lee, J.H. and Iyer, V.R. (2008) 'Global Identification of Myc Target Genes Reveals Its Direct Role in Mitochondrial Biogenesis and Its E-Box Usage In Vivo', *Plos One*, 3(3).

Kohn, E.C., Reed, E., Sarosy, G., Christian, M., Link, C.J., Cole, K., Figg, W.D., Davis, P.A., Jacob, J., Goldspiel, B. and Liotta, L.A. (1996) 'Clinical investigation of a cytostatic calcium influx inhibitor in patients with refractory cancers', *Cancer Research*, 56(3), pp. 569-573.

Korzeniowski, M.K., Manjarres, I.M., Varnai, P. and Balla, T. (2010) 'Activation of STIM1-Orai1 Involves an Intramolecular Switching Mechanism', *Science Signaling*, 3(148).

Kothapalli, D., Flowers, J., Xu, T., Pure, E. and Assoian, R.K. (2008) 'Differential Activation of ERK and Rac Mediates the Proliferative and Anti-proliferative Effects of Hyaluronan and CD44', *Journal of Biological Chemistry*, 283(46), pp. 31823-31829.

Kuang, C.Y., Yu, Y., Guo, R.W., Qian, D.H., Wang, K., Den, M.Y., Shi, Y.K. and Huang, L. (2010) 'Silencing stromal interaction molecule 1 by RNA interference inhibits the

proliferation and migration of endothelial progenitor cells', *Biochemical and Biophysical Research Communications*, 398(2), pp. 315-320.

Kues, W.A., Anger, M., Carnwath, J.W., Paul, D., Motlik, J. and Niemann, H. (2000) 'Cell cycle synchronization of porcine fetal fibroblasts: Effects of serum deprivation and reversible cell cycle inhibitors', *Biology of Reproduction*, 62(2), pp. 412-419.

Langan and Chou, R. (2011) 'Synchronization of mammalian cell cultures by serum deprivation', *Methods Mol Biol*, 761, pp. 75-83.

Lasorsa, F.M., Pinton, P., Palmieri, L., Scarcia, P., Rottensteiner, H., Rizzuto, R. and Palmieri, F. (2008) 'Peroxisomes as novel players in cell calcium homeostasis', *Journal of Biological Chemistry*, 283(22), pp. 15300-15308.

Laude, A.J. and Simpson, A.W.M. (2009) 'Compartmentalized signalling: Ca2+ compartments, microdomains and the many facets of Ca2+ signalling', *Febs Journal*, 276(7), pp. 1800-1816.

Lee, K.P., Choi, S., Hong, J.H., Ahuja, M., Graham, S., Ma, R., So, I., Shin, D.M., Muallem, S. and Yuan, J.P. (2014) 'Molecular Determinants Mediating Gating of Transient Receptor Potential Canonical (TRPC) Channels by Stromal Interaction Molecule 1 (STIM1)', *Journal of Biological Chemistry*, 289(10), pp. 6372-6382.

Lemons, J.M.S., Feng, X.J., Bennett, B.D., Legesse-Miller, A., Johnson, E.L., Raitman, I., Pollina, E.A., Rabitz, H.A., Rabinowitz, J.D. and Coller, H.A. (2010) 'Quiescent Fibroblasts Exhibit High Metabolic Activity', *Plos Biology*, 8(10).

Lemos, D.R., Goodspeed, L., Tonelli, L., Antoch, M.P., Ojeda, S.R. and Urbanski, H.F. (2007) 'Evidence for circadian regulation of activating transcription factor 5 but not tyrosine hydroxylase by the chromaffin cell clock', *Endocrinology*, 148(12), pp. 5811-5821.

Lewis, R.S. (2007) 'The molecular choreography of a store-operated calcium channel', *Nature*, 446(7133), pp. 284-287.

Li, R. and Murray, AW. (1991) 'Feedback control of mitosis in budding yeast'. *Cell*, 66, pp. 519– 31

Li, G.L., Zhang, Z.X., Wang, R.Z., Ma, W.B., Yang, Y., Wei, J.J. and Wei, Y.P. (2013) 'Suppression of STIM1 inhibits human glioblastoma cell proliferation and induces G0/G1 phase arrest', *Journal of Experimental & Clinical Cancer Research*, 32.

Li, J., Sukumar, P., Milligan, C.J., Kumar, B., Ma, Z.Y., Munsch, C.M., Jiang, L.H., Porter, K.E. and Beech, D.J. (2008) 'Interactions, functions, and independence of plasma membrane STIM1 and TRPC1 in vascular smooth muscle cells', *Circulation Research*, 103(8), pp. E97-U311.

Liang, W.G., Ye, D.P., Dai, L.B., Shen, Y. and Xu, J.K. (2012) 'Overexpression of hTERT extends replicative capacity of human nucleus pulposus cells, and protects against serum starvation-induced apoptosis and cell cycle arrest', *Journal of Cellular Biochemistry*, 113(6), pp. 2112-2121.

Liou, J., Fivaz, M., Inoue, T. and Meyer, T. (2007) 'Live-cell imaging reveals sequential oligomerization and local plasma membrane targeting of stromal interaction molecule 1 after Ca2+ store depletion', *Proceedings of the National Academy of Sciences of the United States of America*, 104(22), pp. 9301-9306.

Liou, J., Kim, M.L., Heo, W.D., Jones, J.T., Myers, J.W., Ferrell, J.E. and Meyer, T. (2005) 'STIM is a Ca2+ sensor essential for Ca^{2+}-store-depletion-triggered Ca2+ influx', *Current Biology*, 15(13), pp. 1235-1241.

Litovchick, L., Florens, L.A., Swanson, S.K., Washburn, M.P. and DeCaprio, J.A. (2011) 'DYRK1A protein kinase promotes quiescence and senescence through DREAM complex assembly', *Genes & Development*, 25(8), pp. 801-813.

Liu, J., Xin, L., Benson, V.L., Allen, D.G. and Ju, Y.K. (2015) 'Store-operated calcium entry and the localization of STIM1 and Orai1 proteins in isolated mouse sinoatrial node cells', *Frontiers in Physiology*, 6.

Lopez, E., Jardin, I., Berna-Erro, A., Bermejo, N., Salido, G.M., Sage, S.O., Rosado, J.A. and Redondo, P.C. (2012) 'STIM1 tyrosine-phosphorylation is required for STIM1-Orai1 association in human platelets', *Cellular Signalling*, 24(6), pp. 1315-1322.

Lu, K.P. and Means, A.R. (1993) 'Regulation of the cell-cycle by calcium and calmodulin ', *Endocrine Reviews*, 14(1), pp. 40-58.

Luik, R.M., Wu, M.M., Buchanan, J. and Lewis, R.S. (2006) 'The elementary unit of store-operated Ca^{2+} entry: local activation of CRAC channels by STIM1 at ER-plasma membrane junctions', *Journal of Cell Biology*, 174(6), pp. 815-825.

Machaca, K. and Haun, S. (2000) 'Store-operated calcium entry inactivates at the germinal vesicle breakdown stage of Xenopus meiosis', *Journal of Biological Chemistry*, 275(49), pp. 38710-38715.

Machaca, K. and Haun, S. (2002) 'Induction of maturation-promoting factor during Xenopus oocyte maturation uncouples Ca^{2+} store depletion from store-operated Ca2+ entry', *Journal of Cell Biology*, 156(1), pp. 75-85.

Manji, S.S.M., Parker, N.J., Williams, R.T., van Stekelenburg, L., Pearson, R.B., Dziadek, M. and Smith, P.J. (2000) 'STIM1: a novel phosphoprotein located at the cell surface', *Biochimica Et Biophysica Acta-Protein Structure and Molecular Enzymology*, 1481(1), pp. 147-155.

Matsumoto, Y. and Maller, J.L. (2002) 'Calcium, calmodulin, and CaMKII requirement for initiation of centrosome duplication in Xenopus egg extracts', *Science*, 295(5554), pp. 499-502.

Matsumura, K., Sasaki, K., Tsuji, T., Murakami, T., Takahashi, M. and Shinozaki, F. (1990) 'Changes of agnors in hela-cells during serum starvation', *British Journal of Cancer*, 62(3), pp. 385-387.

McCarron, J.G., Chalmers, S., Bradley, K.N., MacMillan, D. and Muir, T.C. (2006) 'Ca2+ microdomains in smooth muscle', *Cell Calcium*, 40(5-6), pp. 461-493.

Means, A.R. (1994) 'Calcium, calmodulin and cell-cycle regulation', *Febs Letters*, 347(1), pp. 1-4.

Mercer, J.C., DeHaven, W.I., Smyth, J.T., Wedel, B., Boyles, R.R., Bird, G.S. and Putney, J.W. (2006) 'Large store-operated calcium selective currents due to co-expression of Orai1 or Orai2 with the intracellular calcium sensor, Stim1', *Journal of Biological Chemistry*, 281(34), pp. 24979-24990.

Mignen, O., Thompson, J.L. and Shuttleworth, T.J. (2008) 'Both Orai1 and Orai3 are essential components of the arachidonate-regulated Ca^{2+}-selective (ARC) channels', *Journal of Physiology-London*, 586(1), pp. 185-195.

Mitchison, J.M. (1971) *The biology of the cell cycle*.

Miyazaki, S., Shirakawa, H., Nakada, K. and Honda, Y. (1993) 'Essential role of the inositol 1,4,5-trisphosphate receptor/Ca^{2+} release channel in Ca^{2+} waves and Ca^{2+} oscillations at fertilization of mammalian eggs', *Developmental Biology*, 158(1), pp. 62-78.

Murray and Hunt (1993) *The cell cycle*.

Nishikura, K. and Murray, J.M. (1987) 'Antisense rna of protooncogene c-fos blocks renewed growth of quiescent 3T3 cells', *Journal of Cellular Biochemistry*, pp. 146-146.

Ohga, K., Takezawa, R., Arakida, Y., Shimizu, Y. and Ishikawa, J. (2008) 'Characterization of YM-58483/BTP2, a novel store-operated Ca(2+) entry blocker, on T cell-mediated immune responses in vivo', *International Immunopharmacology*, 8(13-14), pp. 1787-1792.

O'Neill K, Aghaeepour N, Špidlen J, Brinkman R (2013) Flow Cytometry Bioinformatics. PLoS Comput Biol 9(12): e1003365. https://doi.org/10.1371/journal.pcbi.1003365

Pardee, A.B. (1992) 'A growth-control event defective in tumors - a citation-classic commentary on a restriction point for control of normal animal-cell proliferation ', *Current Contents/Life Sciences*, (6), pp. 11-11.

Pardee, A.B. (1974) ' A restriction point for control of normal animal cell proliferation. ', *Proc Natl Acad Sci* 71, pp. 1286–1290

Parekh, A.B. (2008) 'Ca ($^{2+}$) microdomains near plasma membrane Ca ($^{2+}$) channels: impact on cell function', *Journal of Physiology-London*, 586(13), pp. 3043-3054.

Parekh, A.B. and Putney, J.W. (2005) 'Store-operated calcium channels', *Physiological Reviews*, 85(2), pp. 757-810.

Park, C.Y., Hoover, P.J., Mullins, F.M., Bachhawat, P., Covington, E.D., Raunser, S., Walz, T., Garcia, K.C., Dolmetsch, R.E. and Lewis, R.S. (2009) 'STIM1 Clusters and Activates CRAC Channels via Direct Binding of a Cytosolic Domain to Orai1', *Cell*, 136(5), pp. 876-890.

Parvez, S., Beck, A., Peinelt, C., Soboloff, J., Lis, A., Monteilh-Zoller, M., Gill, D.L., Fleig, A. and Penner, R. (2008) 'STIM2 protein mediates distinct store-dependent and

store-independent modes of CRAC channel activation', *Faseb Journal*, 22(3), pp. 752-761.

Peacock, M. (2010) 'Calcium Metabolism in Health and Disease', *Clinical Journal of the American Society of Nephrology*, 5, pp. S23-S30.

Peinelt, C., Vig, M., Koomoa, D.L., Beck, A., Nadler, M.J.S., Koblan-Huberson, M., Lis, A., Fleig, A., Penner, R. and Kinet, J.P. (2006) 'Amplification of CRAC current by STIM1 and CRACM1 (Orai1)', *Nature Cell Biology*, 8(7), pp. 771-U231.

Perabo, F.G.E., Wirger, A., Kamp, S., Lindner, H., Schmidt, D.H., Muller, S.C. and Kohn, E.C. (2004) 'Carboxyamido-triazole (CAI), a signal transduction inhibitor induces growth inhibition and apoptosis in bladder cancer cells by modulation of bcl-2', *Anticancer Research*, 24(5A), pp. 2869-2877.

Poenie, M., Alderton, J., Steinhardt, R. and Tsien, R. (1986) 'Calcium rises abruptly and briefly throughout the cell at the onset of anaphase', *Science*, 233(4766), pp. 886-889.

Poenie, M., Alderton, J., Tsien, R.Y. and Steinhardt, R.A. (1985) 'Changes of free calcium levels with stages of the cell-division cycle', *Nature*, 315(6015), pp. 147-149.

Potier, M., Gonzalez, J.C., Motiani, R.K., Abdullaev, I.F., Bisaillon, J.M., Singer, H.A. and Trebak, M. (2009) 'Evidence for STIM1-and Orai1-dependent store-operated calcium influx through I-CRAC in vascular smooth muscle cells: role in proliferation and migration', *Faseb Journal*, 23(8), pp. 2425-2437.

Pozo-Guisado, E., Campbell, D.G., Deak, M., Alvarez-Barrientos, A., Morrice, N.A., Alvarez, I.S., Alessi, D.R. and Martin-Romero, F.J. (2010) 'Phosphorylation of STIM1 at ERK1/2 target sites modulates store-operated calcium entry', *Journal of Cell Science*, 123(18), pp. 3084-3093.

Pozo-Guisado, E., Casas-Rua, V., Tomas-Martin, P., Lopez-Guerrero, A.M., Alvarez-Barrientos, A. and Martin-Romero, F.J. (2013) 'Phosphorylation of STIM1 at ERK1/2 target sites regulates interaction with the microtubule plus-end binding protein EB1', *Journal of Cell Science*, 126(14), pp. 3170-3180.

Prakriya, M., Feske, S., Gwack, Y., Srikanth, S., Rao, A. and Hogan, P.G. (2006) 'Orai1 is an essential pore subunit of the CRAC channel', *Nature*, 443(7108), pp. 230-233.

Prescott, D.M. (1976) 'Cell-cycle and control of cellular reproduction', *Advances in Genetics Incorporating Molecular Genetic Medicine*, 18, pp. 99-177.

Prescott, D.M. (1987) 'CELL REPRODUCTION', *International Review of Cytology-a Survey of Cell Biology*, 100, pp. 93-128.

Prevarskaya, N., Skryma, R. and Shuba, Y. (2011) 'Calcium in tumour metastasis: new roles for known actors', *Nature Reviews Cancer*, 11(8), pp. 609-618.

Putney, J.W. (1986) 'A model for receptor-regulated calcium entry', *Cell Calcium*, 7(1), pp. 1-12.

Putney, J.W. (2005) 'Physiological mechanisms of TRPC activation', *Pflugers Archiv-European Journal of Physiology*, 451(1), pp. 29-34.

Putney, J.W., Broad, L.M., Braun, F.J., Lievremont, J.P. and Bird, G.S.J. (2001) 'Mechanisms of capacitative calcium entry', *Journal of Cell Science*, 114(12), pp. 2223-2229.

Rasband, W.S. (1997-2014) *Image J*. MD thesis.

Rasmussen, C.D. and Means, A.R. (1989) 'Calmodulin is required for cell-cycle progression during g1 and mitosis', *Embo Journal*, 8(1), pp. 73-82.

Ratan, R.R. and Shelanski, M.L. (1986) 'Calcium and the regulation of mitotic events', *Trends in Biochemical Sciences*, 11(11), pp. 456-459.

Raychaudhury, B., Gupta, S., Banerjee, S. and Datta, S.C. (2006) 'Peroxisome is a reservoir of intracellular calcium', *Biochimica Et Biophysica Acta-General Subjects*, 1760(7), pp. 989-992.

Rey, O., Young, S.H., Jacamo, R., Moyer, M.P. and Rozengurt, E. (2010) 'Extracellular Calcium Sensing Receptor Stimulation in Human Colonic Epithelial Cells Induces Intracellular Calcium Oscillations and Proliferation Inhibition', *Journal of Cellular Physiology*, 225(1), pp. 73-83.

Riccardi, D. and Gamba, G. (1999) 'The many roles of the calcium-sensing receptor in health and disease', *Archives of Medical Research*, 30(6), pp. 436-448.

Roderick, H.L. and Cook, S.J. (2008) 'Ca^{2+} signalling checkpoints in cancer: remodelling Ca^{2+} for cancer cell proliferation and survival', *Nature Reviews Cancer*, 8(5), pp. 361-375.

Roos, J., DiGregorio, P.J., Yeromin, A.V., Ohlsen, K., Lioudyno, M., Zhang, S.Y., Safrina, O., Kozak, J.A., Wagner, S.L., Cahalan, M.D., Velicelebi, G. and

Stauderman, K.A. (2005) 'STIM1, an essential and conserved component of store-operated Ca^{2+} channel function', *Journal of Cell Biology*, 169(3), pp. 435-445.

Rossow, P.W., Riddle, V.G.H. and Pardee, A.B. (1979) 'Synthesis of labile, serum-dependent protein in early g1 controls animal-cell growth', *Proceedings of the National Academy of Sciences of the United States of America*, 76(9), pp. 4446-4450.

Rubin, H. and Xu, K. (1989) 'Evidence for the progressive and adaptive nature of spontaneous transformation in the nih 3t3 cell-line', *Proceedings of the National Academy of Sciences of the United States of America*, 86(6), pp. 1860-1864.

Russa, A.D., Ishikita, N., Masu, K., Akutsu, H., Saino, T. and Satoh, Y. (2008) 'Microtubule remodeling mediates the inhibition of store-operated calcium entry (SOCE) during mitosis in COS-7 cells', *Archives of Histology and Cytology*, 71(4), pp. 249-263.

Sauc, S., Bulla, M., Nunes, P., Orci, L., Marchetti, A., Antigny, F., Bernheim, L., Cosson, P., Frieden, M. and Demaurex, N. (2015) 'STIM1L traps and gates Orai1 channels without remodeling the cortical ER', *Journal of Cell Science*, 128(8), pp. 1568-1579.

Shapiro, H.M. (1981) 'Flow cytometric estimation of dna and rna-content in intact-cells stained with hoechst-33342 and pyronin-y', *Cytometry*, 2(3), pp. 143-150.

Sherr, C.J. (1996) 'Cancer cell cycles', *Science*, 274(5293), pp. 1672-1677.

Shin, H.Y., Hong, Y.H., Jang, S.S., Chae, H.G., Paek, S.L., Moon, H.E., Kim, D.G., Kim, J., Paek, S.H. and Kim, S.J. (2010) 'A Role of Canonical Transient Receptor Potential 5 Channel in Neuronal Differentiation from A2B5 Neural Progenitor Cells', *Plos One*, 5(5).

Shuttleworth, T.J. (2012) 'Orai3-the exceptional' Orai?', *Journal of Physiology-London*, 590(2), pp. 241-257.

Smith, P.K., Krohn, R.I., Hermanson, G.T., Mallia, A.K., Gartner, F.H., Provenzano, M.D., Fujimoto, E.K., Goeke, N.M., Olson, B.J. and Klenk, D.C. (1985) 'Measurement of protein using bicinchoninic acid', *Analytical Biochemistry*, 150(1), pp. 76-85.

Smyth, J.T., Petranka, J.G., Boyles, R.R., DeHaven, W.I., Fukushima, M., Johnson, K.L., Williams, J.G. and Putney, J.W. (2009) 'Phosphorylation of STIM1 underlies

suppression of store-operated calcium entry during mitosis (vol 11, pg 1465, 2009)', *Nature Cell Biology*, 12(2), pp. 199-199.

Soboloff, J., Spassova, M.A., Dziadek, M.A. and Gill, D.L. (2006a) 'Calcium signals mediated by STIM and Orai proteins - A new paradigm in inter-organelle communication', *Biochimica Et Biophysica Acta-Molecular Cell Research*, 1763(11), pp. 1161-1168.

Soboloff, J., Spassova, M.A., Hewavitharana, T., He, L.P., Xu, W., Johnstone, L.S., Dziadek, M.A. and Gill, D.L. (2006b) 'STIM2 is an inhibitor of STIM1-mediated store-operated Ca2+ entry', *Current Biology*, 16(14), pp. 1465-1470.

Spencer, S.L., Cappell, S.D., Tsai, F.C., Overton, K.W., Wang, C.L. and Meyer, T. (2013) 'The Proliferation-Quiescence Decision Is Controlled by a Bifurcation in CDK2 Activity at Mitotic Exit', *Cell*, 155(2), pp. 369-383.

Stathopulos, P.B., Li, G.Y., Plevin, M.J., Ames, J.B. and Ikura, M. (2006) 'Stored Ca^{2+} depletion-induced oligomerization of stromal interaction molecule 1 (STIM1) via the EF-SAM region - An initiation mechanism for capacitative Ca2+ entry', *Journal of Biological Chemistry*, 281(47), pp. 35855-35862.

Stathopulos, P.B., Schindl, R., Fahrner, M., Zheng, L., Gasmi-Seabrook, G.M., Muik, M., Romanin, C. and Ikura, M. (2013) 'STIM1/Orai1 coiled-coil interplay in the regulation of store-operated calcium entry', *Nature Communications*, 4.

Stathopulos, P.B., Zheng, L., Li, G.Y., Plevin, M.J. and Ikura, M. (2008) 'Structural and mechanistic insights into STIM1-mediated initiation of store-operated calcium entry', *Cell*, 135(1), pp. 110-122.

Stewart, T.A., Yapa, K. and Monteith, G.R. (2015) 'Altered calcium signaling in cancer cells', *Biochimica Et Biophysica Acta-Biomembranes*, 1848(10), pp. 2502-2511.

Sukumaran, P., Sun, Y., Vyas, M. and Singh, B.B. (2015) 'TRPC1-mediated Ca^{2+} entry is essential for the regulation of hypoxia and nutrient depletion-dependent autophagy', *Cell Death & Disease*, 6.

Sun, Y.H., Cui, X.B., Wang, J., Wu, S., Bai, Y.F., Wang, Y.P., Wang, B.Q. and Fang, J.G. (2015) 'Stromal interaction molecule 1 (STIM1) silencing inhibits tumor growth and promotes cell cycle arrest and apoptosis in hypopharyngeal carcinoma', *Medical Oncology*, 32(5).

Sundivakkam, P., Natarajan, V., Malik, A.B. and Tiruppathi, C. (2012) 'PAR-1 induced AMPK-p38 MAPK signaling axis mediates STIM1 phosphorylation to prevent calcium entry through TRPC channels in endothelial cells', *Faseb Journal*, 26.

Sundivakkam, P.C., Natarajan, V., Malik, A.B. and Tiruppathi, C. (2013) 'Store-operated $Ca^{2(+)}$ Entry (SOCE) Induced by Protease-activated Receptor-1 Mediates STIM1 Protein Phosphorylation to Inhibit SOCE in Endothelial Cells through AMP-activated Protein Kinase and p38 beta Mitogen-activated Protein Kinase', *Journal of Biological Chemistry*, 288(23), pp. 17030-17041.

Takahashi, Y., Murakami, M., Watanabe, H., Hasegawa, H., Ohba, T., Munehisa, Y., Nobori, K., Ono, K., Iijima, T. and Ito, H. (2007a) 'Essential role of the N-terminus of murine Orai1 in store-operated Ca^{2+} entry', *Biochemical and Biophysical Research Communications*, 356(1), pp. 45-52.

Takahashi, Y., Watanabe, H., Murakami, M., Ono, K., Munehisa, Y., Koyama, T., Nobori, K., Iijima, T. and Ito, H. (2007b) 'Functional role of stromal interaction molecule 1 (STIM1) in vascular smooth muscle cells', *Biochemical and Biophysical Research Communications*, 361(4), pp. 934-940.

Takuwa, N., Wei, Z., Kumada, M. and Takuwa, Y. (1993) 'Ca^{2+}-dependent stimulation of retinoblastoma gene-product phosphorylation and p34cdc2 kinase activation in serum-stimulated human fibroblasts', *Journal of Biological Chemistry*, 268(1), pp. 138-145.

Takuwa, N., Zhou, W. and Takuwa, Y. (1995) 'Calcium, calmodulin and cell-cycle progression', *Cellular Signalling*, 7(2), pp. 93-104.

Tani, D., Monteilh-Zoller, M.K., Fleig, A. and Penner, R. (2007) 'Cell cycle-dependent regulation of store-operated I-CRAC and Mg^{2+}-nucleotide-regulated MagNuM (TRPM7) currents', *Cell Calcium*, 41(3), pp. 249-260.

Tao, X., Zhao, N.Q., Jin, H.Y., Zhang, Z.B., Liu, Y.T., Wu, J., Bast, R.C., Yu, Y.H. and Feng, Y.J. (2013) 'FSH enhances the proliferation of ovarian cancer cells by activating transient receptor potential channel C3', *Endocrine-Related Cancer*, 20(3), pp. 415-429.

Targos, B., Baranska, J. and Pomorski, P. (2005) 'Store-operated calcium entry in physiology and pathology of mammalian cells', *Acta Biochimica Polonica*, 52(2), pp. 397-409.

Tsien, R.Y. (1981) 'A non-disruptive technique for loading calcium buffers and indicators into cells', *Nature*, 290(5806), pp. 527-528.

Tupper, J.T., Kaufman, L. and Bodine, P.V. (1980) 'Related effects of calcium and serum on the g1-phase of the human wi38-fibroblast', *Journal of Cellular Physiology*, 104(1), pp. 97-103.

Udagava, T. (2008) 'Tumor dormancy of primary and secondary cancers', *Apmis*, 116(7-8), pp. 615-628.

Umemura, M., Baljinnyam, E., Feske, S., De Lorenzo, M.S., Xie, L.H., Feng, X.F., Oda, K., Makino, A., Fujita, T., Yokoyama, U., Iwatsubo, M., Chen, S.Z., Goydos, J.S., Ishikawa, Y. and Iwatsubo, K. (2014) 'Store-Operated Ca2+ Entry (SOCE) Regulates Melanoma Proliferation and Cell Migration', *Plos One*, 9(2).

Van Rechem, C., Boulay, G., Pinte, S., Stankovic-Valentin, N., Guerardel, C. and Leprince, D. (2010) 'Differential Regulation of HIC1 Target Genes by CtBP and NuRD, via an Acetylation/SUMOylation Switch, in Quiescent versus Proliferating Cells', *Molecular and Cellular Biology*, 30(16), pp. 4045-4059.

Vig, M., Peinelt, C., Beck, A., Koomoa, D.L., Rabah, D., Koblan-Huberson, M., Kraft, S., Turner, H., Fleig, A., Penner, R. and Kinet, J.P. (2006) 'CRACM1 is a plasma membrane protein essential for store-operated Ca^{2+} entry', *Science*, 312(5777), pp. 1220-1223.

Volpi, M. and Berlin, R.D. (1988) 'Intracellular elevations of free calcium induced by activation of histamine-h1 receptors in interphase and mitotic hela-cells - hormone signal transduction is altered during mitosis', *Journal of Cell Biology*, 107(6), pp. 2533-2539.

Whitaker, M. (1995) 'Regulation of the cell-division cycle by inositol trisphosphate and the calcium signaling pathway', *Calcium Regulation of Cellular Function*, 30, pp. 299-310.

Whitaker, M. and Larman, M.G. (2001) 'Calcium and mitosis', *Seminars in Cell & Developmental Biology*, 12(1), pp. 53-58.

Whitaker, M. and Patel, R. (1990) 'Calcium and cell-cycle control', *Development*, 108(4), pp. 525-542.

Whitaker, M.J. and Steinhardt, R.A. (1982) 'Ionic regulation of egg activation', *Quarterly Reviews of Biophysics*, 15(4), pp. 593-666.

Whitfield, J. (1992) ' Calcium signals and cancer', *Crit Rev Oncog* 3(1-2).

Whitfield, J.F., Macmanus, J.P., Rixon, R.H., Boynton, A.L., Youdale, T. and Swierenga, S. (1976) 'Positive control of cell-proliferation by interplay of calcium-ions and cyclic nucleotides', *In Vitro-Journal of the Tissue Culture Association*, 12(1), pp. 1-18.

Whitworth, C. (2015) Phenotype-specific store-operated calcium entry and the differentiation response in neuroblastoma cells. *Institute of Cell and Molecular Biosciences.* PhD Thesis. Newcastle University

Williams, R.T., Manji, S.S.M., Parker, N.J., Hancock, M.S., Van Stekelenburg, L., Eid, J.P., Senior, P.V., Kazenwadel, J.S., Shandala, T., Saint, R., Smith, P.J. and Dziadek, M.A. (2001) 'Identification and characterization of the STIM (stromal interaction molecule) gene family: coding for a novel class of transmembrane proteins', *Biochemical Journal*, 357, pp. 673-685.

Williams, R.T., Senior, P.V., Van Stelenburg, L., Layton, J.E., Smith, P.J. and Dziadek, M.A. (2002) 'Stromal interaction molecule 1 (STIM1), a transmembrane protein with growth suppressor activity, contains an extracellular SAM domain modified by N-linked glycosylation', *Biochimica Et Biophysica Acta-Protein Structure and Molecular Enzymology*, 1596(1), pp. 131-137.

Wu, M.M., Buchanan, J., Luik, R.M. and Lewis, R.S. (2006) 'Ca^{2+} store depletion causes STIM1 to accumulate in ER regions closely associated with the plasma membrane', *Journal of Cell Biology*, 174(6), pp. 803-813.

Wu, Z.S., Qing, J.J., Xia, Y.X., Wang, K. and Zhang, F. (2015) 'Suppression of stromal interaction molecule 1 inhibits SMMC7721 hepatocellular carcinoma cell proliferation by inducing cell cycle arrest', *Biotechnology and Applied Biochemistry*, 62(1), pp. 107-111.

Xiong, W., Jiao, Y., Huang, W.W., Ma, M.X., Yu, M., Cui, Q.H. and Tan, D.Y. (2012) 'Regulation of the cell cycle via mitochondrial gene expression and energy metabolism in HeLa cells', *Acta Biochimica Et Biophysica Sinica*, 44(4), pp. 347-358.

Yang, I.H., Tsai, Y.T., Chiu, S.J., Liu, L.T., Lee, H.H., Hou, M.F., Hsu, W.L., Chen, B.K. and Chang, W.C. (2013) 'Involvement of STIM1 and Orai1 in EGF-mediated cell growth in retinal pigment epithelial cells', *Journal of Biomedical Science*, 20.

Yao, G. (2014) 'Modelling mammalian cellular quiescence', *Interface Focus*, 4(3).

Yeromin, A.V., Zhang, S.Y.L., Jiang, W.H., Yu, Y., Safrina, O. and Cahalan, M.D. (2006) 'Molecular identification of the CRAC channel by altered ion selectivity in a mutant of Orai', *Nature*, 443(7108), pp. 226-229.

Yuan, J.P., Kiselyov, K., Shin, D.M., Chen, J., Shcheynikov, N., Kang, S.H., Dehoff, M.H., Schwarz, M.K., Seeburg, P.H., Muallem, S. and Worley, P.F. (2003) 'Homer binds TRPC family channels and is required for gating of TRPC1 by IP3 receptors', *Cell*, 114(6), pp. 777-789.

Yuan, J.P., Lee, K.P., Hong, J.H. and Muallem, S. (2012) 'The closing and opening of TRPC channels by Homer1 and STIM1', *Acta Physiologica*, 204(2), pp. 238-247.

Yuan, J.P., Zeng, W.Z., Huang, G.N., Worley, P.F. and Muallem, S. (2007) 'STIM1 heteromultimerizes TRPC channels to determine their function as store-operated channels', *Nature Cell Biology*, 9(6), pp. 636-U38.

Zeng, W.Z., Yuan, J.P., Kim, M.S., Choi, Y.J., Huang, G.N., Worley, P.F. and Muallem, S. (2008) 'STIM1 Gates TRPC Channels, but Not Orai1, by Electrostatic Interaction', *Molecular Cell*, 32(3), pp. 439-448.

Zetterberg, A. and Larsson, O. (1985) 'Kinetic-analysis of regulatory events in g1 leading to proliferation or quiescence of swiss 3t3 cells', *Proceedings of the National Academy of Sciences of the United States of America*, 82(16), pp. 5365-5369.

Zhang, S.L., Yeromin, A.V., Zhang, X.H.F., Yu, Y., Safrina, O., Penna, A., Roos, J., Stauderman, K.A. and Cahalan, M.D. (2006) 'Genome-wide RNAi screen of Ca2+ influx identifies genes that regulate Ca^{2+} release-activated Ca^{2+} channel activity', *Proceedings of the National Academy of Sciences of the United States of America*, 103(24), pp. 9357-9362.

Zhang, S.Y.L., Yu, Y., Roos, J., Kozak, J.A., Deerinck, T.J., Ellisman, M.H., Stauderman, K.A. and Cahalan, M.D. (2005) 'STIM1 is a Ca^{2+} sensor that activates CRAC channels and migrates from the Ca^{2+} store to the plasma membrane', *Nature*, 437(7060), pp. 902-905.

Zheng, L., Stathopulos, P.B., Li, G.Y. and Ikura, M. (2008) 'Biophysical characterization of the EF-hand and SAM domain containing Ca^{2+} sensory region of STIM1 and STIM2', *Biochemical and Biophysical Research Communications*, 369(1), pp. 240-246.

Zhivotovsky, B. and Orrenius, S. (2010) 'Cell cycle and cell death in disease: past, present and future', *Journal of Internal Medicine*, 268(5), pp. 395-409.

Zhou, Y.D., Lewis, T.L., Robinson, L.J., Brundage, K.M., Schafer, R., Martin, K.H., Blair, H.C., Soboloff, J. and Barnett, J.B. (2011) 'The Role of Calcium Release Activated Calcium Channels in Osteoclast Differentiation', *Journal of Cellular Physiology*, 226(4), pp. 1082-1089.

Zucker, R.S. and Steinhardt, R.A. (1978) 'Prevention of cortical reaction in fertilized sea-urchin eggs by injection of calcium-chelating ligands', *Biochimica Et Biophysica Acta*, 541(4), pp. 459-466.

Zucker, R.S., Steinhardt, R.A. and Winkler, M.M. (1978) 'Intracellular calcium release and mechanisms of parthenogenetic activation of sea-urchin egg', *Developmental Biology*, 65(2), pp. 285-295.